



TECHNISCHE
UNIVERSITÄT
DARMSTADT

Impact of Low-Dose Ionizing Radiation on Cognitive Abilities
in the Mouse: Assessment of Radiation Sensitivity during
Pre- and Postnatal Brain Development

vom Fachbereich Biologie
der Technischen Universität Darmstadt

zur Erlangung des Grades
Doctor rerum naturalium
(*Dr. rer. nat.*)

Dissertation
von Axel Klink

Erstgutachter: Prof. Dr. Bodo Laube
Zweitgutachter: Prof. Dr. Ralf Galuske

Darmstadt 2021

Klink, Axel: Impact of Low-Dose Ionizing Radiation on Cognitive Abilities in the
Mouse: Assessment of Radiation Sensitivity during Pre- and Postnatal Brain
Development
Darmstadt, Technische Universität Darmstadt
Jahr der Veröffentlichung der Dissertation auf TUpriints: 2021
Tag der mündlichen Prüfung: 26.01.2021
urn:nbn:de:tuda-tuprints-175351
Veröffentlicht unter CC BY-SA 4.0 International
<https://creativecommons.org/licenses/>

Ehrenwörtliche Erklärung

Ich erkläre hiermit, dass ich die vorliegende Arbeit entsprechend den Regeln guter wissenschaftlicher Praxis selbstständig und ohne unzulässige Hilfe Dritter angefertigt habe. Sämtliche aus fremden Quellen direkt oder indirekt übernommenen Gedanken sowie sämtliche von Anderen direkt oder indirekt übernommenen Daten, Techniken und Materialien sind als solche kenntlich gemacht. Die Arbeit wurde bisher bei keiner anderen Hochschule zu Prüfungszwecken eingereicht. Die eingereichte elektronische Version stimmt mit der schriftlichen Version überein.

Darmstadt, den 16.12.2020



OMNIA TEMPUS HABENT.

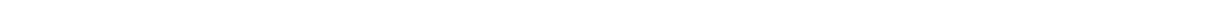


TABLE OF CONTENT

1	Abbreviations	I
2	Summary	III
3	Zusammenfassung	V
4	Introduction	1
4.1	Ionizing Radiation	3
4.1.1	Physical Interaction of Photons and Matter	4
4.1.2	Radiation Sensitivity	4
4.2	Learning, Memory and Spatial Navigation	5
4.2.1	The Hippocampal Formation	5
4.2.2	Development of the Murine Hippocampus	6
4.2.3	Anatomy of the Hippocampal Circuitry	8
4.2.4	The Dentate Gyrus – Adult Hippocampal Neurogenesis	12
4.2.5	Navigation, Spatial Cells and Cognitive Maps	17
5	Purpose	25
6	Material	26
6.1	Chemicals and Reagents	26
6.2	Consumable Material	26
6.3	Equipment	27
6.4	Buffers and Solutions	28
6.5	Primary Antibodies	29
6.6	Secondary Antibodies	29
6.7	Computer Software	29
7	Methods	30
7.1	Laboratory Animals	30
7.2	Experimental Timeline: E14.5 and P10	30
7.3	Experimental Timeline: Short-term Learning Phase Experiments	32
7.4	Irradiation	33

7.5	Behavioural Experiments	33
7.5.1	Rotarod	33
7.5.2	Elevated Zero Maze (EZM)	35
7.5.3	Morris Water Maze (MWM)	36
7.5.4	Video Tracking Analysis with <i>EthoVisionXT</i> 11.5	39
7.6	Histology	45
7.6.1	Tissue Preparation	45
7.6.2	Nissl Staining	46
7.6.3	Immunohistochemistry (IHC)	47
7.6.4	Fluorescence Microscopy and Quantifications	48
7.7	Data Generation and Analysis	48
7.7.1	Rotarod Data and EZM Data	49
7.7.2	MWM Data	49
8 Chapter I – Evaluation of Long-term Radiation Risk and Sensitivity for Time Point E14.5	53
8.1	Results	53
8.1.1	Effects on Motor Function and Anxiety/Exploration Behaviour (E14.5)	53
8.1.2	Initial Learning Revealed Dose-dependent Learning Delays	55
8.1.3	Probe Trial Revealed Disturbed Reference Memory	59
8.1.4	Initially Affected Spatial Memory was Improved during Reversal Learning	62
8.1.5	Reversal Probe Testing Confirmed Proper Formation of Reference Memory	64
8.1.6	Conclusion – Chapter I (E14.5)	67
9 Chapter II – Evaluation of Long-term Radiation Risk and Sensitivity for the Time Point P10	68
9.1	Results	68
9.1.1	Effects on Motor Performance and Activity/Exploration Behaviour (P10)	68
9.1.2	Initial Learning Uncovers Dose-dependent Learning Delays	70
9.1.3	Disturbed Reference Memory during Probe Trial	73
9.1.4	Performance of Irradiated Mice was Improved during Reversal Training	76
9.1.5	Reversal Probe Test Confirmed Improved Reference Memory	78

9.2 Conclusion – Chapter II (P10)	80
10...Chapter III – Effects of LDIR on MWM Learning Phases	81
10.1 Results	81
10.1.1 Similar Rotarod and EZM Performance in all Cohorts	81
10.1.2 Minimal Difference in the Acquisition of Spatial Memory in Cohort 1	84
10.1.3 Mice in Cohort 2 Displayed Equal Spatial Learning Abilities	89
10.1.4 IR Mice of Cohort 3 Performed Worse at the Start of Reversal Learning	95
10.2 Conclusion – Chapter III (learning phases)	100
11...Chapter IV – Immunohistological Analysis of Neural Progenitors in the Dentate Gyrus	102
11.1 Results	103
11.1.1 Irradiation with 0.5 Gy Reduced DCX ⁺ Progenitor Cells and Resulted in Diminished DG Area	103
11.2 Conclusion – Chapter IV (Immunohistological Analysis)	105
12...Chapter V – Overarching Comparison of the Distinct Irradiation Time Points	106
12.1 Results	106
12.1.1 Different Sham Groups Performed Similar in the MWM Task	106
12.1.2 Differences in Spatial Searching and Reference Memory Depending on Irradiation Time Point	108
12.1.3 Evaluation of Searching Strategy Profiles	111
12.2 Conclusion – Chapter V (Overarching Comparison)	114
13...Discussion	115
13.1 Impact of LDIR on Motor Function and Anxiety-like Behaviour	117
13.2 Impact of LDIR on Hippocampus-dependent Spatial Navigation	120
13.2.1 Initial MWM Phase	120
13.2.2 Initial Deficit in Spatial Navigation Could Result from Impairment of the Neurogenic Niche	125
13.2.3 Reversal MWM Phase	132
13.3 Relevance of Medical Radiation Treatments for Human Brain Development	140
14...List of figures	143
15...List of tables	145

16...References	146
17...Acknowledgments	170
18...Curriculum Vitae	171

1 Abbreviations

ANOVA	Analysis of Variance
Arc	Activity-regulated cytoskeleton-associated protein
BrdU	5-bromo-2'-deoxyuridine
CA	Cornu ammonis
CET	Central european time
cGy	Centigray
CH	Cortical hem
cm	Centimeter
CNS	Central nervous system
CREB	cAMP response element-binding protein
CT	Computer tomography
DG	Dentate gyrus
DNA	Deoxyribonucleic acid
DNE	Dentate neuroepithelium
E	Embryonic day
EC	Entorhinal cortex
EdU	5-Ethynyl-2'-desoxyuridin
et al.	<i>et alii</i>
EtOH	Ethanol
F	F-ratio (ANOVA)
g	Gram
Gy	Gray
H	H value (Kruskal-Wallis statistic)
h	Hour
HC	Hippocampus
HNE	Hippocampal neuroepithelium
IHC	Immunohistochemistry
IPC	Intermediate progenitor cells
IR	Ionizing radiation or irradiated
kV	Kilovolt
L	Liter
LDIR	Low-dose ionizing radiation (here defined as ≤ 0.5 Gy)
LTP	Long-term potentiation
mA	Milliampere
mg	Milligram
min	Minute / minutes
mL	Milliliter
mm ²	Square millimeter
MWM	Morris Water Maze
μ L	Microliter
μ m	Micrometer
n	Number of animals
NE	North-East quadrant
NIH	National Institutes of Health
NPC	Neural progenitor cell
NSC	Neural stem cell
NW	North-West quadrant
P	Postnatal day or P value/level of significance
ParaSub	Parasubiculum
PBS	Phosphate buffered saline
PFA	Paraformaldehyde
PreSub	Presubiculum
PSD95	Postsynaptic density protein 95
PVC	Polyvinyl chloride

P _{X/Y}	P value for specific comparisons, possibilities to substitute X and Y: S (Sham) / 0.125 (0.125 Gy) / 0.25 (0.25 Gy) / 0.5 (0.5 Gy) SW / NE / NW / SE 1 (day 1) / 2 (day 2) / 3 (day 3) / 4 (day 4) / 5 (day 5) E (embryonic), P (postnatal), C1 (Cohort 1), C2 (Cohort 2), C3 (Cohort 3)
Rac1	Ras-related C3 botulinum toxin substrate 1
rpm	Revolutions per minute
RT	Room temperature
s/secs	Seconds
SD	Standard deviation
SE	South-East quadrant
SEM	Standard error of the mean
SGZ	Subgranular zone
Sub	Subiculum
SVZ	Subventricular zone
SW	South-West quadrant
TUD	Technische Universität Darmstadt
Two-way RM ANOVA	Two-way Repeated Measures ANOVA
vs.	Versus
VZ	Ventricular zone
<	Less than
≤	Less or equal
>	Greater than
≥	Equal to or greater
°C	Degree Celsius
∅	Diameter
%	Percentage
±	Plus-or-minus sign
*	P < 0.05
**	P < 0.01
***	P < 0.001
****	P < 0.0001

2 Summary

In our modern society various sources of radiation are omnipresent. Sectors like nuclear power generation, long distance air travel and medical radiation diagnostics rank among the most prominent. Especially, the amount of medically necessary radiation is increasing and represents a major source of exposure in the general population. Therefore, radiation protection and the epidemiology of radiation have gained in importance. The risk possibly arising from exposure to low-dose radiation is still part of intensive and ongoing debates, demonstrating that current results are still controversial. Consequently, further studies on the effects of low-dose radiation are of great social relevance. Systemic studies within animals could provide additional information about radiation impact on behaviour and neurogenesis within the hippocampus, thus contributing to a better understanding of radiation induced sequelae and improving current risk assessment.

This thesis evaluates the effects of low-dose ionizing radiation (LDIR, defined as ≤ 0.5 Gy) on murine behaviour and neurogenesis. Chapter I and II deal with irradiations at specific time points during prenatal (E14.5) and early postnatal (P10) brain development and provide results on the long-term sensitivity to low-dose radiation. Chapter III deals with low-dose irradiation during different learning phases at an early adult stage (two months) and provides results on the short-term sensitivity to low-dose radiation. Chapter IV deals with the long-term effects of low-dose irradiation at E14.5 or P10 on neurogenesis. Chapter V provides an overarching comparison of all time points of irradiation.

Mice performed a set of behavioural tasks including the Rotarod performance test for the analysis of motor function and coordination, the Elevated-Zero-Maze for evaluation of anxiety and exploration, and the Morris Water Maze for the analysis of spatial learning and memory abilities. Furthermore, naïve mice were irradiated at E14.5 or P10 and analyzed immunohistologically at the age of two months. Here, the focus was on quantification of DCX⁺ neural progenitor cells in the neurogenic niche of the dentate gyrus.

Substantial dose-dependent effects during MWM testing were detected after irradiation at the time points E14.5 and P10, but not after irradiations in two months old mice compared to Sham controls. Impairment of MWM performance was characterized by

decreasing efficiencies in spatial searching and disturbed reference memory with increasing irradiation dose. The comparison of E14.5 and P10 revealed only slight differences, so that a similar sensitivity to low-dose irradiation was ascribed to both time points. Immunohistological analysis revealed that irradiation with 0.5 Gy reduced the number of DCX⁺ progenitor cells in the adult dentate gyrus of naïve mice after both the embryonic and the early postnatal irradiation. However, a significant cell loss was only observed in mice irradiated at E14.5 compared to the P10. My data show that the neurogenic niche in the dentate gyrus reacts very sensitive to radiation exposure, even if doses are low. The alterations in neurogenesis are certainly associated with learning and memory deficits. As the observed impact on neurogenesis was differently pronounced in naïve animals irradiated at E14.5 or P10, whereas the observed cognitive effects were quite similar, the reduced number of progenitor cells within the hippocampal network was probably not the only relevant trigger for cognitive impairment. It is conceivable that migration of progenitor cells and synaptogenesis which are crucial steps during murine brain development at E14.5 and P10, respectively, add an extra layer of complexity to radiation-induced sequelae that should be also taken into consideration in the human brain.

3 Zusammenfassung

In unserer modernen Gesellschaft sind vielfältige Strahlungsquellen allgegenwärtig. Bereiche wie Kernenergieerzeugung, Langstreckenflugreisen und medizinische Strahlendiagnostik zählen zu den bekanntesten. Insbesondere medizinische Untersuchungen mittels Strahlung nehmen zu, sodass darin eine Hauptquelle für Strahlenexposition in der Allgemeinbevölkerung besteht. Daher haben sowohl der Strahlenschutz als auch die epidemiologische Aufarbeitung möglicher Folgen an Wichtigkeit zugenommen. Mögliche Risiken einer Niedrigdosis-Strahlenexposition werden aufgrund kontroverser Resultate derzeit immer noch stark diskutiert. Folglich sind weitere Studien zu den Auswirkungen niedrig dosierter Strahlung von großer sozialer Relevanz. Systemische Studien an Tieren können zusätzliche Informationen über die Auswirkungen der Strahlung auf das Verhalten und die Neurogenese im Hippocampus liefern und so zu einem besseren Verständnis der strahleninduzierten Folgen und zur Verbesserung der aktuellen Risikobewertung beitragen.

In dieser Arbeit werden die Auswirkungen niedrig dosierter ionisierender Strahlung (LDIR, definiert als $\leq 0,5$ Gy) auf das Verhalten und die Neurogenese von Mäusen untersucht. Kapitel I und II befassen sich mit Bestrahlungen zu bestimmten Zeitpunkten während der pränatalen (E14.5) und frühen postnatalen (P10) Gehirnentwicklung und liefern Ergebnisse zur Langzeitempfindlichkeit gegenüber niedrig dosierter Strahlung. Kapitel III befasst sich mit niedrig dosierter Bestrahlung während verschiedener Lernphasen in einem frühen Erwachsenenstadium (zwei Monate) und liefert Ergebnisse zur kurzfristigen Empfindlichkeit gegenüber niedrig dosierter Strahlung. Kapitel IV befasst sich mit den Langzeiteffekten einer Bestrahlung mit niedriger Dosis bei E14.5 oder P10 auf die Neurogenese. Kapitel V bietet einen umfassenden Vergleich aller Bestrahlungszeitpunkte.

C57BL/6 Mäuse wurden in einer Reihe kognitiver Tests analysiert. Mittels Rotarod Test wurden zunächst motorische Fähigkeiten und Koordination untersucht. Im Anschluss daran wurde ein Elevated-Zero-Maze Test zur Bewertung des Angst- und Erkundungsverhaltens durchgeführt. Schließlich wurden räumliches Lernen und Gedächtnisfunktion im Morris Water Maze (MWM) analysiert. Darüber hinaus wurden naive Mäuse an E14.5 oder P10 bestrahlt und im Alter von zwei Monaten

immunhistologisch analysiert. Hier lag der Fokus auf der Quantifizierung von DCX⁺ neuronalen Vorläuferzellen in der neurogenen Nische des Gyrus dentatus.

Im Vergleich zu Sham Kontrollen wurden nach Bestrahlung zu den Zeitpunkten E14.5 und P10 erhebliche dosisabhängige Effekte während des MWM-Tests festgestellt, jedoch nicht nach Bestrahlung in zwei Monate alten Mäusen. Die Beeinträchtigung der MWM-Leistung war durch eine ineffizientere räumliche Suche und ein gestörtes Referenzgedächtnis mit zunehmender Bestrahlungsdosis gekennzeichnet. Der Vergleich von E14.5 und P10 ergab nur geringe Unterschiede, so dass beiden Zeitpunkten eine ähnliche Empfindlichkeit gegenüber Bestrahlung mit niedriger Dosis zugeschrieben wurde. Die immunhistologische Analyse ergab, dass eine Bestrahlung mit 0,5 Gy die Anzahl der DCX⁺ Vorläuferzellen im adulten Gyrus dentatus naiver Mäuse sowohl nach der embryonalen als auch nach der frühen postnatalen Bestrahlung verringerte. Ein signifikanter Zellverlust wurde jedoch nur bei Mäusen beobachtet, die an E14,5 bestrahlt wurden, im Gegensatz zu P10. Meine Daten zeigen, dass die neurogene Nische im Gyrus dentatus sehr empfindlich auf Strahlenexposition reagiert, selbst wenn die Dosen niedrig sind. Veränderungen in der Neurogenese sind höchstwahrscheinlich ursächlich für die beobachteten Lern- und Gedächtnisdefizite. Jedoch waren die strahleninduzierten Effekte auf die Neurogenese bei naiven Tieren, die an E14.5 oder P10 bestrahlt wurden, unterschiedlich stark ausgeprägt, während die kognitiven Defizite ähnlich stark ausgeprägt waren. Daher muss man davon ausgehen, dass eine verringerte Anzahl von Vorläuferzellen innerhalb des hippocampalen Netzwerks nicht der einzige relevante Auslöser für kognitive Beeinträchtigungen ist.

Es ist vorstellbar, dass sowohl Migration von Vorläuferzellen als auch Synaptogenese, welche entscheidend an der Gehirnentwicklung von Mäusen bei E14.5 bzw. P10 beteiligt sind, die Komplexität der strahleninduzierten Folgen zusätzlich erhöhen. Diese Prozesse sollten daher auch bei der Bewertung strahleninduzierter Folgen im menschlichen Gehirn berücksichtigt werden.

4 Introduction

Life on earth developed in continuous interaction with radiation and has to deal with radiation permanently, even today. The human population is exposed to ionizing radiation in a variety of ways. On the one hand, this radiation exposure is composed of a natural proportion, on the other hand there is an additional proportion in terms of civilization. In a modern and critical society, radiobiological issues possess considerable significance regarding the discussion of advantages and drawbacks of radiation use. Thus, an appropriate evaluation of the radiation risks to the general population and the development of suitable radiation protection measures taking account of radiobiological aspects are necessary and reasonable.

It is known for a while that exposure to ionizing radiation during critical phases of prenatal development can have detrimental effects on human health that include brain damage and growth retardation (Otake & Schull, 1998). As part of these effects, severe mental deficiencies constitute a tremendous interference with broad impact on everyday life (Otake & Schull, 1993, 1998). Here gestational age at the time of exposure seems to be a very important constant regarding the determination of the injury severity (Otake & Schull, 1998). Today's knowledge regarding the health risks of ionizing radiation is based mainly on the numerous well-known epidemiological studies about the survivors of the atomic bombings of Hiroshima and Nagasaki (6/9 August 1945) conducted by the ABCC (Atomic Bomb Casualty Commission) and the RERF (Radiation Effects Research Foundation). These indicate that affected children are at risk to become mentally retarded. Thus, *in utero* exposed children showed higher incidence of small head size and lower IQ values as well as seizures. Interestingly, the gestational weeks 8 and 15 and to a lower extent the gestational weeks 16 and 25 were sensitive to radiation. Thus, the timing of exposure seemed to be very crucial (Otake & Schull, 1998; Schull et al., 1990). These epidemiological studies about the survivors of the atomic bombings are important milestones in the description of the deleterious effects on human health (Blot, 1975; Dunn et al., 1990; R. Miller, 1969; R. Miller & Blot, 1972; Otake & Schull, 1993, 1998; Otake et al., 1988, 1996, 1987; Schull & Otake, 1986; J. Wood et al., 1967).

Various sources of radiation in our modern society can be found in the sectors such as nuclear power generation, long distance air travel or medical radiation diagnostics (e.g. Computer Tomography, curative/palliative radiotherapy). Especially, the amount of medical radiation is increasing and represents the major source of exposure in the general population (Bernier et al., 2012; Mettler Jr et al., 2008, 2000). According to the Federal Office for Radiation Protection in Germany, the estimated total number of X-ray examinations in 2016 amounted to approximately 135 million. This number does not include the dental sector which additionally comprised approximately 80 million examinations.

Between 2007 and 2017, a steady increase by about 45 % in CT examinations was very prominent (<https://www.bfs.de/DE/themen/ion/anwendung-medizin/diagnostik/roe-ntgen/haeufigkeit-exposition.html>; Status: 13 February 2020). Radiation protection and the epidemiology of radiation have gained in importance based on the steady increase in medical radiation exposure and the high number of occupationally exposed persons. Today, pregnant women can still be exposed to radiation sources during medical examinations or treatments. For example, radiation therapy is sometimes required for treating cancer patients during pregnancy, however, the available information on the long-term outcome of the exposed embryos or fetuses is incomplete (van Calsteren & Amant, 2014).

Recent studies emphasized the relevance of *in utero* or postnatal irradiation regarding neuronal cell death in the developing brain (Gatz et al. 2011; Fike et al. 2009; Michelin et al. 2004). It has been shown that a fetal and neonatal brain developmental period (brain growth spurt) seems to be particularly vulnerable to radiation (Fukuda et al., 2005). This phase is characterized by cell differentiation, dendrite formation, synaptogenesis and physiological apoptosis. Especially, irradiation during sensitive phases could be responsible for impairment of cognitive function via impact on the neurogenic niche of the dentate gyrus, an issue of great personal and social relevance. A further study evaluated cognitive deficits in men at the time of military enlistment who were exposed to low-dose ionizing radiation in early childhood. Treatments against cutaneous haemangiomas in those children under 18 months of age showed a negative correlation with intellectual capacity at 18-19 years of age. The results showed a reduced probability of attending high school when irradiation dose was higher than

0.1 Gy (Hall et al., 2004). This indicates that brain development is extremely sensitive to radiation not only during the fetal phase, but also during toddler age. The high radiation sensitivity of the developing brain can be explained by its high number of undifferentiated, proliferating neural precursor cells (Jacquet, 2004). Despite neural proliferation is declining after birth, cells in specific regions, like the dentate gyrus, continue to divide up into adulthood (Verheyde & Benotmane, 2007). Consequently, those regions remain sensitive to radiation.

There have been numerous efforts to reduce the exposure of children to radiation. However, a commissioned investigation of the BMU (Bundesministerium für Umwelt, Naturschutz und nukleare Sicherheit) has shown that 1 to 6 % of all CT examinations are done in children. The age distribution for paediatric CT examinations was almost uniform with 40 % in 0- to 5-year-old children, 28 % in 6- to 10-year-old children and 32 % in 11- to 15-year-old children. The vast majority of CT examinations in children (52%) involved the skull and brain (Galanski et al., 2007). Brain doses received during a single typical CT scan of the head in children younger than 5 years have been estimated within the range of 50-100 mGy (Brenner & Hall, 2007).

So far, consequences of low-dose irradiation on cognitive abilities are less well characterized. It is particularly urgent to acquire knowledge about the risks of the increased use of CT, especially in children. Thus, there is still need for information and clarification, as the *Multidisciplinary European Low Dose Initiative* has particularly pointed out (MELODI; Kreuzer *et al.* 2017, 2018). On that basis, it is essential to characterize specific brain developmental phases according to their radio sensitivity towards a range of applied low doses of ionizing radiation. Moreover, it is crucial to evaluate low-dose radiation exposure in the young adult brain and its impact on individuals who are going through distinct learning processes. Therefore, this study was based on a standardized behavioural approach using C57BL/6 mice to mimic the radiation risk for two different phases of brain development (E14.5, P10) as well as to elucidate the influence of low radiation doses during learning phases in the young adult mouse.

4.1 Ionizing Radiation

Ionizing radiation includes electromagnetic radiation (X-ray or γ -radiation) and particle radiation. By interacting with atoms, ionizing radiation is able to release electrons from

the atomic shell. Through the loss of an electron, the atom becomes a positively charged ion, which is why this process is called ionization. If this atom is part of a macromolecule, an induced positive charge will at first influence the chemical properties of this molecule by, for example, breaking up of atomic bonds. Thus, it is possible that functional groups, important for the interaction with other molecules, are modified. Subsequently, this will also induce changes in the biological properties of the macromolecule (Kelsey et al., 2014; Krieger, 2011; Matthews, 2019).

4.1.1 Physical Interaction of Photons and Matter

X-rays are photons. They do not have a mass, are highly energetic and can travel over long distances. Depending on their energy, photons can interact with atomic shells or atomic nuclei of the permeated matter. When photons interact with the atomic shell, they can become scattered (change of direction) without any energy transfer. Alternatively, photons interact via the photoelectric effect or the Compton effect, causing energy transfer. The energy transfer to an electron in the atomic shell causes its release from the atomic association, leading to the ionization of the energy absorbing atom. When high-energy photons (> 1 MeV) interact with the electric field of the atomic nucleus, this can convert the energy of the photon into an electron and a positron (pair production). Electrons released by ionization are called secondary electrons that can excite or ionize further atoms or molecules, depending on their energy. Based on their charge and their low mass, the secondary electrons interact with almost all passed atoms and often become scattered. In this way, electrons create a homogeneous dose deposition in the matter penetrated by X-rays which is why X-rays are often referred to as indirect ionizing radiation (Kelsey et al., 2014; Krieger, 2011).

In cells, photons and secondary electrons interact mainly with water molecules. Ionization of water molecules results in secondary electrons and highly reactive radicals, such as the hydroxyl radical. As a result, damages to the DNA backbone (single and double strand breaks) or loss and modifications of DNA bases can be induced (Bolus, 2017; Krieger, 2011).

4.1.2 Radiation Sensitivity

The term radiation sensitivity describes the sensitivity of organisms to the effects of ionizing radiation. This susceptibility can affect the level of individual cells, tissues and

organs and thus affect the entire organism. The "Law of Bergonié and Tribondeau" from 1906 postulates a connection between the proliferation rate and radiation sensitivity (Bergonié & Tribondeau, 1906, 1959). The authors concluded from their observations that tumor cells with higher reproductive activity are generally more sensitive to radiation compared to the majority of body cells. Indeed, a directly/reciprocally proportional relationship between the radiation sensitivity of cells and proliferation rate or differentiation stage has been demonstrated (Rubin & Casarett, 1968). Consequently, actively dividing cells and more immature cells show the highest susceptibility towards radiation.

4.2 Learning, Memory and Spatial Navigation

The major part of our knowledge and our abilities are not inherent but learned. Learning involves processes of gaining new knowledge about our environment. However, each new piece of knowledge is only useful if we can memorize and reconstruct it over time. Therefore, memory impairment can influence cognitive abilities and subsequently the quality of living at all stages of age.

4.2.1 The Hippocampal Formation

The human medial temporal lobe and memory function are closely intertwined, a connection that has already been noticed more than 100 years ago (von Bechterew, 1900). Von Bechterew described a patient suffering from massive memory deficits. Post mortem, the patient's brain was found to have bilateral aberrations within this brain area, especially the hippocampal formation and the underlying structures were affected. However, linking those brain regions systematically to memory function took several decades, until Brenda Milner documented the probably best known patient in history, Henry Gustav Molaison, patient H.M. (Scoville & Milner, 1957). Since he was involved in a bicycle accident as a child, H.M. started suffering from epileptic seizures at the age of ten (Squire, 2009). His convulsions became progressively more severe with age, why Patient H.M. underwent a neurosurgery in 1953 at the age of 27 to resect portions of the medial temporal lobe bilaterally, including parts of the hippocampus (Milner et al., 1998; Squire, 2009). Although, the intervention alleviated his epileptic seizures, H.M. instantaneously showed deficiencies regarding recent memories, while other intellectual abilities and his personality were unaffected (Annese et al., 2014; Milner et

al., 1998; Scoville, 1954). Patient H.M. developed an anterograde amnesia and a partial retrograde amnesia for memories spanning the last three years before the resection, while old childhood memories seemed to be available (Milner et al., 1998; Scoville & Milner, 1957; Squire, 2009).

Interestingly, Milner found that H.M. was able to retain new information for a certain amount of time, for example a number of three digits, as long as he could continuously focus on that task and his attention was not diverted (Milner et al., 1998). Thus, H.M.'s short term memory was normal and his case provides marked evidence for the difference between short-term and long-term memory and the involvement of the hippocampal formation in memory processes. As a whole, the hippocampal formation is crucially involved in both spatial and non-spatial forms of declarative or explicit memory, our knowledge about people, places, objects and happenings. Additionally, it may also be involved in the processing of temporally structured events and experiences (Basu & Siegelbaum, 2015; Buzsáki & Llinas, 2017; Kraus et al., 2013; MacDonald et al., 2013; Pastalkova et al., 2008a, 2008b; Squire et al., 2004).

4.2.2 Development of the Murine Hippocampus

Important stages of hippocampal development in the mouse are shown in Figure 4-1. Embryonic development of the dentate gyrus is characterized by migration of proliferative progenitor cells and the formation of the dentate migratory stream (DMS) that starts from the dentate neuroepithelium (primary matrix) and spreads out to the future dentate gyrus in late embryonic development (Altman & Bayer, 1990a, 1990b; Nelson et al., 2020; Urban & Guillemot, 2014). Dentate neurogenesis in mice starts around E10 (Hatten, 1999; Rice & Barone Jr., 2000; Stagni et al., 2015). The primary matrix is a part of the ventricular zone and becomes discernible from embryonic day 14.5 on, the time point of initial DMS formation. Embryonic day 14.5 coincides with the start of migration of precursors and immature neurons in direction of the pial surface and hippocampal fissure, a process that is conveyed by Cajal-Retzius cells (Altman & Bayer, 1990a, 1990b; Del Río et al., 1997; Nelson et al., 2020; Rickmann et al., 1987; Urban & Guillemot, 2014).

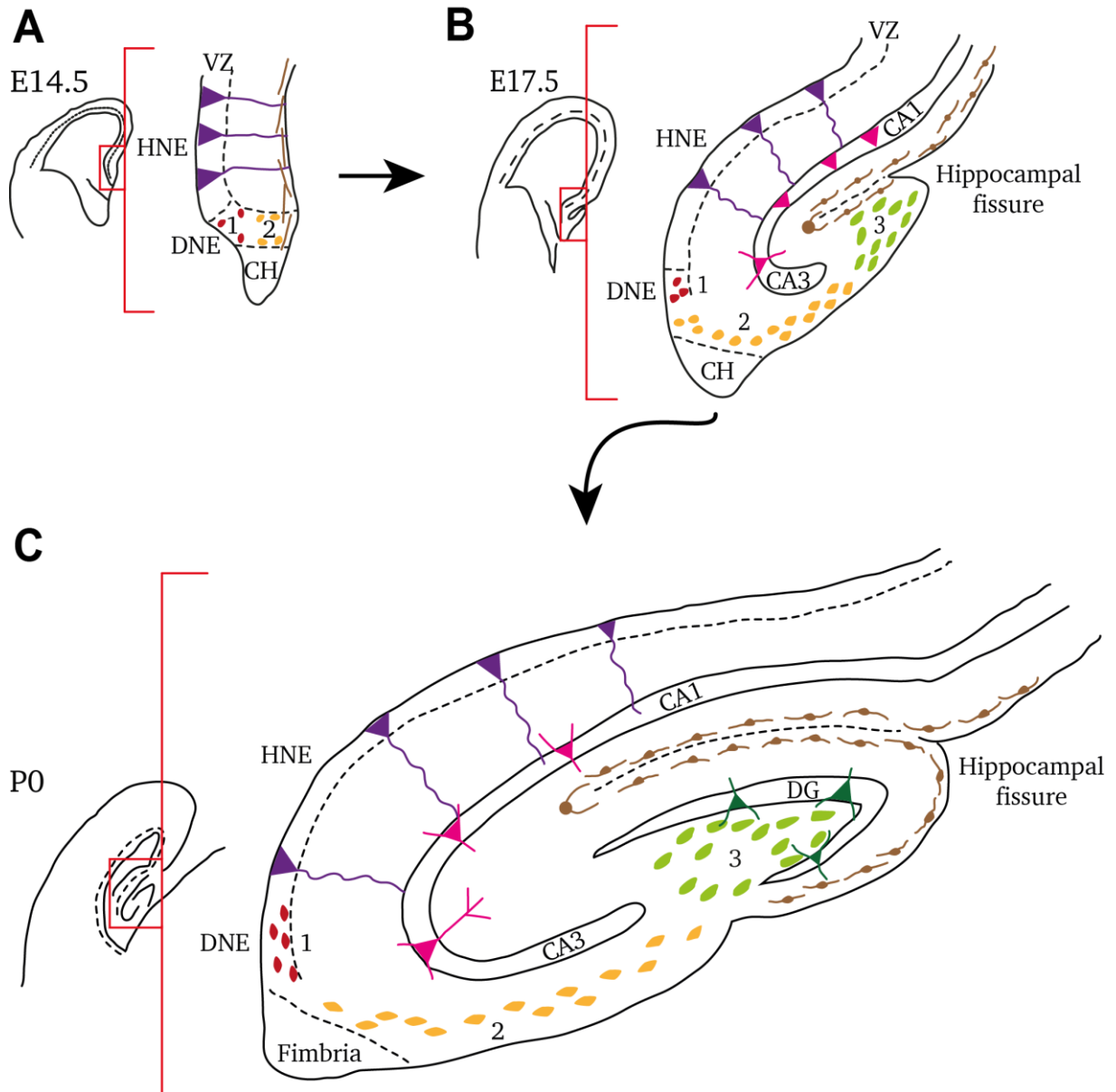


Figure 4-1: Stages of hippocampal development in the dorsal telencephalon of the mouse. (A) E14.5: Precursor cells of the future dentate gyrus (red ovals) are found in the VZ where they settle in the prospective DNE and form the primary matrix (1). Here, precursors spread out and migrate in direction of the pial surface of the cortex (yellow ovals), establishing the secondary matrix (2). Radial glial progenitors in the VZ of the HNE (violet triangles) are going to generate cells of the future hippocampus proper. Cajal-Retzius cells, generated by the CH, line the pial surface of the cortex (B) E17.5: Dentate precursor cells migrate further (light green ovals) and accumulate at the hippocampal fissure, establishing the tertiary matrix (3). The Cajal-Retzius cells align with the structural formation of the hippocampal fissure. A glial scaffold (not depicted) between CH and hippocampal fissure determines the route of migration. Hippocampal cells (magenta triangles), derived from the HNE, migrate along radial glial fibers and settle in the subfields of the cornu ammonis. (C) P0: The typical blade form of the DG becomes apparent. Dentate granule cells (dark green triangles) first occupy the upper blade and then the lower blade. The shaping of the DG is induced by positioning signals from the Cajal-Retzius cells that settle around the DG. The primary and secondary matrix will lose their proliferative potential, in contrast to cells in the tertiary matrix that continue to generate granule cells during postnatal development. Within two weeks after birth, neurogenesis in the DG becomes restricted to the subgranular zone. VZ = ventricular zone, HNE = hippocampal neuroepithelium, DNE = dentate neuroepithelium, CH = cortical hem, 1 = primary matrix, 2 = secondary matrix, 3 = tertiary matrix, CA = cornu ammonis, DG = dentate gyrus. (modified according to Urbán and Guillemot 2014).

On their further way, the progenitor cells form a new migratory population called the secondary matrix while simultaneously glial scaffolding starts. This, together with Cajal-Retzius cells, has crucial functions in the organization of progenitor and dentate granule cells (Urban & Guillemot, 2014). A proliferative tertiary matrix is formed when the progenitor cells arrive and accumulate in the hippocampal fissure around E17.5. Subsequently, the granule cell layer is built up and adapts its final shape to the surrounding Cajal-Retzius cells that secrete reelin, acting as a positioning signal. In early postnatal life, the tertiary matrix remains the only source of dentate progenitors and granule cells (Frotscher, 1998; Li et al., 2009; Nelson et al., 2020; Urban & Guillemot, 2014).

4.2.3 Anatomy of the Hippocampal Circuitry

The network of brain areas which is referred to as hippocampal formation, consists of entorhinal cortex (EC, lateral and medial), hippocampus (dentate gyrus (DG) + hippocampus proper (CA3, CA2, CA1)), subiculum (Sub), presubiculum (PreSub) and parasubiculum (ParaSub) as shown in Figure 4-2.

Generally, mammals display a very similar conserved basic layout of cells and corresponding projections within the pathways of the hippocampal formation (West, 1990; Witter et al., 1989). The hippocampus receives neocortical information from the superficial layers of the EC which displays the most important glutamatergic input to this area. The input information is processed by several parallel circuits within the hippocampus (Hartley et al., 2014; van Strien et al., 2009). The deep layers of the EC and the Sub provide the information deriving from pyramidal cells in the hippocampal CA1 subfield to the rest of the brain, thus representing the major output zone (Hartley et al., 2014; van Strien et al., 2009).

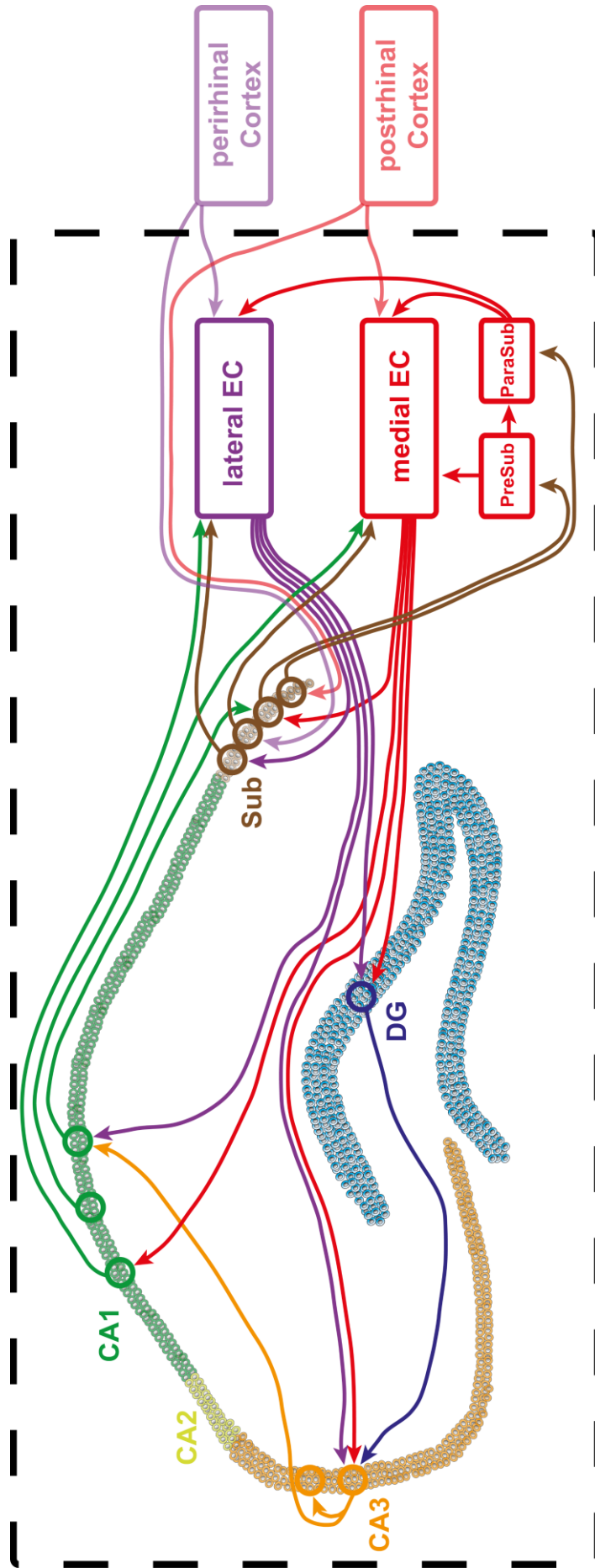


Figure 4-2: Schematic overview about the hippocampal network. The classical trisynaptic pathway is formed by projections from both the lateral and medial EC to the DG (perforant pathway), from there to the CA3 subfield (mossy fiber pathway) and further to the CA1 area (Schaffer collateral pathway). Projections from CA1 to the Sub and to the lateral and medial EC as well as from the Sub to the lateral and medial EC complete the circuit. There is also a direct monosynaptic input from the lateral and medial EC to CA3, CA1 and the Sub. Further circuits consist of CA3 recurrent collaterals and projections from the Sub to the PreSub and to the ParaSub. The PreSub projects to the ParaSub and the medial EC, while the ParaSub forms projections to both the medial and the lateral EC. Both perirhinal and postrhinal cortices project to the Sub. Furthermore, the perirhinal cortex projects to the lateral EC and the postrhinal cortex projects to the medial EC. The perirhinal cortex is involved in object processing while the postrhinal cortex is involved in visuo-spatial processing. Colored arrows delineate the projections. Projections from CA2 are not shown for simplicity. The hippocampal formation is highlighted by the dashed box. EC = entorhinal cortex, DG = dentate gyrus, CA = cornu ammonis, Sub = subiculum, PreSub = presubiculum, ParaSub = parasubiculum (modified according to Hartley et al., 2014).

There are two classical excitatory pathways by which information is transferred from the superficial layers of the EC to CA1. First, there is the indirect trisynaptic circuit, originating in EC layer II. In a first step, stellate cells project excitatory input to the dendritic tree of granule cells in the molecular layer (stratum moleculare) of the DG (perforant pathway). In a second step, the granule cells themselves project further to CA3 where they excite the local pyramidal cells (mossy fiber pathway). Granule cells within the DG represent the first stage that processes EC input to the hippocampal circuitry (Amaral et al., 2007; Basu & Siegelbaum, 2015; van Strien et al., 2009). This cell population interacts with excitatory mossy fiber cells, located in the hilus region and with GABAergic interneurons (Amaral & Lavenex, 2007, Hippocampus Book). Furthermore, the DG is involved in the process of pattern separation that accomplishes the transformation of similar into non-overlapping representations or memories (Bakker et al., 2008; Knierim & Neunuebel, 2016; McHugh et al., 2007). Forming distinguishable representations of multiple contexts, places or episodes is essential for hippocampal function.

An important anatomical feature of the CA3 subregion are projections of local pyramidal cells to other CA3 pyramidal cells. These so-called recurrent collaterals play a significant role in pattern completion. This process is characterized by the ability to use fragmentary information (subset of cues associated with an event) to fully retrieve complete memories about an original event (Marr, 1971; Nakazawa et al., 2002; Rolls, 2013). In a next step of the trisynaptic circuit, the pyramidal cells of CA3 form excitatory synapses on proximal regions of CA1 pyramidal cell apical dendrites in a layer called stratum radiatum via the Schaffer collateral pathway (Basu & Siegelbaum, 2015). Besides this indirect pathway, there are also direct projections from layer III of the EC that form synapses with CA1 pyramidal cells through the temporoammonic pathway (Basu & Siegelbaum, 2015). Contrary to the indirect route, projections through the temporoammonic pathway target CA1 neurons on more distal areas of the apical dendrites that are located in a layer called stratum lacunosum moleculare (Basu & Siegelbaum, 2015; Kajiwara et al., 2008). This double input mechanism via two pathways projecting directly or indirectly to different dendritic regions on common target pyramidal cells, may provide the hippocampal system with a comparative function (E. Moser & Paulsen, 2001; Nakazawa et al., 2003; O'Keefe & Nadel, 1978).

Besides those classical input pathways, CA1 pyramidal cells additionally receive excitatory input in parallel from the CA2 subregion of the hippocampus, a small region between CA3 and CA1 (Chevalyere & Siegelbaum, 2010). On the one hand, neurons in layer II of the EC directly project to pyramidal cells within CA2, forming synapses with distal CA2 dendrites (Cui et al., 2013; Hitti & Siegelbaum, 2014). On the other hand, CA2 pyramidal cells receive indirect EC input through either granule cells within the DG or via CA3 projections onto their proximal dendrites (Chevalyere & Siegelbaum, 2010; Kohara et al., 2014).

While the EC plays a fundamental role for input of neocortical information to the hippocampal circuitry and thus for memory processes, there are also many subcortical inputs that are vital for spatial memory and representation. One example are head direction cells found in the anterior thalamus which has strong projections to the hippocampal network (Taube, 1995, 1998). Furthermore, there are also interesting subcortical outputs from the hippocampal formation. An example of this is a projection from the CA3 subregion to the ventral tegmental area via the lateral septum that regulates associations between reward and spatial contexts (Luo et al., 2011).

It is important to note that a highly interconnected region in the basal forebrain containing the medial septum and the diagonal band of Broca projects to all regions of the hippocampal formation (Fuhrmann et al., 2015; Swanson & Cowan, 1979). These connections contribute fundamentally to the generation and the shaping of high amplitude 4-12 Hz Theta oscillations, observed when animals move and explore (Buzsáki et al., 1983; Hartley et al., 2014; Vanderwolf, 1969). This Theta rhythm is tightly linked to the hippocampal network and may be crucial for signaling of environmental novelty (Jeewajee et al., 2008), coordination of memory encoding and retrieval (Douchamps et al., 2013; Hasselmo et al., 2002) as well as representation of space (Burgess & O'Keefe, 2011; O'Keefe & Recce, 1993).

4.2.4 The Dentate Gyrus – Adult Hippocampal Neurogenesis

Several decades ago, in 1965, Altman and Das were the first who reported on neurogenesis in the dentate gyrus of the hippocampal formation of adult rodents. The discovery that the adult mammalian brain is capable of generating new neurons throughout life superseded the long-held view that a process like neurogenesis could be present in the adult brain (Altman & Das, 1965). The idea that new nerve cells are permanently added in specific neurogenic niches of the adult brain throughout life is now generally accepted and outlines a mechanism with important functions in learning and memory processes and a role in the regulation of emotional status (Akers et al., 2014; Clelland et al., 2009; Deng et al., 2010, 2009; Encinas et al., 2006; Garthe & Kempermann, 2013; Gonçalves et al., 2016; Shors et al., 2001; Spalding et al., 2013; Zhao et al., 2008).

The subventricular zone (SVZ) and the subgranular zone (SGZ) within the hippocampal dentate gyrus (DG) represent two of these neurogenic niches (Götz & Huttner, 2005; Ming & Song, 2011; Paridaen & Huttner, 2014). New neurons generated by the SVZ migrate through the rostral migratory stream (RMS) to the olfactory bulb where they become interneurons (Gage, 2000; Ming & Song, 2011). In contrast to that, the SGZ harbors a pool of neural stem (NSCs) and progenitor cells (NPCs) designated to generate future granule cells which will integrate into the DG and thus contribute to the hippocampal circuitry (Altman & Das, 1965; Gage, 2000; Spalding et al., 2013; Urban & Guillemot, 2014). With regard to the molecular and cellular mechanisms of neurogenesis, several reports indicate that both the adult and the developing brain share many properties, even if there are key differences as well (Esposito, 2005; Götz et al., 2016; Ming & Song, 2011; Nacher et al., 2005; Song et al., 2005). For example, embryonic and adult neurogenesis share several regulators of transcription, such as Pax6, Gsx2 and Dlx (Brill et al., 2008; Hack et al., 2005; Kohwi et al., 2005; López-Juárez et al., 2013; Ninkovic et al., 2013) or the basic helix-loop-helix transcription factors *Ascl1*, *Ngn2*, and *Neurod1* (Andersen et al., 2014; Brill et al., 2009; E. Kim et al., 2007; Parras et al., 2004; Roybon et al., 2009). However, several studies also demonstrated that the mode of their molecular function in the developing and adult brain vary (Andersen et al., 2014; López-Juárez et al., 2013; Ninkovic et al., 2013; Urban & Guillemot, 2014; Walcher et al., 2013).

The subgranular zone (SGZ; Figure 4-3) of the hippocampal DG is situated between the granule cell layer and the hilus region and simultaneously provides the microenvironment for proliferation of NSCs and the differentiation of intermediate precursors into mature dentate granule cells. Newly generated dentate granule cells in the adult brain become functionally integrated into the hippocampal network after running through a sequence of maturation stages, taking approximately 4-7 weeks (Ehninger & Kempermann, 2008; Gonçalves et al., 2016; Hodge & Hevner, 2011; van Praag et al., 2002). The pool containing cells that potentially become recruited and exit the cell cycle expands at the precursor stage. However, the majority of those newly generated cells undergoes apoptosis, while 10 % to 50 % of them persist and functionally integrate into the existing hippocampal network. This process involves the building of synaptic connections, projecting axons through the mossy fiber tract and adopting the electrophysiological properties of mature granule cells (Hastings & Gould, 1999; Stanfield & Trice, 1988; van Praag et al., 2002; Zhao et al., 2006). As the hippocampus plays an outstanding role for learning and memory, the generation of new neurons in the dentate gyrus during adulthood likely contributes to this cognitive process. Fully integrated dentate granule cells can survive for months or even a whole life (Garthe & Kempermann, 2013). The different cell maturation stages can be distinguished by expression of specific markers and changing morphologies and allow the categorization into different cell types (Figure 4-3).

Type-1 cells (Figure 4-3) are neural stem or primary progenitor cells with self-renewing and multipotent properties that display glial-like morphological and functional characteristics and produce neurons and glia (Ehninger & Kempermann, 2008; Hodge & Hevner, 2011; Kempermann et al., 2004). Two type-1 subpopulations can be distinguished, namely active and quiescent type-1 cells (Hodge & Hevner, 2011; Lugert et al., 2010). The quiescent subtype which makes up small part of the dividing subgranular cells is characterized by a radial morphology and a triangular shape of the soma. A long radial process originates from the soma and extends through the dentate granular layer to the molecular layer where it forms several shorter processes (Hodge & Hevner, 2011; Kempermann et al., 2004; Lugert et al., 2010). The rarely dividing quiescent type-1 cells further display a characteristic expression pattern, consisting of the glial cell marker GFAP, the neural progenitor marker Nestin and the stem cell

protein Sox2 (Encinas et al., 2006; Seri et al., 2004; Steiner et al., 2006; Suh et al., 2007).

The active type-1 cell subtype differs from the quiescent form by a horizontal morphology with short processes, but displays a similar expression pattern. These cells divide at higher rates and represent a greater fraction of dividing cells within the adult DG (Encinas et al., 2006; Lugert et al., 2010; Suh et al., 2007). Emanating from type-1 cells, further development progresses over at least two stages of intermediate progenitor cells (IPCs), namely type-2 (a and b) and type-3 neuroblasts (Gonçalves et al., 2016; Hodge & Hevner, 2011; Kempermann et al., 2004).

Type-2 cells (Figure 4-3) exhibit transient amplifying characteristics and are responsible for the bulk of the cell pool expansion and the production of type-3 cells (Ehninger & Kempermann, 2008; Kempermann et al., 2015). They have short, horizontal but no radial processes, a small soma and can be further subdivided into type-2a and type-2b which show overlapping expression of different markers (Ehninger & Kempermann, 2008; Gonçalves et al., 2016; Hodge & Hevner, 2011). Type-2a IPCs are positive for Nestin and Sox2 but not for DCX and represent the more immature subtype (Ehninger & Kempermann, 2008; Hodge & Hevner, 2011; Steiner et al., 2006). In addition to Nestin, type-2b IPCs express the microtubule-associated DCX which is a first sign of their neuronal commitment (Brandt et al., 2003; J. Brown et al., 2003; Hodge & Hevner, 2011).

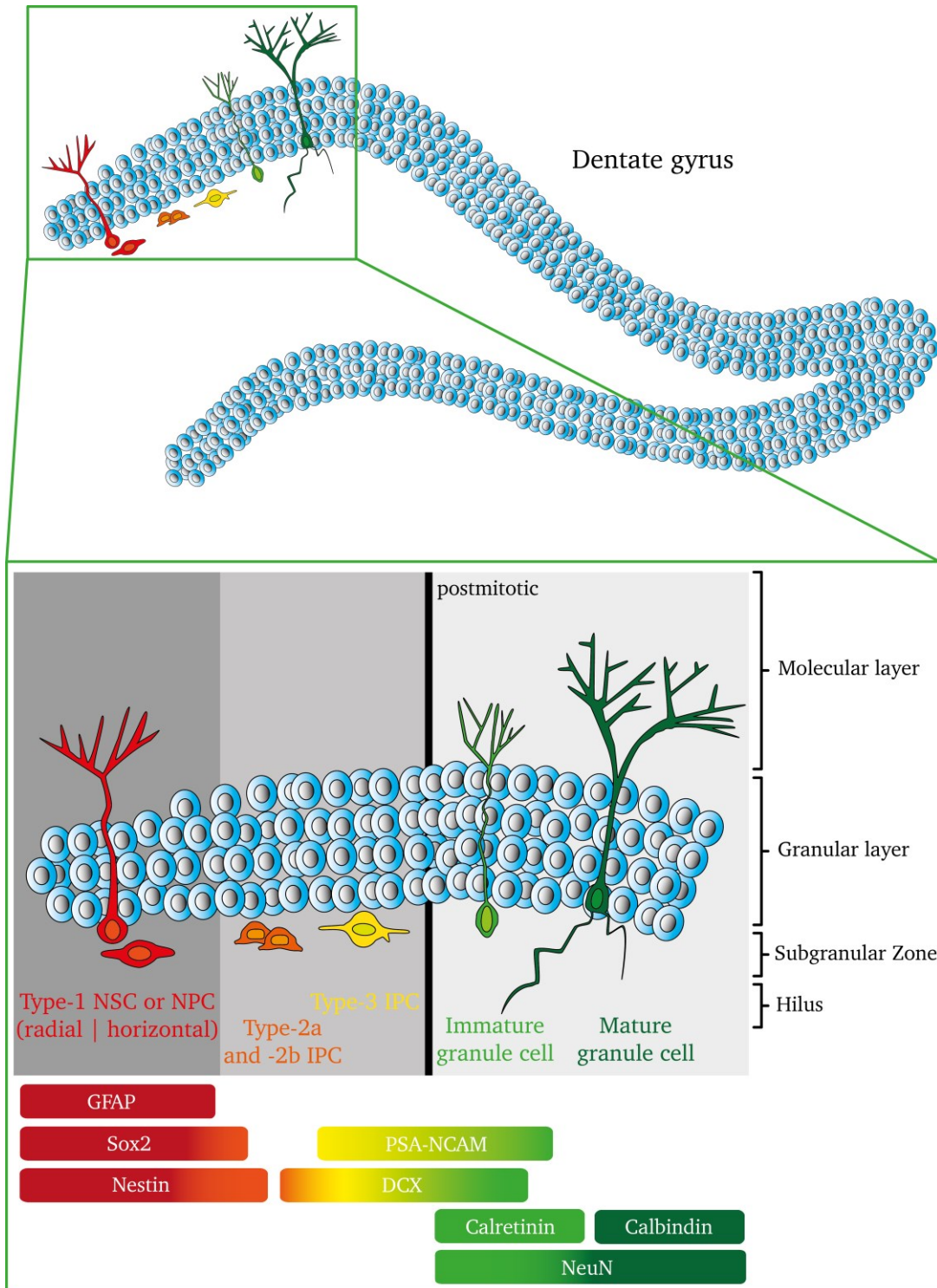


Figure 4-3: Adult hippocampal neurogenesis in the subgranular zone of the dentate gyrus. Schematic illustration of neural progenitor cell development and maturation. The subgranular zone (SGZ) of the dentate gyrus (DG) is situated between the granular cell layer and the hilus. The SGZ harbors a pool of type-1 neural stem (NSC)/progenitor cells (NPC) which are designated to produce intermediate progenitor cells (IPCs). At least two stages of IPCs, namely type-2 (a and b) and type-3 (neuroblasts) go through several rounds of cell division and maturation to produce future postmitotic granule cells which will integrate into the DG and thus contribute to the function of the hippocampal circuitry.

Type-3 cells or neuroblasts (Figure 4-3) remain mitotically active and are characterized by lack of Nestin expression (Hodge & Hevner, 2011). This cell stage represents the transition to the postmitotic immature granule cell. Therefore, type-3 cells are morphologically diverse, displaying differences in the complexity of their processes and their orientation (Ehninger & Kempermann, 2008). The characteristic simultaneous expression of DCX and PSA-NCAM starts with the neuroblast stage and persists up to the first two to three weeks of postmitotic maturation (Brandt et al., 2003; Couillard-Despres et al., 2005; Plümpe et al., 2006; Rao & Shetty, 2004). The DCX expression pattern also highlights the migratory phenotype of type-3 neuroblasts which settle down in the granular layer where they finally differ into postmitotic immature dentate granule cells (Ehninger & Kempermann, 2008; Hodge & Hevner, 2011; Kempermann et al., 2004).

Postmitotic immature granule cells (Figure 4-3) are characterized by the transient expression of the calcium binding protein Calretinin and the upregulation of NeuN expression that marks postmitotic neuronal nuclei (Ehninger & Kempermann, 2008; Hodge & Hevner, 2011; Kempermann et al., 2004). The expression of Calretinin continues for approximately two weeks until it is exchanged for Calbindin in mature granule cells (Figure 4-3) (Ehninger & Kempermann, 2008; Hodge & Hevner, 2011).

Most of the early postmitotic granule cells are eliminated by apoptosis which occurs within these first two weeks at the stage of simultaneous DCX and Calretinin expression (Biebl et al., 2000; Ehninger & Kempermann, 2008; Kuhn et al., 2005). The survival of maturing granule cells is mediated by the activation of NMDA (N-methyl-D-aspartate) receptors (Tashiro et al., 2006). The gradual addition of newly generated granule cells results in overall growth of the dentate gyrus over time (Crespo et al., 1986). However, growth of the structure is thought to take place to a large extent in the first year of rodent life (Altman & Das, 1965; Bayer et al., 1982). A recent study revealed that neurogenesis sharply declines between 1.5 and 3 months of age in mice and then continues to decline constantly (Gil-Mohapel et al., 2013).

During the immature granule cell stage, development and refinement of the dendritic trees and axonal outgrowth towards the CA3 subfield take place simultaneously, but axons reach their targets before the synaptic contacts on the dendritic tree are formed (Ehninger & Kempermann, 2008; Zhao et al., 2006). Studies report that immature granule cells extend axons into CA3 very rapidly and that axonal contact is established

already within 4 to 11 days after their generation (Hastings & Gould, 1999; Markakis & Gage, 1999; Zhao et al., 2006), leading to the conclusion that these cells could influence normal hippocampal function despite their immature stage. In contrast, dendritic spines first appear approximately one week afterwards and continue to be formed over a period of months (Zhao et al., 2006). New dentate granule cells receive full excitatory input about two months following cell division (Toni et al., 2007).

4.2.5 Navigation, Spatial Cells and Cognitive Maps

The hippocampal formation plays important roles for different forms of memory. Thus, it is crucial for declarative memories (semantic and episodic) and navigational learning (Buzsáki & Moser, 2013; Neves et al., 2008; O'Keefe & Nadel, 1978; Scoville & Milner, 1957; Squire et al., 2004). Theta oscillations describe a coordinated interaction of cells in the hippocampal network and are thought to provide the basis for these kinds of memory functions by evoking spike timing-dependent plasticity (Dragoi & Buzsáki, 2006; Foster & Wilson, 2007; Gupta et al., 2012; Hebb, 1949).

The ability to navigate in environments is critical to the survival of several species. Navigation through environments requires that animals memorize locations and routes. Thus, the ability to navigate through space and form spatial memories, highly depends on the accurate formation of environmental representations of past, present and future locations (Buzsáki & Moser, 2013). These are thought to be deposited in the hippocampus in form of cognitive maps which provide a remarkable flexibility.

However, it should also be mentioned that navigation can depend on the dynamic interaction of the hippocampus and other brain regions like the striatum. The striatum participates in the circuitry regulating reward and addiction. It is connected to the hippocampus, the amygdala, and the thalamus from where it receives glutamatergic input and to the ventral tegmental area and the substantia nigra that send dopaminergic inputs to the striatum (Goodroe et al., 2018; Haber & Knutson, 2010; Yager et al., 2015). Furthermore, it plays a role in keeping decisions and responses flexible by interacting with regions involved in memory, emotion and cognitive processing (T. Brown et al., 2012; Ferbinteanu & McDonald, 2000; Haber & Knutson, 2010; Scimeca & Badre, 2012; Yager et al., 2015). Thus, the striatum is thought to provide response-learning strategies and procedural memory that can automatically be used by following

familiar routes during spatial navigation. (Goodroe et al., 2018; Hartley et al., 2003; Iaria et al., 2003; Packard & McGaugh, 1996).

Generally, two intertwined types of navigation can be distinguished (Buzsáki & Moser, 2013; Mcnaughton et al., 1996; O'Keefe & Nadel, 1978). On the one hand, allocentric navigation (map-based spatial navigation) relies on the use of external distant visual cues (landmarks) that provide information about where the animal is in relation to other landmarks. The spatial metric used to evaluate the distances between such landmarks probably results from an alternative mechanism called egocentric navigation or path integration (Buzsáki & Moser, 2013). During egocentric navigation animals make use of internal cues like feedback after movements to assess speed, direction or sequential turns as well as closer signposts that mark locations where the animal has to change direction to continue its path. Thus, egocentric navigation is based on the calculation of coordinates by integrating motion and knowledge of previous positions (Buzsáki & Moser, 2013; Mcnaughton et al., 1996; O'Keefe & Nadel, 1978; Rogers et al., 2017; Vorhees & Williams, 2014). Interestingly, egocentric navigation also functions when animals navigate in darkness, showing that this type of navigation does not necessarily depend on visual cues compared to allocentric navigation (Moghaddam & Bures, 1996; Vorhees & Williams, 2014). Map-based allocentric and path integration-based egocentric mechanisms always interoperate, however, the availability of external landmarks probably determines which of them is used as the prevailing strategy (Buzsáki & Moser, 2013).

The hippocampal network and its pathways contain specialized cell types that play fundamental roles in navigation and that function as a neural positioning system, a kind of GPS within the brain. Edward Tolman's famous publication (Tolman, 1948) first proposed the idea of a cognitive map which provides the basis for the respective memory representations that underlie navigation through space. The discovery of place cells in 1971 by O'Keefe and Dostrovsky (O'Keefe & Dostrovsky, 1971) should lead to the link between hippocampal function and the development of cognitive maps that was discussed and substantiated by O'Keefe and Nadel a few years later (O'Keefe & Nadel, 1978). Subsequent studies highlighted further types of neurons that are involved in spatial coding and constantly interact with the hippocampus, namely grid cells in the medial entorhinal cortex (Fyhn et al., 2008; Hafting et al., 2005), head direction cells

(Sargolini et al., 2006; Taube et al., 1990) and neurons responding to borders (Solstad et al., 2008). All these cells are thought to constitute the main units of the GPS-like neural positioning system in the brain.

Place Cells

Place cells can be found in the hippocampus proper and the DG. They display a characteristic baseline with low firing rates. However, each cell has its own specifically increased firing pattern when the animal enters a defined area in the environment, corresponding to its place field (Hartley et al., 2014). Thus, different place cells have different firing locations or place fields (O'Keefe, 1976). Place fields of neighboring cells are no more similar than those of cells that are far apart from each other, leading to the assumption that place is mapped in a non-topographical manner (O'Keefe, 1976; Wilson & McNaughton, 1993). Place fields differ in size, dependent on the site of recording. Place cells recorded more dorsally have smaller fields compared to cells recorded more ventrally (Jung et al., 1994; Kjelstrup et al., 2008).

Interestingly, the location of an animal in an environment can be determined quite exactly by place field recordings, as it is possible to differ between place cells recorded at the same time and as each location is represented by a small subset of place cells that show strong firing (O'Keefe & Dostrovsky, 1971; Wilson & McNaughton, 1993; Zhang et al., 1998).

The specific spatial firing pattern and the place field, respectively, can be delineated by color-coded firing rate maps showing the mean firing rate for each area of the environment (Figure 4-4).

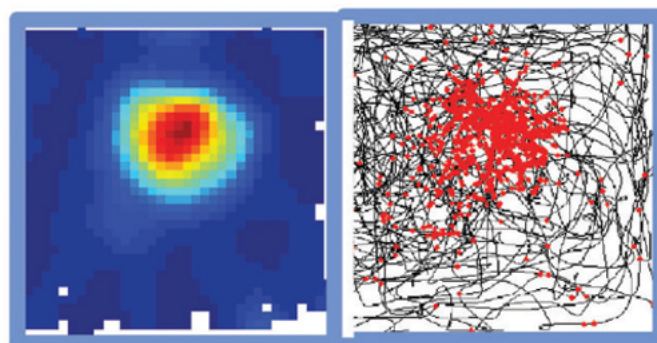


Figure 4-4: Place cell. Color-coded firing rate map on the left with red showing high activity and blue showing low activity. Tracked path (black) on the right with plotted locations (red) at which spikes were recorded (modified according to Moser et al., 2015).

The firing pattern of a specific place cell appears very stable when recorded during multiple trials in the same environment. However, if the environment differs or if the animal gets adequately experienced with an environment, distinct firing patterns and subsets of place cells will occur (Bostock et al., 1991; Kentros et al., 1998; Knierim, 2002; Leutgeb et al., 2004; Lever et al., 2002; Muller & Kubie, 1987; Sharp, 1997). O'Keefe and Conway could further show that even removal of individual cues does not particularly change place field specifications, showing that there are differences in the importance of the available cues (O'Keefe & Conway, 1978). Moreover, place cells definitely respond to changes in context or environmental factors, like colors or odors (Anderson & Jeffery, 2003). Typically, place fields can be recorded from the first exposure to a new environment within minutes and develop independently of a specific mode of behaviour (Bostock et al., 1991; Hartley et al., 2014; Wilson & McNaughton, 1993). However, in what way spatial selectivity of place field activity is formed with experience during learning of an environment is not entirely clear. Recent studies give evidence for a competitive learning model of the DG as a possible mechanism that enables both formation of single place fields and persistent spatial mapping by granule cells (S. Kim et al., 2020; Rolls et al., 2006; Si & Treves, 2009).

Grid Cells

The medial EC was the first site where grid cells have been identified. Since then, grid cells have also been found in the PreSub and ParaSub (Boccaro et al., 2010; Buzsáki & Moser, 2013). Similar to place cells, grid cells display defined firing locations in an environment, however, they also show multiple firing fields of similar amplitude that are characterized by a remarkably regular triangular or hexagonal grid structure as shown in Figure 4-5 (Hafting et al., 2005; M. Moser et al., 2015).

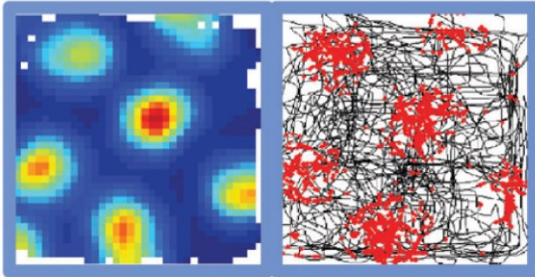
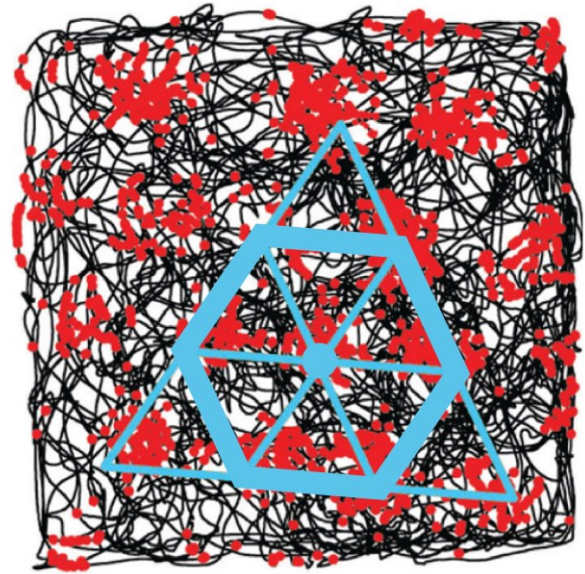
A**B**

Figure 4-5: Grid cell. (A) Color-coded firing rate map on the left with red showing high activity and blue showing low activity. Tracked path (black) on the right with plotted locations (red) at which spikes were recorded. (B) Equilateral triangles (blue) illustrating the regular triangular or hexagonal structure of the grid pattern (modified according to Moser et al., 2015).

Hafting et al. report that the geometric structure displayed a constant scale that was determined by the distance from the central grid field peak to the nearest six equidistant peaks, forming an inner hexagon. The vertices of this hexagon were separated by 60 degree angles, leading to an equilateral triangle as a basic grid unit. Besides the distance between grid fields (spacing), the grid was characterized by its orientation in relation to an external reference axis and its phase. The latter one describes a two-dimensional shift relative to an external reference point (E. Moser et al., 2008). Interestingly, the grid structure was preserved when the size of available environment was expanded. Thus, the spacing of the grid was not confined by the external boundaries (Hafting et al., 2005). When they compared different grid fields at nearby recording locations, similarities in terms of spacing, orientation and field size became apparent. Despite that, the grid phase seemed to vary randomly among cells at the same recording location. They suggested that the entire surface of the environment could be represented by a local subset of cells with common grid spacing and orientation and that the spatial map in the EC was organized in local modules (Hafting et al., 2005).

The comparison between more ventral and more dorsal recording locations revealed systematic variations in grid field properties. Grid fields recorded from cells in more dorsal portions of the medial EC were smaller and denser, whereas grid fields recorded from more ventral parts of the medial EC were larger with increased spacing. Even if

the site of recording also influenced the grid orientation, a systematic change from dorsal to ventral medial EC could not be demonstrated for this parameter. Thus, spacing of the grids was organized in a topographical manner from the dorsal to the ventral medial EC (Brun et al., 2008; Fyhn et al., 2008, 2004; Hafting et al., 2005; Hartley et al., 2014). However, it was still questionable how grid scale is distributed in animals, even if evidence for a clustering of grid cells and a modular organization came from another study (Barry et al., 2007). Stensola et al. could finally show that the grid map is indeed based on a combination of sub-maps or modules and that grid scale is progressed in clear steps rather than as a continuum (Stensola et al., 2012).

Grid cells function as a metric for space. Thus, the spatial information that can be extracted theoretically from these cells is first, the animal's position within an environment and second, its distance relative to a reference point (Fiete et al., 2008). However, it is still unclear how effectively this information can be used by downstream target cells (Rowland et al., 2016).

Boundary (Border) Cells and Head Direction Cells

Additional cell types in the entorhinal cortex involved in the GPS-like neural positioning system are boundary (border) cells (Figure 4-6 A) and head direction cells (Figure 4-6 B).

Head direction cells were first discovered in the dorsal PreSub (= postsubiculum) by Ranck in 1984 (Taube et al., 1990). Since then, they also have been found in other areas of the brain, such as the anterior dorsal thalamic nucleus (Taube, 1995), entorhinal cortex (Sargolini et al., 2006), dorsal striatum (Mizumori et al., 2000; Wiener, 1993), as well as in smaller numbers in several other areas like the CA1 subregion of the hippocampus proper (Leutgeb et al., 2000).

Boundary or border cells are found in the medial EC, the subiculum, PreSub and ParaSub. They exclusively fire along geometric borders within an environment, including walls and along the edges of elevated open platforms (Hartley et al., 2014; E. Moser et al., 2017; Solstad et al., 2008). These cells may have a role in the calculation of allocentric distances by triangulation and in fitting the grid size to the specific environment (Butler et al., 2017; Buzsáki & Moser, 2013; Calton et al., 2003; Fyhn et al., 2008, 2004; Hafting et al., 2005; O'Keefe & Dostrovsky, 1971; O'Keefe & Nadel, 1978; Solstad et al., 2008; Taube et al., 1990).

A head direction cell increases its firing rate specifically when the animal is heading in a single direction of the horizontal plane, whereas it does not respond to other directions. The direction at which a head direction cell has its firing peak is defined as its preferred firing direction which is independent of the animal's current location (Hartley et al., 2014; Taube, 2007). The entire directional range is displayed in such a way that firing of a subset of head direction cell is triggered at any time (Hartley et al., 2014). The firing of a head direction cell can be expressed as a polar plot (Knierim et al., 1995) of head direction in the horizontal plane and firing rate, displaying the preferred direction of spiking. Firing of head direction cells may play important roles for the spatial tuning of grid cells and place cells and thus provides animals with an internal neural compass due to their directional representation (Calton et al., 2003; Taube, 2007; Winter et al., 2015).

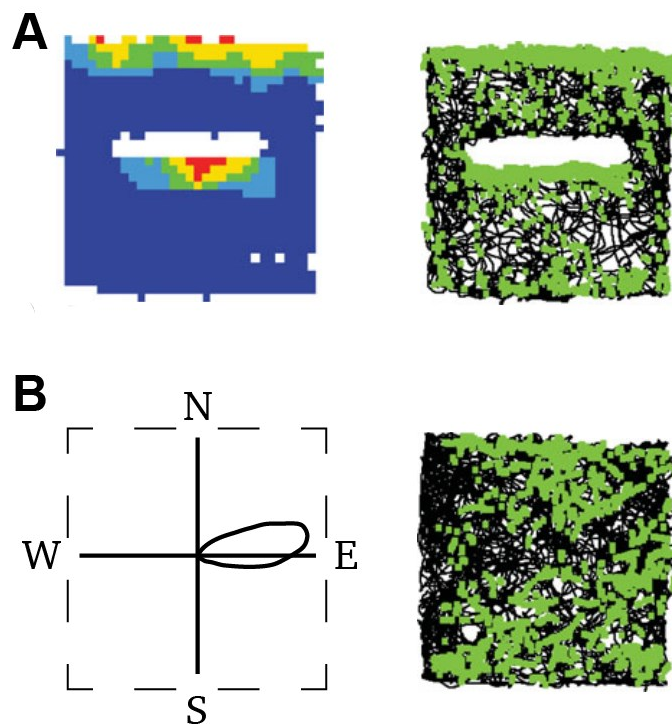


Figure 4-6: Border cells and head direction cells. (A) **Border cell:** On the left, color-coded firing rate map with red showing high activity and blue showing low activity. On the right, travel path taken over a testing period in black with the locations where firing activity was recorded plotted as an overlay in green. (B) **Head direction cell:** On the left, directional firing polar plot of head direction cell when the animal faces North-East. On the right, travel path taken over a testing period in black with the locations where firing activity was recorded plotted as an overlay in green (modified according to Hartley et al. 2014).

In contrast to place cells that exhibit varying firing patterns dependent on the specific environment (Muller & Kubie, 1987), grid cells, head direction cells and border cells display interrelated firing activities in any environment (Solstad et al., 2008). Thus, this combination of cells provides an overarching metric system that is universally usable independent of the environment (Hafting et al., 2005; McNaughton et al., 2006; E. Moser et al., 2008).

5 Purpose

This PhD project aimed at understanding the effects of low-dose ionizing radiation (LDIR, defined here as ≤ 0.5 Gy) exposure on cognitive abilities during pre- and postnatal brain development (E14.5, P10) and its influence in the young adult mouse (2 months of age).

Therefore, a set of behavioural tests for motor function (Rotarod), anxiety/exploration behaviour (Elevated-Zero-Maze) and spatial learning (Morris Water Maze) was established and used to analyze the long- and short-term effects of LDIR on cognitive performance. Furthermore, the progenitor cell pool within the dentate gyrus was immunohistologically analyzed after application of LDIR. Here, the focus was on quantification of DCX⁺ neural progenitor cells in the neurogenic niche of the dentate gyrus.

Understanding the consequences of LDIR on the organism is not only interesting for academic reasons, it is rather important to estimate the radiation risk for individuals and the population, as radiation induced cognitive deficiencies constitute both personal and socially relevant drawbacks. Especially, the impairment of mental functions potentially occurs after LDIR, an issue of great social relevance. In regard of radiation protection, it is important to estimate consequences of LDIR on the developing fetus and the developing brain as well as during learning processes. Understanding the impact of LDIR on specific phases of brain development and maturation can shed light on the LDIR sensitivity of the neurogenic milieu and help to prevent radiation induced cognitive deficits.

6 Material

6.1 Chemicals and Reagents

<i>Name</i>	<i>Provider</i>
Acetic acid	Sigma-Aldrich
Chromium(III) potassium sulfate dodecahydrate, $\text{KCr}(\text{SO}_4)_2 \times 12 \text{H}_2\text{O}$	Carl Roth
Citric acid monohydrate, $\text{C}_6\text{H}_8\text{O}_7 \times \text{H}_2\text{O}$	VWR International
Cresyl violet	Sigma-Aldrich
Hoechst 33342, 200 $\mu\text{g}/\text{mL}$	Sigma-Aldrich
iso-Pentane	VWR International
Paraformaldehyde	Sigma-Aldrich
Potassium disulfite	Sigma-Aldrich
Roti [®] -ImmunoBlock, 10x	Carl Roth
Roti [®] -Mount FluorCare	Carl Roth
Sodium acetate	Sigma-Aldrich
Sodium citrate dihydrate, $\text{C}_6\text{H}_5\text{O}_7 \times 2 \text{H}_2\text{O}$	Sigma-Aldrich
Sodium hydroxide pellets	Merck
Sucrose	Sigma-Aldrich
Triton [®] X-100	Sigma-Aldrich

6.2 Consumable Material

<i>Name</i>	<i>Provider</i>
Bacillol [®] AF	BODE Chemie
Centrifuge tubes, 15/50 mL	STARLAB
CoverGrip [™] Coverslip Sealant	Biotium
Coverslips, 24 x 60 mm, #1	Carl Roth
Dissecting set	Fine Science Tools
ecoSHIELD [™] Eco Nitrile PF 250, Category III	SHIELD Scientific
Entellan [®]	Merck
Ethanol	Carl Roth
Ever-Sharp-Blades	Apollo Herkenrath
Folded Filters 595 ½, Ø 270 mm	Schleicher & Schuell
Gelatin	Merck
Gouache Tempera paint, white	LEFRANC & BOURGEOIS
Infrared Basking Spot	Philips
Kimtech Science [*] Precision wipes	Kimberly-Clark
Microscope slides	Carl Roth
Parafilm [®]	VWR International
Phosphate buffered saline, 10x	Sigma-Aldrich
Scalpel handle and Sterile Surgical Blades, No. 21	BAYHA

Shandon™ Peel-A-Way embedding molds, 1220	Thermo Fisher Scientific
Thermo Scientific™ Microtome Blades MX35 Ultra, 34°/80 mm	Thermo Fisher Scientific
TipOne® Pipet tips, 10/20/200/1250 µL	STARLAB
Tissue-Tek® O.C.T.™ Compound	Sakura Finetek Europe
TubeOne® Natural Flat Cap Microcentrifuge Tubes, 1.5 mL	STARLAB

6.3 Equipment

<i>Name</i>	<i>Provider</i>
Aperio CS2 slide scanner	Leica
Camera acA1300-60gm	Basler AG
DeltaRange® Analytical Balance AT261	Mettler Toledo
Duran® Glass bottles, 250/500/1000 mL	Schott AG
Duran® Staining trays	VWR International
Elevated Zero Maze	Workshop TUD, Department of Biology
Fisherbrand™ Electric Pipet Controller	Thermo Fisher Scientific
Fluorescence Light Source X-Cite exacte	Olympus Europe
Fluorescence microscope Axio Observer.Z1	Zeiss
Hotplate H22 electronic	Gerhardt Analytical Systems
Humidified chamber for IHC	Workshop TUD, Department of Biology
Magnetic hotplate stirrer IKAMAG® RCT	IKA®-Werke
Measuring cylinders, 250/500/1000 mL	VWR International
Morris Water Maze	Ugo Basile S.R.L.
Optiplex 4020 High-end workstation	Dell
pH meter CG840	Schott AG
Pipets, 10/20/200/1000 µL	Gilson
Precision Balance Universal	Sartorius
REAX 2000 Vortex	Heidolph Instruments
Rotarod	Hugo Sachs Elektronik – Harvard apparatus
Rotilabo® mini centrifuge	Carl Roth
Slide Boxes	VWR International
Slide Folders	VWR International
Thermostatic Water Bath WBS-4	Fried Electric
-85 °C Ultra Low Freezer	New Brunswick Scientific
X-ray tube Isovolt 320 Titan	GE Sensing & Inspection Technologies

6.4 Buffers and Solutions

Cresyl violet solution for Nissl staining

1.5 g Cresyl violet in 98 mL ddH₂O
1 mL 1 M Sodium acetate (0.82 g in 10 mL ddH₂O)
1 mL Acetic acid (60 μL in 940 μL ddH₂O)

Potassium disulfite for Nissl staining

150 g K₂S₂O₅ in 300 mL ddH₂O (heated with stirring)

Acetate buffer (pH 4.6), final concentration 0.1 M for Nissl staining

Solution A: 0.2 M Sodium acetate (16.4 g in 1 L ddH₂O)
Solution B: 0.1 M Acetic acid (11.6 mL in 1 L ddH₂O)
Solutions were stored at RT
98 mL A + 102 mL B

Blocking solution for IHC

Blocking step: Roti[®]-ImmunoBlock 1:10 in ddH₂O + 0.5 % Triton[®] X-100
Antibody dilution: Roti[®]-ImmunoBlock 1:10 in 0.01 M PBS + 0.1 % Triton[®] X-100

Citrate buffer (10 mM, pH 6) for antigen retrieval

Solution A: 0.1 M Citric acid (21.01 g C₆H₈O₇ x H₂O in 1 L ddH₂O)
Solution B: 0.1 M Sodium citrate (29.41 g C₆H₅O₇ x 2 H₂O in 1 L ddH₂O)
Solutions were stored at 4 °C
9 mL A + 41 mL B + 450 mL ddH₂O

Gelatin solution for slide coating

0.5 % gelatin + 0.05 % Chromium(III) potassium sulfate dodecahydrate
KCr(SO₄)₂ x 12 H₂O

10 g gelatin were dissolved in 2 L ddH₂O at 40 °C with stirring and then filtered. 1 g Chromium(III) potassium sulfate dodecahydrate were added. Slides were washed in 70 % ethanol (2x) and then in ddH₂O (2x). Slides were dipped in gelatin and drained for 2 minutes. The previous step was repeated once. The slides were dried over night at 37 °C.

Paraformaldehyde/0.01 M PBS solution for fixation (4 % PFA)

40 g PFA were dissolved in 800 mL preheated ddH₂O + 1 mL 10 M NaOH (55-60 °C) with stirring. After cooling down to RT, 100 mL 0.1 M PBS were added and the solution was mixed and filtered. Next, the solution was filled up to 1 L with ddH₂O and pH was adjusted with 1 M HCl to 7.4. The solution was aliquoted and stored at -20 °C.

Hoechst 33342 staining solution (2 µg/mL)

1:100 dilution of Hoechst 33342 stock solution (200 µg/mL)

6.5 Primary Antibodies

<i>Name</i>	<i>Host species</i>	<i>Dilution</i>	<i>Code</i>	<i>Provider</i>
Anti-DCX (Doublecortin)	Rabbit	1:1500	ab18723	Abcam
Anti-SOX2 (Sex determining region Y-box 2)	Mouse	1:1000	ab79351	Abcam

6.6 Secondary Antibodies

<i>Name</i>	<i>Dilution</i>	<i>Code</i>	<i>Provider</i>
Donkey anti-Rabbit Alexa Fluor® 594	1:800	ab150076	Abcam
Donkey anti-Mouse Alexa Fluor® 488	1:800	ab150105	Abcam

6.7 Computer Software

<i>Name</i>	<i>Provider</i>
Aperio ImageScope	Leica
EthoVisionXT 11.5	Noldus
Excel 2010/2016	Microsoft
Illustrator CS5	Adobe
ImageJ	NIH
Micromanager 1.4	µManager (http://www.micro-manager.org)
Photoshop CS5	Adobe
Prism 7.0	GraphPad Software
Word 2010/2016	Microsoft

7 Methods

7.1 Laboratory Animals

In general, the conditions of all animal experiments performed during this project comprised best possible standardizations. These basically included habituation to the experimenter and the behavioural apparatuses or mazes, as well as blinding during to the treatment during the experiments and evaluation of the data sets. Specific experimental procedures are explained in the sections below. All experiments were performed with age- and sex-matched C57BL/6 mice, housed in common type II long cages (n = 2-4 mice/cage, with nesting material and hideaway) in the animal facility of the Technische Universität Darmstadt. The mice were provided with *ad libitum* access to food and water and kept under 12 h light/dark cycle, 22 °C (\pm 1 °C) room temperature and 50 % - 65 % relative humidity (according to the guidelines of the GV-SOLAS). All experiments were carried out according to an animal test proposal approved by the regional authority in Darmstadt/Hesse (approval number: V54 – 19c 20/15 – DA8/1004).

7.2 Experimental Timeline: E14.5 and P10

The animals were whole-body irradiated with a single X-ray dose (Sham, 0.125 Gy, 0.25 Gy or 0.5 Gy) at E14.5 or P10. On the one hand, mouse brains (Sham and 0.5 Gy) were used for immunohistochemical analyses (IHC; Figure 7-1), on the other hand mice were tested in a set of behavioural tasks at the age of two months (Figure 7-2).

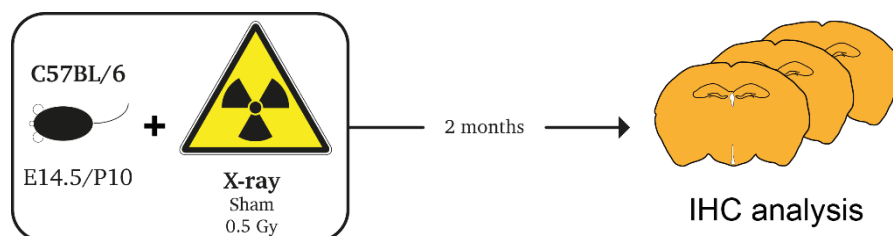


Figure 7-1: Experimental timeline for immunohistochemical (IHC) analysis. Naïve mice, irradiated at E14.5 or P10 (Sham and 0.5 Gy) were sacrificed at two months of age to remove their brains for IHC analysis. Cerebellum and Bulbus olfactorius from freshly prepared brains were removed and the remaining tissue was fixed in 4 % PFA for 24-48 h, cryoprotected in sucrose solutions and embedded in OCT before snap freezing.

The mice were tested for their motor performance (Rotarod) and activity/exploration and anxiety behaviour (Elevated Zero Maze). Afterwards, a spatial learning test (Morris Water Maze) was performed.

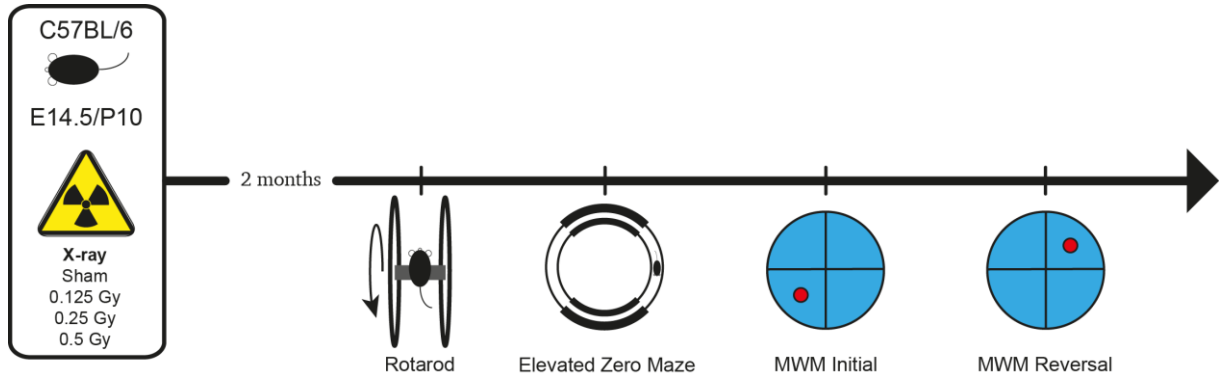


Figure 7-2: Experimental timelines for the analysis of sensitive phases of brain development/maturation. The experiments were performed in male and female C57BL/6 mice. The animals received a single whole-body irradiation either at E14.5 or at P10. The different X-ray doses were Sham = 0 Gy, 0.125 Gy, 0.25 Gy or 0.5 Gy. For both time points, the animals were analyzed at the age of two months and each compared with their respective Sham control group. The behavioural testing started with the evaluation of the motor performance (Rotarod) that comprises motor coordination and balance, followed by the assessment of the activity, exploration and anxiety behaviour in the Elevated Zero Maze. Afterwards, the spatial learning abilities were analyzed in the Morris Water Maze (MWM).

Table 7-1 contains the number of investigated animals.

	<i>E14.5</i>				<i>P10</i>			
<i>IHC</i>	Sham		0.5 Gy		Sham		0.5 Gy	
	5	6	3	3				
<i>Behaviour</i>	Sham	0.125 Gy	0.25 Gy	0.5 Gy	Sham	0.125 Gy	0.25 Gy	0.5 Gy
	10	10	8	10	10	10	10	12

Table 7-1: Number of animals investigated at E14.5 and P10.

The figures 7-1 and 7-2 show the experimental time lines and summarize schematically the used mouse model, time points for irradiation, IHC and behavioural testing, the applied irradiation doses and the different behavioural tasks (detailed experimental protocols are described in the corresponding sections below). The mice passing through the behavioural tests were subsequently analyzed with fMRI at the University of Erlangen in the lab of Prof. Dr. Andreas Hess.

7.3 Experimental Timeline: Short-term Learning Phase Experiments

The animals were assigned to three distinct cohorts and whole-body irradiated with a single X-ray dose (Sham or 0.5 Gy) at a specific time point in relation to the Morris Water Maze (MWM) test. In advance of the MWM, the mice were tested for their motor skills and their activity/exploration and anxiety behaviour.

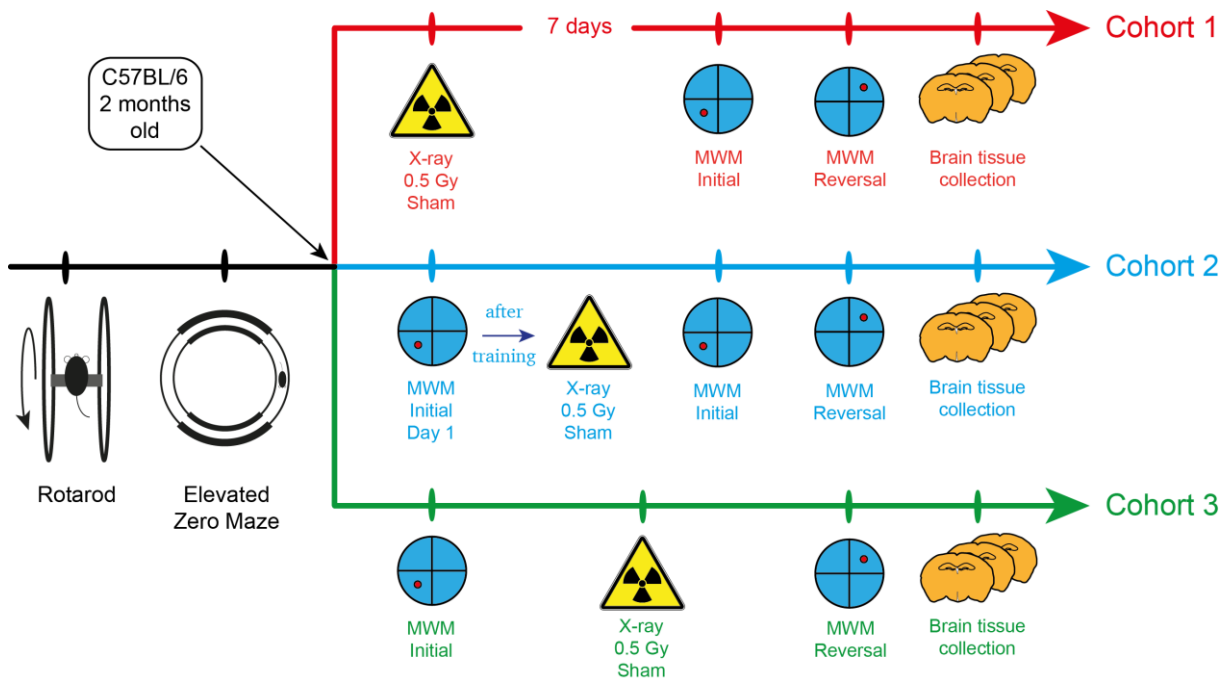


Figure 7-3 Experimental timelines for the analysis of short-term IR effects during learning phases. The experiments were performed in male and female C57BL/6 mice. Two month old animals were divided into three cohorts and received a single whole-body irradiation at a specific time interval in relation to the Morris Water Maze (MWM). The different X-ray doses were Sham = 0 Gy or 0.5 Gy. Prior to the start of the MWM, the mice were analyzed for their motor performance (Rotarod) that comprises motor coordination and balance, and their activity, exploration and anxiety behaviour in the Elevated Zero Maze.

Table 7-2 contains the number of investigated animals.

	Cohort 1		Cohort 2		Cohort 3	
IHC	Sham	0.5 Gy	Sham	0.5 Gy	Sham	0.5 Gy
	1	1	-	-	-	-
Behaviour	Sham	0.5 Gy	Sham	0.5 Gy	Sham	0.5 Gy
	9	10	10	10	8	9

Table 7-2: Number of animals investigated during short-term experiments.

After finishing the behavioural testing, the mice were sacrificed and their brains were collected for prospective immunohistochemical analyses. Figure 7-3 depicts the experimental time lines and summarizes schematically the used mouse model, the time points for irradiation and behavioural testing, the analyzed irradiation doses and the different behavioural tasks (detailed experimental protocols are described in the corresponding sections below).

7.4 Irradiation

Irradiation was performed with an *Isovolt 320 Titan* x-ray tube (GE Sensing & Inspection Technologies) and 250 kV/10 mA. The mice (irradiated and Sham control animals) were transferred to an irradiation box (10 cm x 10 cm x 6 cm, plastic, with breathing holes) that restricted the movement range to the size of the irradiation field inside the X-ray tube. Animals received a single whole-body irradiation with 1,0356 Gy/min at a source-object distance of 75 cm. All control animals were treated exactly the same way like the irradiated groups, but without being exposed to radiation. The applied doses were Sham, 0.125 Gy, 0.25 Gy and 0.5 Gy.

The irradiation time point E14.5 was determined as follows: Males and females were placed together in the evening. Females were checked early the following morning for a vaginal plug (E0). The first day of gestation (E1) was considered to be the day after the plug was found. Females were daily checked for pregnancy and irradiated on day 14 at noon (E14.5). The experimenter was blinded to the treatment during the experiments and evaluation of the data sets.

7.5 Behavioural Experiments

All animals were habituated to the test room and to the experimenter before the beginning of the behavioural experiments to ensure acclimation and to minimize handling stress.

7.5.1 Rotarod

The accelerating Rotarod performance test (Jones & Roberts, 1968) was used to analyze the gross motor abilities of the animals. The mice must permanently walk forward to prevent falling off the rotating bar. Mice with motoric impairments or deficits in balance will drop down the rotating bar usually during the first minute of the test, while mice

with intact motor coordination have no difficulties in maintaining balance for several minutes. The Rotarod apparatus (Hugo Sachs Elektronik, Harvard apparatus GmbH, Germany) consisted of a horizontal rotatable bar with a diameter of approximately 3 cm, 20 cm raised above the surface area. The Rotarod was divided into four sections by movable screen walls. The rotational speed could be gradually increased via the corresponding device.

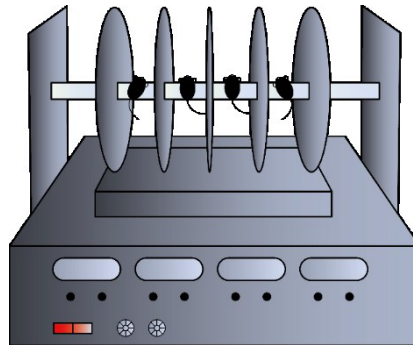


Figure 7-4: Schematic figure of the Rotarod. The apparatus consisted of rotatable bar (diameter: approx. 3 cm, 20 cm raised above the surface area). Five movable screen walls divided the apparatus into four running sections. So, four mice at the same time could be tested.

The experimental procedure to evaluate the gross motor skills was divided into two phases. First, the mice were given one practice trial on the unrevolving bar for habituation to the apparatus (60 s followed by a 10-minute break). Afterwards, each mouse performed two sessions (60 s each) on the slowly rotating bar (4 rpm). The mice were lifted back onto the rod when they fell off before this time elapsed and the habituation was continued. Afterwards, the mice had a 30-minute break in their home cages.

During the second phase, the mice were tested for their gross motor skills. The mice performed three trials, each of 300 s maximum time, on the rotating bar. The rotational speed was gradually increased from 4 to 40 rpm over the 300-second test period. Between the trials, the mice had 15-minute breaks in their home cages. The test trials were finished as soon as the mice fell off the rotating bar or after the maximum time of 300 s. The Rotarod was cleaned with ethanol between the trials. The latency time that the mice stayed on the rotating bar served as a measure of their balance, motor coordination and physical condition.

7.5.2 Elevated Zero Maze (EZM)

The EZM (Heisler et al., 1998; Shepherd et al., 1994) is based on a natural conflict in rodents between exploration of novel environments and the aversive features of brightly lit, exposed areas (Lister, 1987; Montgomery, 1955; Pellow et al., 1985). On the one hand, mice tend to explore novel environments. On the other hand, they avoid to expose themselves to brightly lit, open areas and instead seek for shelter by hiding away or showing for example Thigmotaxis (tendency to remain close to a wall). The EZM provides both sheltered and aversive properties that allow the investigation of the anxiety, exploration and activity status of the animals. Here, a narrow and elevated running track challenges the animals.

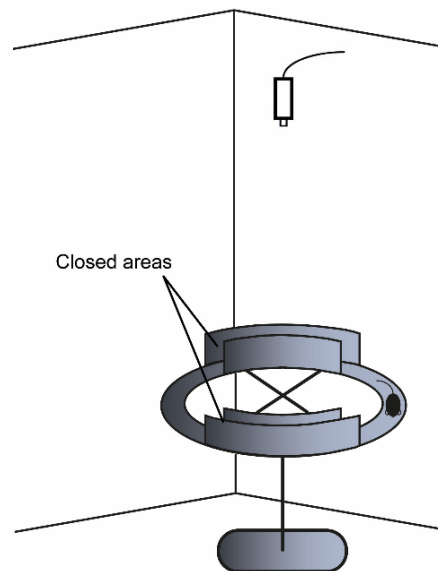


Figure 7-5: Schematic figure of the Elevated Zero Maze. The Elevated Zero Maze (EZM, produced by the departments own workshop) consisted of a ring-shaped PVC platform (width 5 cm, outer diameter 50 cm) mounted 60 cm above the floor level. Two opposing 90° sectors of the running track were surrounded by 15 cm high PVC panels at the inner and outer edge of the ring. Depicted are closed and open areas of the maze. The mice were recorded during the experiments using a Basler ace camera (acA1300-60gm, Basler AG, Ahrensburg, Germany) mounted centrally above the maze on a boom stand. The video tracking software *EthoVisionXT 11.5* (Noldus, Wageningen, the Netherlands) was used to evaluate movements and whereabouts of the animals.

Mice were recorded during the experiments using a Basler ace camera (acA1300-60gm, Basler AG, Ahrensburg, Germany) mounted centrally above the maze on a boom stand. *EthoVisionXT 11.5* (Noldus, Wageningen, the Netherlands) was used to perform the

video tracking analysis. The Elevated Zero Maze (EZM, produced by the departments own workshop) consisted of a ring-shaped PVC platform (width 5 cm, outer diameter 50 cm) mounted 60 cm above the floor level. Two opposing 90° sectors of the running track were surrounded by 15 cm high PVC panels at the inner and outer edge of the ring. In this way, the EZM platform was divided into four equally sized zones, two exposed and two sheltered. The mice were placed in one of the protected areas and allowed to explore the maze for 30 min.

The frequency and retention time in the open areas of the maze, the distance covered and the velocity during the test period served as measures of the general activity, the anxiety and the exploration behaviour. For time course analysis, the 30-minute test period was divided into six 5-minute time bins. Between trials, the setup was thoroughly cleaned with ethanol to get rid of odors caused by preceding animals. The experimenter was separated from the maze by screen walls.

7.5.3 Morris Water Maze (MWM)

The Morris Water Maze (Morris, 1984; Morris et al., 1982) was used to analyze the spatial learning and memory abilities of the mice. The MWM is a spatial navigation task in which the mice must swim to find a hidden platform. Locating the platform requires the use of distant visual cues in the surrounding of the maze. The possibility to escape the water by finding the platform works as positive reinforcement. The MWM is based on the natural aversion of mice towards swimming that motivates them to escape from the water as quickly as possible by developing most effective and efficient spatial search strategies, reflecting the formation of a proper allocentric reference map (Morris, 1984). The mice were recorded during the experiments using a Basler ace camera (acA1300-60gm, Basler AG, Ahrensburg, Germany) mounted centrally above the maze on a boom stand. The video tracking analysis was performed with *EthoVisionXT 11.5* (Noldus, Wageningen, the Netherlands). The circular water pool (Ugo Basile s.r.l., Varese, Italy; white, diameter: 120 cm, height: 60 cm; schematic illustration in figure 8-6) was halfway filled with water (water temperature 22 ± 1 °C). The water was opacified with nontoxic white tempera paint. A round transparent platform (Ugo Basile s.r.l., Varese, Italy; acrylic glass, diameter: 10 cm, height: 30 cm) was hidden 1.5 cm below the water surface (during initial learning in the center of the South-West/SW quadrant; during reversal learning in the center of the North-East/NE quadrant). Distant extramaze visual

cues (size: approx. 50 x 50 cm, high contrast, different shapes) and room equipment were maintained constant during the test and served as reference points to localize the hidden platform. The ceiling lights were covered with a tarpaulin to provide diffuse lighting and to avoid reflections on the water surface. The experimenter was separated from the maze by sliding panels to avoid misleading, inconsistent cues.

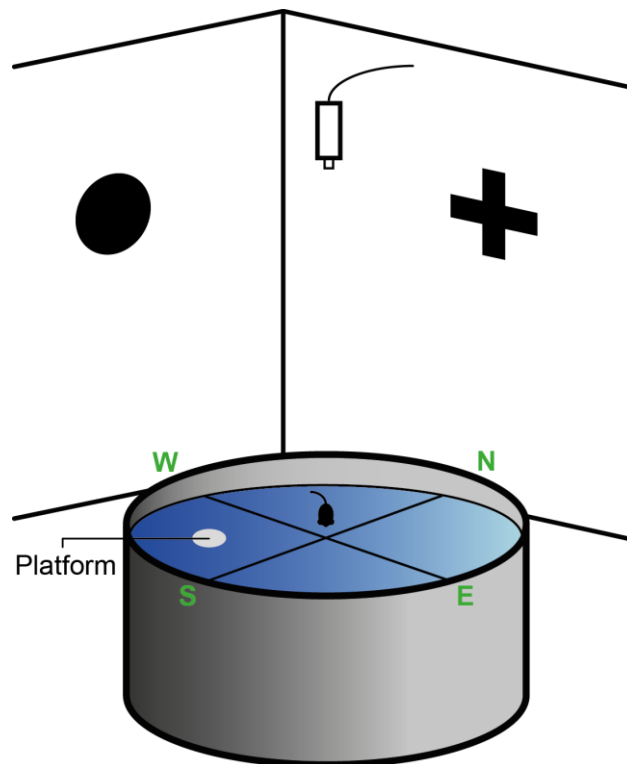


Figure 7-6: Schematic figure of the Morris Water Maze (MWM). Maze testing was conducted in a large circular pool (diameter: 120 cm, height: 60 cm). The pool was filled approximately halfway with water (maintained at $22\text{ }^{\circ}\text{C} \pm 1\text{ }^{\circ}\text{C}$) to cover a circular transparent platform (diameter: 10 cm). The platform was submerged 1.5 cm below the water surface in the center of one of the four quadrants. Additionally, the water was opacified with nontoxic white tempera paint. The pool was located in a large room with a number of extramaze visual cues, including sharp contrasted wall-mounted geometric images (cross, circle, triangle and rhombs). The experimenter was separated from the arena by sliding panels, so as not to offer an inconstant visual cue. Ceiling lights were covered with a tarpaulin to provide diffuse lighting and to avoid reflections on the water surface. The mice were recorded with a video camera connected to a video tracking system (*EthoVisionXT 11.5*, Noldus, Wageningen, the Netherlands).

First of all, the mice were gently habituated to the maze. For this purpose, the platform was initially centered in the pool and the water level was adjusted so that the platform was sticking out of the water (1 cm). The mice were then lifted onto the platform. The mice either left the platform within the next 30 s or if not were gently lifted into the

water. In either case, the mice had to swim for 15 s. Mice that did not reenter the platform by themselves were gently guided back. Independently, mice stayed 15 s on the platform before they were put back to their home cages. Habituation was performed three times with each mouse.

For both the initial and the reversal learning phase, mice were trained on 5 consecutive days with 4 trials (maximum 120 s each) per mouse and day for the hidden platform task. Normally, 5 training days are suitable to acquire robust learning and memory formation of a hidden platform position in mice, matching with established standard protocols (Vorhees & Williams, 2006). The mice were lifted into the water facing the wall. The starting positions for each trial were semi-randomly chosen to reinforce allocentric spatial orientation (see figures 7-7 and 7-8 for description of starting positions).

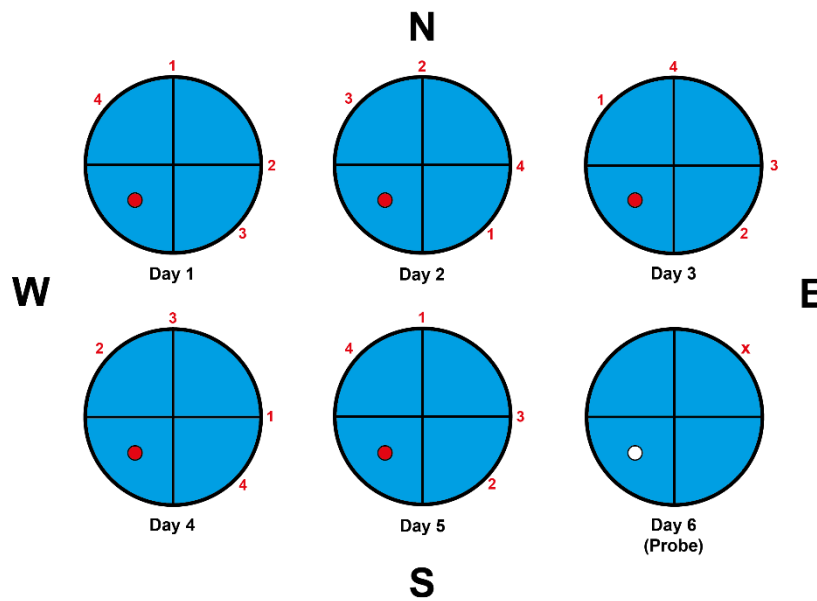


Figure 7-7: Starting positions MWM Initial learning phase. Semi-randomly chosen starting positions are depicted as red numbers. The sequences varied over the course of the 5 training days. During the probe trial on day 6 (without platform), mice started from the red “X” in the north-east quadrant.

A trial was rated as finished when the mice found the platform and stayed there for a minimum time of 3 s or after the maximum time of 120 s. In the latter case, the mice were gently guided to the platform. In either case, the mice stayed in total 15 s on the platform for orientation before they were returned to their home cages. A probe trial (60 s) without platform was performed 24 hours after the last initial and reversal

learning day, respectively, to test the reference memory of the mice. During the analysis of short-term IR effects on learning phases of the MWM, an additional visible trial (platform marked with flag; end of each training day to monitor the form on the day) and a second reversal probe trial were performed (five days after the last reversal learning trial). The start positions for the probe trials were located in the middle of the wall in the quadrant opposing the former platform position (Figure 7-7 and 7-8). Between all trials, the mice could warm up under an infrared lamp to avoid hypothermia and rest in their home cages for 10-15 min.

Following the initial learning phase, the platform position was switched from the SW quadrant to the NE quadrant. During this reversal learning phase, the mice' capacity for memory extinction of the old platform location and acquiring knowledge about the new location was tested. The experimental procedure corresponded basically to that of the initial phase with the exceptions of different platform location and starting positions (Figure 7-8).

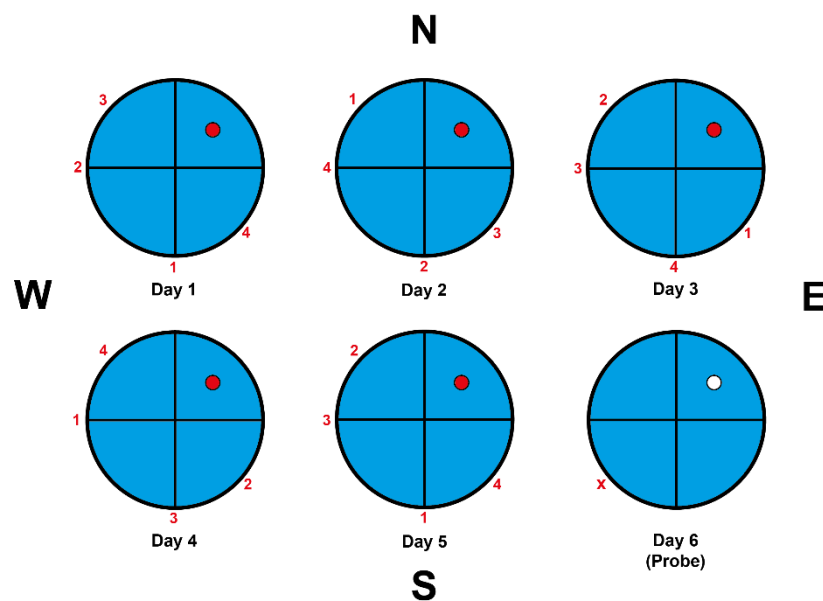


Figure 7-8: Starting positions MWM Reversal learning phase. Semi-randomly chosen starting positions are depicted as red numbers. The sequences varied over the course of the 5 training days. During the probe trial on day 6 (without platform), mice started from the red “X” in the south-west quadrant.

7.5.4 Video Tracking Analysis with *EthoVisionXT* 11.5

EthoVisionXT 11.5.1026 (Noldus, Wageningen, the Netherlands) is a video tracking and motion analysis system. It offers a wide range of video tracking options, and extensive

analysis of locomotor tracks. Video tracking analyses were performed for the EZM and MWM. For this purpose, mice were recorded during the experiments within the particular arenas using a Basler ace camera (acA1300-60gm, Basler AG, Ahrensburg, Germany) mounted centrally above the mazes on a boom stand. In general, images of the animals are passed from the video camera to a computer, where a digital video file is encoded. *EthoVisionXT* first detects the subjects and then extracts their size and the positions of one or more body points in each image. These data are then transformed into a series of dependent variables which can be used to quantify the animals' behaviour.

In general, a background image of the arenas was taken that served as a template for the definition of the virtual arena and its specific zones within the tracking software. The layers of the distinct zones were superimposed onto the predefined arena. Furthermore, test specific start/stop trial conditions with intermediate operators were created that served as regulations for the test procedure.

EthoVisionXT needs a few criteria to track moving subjects. Here, the specification how different the subject is from the background in terms of grey scale values is important. Therefore, the method to distinguish the subjects from the background, number of images per second analyzed by *EthoVisionXT* (sample rate) and the average subject size have to be defined in the detection settings menu.

Basic Software Settings EZM

During the Elevated Zero Maze (EZM), the “multiple body points” module of the software was used to track the nose-point, the center and the tail-base of the animals. The 5 cm broad running track of the EZM described under section 7.5.2 was defined as arena (Figure 7-9; Calibration → inner Ø: 40 cm, outer Ø: 50 cm).

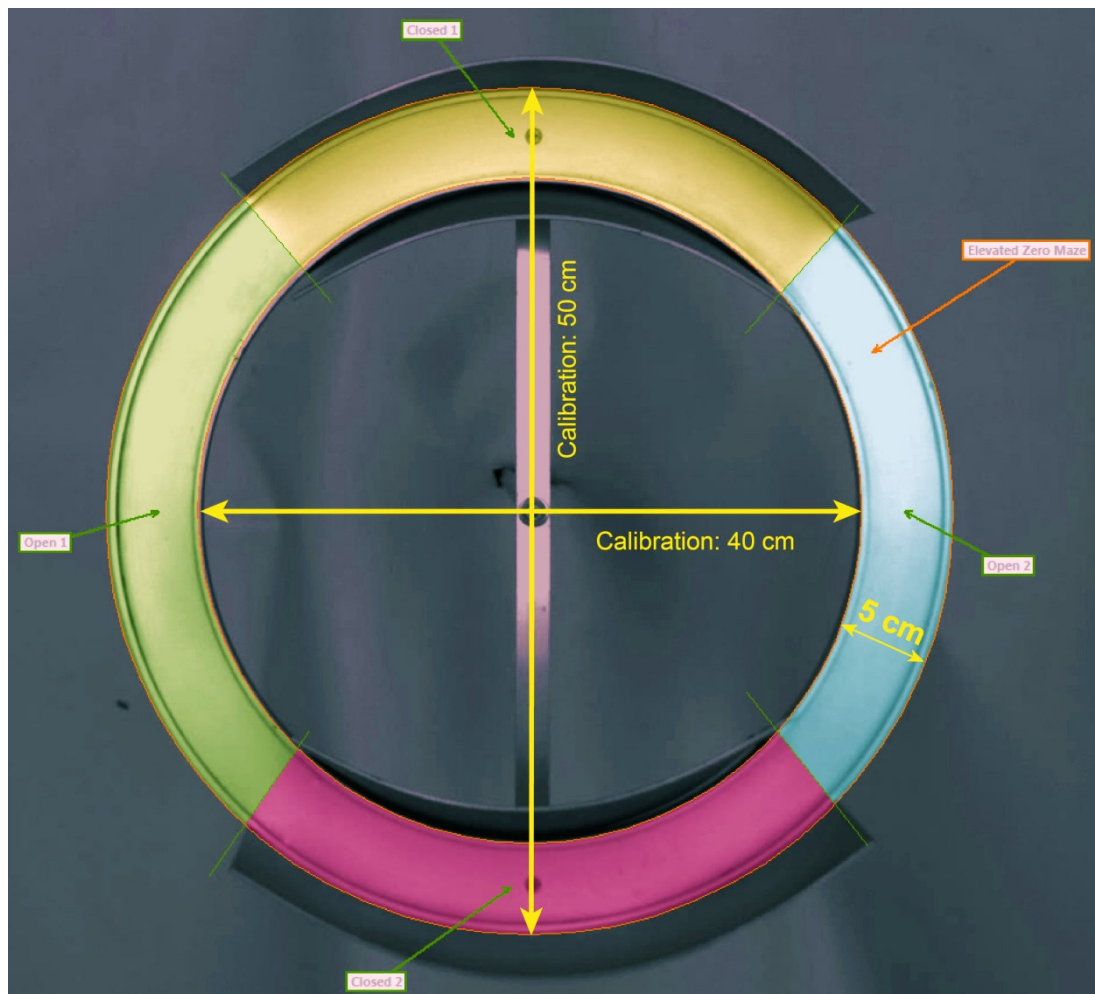


Figure 7-9: Zone definitions and dimensions for the Elevated Zero Maze (EZM). Displayed is the EZM arena and its different virtual zones created in *EthoVisionXT*. Two open and two closed zones were superimposed onto the arena. The 5 cm broad running track was defined as arena (inner diameter: 40 cm, outer diameter: 50 cm).

The described open and closed zones were defined by subdivision of the arena with intersection lines. Thus, four equally spaced zones, two open and two closed, were created. Both open and closed zones were created as cumulative zones, so that the measured parameters regarding the animals' positions were displayed as total values. Under the trial control settings, the start tracking action was executed via the condition "Current = true, when center-point is in arena". The stop tracking action was linked to the stop condition: "Stop after a delay of 30 min" The start/stop trial rules for the EZM are displayed in Figure 7-10.

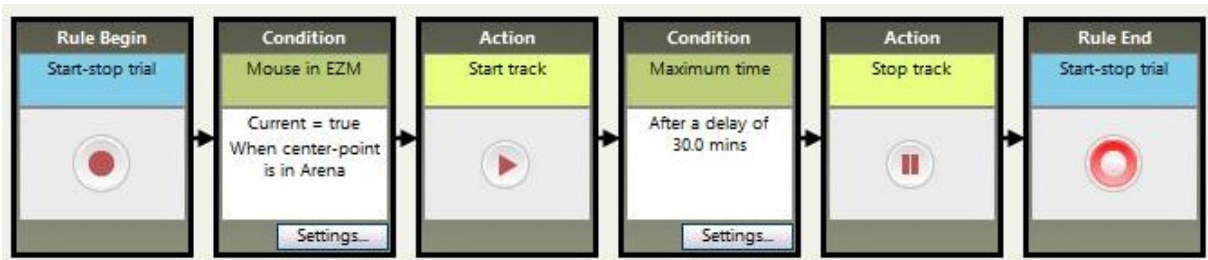


Figure 7-10: Trial control settings for Elevated Zero Maze data acquisition. The depicted start/stop trial rules were maintained for all experiments.

In the detection settings menu, the sample rate was set as 25. Best detection results were obtained with the *Dynamic subtraction* method. This method is recommended when the background or the light conditions within the arena change gradually over the testing time. This is the case when mouse droppings appear, the animals micturate or a water surface moves (see also section 7.5.4.2 basic software settings MWM), leading to adverse light reflections. Thus, the program compares each sampled image with a reference image (without animal) that is updated regularly. This compensates for temporal changes in the background. In detail, for the adapted detection configuration the animal color compared to background was chosen as “darker”, as the investigated mice had black fur and the arena was light grey. Each pixel in the image matches a grey scale value, ranging from 0 (= black) to 255 (= white). As described above, a reference image of the arena without animal was taken. When analyzing the images, *EthoVisionXT* subtracts the grey scale value of each pixel in the reference image from the grey scale value of the corresponding pixel in the current image. Those pixels with non-zero difference and within the grey scale range from 70 to 255 were considered as the animal. Additionally, the frame weight value was set to a low value (1), as the background changed slowly during the test. Thus, a large number of past images contributed to each updated reference image. Consequently, changes in the background were diluted over many images. Moreover, it was important to adjust the animals’ contours within the software because their complete body (including the tail base, but not the tail itself) should be detected. The elimination of the tail is necessary, since its movements could incorrectly be detected as distance moved, even if the animals do not move. Therefore, the “Erode first, then dilate” method was used (Contour erosion = 1 pixels, Contour dilation = 1 pixels) which first removes a pixel layer (including the tail) and then adds a pixel layer back, restoring the original subject size. Next, as the animals differed slightly from one another in size, the subject size

settings were adapted. These settings model the animal's body size by using the results of the body detection. Thus, objects like droppings or large reflections were excluded from the detection. The subject size range was adjusted to cover the complete size range of the currently analyzed animals. Now, the data acquisition was performed. When tracking a moving animal with a high sample rate, sideward movements resulting from wobbling of the animal's body are also tracked. This causes an overestimation of, for example, the distance covered. Therefore, the acquired tracks were smoothed with the Lowess method (Locally weighted scatter plot smoothing) and a half window size of 10 (recommended by the manufacturer; based on 10 samples before and after every sample point) to eliminate such small movements. During the "multiple body points" detection, *EthoVisionXT* sometimes incorrectly assigns nose-point and tail-base of the animals resulting from sudden or large turns. In such a case, both body points were manually swapped in the generated tracking files.

Basic Software Settings MWM

During the Morris Water Maze (MWM), only the center point detection was used to track the animals. The MWM arena described under section 8.5.3 was defined according to the water level in the pool ((Figure 7-11; Calibration → diameter: 120 cm). The arena was divided in distinct zones that were organized as superimposed zone groups. For the initial learning, four equally sized quadrants (SW, NW, NE, SE), a thigmotactic zone in the periphery (width: 15 cm), a circular critical zone around the platform (width: 10 cm) and a platform zone (diameter: 10 cm) within the center of the SW quadrant were defined (Figure 7-11). For the reversal learning, the original critical zone and platform zone position were retained and marked as "old". Additionally, both a new critical and platform zone were created in the center of the NE quadrant (Figure 7-11).

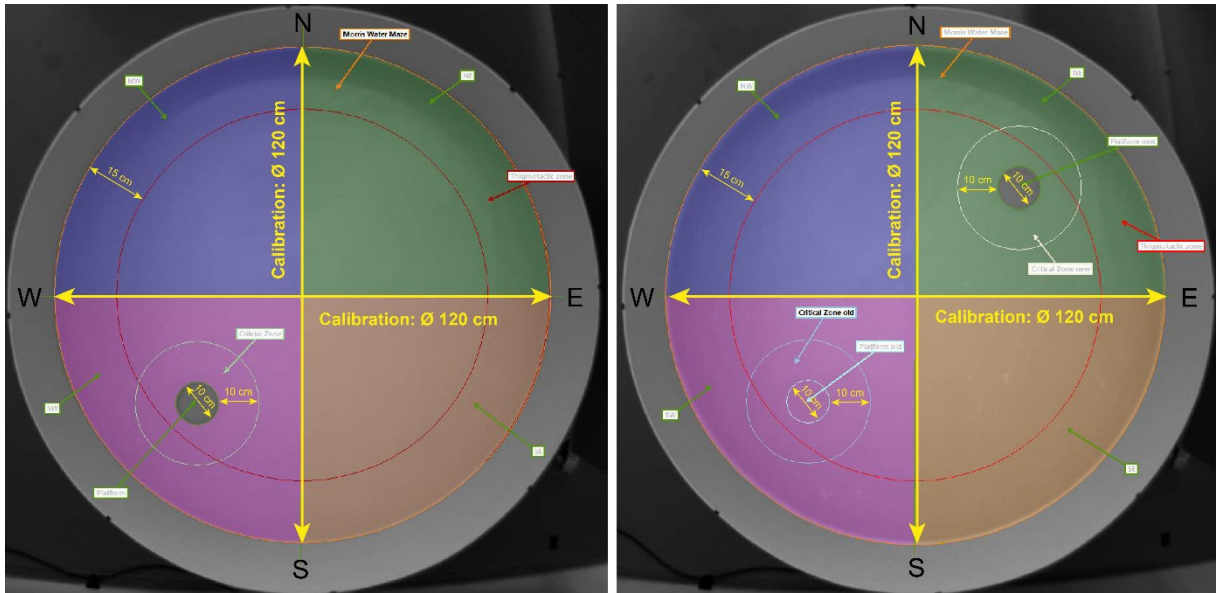


Figure 7-11: Zone definitions and dimensions for the Morris Water Maze (MWM) during initial and reversal learning. Displayed is the MWM arena for the initial and the reversal learning phase and its different virtual zones created in *EthoVisionXT*. Four equally sized quadrants (SW, NW, NE, SE), a thigmotactic zone in the periphery (width: 15 cm), circular critical zones around the platform (width: 10 cm) and platform zones (diameter: 10 cm) within the center of the SW/NE quadrant were defined and superimposed onto the arena.

In the trial control settings menu, the start tracking action for the training period was executed via the condition “Current = true, when center-point is in arena”. The stop tracking action was linked to two stop conditions: “Stop after a delay of 120 s” or “Current duration \geq 3 s, when center-point is in platform” via the “any input true” operator. The start/stop trial rules for the MWM training period are displayed in Figure 7-12.

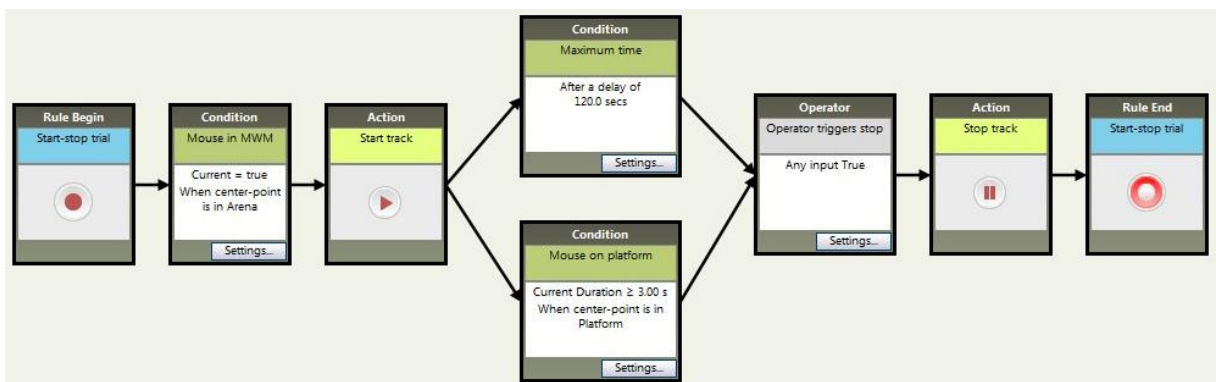


Figure 7-12: Trial control settings for data acquisition during the MWM training period. The depicted start/stop trial rules were maintained for all experiments.

The start/stop trial rules for the MWM probe trials differed from the rules during the training period. Here, only one stop condition “after a delay of 60 secs” was defined as shown in Figure 7-13.

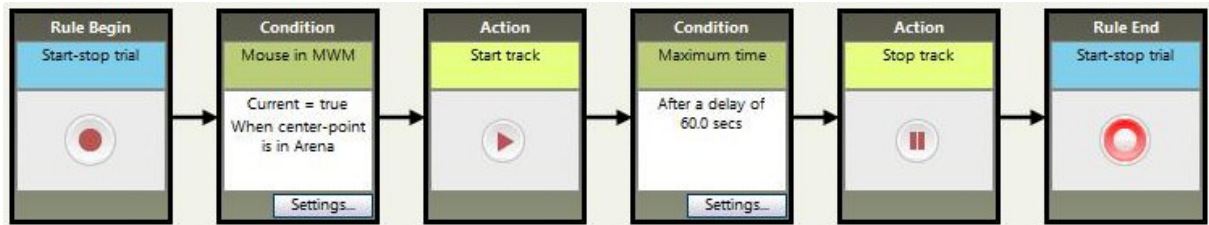


Figure 7-13: Trial control settings for data acquisition during probe trials. The depicted start/stop trial rules were maintained for all probe trials.

In the detection settings menu, the sample rate was set as 25. Best detection results were obtained with the *Dynamic subtraction* method. This method is recommended because the water surface is in motion when mice swim, causing adverse light reflections. The animal color compared to background was chosen as “darker”, as the investigated mice had black fur and a white pool with opacified water (white tempera paint) was used. The pixels with non-zero difference and within the grey scale range from 70 to 255 were considered as the animal. Additionally, the frame weight value was set to a low value (1), as the background changed slowly during the test. The “Erode first, then dilate” method was used (Contour erosion = 1 pixels, Contour dilation = 1 pixels) to adapt the body contours. The subject size range was adjusted to cover the complete size range of the currently analyzed animals. Afterwards, the data acquisition was performed. The acquired tracks were smoothed with the Lowess method (Locally weighted scatter plot smoothing) and a half window size of 10 (recommended by the manufacturer; based on 10 samples before and after every sample point) to eliminate small movements. For more detailed information about the general settings, see section 7.5.4.1 Basic software settings EZM.

7.6 Histology

7.6.1 Tissue Preparation

The mice were sacrificed by CO₂-inhalation and decapitated. The brains were dissected out and transferred into 4 % PFA/0.01 M PBS fixative (pH 7.4) for 24 to 48 h after removal of the olfactory bulb and the cerebellum. After fixation, brains were first

washed in 0.01 M PBS to get rid of excess PFA solution and then cryoprotected in serial sucrose solutions (in 0.01 M PBS, pH 7.4) with increasing concentrations (10 % → 20 % → 30 %) each for at least 24 hours. Proper incubation was confirmed by sinking down of the brains. Then, the brains were snap frozen with isopentane (chilled in liquid nitrogen) in embedding molds filled with O.C.T compound (Tissue-Tek) and finally sectioned using a CryoStar NX50 cryostat (Thermo Scientific). First, the frozen blocks containing the brains were trimmed from anterior to posterior until reaching the level with the typical C-shaped structure of the hippocampus. Coronal sections (10 μ m) from the rostral to caudal extension of the hippocampus were directly collected on gelatin-coated slides (0.5 % gelatin + 0.05 % Chromium(III) potassium sulfate dodecahydrate) and stored at -20 °C after thorough drying until further use.

7.6.2 Nissl Staining

The Nissl staining is a widely used method to study the morphology of nervous tissue and is based on blue coloring of neuronal and glial cell bodies. Its staining capacity is based on interactions between the basic dye cresyl violet and the negatively charged DNA and RNA as well as the endoplasmic reticulum, resulting in blue coloring of nucleoli and ribosomes (Mulisch & Welsch, 2010). This causes the cell bodies to stand out from the white matter fibers. Nissl staining highlights the somata of neurons but omits dendrites and axons. In every fourth brain section, cell bodies were stained with the Nissl method to provide an overview about the sectional plane and brain areas for later IHC stainings (Figure 7-14). The staining protocol is shown in Table 7-3. All steps were conducted at RT.

No.	Step	Time
1	ddH ₂ O	2 min
2	EtOH 70%	5 min
3	EtOH 96%	5 min
4	EtOH 70%	2 min
5	ddH ₂ O	2 min
6	Potassium disulfite	12 min
7	ddH ₂ O	2 min
8	ddH ₂ O	2 min
9	Cresyl violet	1-2 min
10	Acetate Buffer	2 min
11	EtOH 70%	>2 min
12	EtOH 96%	>2 min
13	EtOH 100% (or 2-Propanol)	>2 min
14	Xylol	5 min
15	Xylol	5 min

Table 7-3: Protocol of Nissl staining.

→ Sections were coverslipped with Entellan® (Merck). Images were taken at 20x with an Aperio CS2 slide scanner (Leica).

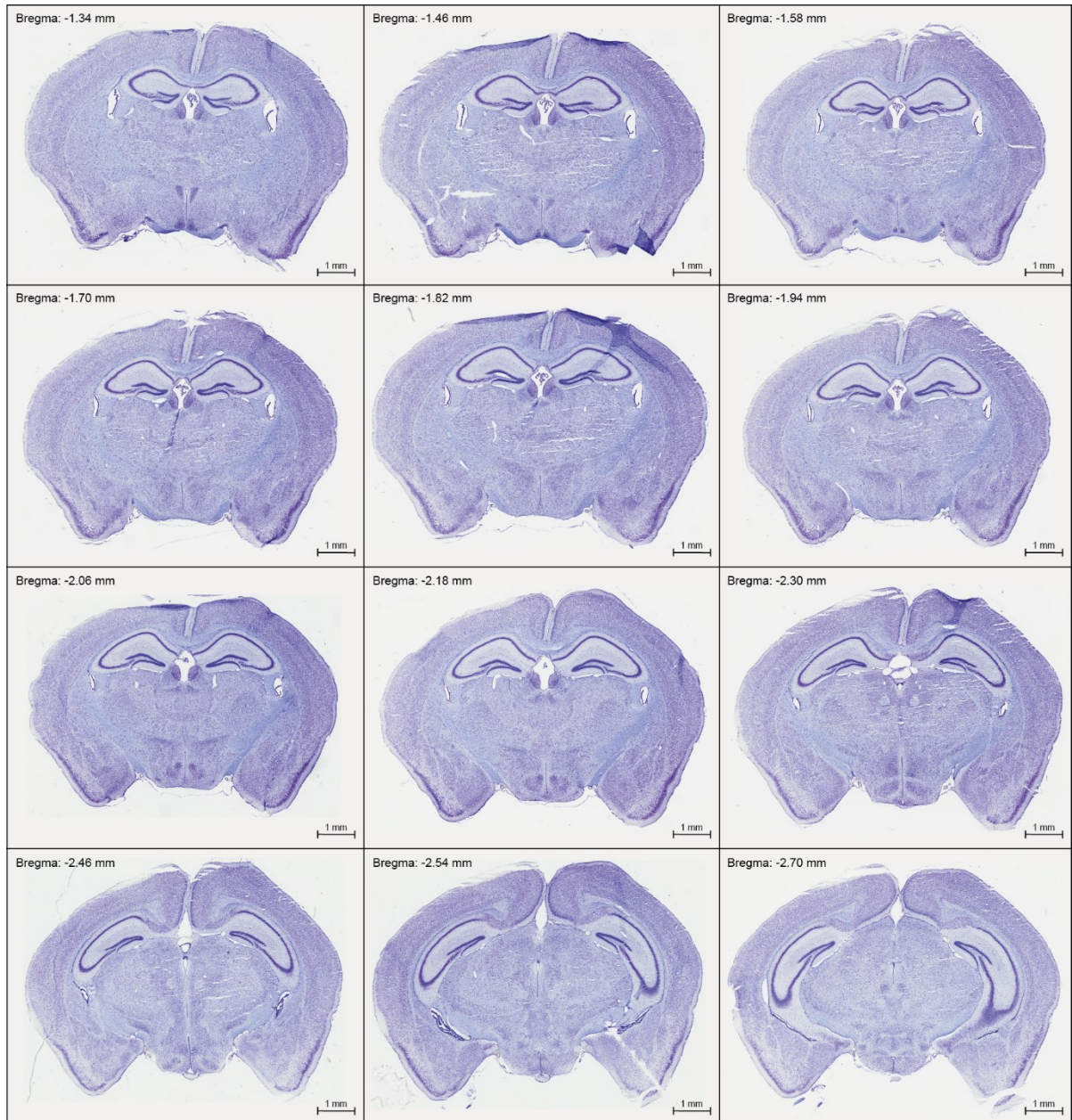


Figure 7-14: Murine coronal sections stained with Nissl. Depicted are coronal sections of mouse brains ranging from Bregma -1.34 mm to Bregma -2.70 mm and stained with Nissl. Bregma is a skull reference point and delineates here the different levels across which IHC was performed. Images were taken at 20x with an Aperio CS2 slide scanner (Leica).

7.6.3 Immunohistochemistry (IHC)

IHC was performed according to a protocol with preceding antigen retrieval as detailed below: First, the slides were brought to room temperature while citrate buffer (10 mM, pH 6) was boiled up in a microwave. The hot citrate buffer was transferred into a staining tray, placed in a preheated water bath (100 °C). Next, the slides were placed

in the staining tray and incubated for 30 min with the citrate buffer. Afterwards, the slides within the citrate buffer cooled down to RT, before the sections were washed 3 x 10 min in 0.01 M PBS and incubated for 45 min in blocking solution (Roti®-ImmunoBlock, Carl Roth, 1:10 in ddH₂O). Sections were incubated overnight at 4 °C with the primary antibody diluted in blocking solution (Roti®-ImmunoBlock, Carl Roth, 1:10 in 0.01 M PBS) using a humidified chamber. The next day, the sections were washed 3 x 10 min in 0.01 M PBS and incubated for 1 h at room temperature with the secondary antibody diluted in blocking solution (Roti®-ImmunoBlock, Carl Roth, 1:10 in 0.01 M PBS). Then, the sections were washed 3 x 10 min in 0.01 M PBS and incubated for 10 min in Hoechst 33342 solution (2 µg/mL) to label nuclei. The sections were washed 3 x 10 min in 0.01 M PBS. The slides were coverslipped with antifade mounting medium (Roti®-Mount FluorCare, Carl Roth) and sealed with CoverGrip™ Coverslip Sealant (Biotium). The primary antibody was anti-DCX (1:1500, Abcam, ab18723). The secondary antibody was donkey anti-rabbit Alexa Fluor® 594 (1:800, Abcam, ab150076).

7.6.4 Fluorescence Microscopy and Quantifications

Fluorescence images were taken on a fluorescence microscope (Axio Observer.Z1, Zeiss) combined with a computer-assisted imaging system (ImageJ-based Micromanager 1.4). The Paxinos mouse brain atlas and Nissl stainings were used to identify and delineate the analyzed DG regions (Paxinos & Franklin, 2004). For quantification of DCX⁺ cells, 8-10 randomly chosen, non-overlapping sections per animal among the rostral-caudal extension of the dorsal dentate gyrus (DG; Bregma: from -1.34 to -2.70) were analyzed. Cells were quantified per DG/section in Sham (n = 8) and 0.5 Gy animals (E14.5: n = 6, P10: n = 3) using the ImageJ (NIH) cell counter plugin. The area (mm²) of the hippocampus was measured with the ImageJ (NIH). Quantifications were performed blinded.

7.7 Data Generation and Analysis

Generally, all data sets were preprocessed with Microsoft Excel 2010/2016 and statistically analyzed with Prism 7 (GraphPad Software Inc.). Error bars represent SEM or SD, as indicated in the respective figure legends. Behavioural data derived from Elevated Zero Maze (EZM) and Morris Water Maze (MWM) were generated and

presorted with *EthoVisionXT 11.5* (Noldus, Wageningen, the Netherlands). First, the data sets were checked for normality distribution (D'Agostino-Pearson normality test, Shapiro-Wilk normality test). The specific statistical tests used are described below. Significances were assumed when $P < 0.05$ (* $P < 0.05$, ** $P < 0.01$, *** $P < 0.001$, **** $P < 0.0001$), if not otherwise stated. All graphics have been developed by the author if not otherwise stated.

7.7.1 Rotarod Data and EZM Data

E14.5 / P10

The Kruskal-Wallis statistic was used to evaluate latency outcomes in the Rotarod test and distance, velocity, frequencies and retention times in open areas of the EZM and if required followed by Dunn's multiple comparisons test.

2 months

The Mann-Whitney test was used to evaluate latency outcomes in the Rotarod test, frequencies and retention times in open areas of the EZM.

7.7.2 MWM Data

E14.5 / P10

Swimming distances and velocities over the 5 training days were analyzed with a Two-way RM ANOVA and if required followed by Tukey's multiple comparisons test. Escape latencies during the five MWM training days (cumulative incidence of escape in %) were evaluated using cumulative Kaplan-Meier plots which are most appropriate to analyze time to event data. These plots are convenient as they also take right-skewed and censored data into consideration, as it is commonly used in survival studies and thus also suitable for analysis of escape latencies (Jahn-Eimermacher et al., 2011). Each data point represents the mean of four training trials and corresponds to one animal within the particular group. A left shift of the curves indicates a decline in the escape latencies shown on the x-axis while the y-axis shows the percentage of animals that found the platform within 120 s. The survival distributions of the samples were compared statistically pairwise with the Log-rank test followed by Bonferroni test to correct for alpha error accumulation during multiple comparisons. Based on six group comparisons, a P value lower than 0.0083 was accepted as significant ($\alpha/K = 0.0083$,

with $\alpha = 0.05$, $K = 6$). The Log-rank test is a nonparametric hypothesis test to compare the survival distributions of two samples. It is suitable when the data are right skewed and censored. In terms of survival analysis, the median overall survival of the four groups was calculated. In clinical studies, measuring the median survival is used to see how well a new treatment works. Here, survival corresponds to the length of time on each training day that half of the animals in a group are still searching for the platform and will be called here conveniently median overall swimming time (MOST [s]). Searching strategies were differentiated into spatial and non-spatial, whereby five categories were classified as non-spatial and three as spatial (as shown exemplarily with the scheme in Figure 7-15 and described in Table 7-4).

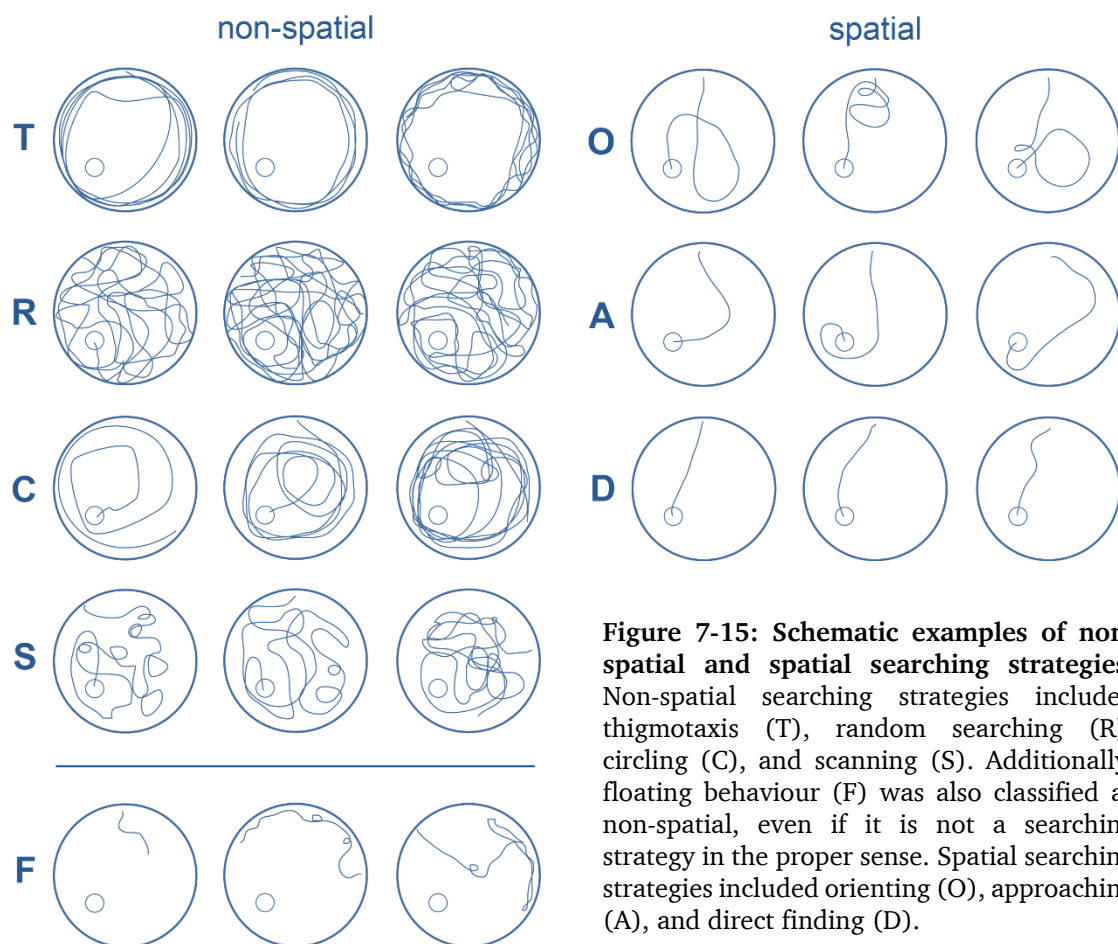


Figure 7-15: Schematic examples of non-spatial and spatial searching strategies. Non-spatial searching strategies included thigmotaxis (T), random searching (R), circling (C), and scanning (S). Additionally, floating behaviour (F) was also classified as non-spatial, even if it is not a searching strategy in the proper sense. Spatial searching strategies included orienting (O), approaching (A), and direct finding (D).

The predominant searching strategy used in each trial was classified according to the criteria in Table 7-4 by the experimenter blind to the irradiation dose.

Differences between groups in the percentage of spatial searching strategies and direct finding were calculated with a Two-way RM ANOVA and if required followed by Tukey’s multiple comparisons test.

	<i>Category</i>	<i>Description</i>
<i>non-spatial</i>	Thigmotaxis (T)	<ul style="list-style-type: none"> ▪ Mice mainly in the peripheral zone of the pool ▪ Contact to arena wall interrupted by sporadic pushing away ▪ Seldom entries into more central parts of the maze may randomly lead to platform finding
	Random (R)	<ul style="list-style-type: none"> ▪ Unfocused, wide exploration in all parts of the pool ▪ Occasional success in finding the platform ▪ Swimming paths are jagged with frequent changes of direction and velocity
	Circling (C)	<ul style="list-style-type: none"> ▪ Mice use concentric, circular swimming patterns ▪ Increased probability of encountering the platform
	Scanning (S)	<ul style="list-style-type: none"> ▪ Searching is shifted away from the periphery and becomes more focused to the pool center ▪ Swimming paths with reduced length
	Floating (F)	<ul style="list-style-type: none"> ▪ Non-performance
<i>spatial</i>	Orienting (O)	<ul style="list-style-type: none"> ▪ Option 1 – Mice make first attempt to reach the platform but miss it by a few degrees. They then re-orientate themselves by returning near the start position or the center of the maze and finally find the platform ▪ Option 2 – Mice orientate themselves by swimming around in front of the start position and then find the platform ▪ Swimming paths clearly reduced compared to non-spatial strategies
	Approaching (A)	<ul style="list-style-type: none"> ▪ Mice adjust their swimming paths only by a few degrees while approaching/reaching the platform ▪ Short swimming paths
	Direct (D)	<ul style="list-style-type: none"> ▪ Straight finding of the platform following the linear distance from start position to target ▪ Most effective and fastest strategy

Table 7-4: Searching strategies.

Swimming distances during probe trials were analyzed with a One-way ANOVA and if required followed by Tukey’s multiple comparisons test. Frequency and cumulative retention time in critical zone and proximity to former platform position were analyzed with Kruskal-Wallis statistic and if required followed by Dunn’s multiple comparisons test. The cumulative retention time in quadrants was analyzed with a Two-way RM ANOVA and if required followed by Tukey’s multiple comparisons test. Heat maps were generated with *EthoVisionXT 11.5* (Noldus, Wageningen, the Netherlands).

2 months

Escape latencies during the five MWM training days (cumulative incidence of escape in %) were evaluated using cumulative Kaplan-Meier plots (see section 7.7.2 MWM data *E14.5/P10* for explanation). Each data point represents the mean of four training trials and corresponds to one animal within the particular group. The survival distributions of the samples were compared statistically pairwise with the Log-rank test. Based on only one group comparison, already a P value lower than 0.05 was accepted as significant. Differences between groups in the percentage of spatial searching strategies or direct finding were calculated with a Two-way RM ANOVA and if required followed by Sidak's multiple comparisons test. Differences between days in the percentage of spatial searching strategies or direct finding were calculated with a Two-way RM ANOVA and if required followed by Tukey's multiple comparisons test (for explanation of searching strategies see section 7.7.2 MWM data *E14.5/P10*).

The initial probe trial results were either analyzed with the Mann-Whitney test (swimming distance, frequency and cumulative retention time in critical zone) or with a Two-way RM ANOVA and if required followed by Tukey's multiple comparisons test (cumulative retention time in quadrants).

The cumulative retention times in quadrants during reversal probe testing were analyzed with a Two-way RM ANOVA and if required followed by Tukey's multiple comparisons test. Heat maps were generated with *EthoVisionXT 11.5* (Noldus, Wageningen, the Netherlands).

Histology

Quantifications of DCX⁺ progenitor cells in the dentate gyrus of naïve, two months old mice were analyzed with Mann-Whitney test.

Comparison E14.5 / P10 / 2 months

Differences in spatial searching during training and cumulative retention times in quadrants during probe testing were calculated with a Two-way RM ANOVA and if required followed by Tukey's multiple comparisons test.

8 Chapter I – Evaluation of Long-term Radiation Risk and Sensitivity for Time Point E14.5

The first chapter describes the long-term effects of prenatal low-dose irradiation in C57BL/6 mice that were characterized in a series of behavioural tests addressing the motor abilities, exploration- and anxiety-related properties and the development of spatial reference memory. Single low X-ray doses from 0 Gy (Sham) to 0.5 Gy were whole-body applied at E14.5. The offspring was analyzed for the different behavioural aspects at the age of two months to evaluate the risk of radiation exposure and the sensitivity of this specific time point of brain development.

8.1 Results

8.1.1 Effects on Motor Function and Anxiety/Exploration Behaviour (E14.5)

In order to analyze motor function, the accelerating Rotarod test was used during which the mice had to balance on a rotating bar. The latency until the mice fell off the bar served as a measure for their motor coordination and balance. The Kruskal-Wallis test was conducted to evaluate statistical effects. Considerable deficiencies between the group means of time spent on the rotating bar could not be detected (Fig. 8-1 A). All animals were able to maintain balance on the Rotarod and reached more than 90 % of the maximum time on average ($H = 1.8, P = 0.61$). Thus, the motor function was not affected by prenatal irradiation and a physical handicap during the following tests could be excluded.

Next, the Elevated Zero Maze (EZM) was performed that is based on a natural conflict in rodents between exploration of novel environments and the aversive features of brightly lit, exposed areas (Lister, 1987; Montgomery, 1955; Pellow et al., 1985). The mice were allowed to explore the maze for 30 minutes. There were neither statistically significant differences between the group means of the distance covered nor the velocity during exploration as determined by Kruskal-Wallis test (Figure 8-1 B; distance: $H = 1.1, P = 0.78$; velocity: $H = 1.4, P = 0.71$).

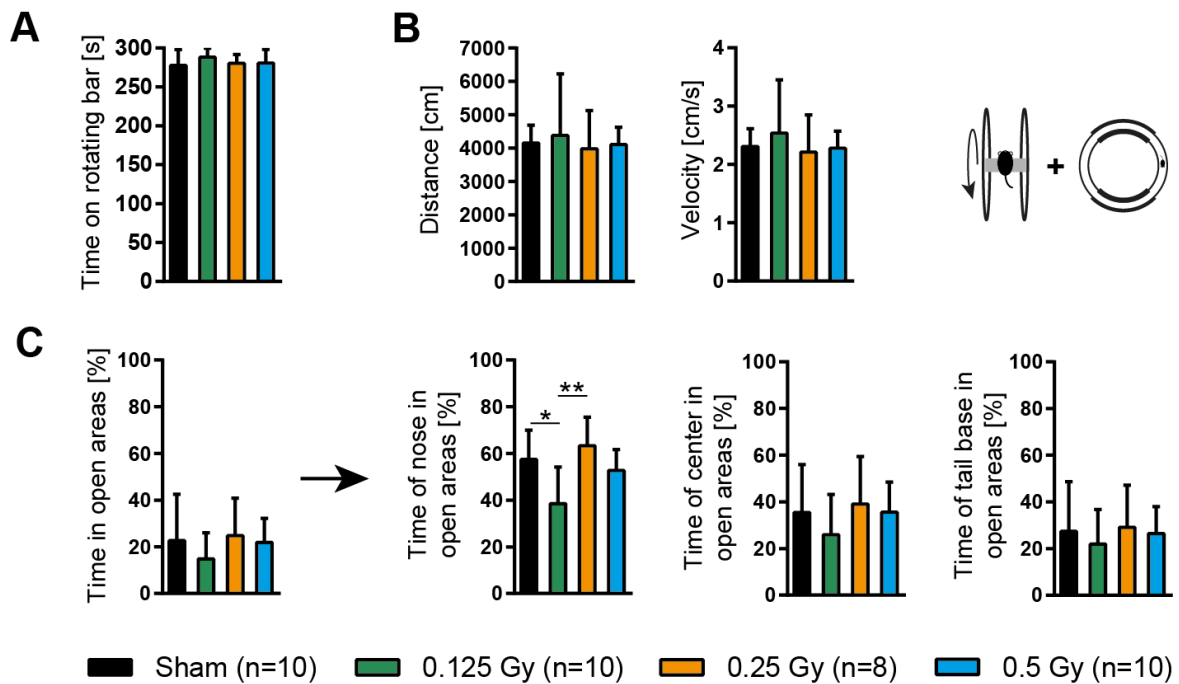


Figure 8-1: E14.5 LDIR did not affect motor performance (Rotarod) but caused dose-specific effects on anxiety/exploration behaviour (Elevated Zero Maze). 0.125 Gy mice displayed reduced retention times of their nose point in the open areas of the maze. (A) Time spent on the rotating bar [s]. Statistics: Kruskal-Wallis test. (B) Distance [cm] and velocity [cm/s] during the 30-minute EZM testing phase. Statistics: One-way ANOVA. (C) Time spent in open areas [%] of the EZM for the case when animals left the sheltered areas with their entire body contour and for the three individually tracked body points (nose, center, tail base). Statistics: Kruskal-Wallis test (for nose: followed by Dunn’s multiple comparisons test). * = $P < 0.05$, ** = $P < 0.01$. Black bars represent Sham (n = 10), green bars represent 0.125 Gy (n = 10), orange bars represent 0.25 Gy (n = 8), blue bars represent 0.5 Gy (n = 10). All values are expressed as mean (SD).

Accordingly, the mice’s basic activity and exploration abilities seemed to be unaffected by low-dose ionizing radiation (LDIR).

It was obvious that all groups preferred the closed over the open areas. Evaluation of time spent in open areas, describing the case when all body points are situated in the open compartments, gave a minor percentage of approximately 20 %, with the lowest value in the 0.125 Gy group. However, testing with Kruskal-Wallis analysis could not reveal any statistical difference between the groups (Figure 8-1 C). Interestingly, when looking in more detail at the three body points, the 0.125 Gy group explored the open areas less intensive than all other groups, as indicated by the statistically significant effect on the group means of time of nose point in open areas (Kruskal-Wallis statistic: $H = 12.6, P = 0.0056$). Post hoc testing with Dunn’s multiple comparisons test revealed a significantly decreased percentage in the 0.125 Gy animals compared to Sham ($P = 0.028$) and 0.25 Gy animals ($P = 0.0024$), as shown in Figure 8-1 C. The follow-up comparison between 0.125 Gy and 0.5 Gy could not demonstrate a statistical disparity

(Figure 8-1 C). Sham, 0.25 Gy and 0.5 Gy animals were on similar levels regarding the time in open areas of the maze (Figure 8-1 C). Consequently, the 0.25 Gy and 0.5 Gy dose were estimated to have no effect on the basic exploration and anxiety behaviour of the animals. In contrast to that, eight out of ten 0.125 Gy animals were clearly below the average of the Sham control group. The 0.125 Gy dose clearly reduced the time of nose point in open areas, thus giving a hint of an increased anxiety behaviour.

8.1.2 Initial Learning Revealed Dose-dependent Learning Delays

The mice were trained for five days in an initial learning phase of the Morris Water Maze (MWM) and analyzed for their hippocampus-dependent spatial learning abilities. The platform was constantly located in the center of the SW quadrant.

First, the cumulative incidence of escape [%] was evaluated over the training period of five days. Figure 8-2 A shows the corresponding Kaplan-Meier plots which are most appropriate to analyze time to event data (for explanation see section 7.7.2). A left shift of the curves indicates a decline in the escape latencies. The Kaplan-Meier curves were compared statistically pairwise with the Log-rank test followed by Bonferroni correction. In terms of survival analysis, the median overall survival of the four groups was calculated. Here, survival corresponds to the length of time on each training day that half of the animals in a group are still searching for the platform and will be called here conveniently median overall swimming time (MOST [s]).

Significant differences were observed between the 0.5 Gy group and the Sham animals on day 2 (Figure 8-2 A; $P = 0.0049$) and day 3 (Figure 8-2 A; $P = 0.0007$). On day 4, the 0.25 Gy group showed significantly prolonged escape times compared to the Sham treated group (Figure 8-2 A; $P = 0.0077$). In general, dose-dependent prolonged escape times were detectable for all IR groups compared to Sham, most evident from training day 3 to 5. However, in contrast to the 0.125 Gy group, several animals of both the 0.25 Gy and the 0.5 Gy group could not catch up on the delay, so that the MOST on training day 5 was still increased (Figure 8-2 A).

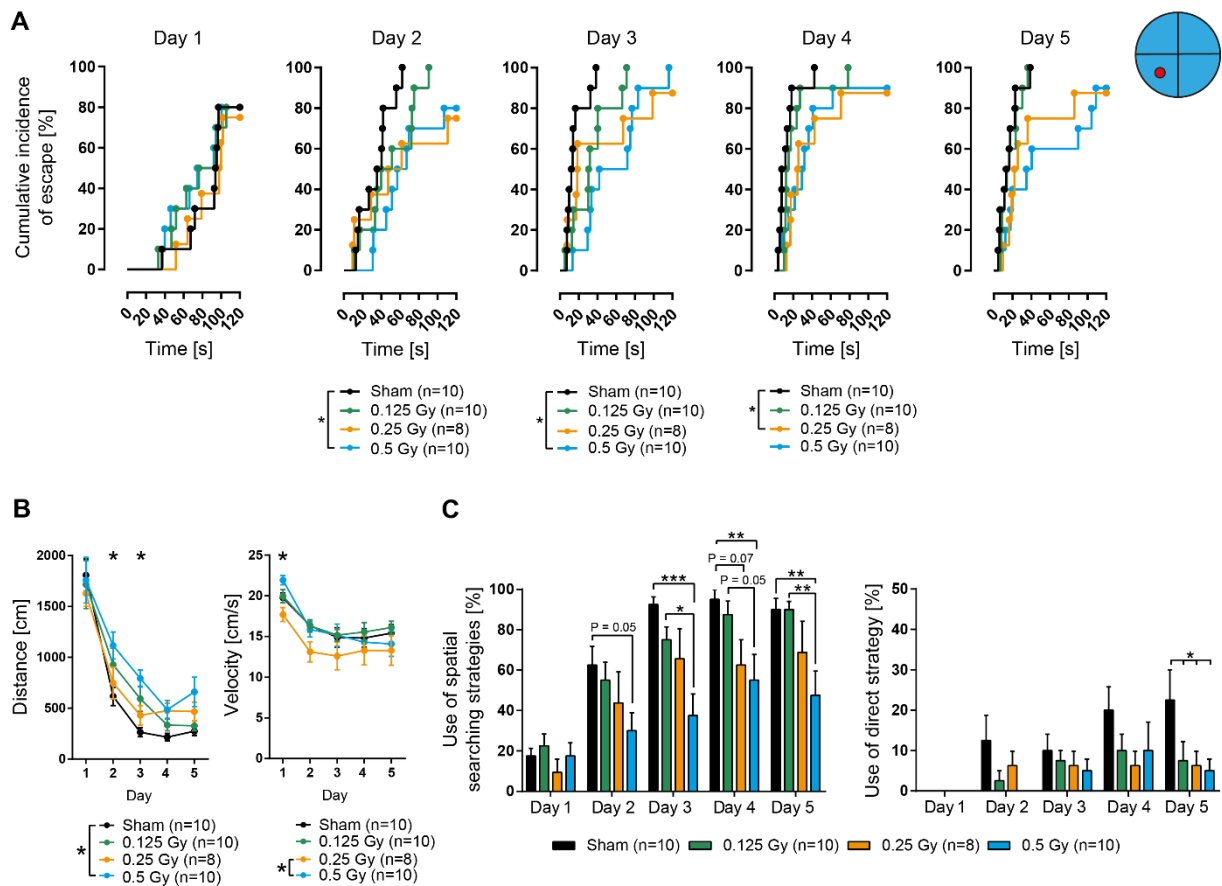


Figure 8-2: E14.5 MWM initial learning phase revealed dose-dependent deficiencies after irradiation, expressed by a delayed learning process and a reduced amount of spatial searching. (A) Cumulative incidence of escape [%] from Day 1 to Day 5. Statistics: Log-rank test followed by Bonferroni correction, * = $P < 0.0083$. Each data point represents the mean of four training trials. (B) Swimming distance [cm] and swimming velocity [cm/s] over the course of five training days. Statistics: Two-way RM ANOVA followed by Tukey's multiple comparisons test, * = $P < 0.05$. Values are expressed as mean (SEM). (C) Use of spatial searching strategies [%] and direct finding [%] over the course of five training days. Statistics: Two-way RM ANOVA followed by Tukey's multiple comparisons test, * = $P < 0.05$, ** = $P < 0.01$, *** = $P < 0.001$. Values are expressed as mean (SEM). Black curves/bars represent Sham ($n = 10$), green curves/bars represent 0.125 Gy ($n = 10$), orange curves/bars represent 0.25 Gy ($n = 8$), blue curves/bars represent 0.5 Gy ($n = 10$).

The swimming distance and the swimming velocity over the course of the five training days were statistically compared using a Two-way RM ANOVA followed by Tukey's multiple comparisons test. Generally, a decline of the swimming distance is expected when learning proceeds. Such a decline was present in all groups from day 1 to day 5 of training. However, the Sham animals always swam shorter distances than the IR groups. There was an overall effect of training day ($F(4, 136) = 101.5, P < 0.0001$) and irradiation dose ($F(3, 34) = 3.2, P = 0.04$) without interaction ($F(12, 136) = 1.2, P = 0.28$). In accordance with the escape latencies, follow-up testing showed that the distance in the 0.5 Gy group dropped significantly less sharply compared to the Sham group on day 2 (Figure 8-2 B; $P = 0.02$) and day 3 (Figure 8-2 B; $P = 0.01$). Further,

both groups still differed in their swimming distance on day 4 and day 5 by tendency. The 0.125 Gy and 0.25 Gy irradiation dose had only lower impact, resulting in slightly increased distances from day 2 to day 5 of training compared to the Sham group (Figure 8-2 B). The swimming velocity of the animals dropped in all groups over the training phase. Overall, a main effect of training day ($F(4, 136) = 39.6, P < 0.0001$) was observed by ANOVA, but not for IR dose ($F(3, 34) = 1.6, P = 0.21$). Furthermore, post hoc testing showed that the 0.25 Gy animals swam significantly slower than 0.5 Gy animals on day 1 (Figure 8-2 B; $P = 0.049$). There was no difference between the Sham and the 0.125 Gy or 0.5 Gy group. Generally, all groups reached a plateau with ongoing training, albeit the 0.25 Gy mice still showed slightly decreased velocities from day 2 to 5. The development and the use of spatial searching strategies during the MWM are important parameters during proper spatial learning behaviour. Normally, mice first go through a set of non-spatial searching strategies, characterized by complex and inefficient swimming patterns. However, after a few training sessions the initially used strategies are superseded by more efficient spatial strategies, characterized by more targeted searching with shorter escape latencies and swim distances. These spatial strategies mirror the formation of an allocentric spatial map and thus the proper function of the hippocampus-dependent allocentric place navigation (Moghaddam & Bures, 1996; Morris, 1984; Morris et al., 1982, 1986; Vorhees & Williams, 2014). Accordingly, each MWM trial was assigned to one of eight searching strategies, based on the swimming paths and its prevailing pattern. Three of these searching strategies have been defined as spatial (for detailed explanation, see section 7.7 Data Generation and Statistics and Figure 7-15/Table 7-4). Spatial searching strategies were statistically compared using a Two-way RM ANOVA followed by Tukey's multiple comparisons test. Figure 8-2 C shows the percentage of spatial searching strategies used over the course of the five training days. Generally, the Sham animals reached higher amounts of spatial searching in the course of the training than the IR groups. Overall, there was a significant main effect of training day ($F(4, 136) = 44.8, P < 0.0001$) and applied dose ($F(3, 34) = 6.2, P = 0.002$). On day 1, all groups used on average less than 25 % spatial searching. This corresponds to less than one spatial trial per day and can be accepted as the expected value for the first training day. Despite the similar baseline, post hoc testing revealed a first trend for a lower amount of spatial searching in the IR groups on day 2, with $P = 0.05$ for the comparison between Sham and 0.5 Gy (Figure

8-2 C). Sham and 0.125 Gy animals used similar amounts of spatial strategies from day 1 to day 5, with the greatest, but not significant, difference on day 3 (Figure 8-2 C). The 0.25 Gy group assumed an intermediate position that was not significant compared to all the other IR groups, however follow-up testing gave a $P = 0.07$ for the comparison of 0.25 Gy and Sham on day 4 (Figure 8-2 C). The 0.125 Gy mice showed significantly more spatial searching strategies compared to 0.5 Gy animals on day 3 (Figure 8-2 C; $P = 0.02$) and day 5 (Figure 8-2 C; $P = 0.005$). Additionally, Tukey's multiple comparisons test gave $P = 0.05$ on day 4 for the comparison of 0.125 Gy and 0.5 Gy (Figure 8-2 C). The Sham group developed significantly more spatial searching compared to the 0.5 Gy mice on day 3, 4 and 5 (Figure 8-2 C; day 3: $P = 0.0001$, day 4: $P = 0.009$, day 5: $P = 0.005$). These results highlighted that the development of efficient spatial searching strategies was affected in a dose-dependent manner, prominent on each of the training days except day 1. Thus, the hippocampus-dependent allocentric place navigation was impaired after low-dose irradiation at E14.5.

Straight swimming paths to the hidden platform represent the most efficient spatial escape strategy during the MWM and highlight the accuracy of the formed allocentric spatial map. Therefore, effects of ionizing radiation on the firmness or precision of search and thus on the ability of direct platform localization were evaluated.

Accordingly, the percentage of this specific strategy was calculated. The use of the direct strategy was statistically compared using a Two-way RM ANOVA followed by Tukey's multiple comparisons test. Main effects of training day ($F(4, 48) = 5.9$, $P = 0.0006$) and IR dose ($F(3, 12) = 3.79$, $P = 0.04$) were evident. The Sham group developed the highest amount of direct platform search which tended to be greatly increased on day 4 compared to 0.25 Gy animals and significantly differed compared to all IR groups on day 5, as shown by follow-up testing (Figure 8-2 C; day 4: $P_{S/0.25} = 0.08$, day 5: $P_{S/0.125} = 0.047$, $P_{S/0.25} = 0.027$, $P_{S/0.5} = 0.015$).

Altogether, these results demonstrate that irradiation at E14.5 deteriorated the performance in an initial MWM phase in a dose-dependent manner compared to Sham irradiated animals. LDIR caused a delay in spatial memory acquisition in animals irradiated with 0.125 Gy, 0.25 Gy and 0.5 Gy. Interestingly, 0.125 Gy animals were able to catch up with the control group until day 5 of training regarding almost all analyzed parameters, except the direct platform finding. In contrast to that, a substantial number

of 0.25 Gy and 0.5 Gy mice still failed to achieve the Sham level on day 5 for those variables.

8.1.3 Probe Trial Revealed Disturbed Reference Memory

Following the training phase, a 60 s probe trial without platform was performed 24 h after the last training day. This procedure should reveal if the mice developed a proper reference memory of the platform position. Under normal circumstances, mice that successfully learned the current platform position are going to spend a substantial amount of time in the target quadrant searching for the platform.

First, a One-way ANOVA was conducted to compare the effect of IR dose on the distance covered. The analysis could not ascertain any significant overall effect of IR dose on the group means of distance (Figure 8-3 A; $F(3, 34) = 1.28, P = 0.3$). As a consequence, both the Sham and the IR groups searched with similar effort during probe testing. Subsequently, different parameters suitable to elucidate the consolidation of the reference memory for the trained platform position were evaluated. Therefore, the cumulative retention times within each of the four quadrants were compared, using a Two-way RM ANOVA followed by Tukey's multiple comparisons test. Overall, there was a significant main effect of quadrant ($F(3, 102) = 15.32, P < 0.0001$) and applied dose ($F(3, 34) = 4.09, P = 0.014$), as well as a significant effect on quadrant x dose interaction ($F(9, 102) = 2.72, P = 0.0069$). In contrast to the 0.5 Gy mice, the Sham, the 0.125 Gy and the 0.25 Gy group exceeded the statistical 25 % chance level within the SW sector and not in NE, NW and SE, indicating a preference for the target quadrant. Follow-up testing to assess between-group differences within the individual quadrants revealed a significantly decreased cumulative retention time for the SW target quadrant in the 0.5 Gy mice compared to Sham and 0.125 Gy. Even though, the 0.25 Gy animals outreached the 25 % chance level for SW, this difference was not significant towards the 0.5 Gy group (Figure 8-3 B; $P_{S/0.5} < 0.0001, P_{0.125/0.5} = 0.026$). Significant between-group differences could also be ruled out for the remaining three quadrants. When testing the individual groups for between-quadrant differences, both Sham and 0.125 Gy animals spend significantly more time in the SW quadrant compared to NE, NW and SE, highlighting the previously mentioned preference for the target sector (Figure 8-3 B; Sham: $P_{SW/NE} < 0.0001, P_{SW/NW} < 0.0001, P_{SW/SE} < 0.0001$; 0.125 Gy: $P_{SW/NE} = 0.0095, P_{SW/NW} = 0.0062, P_{SW/SE} = 0.0081$). In spite of the fact that

the 0.25 Gy mice exceeded the statistical 25 % chance level for the target sector, a significant time difference could only be determined for the comparison between SW and NW (Figure 8-3 B; $P_{SW/NW} = 0.016$). Thus, the assumed preference for the SW quadrant could not statistically be confirmed for the 0.25 Gy mice. Additionally, the representative heat maps in Figure 8-3 B also indicate a less focused, but rather a broadly expanded search window with longer retention times for the 0.5 Gy animals. In order to take a closer look at the effects of IR dose on the precision of search, a Kruskal-Wallis statistic was employed to compare the group means of frequency and cumulative retention time in the critical zone as well as the proximity to the former platform position (Figure 8-3 C, D and E). Overall, a progressive decrease in frequency and cumulative retention time as well as an increase in the distance between subject and platform were observed with increasing IR dose compared to Sham. The Kruskal-Wallis test revealed significant effects of IR dose on the cumulative retention time in the critical zone ($H = 11.5$, $P = 0.009$) and the proximity to former platform position ($H = 8.6$, $P = 0.035$). Even if the analysis could not reveal a statistical effect on the frequency in critical zone, the 0.5 Gy group was clearly reduced compared to Sham. Dunn 's multiple comparisons test showed statistically significant differences between Sham and 0.5 Gy for the cumulative retention time in the critical zone and the proximity to former platform position, but not for the frequency in critical zone (Figure 8-3 C, $P_{S/0.5} = 0.056$; Figure 8-3 D, $P_{S/0.5} = 0.005$; Figure 8-3 E, $P_{S/0.5} = 0.02$).

So far, the probe trial has corroborated the dose-dependent impairment of the learning process observed during the training. Additionally, the animals' reference memory which is addressed by removing the platform was significantly affected after irradiation with 0.5 Gy and at least a tendential memory deficit could be observed for 0.125 Gy and 0.25 Gy.

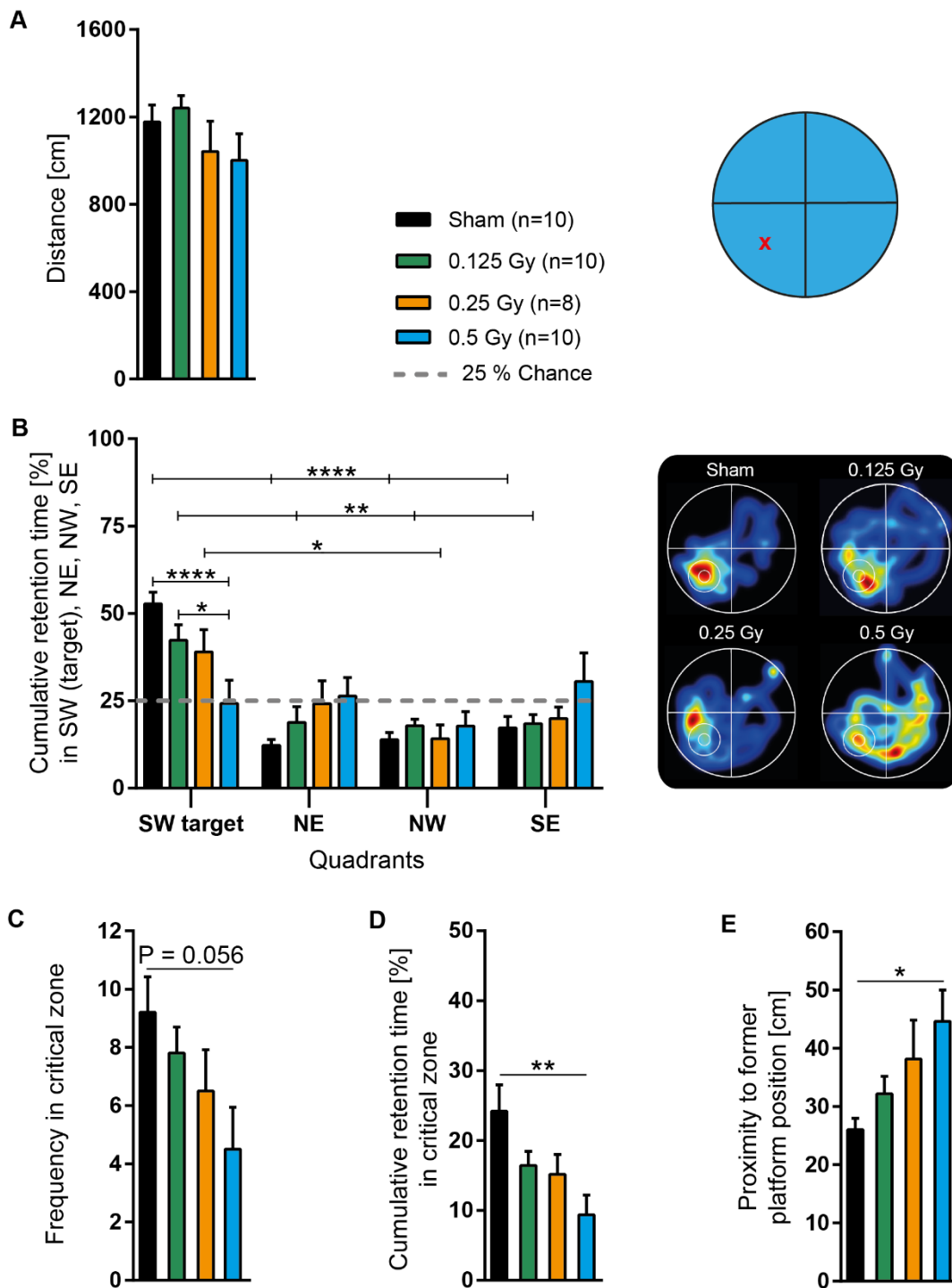


Figure 8-3: E14.5 MWM initial probe trial without platform revealed a dose-dependent decline in the preference for the target zones. (A) Swimming distance [cm] during the 60-second probe trial. Statistics: One-way ANOVA. (B) Cumulative retention time [%] in South-West (SW) target quadrant, North-East (NE), North-West (NW), South-East (SE). The dashed grey line represents 25 % chance. Statistics: Two-way RM ANOVA followed by Tukey's multiple comparisons test, * = $P < 0.05$, ** = $P < 0.01$, **** = $P < 0.0001$. Representative heat maps depicting both former position of platform/critical zone and areas of long retention time (red colors) and areas of short retention time (blue colors) within the MWM pool. (C) Frequency in critical zone. Statistics: Kruskal-Wallis test followed by Dunn's multiple comparisons test. (D) Cumulative retention time [%] in critical zone. Statistics: Kruskal-Wallis test followed by Dunn's multiple comparisons test, ** = $P < 0.01$. (E) Proximity to former platform position [cm]. Statistics: Kruskal-Wallis test followed by Dunn's multiple comparisons test, * = $P < 0.05$. Black bars represent Sham (n = 10), green bars represent 0.125 Gy (n = 10), orange bars represent 0.25 Gy (n = 8), blue bars represent 0.5 Gy (n = 10). All values are expressed as mean (SEM).

8.1.4 Initially Affected Spatial Memory was Improved during Reversal Learning

Accordingly, the platform was now centered in the North-East (NE) quadrant and a reversal learning phase was performed to test the memory acquisition for a new platform location.

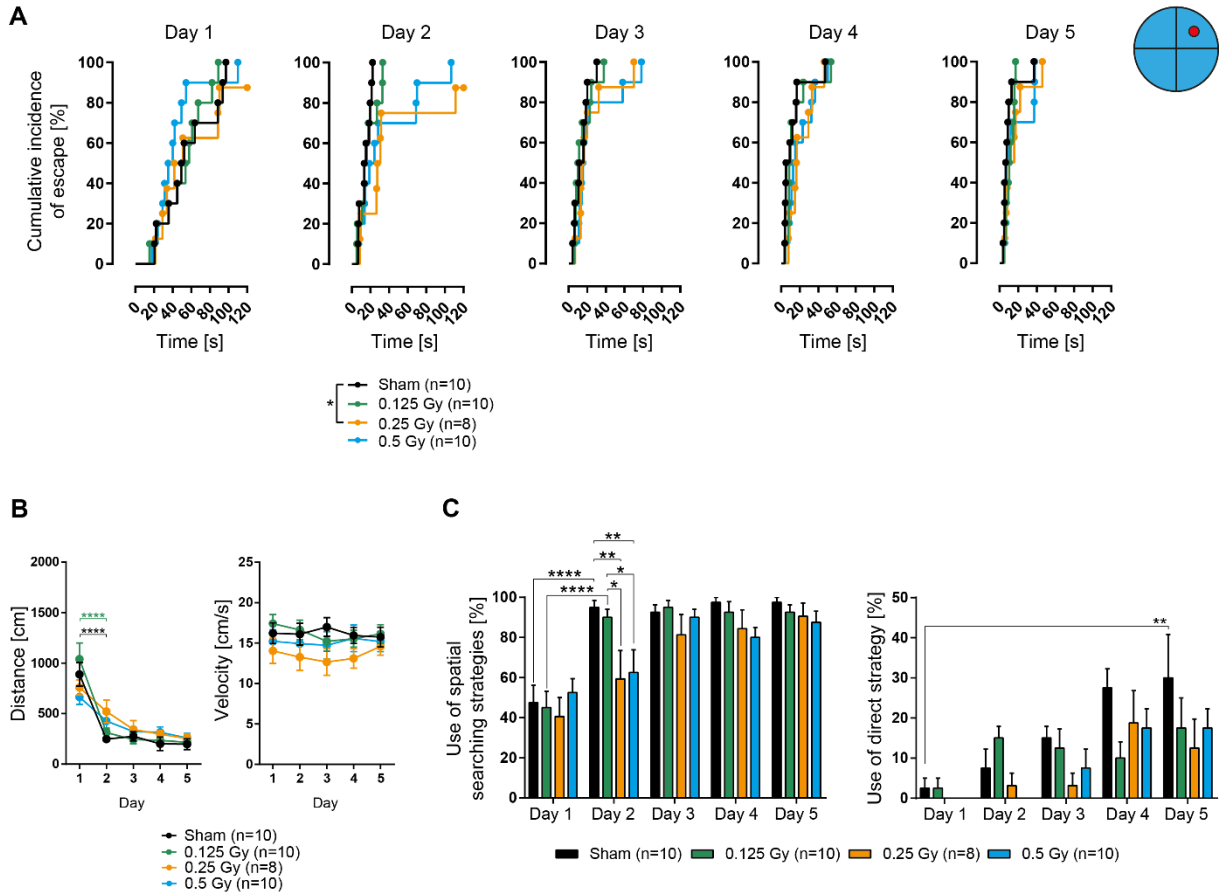


Figure 8-4: E14.5 MWM reversal learning phase revealed deficits after irradiation in the beginning of the training for a new platform location. (A) Cumulative incidence of escape [%] from Day 1 to Day 5. Statistics: Log-rank test followed by Bonferroni correction, * = $P < 0.0083$. Each data point represents the mean of four training trials. (B) Swimming distance [cm] and swimming velocity [cm/s] over the course of five training days. Statistics: Two-way RM ANOVA followed by Tukey's multiple comparisons test. Values are expressed as mean (SEM). (C) Use of spatial searching strategies [%] and direct finding [%] over the course of five training days. Statistics: Two-way RM ANOVA followed by Tukey's multiple comparisons test, * = $P < 0.05$, ** = $P < 0.01$, **** = $P < 0.0001$. Values are expressed as mean (SEM). Black curves/bars represent Sham (n = 10), green curves/bars represent 0.125 Gy (n = 10), orange curves/bars represent 0.25 Gy (n = 8), blue curves/bars represent 0.5 Gy (n = 10).

First, the cumulative incidence of escape was evaluated for the five reversal training days. Figure 8-4 A shows the corresponding Kaplan-Meier plots. In general, increased escape latencies were observed for Sham, 0.125 Gy and 0.25 Gy on the reversal training day 1, compared to day 5 of initial learning, as also indicated by their increased MOST. In contrast, the MOST of the 0.5 Gy group was on the same level as on day 5 of initial training (Figure 8-4 A).

On the second day of training, the Sham and the 0.125 Gy mice already strongly improved their performance and were able to outpace the 0.25 Gy and 0.5 Gy animals (Figure 8-4 A). A Log-rank analysis of this day showed a significant difference between the Sham and the 0.25 Gy curve ($P = 0.0037$). There was neither a statistical difference between 0.125 Gy and 0.25 Gy/0.5 Gy nor between Sham and 0.5 Gy, even if there were three animals in the 0.5 Gy group that showed increased mean latencies (Figure 8-4 A; 106.9 s, 70.1 s, 69.1 s). Regarding the comparison of Sham and 0.25 Gy, one mouse of the 0.25 Gy group had a very high mean escape latency of 111.5 s. A second mouse was not able to find the platform just one single time within four trials (120 s), thus leading to only 87.5 % of the animals being successful on this training day, while the other groups reached 100 %. In the course of the last three days of reversal training, all groups reached similar escape latencies with only minor differences (Figure 8-4 A). Figure 8-4 B reports the mean distance covered and the velocity over the training phase. The first reversal day was associated with increased swimming distances in Sham, 0.125 Gy and 0.25 Gy animals, matching the escape latency outcomes. Overall, Two-way RM ANOVA showed a main effect of training day ($F(4, 136) = 56.2, P < 0.0001$) but not of irradiation dose ($F(3, 34) = 0.54, P = 0.66$). Follow-up analysis with Tukey's test showed that the distance in Sham and 0.125 Gy animals dropped significantly in contrast to 0.25 Gy and 0.5 Gy mice between day 1 and 2 (Figure 8-4 B; Sham: $P_{1/2} < 0.0001$, 0.125 Gy: $P_{1/2} < 0.0001$). From day 3 to day 5, all group means reached plateaus at 200 to 300 cm. Distances between day 1 and 5 were significantly reduced in all groups (not highlighted in Figure 8-4 B; Sham: $P_{1/5} < 0.0001$; 0.125 Gy: $P_{1/5} < 0.0001$; 0.25 Gy: $P_{1/5} < 0.0001$; 0.5 Gy: $P_{1/5} = 0.0002$). The mean velocity remained constant in all groups during the whole training phase with slightly reduced velocities in the 0.25 Gy group (Figure 8-4 B). ANOVA testing could not reveal any significant effect of training day ($F(4, 136) = 1.8, P = 0.13$) or IR dose ($F(3, 34) = 0.9, P = 0.46$).

The groups started with a higher amount of spatial searching strategies on the first reversal day compared to day 1 of initial learning, indicating that the mice interiorized the test concept of finding a hidden platform to escape from the water (Figure 8-4 C). Interestingly, the Sham and 0.125 Gy animals were able to approximately double their amount of spatial searching already on day 2 of training, whereas 0.25 Gy and 0.5 Gy mice hardly improved. On the remaining three training days, all groups reached a high

level of spatial searching ($\geq 80\%$). Overall, there was a significant main effect of training day ($F(4, 136) = 42.6, P < 0.0001$), while the effect of the applied dose was not significant ($F(3, 34) = 2.4, P = 0.08$). Follow-up analysis with Tukey's multiple comparisons test disclosed a significant increase of spatial searching in the Sham and the 0.125 Gy animals from day 1 to day 2 in contrast to the 0.25 Gy/0.5 Gy mice (Figure 8-4 C; Sham: $P_{1/2} < 0.0001$, 0.125 Gy: $P_{1/2} < 0.0001$). Moreover, both Sham and 0.125 Gy mice showed significantly more spatial searching on day 2 compared to 0.25 Gy and 0.5 Gy ($P_{S/0.25} = 0.002, P_{S/0.5} = 0.004, P_{0.125/0.25} = 0.013, P_{0.125/0.5} = 0.02$). On that basis, the percentage of direct finding was further evaluated. Sham and 0.125 Gy animals used the direct platform localization from day 1 onwards, while 0.25 Gy animals started with direct localization on day 2 and 0.5 Gy animals on day 3. A higher amount of direct localization was found in Sham on day 4 and 5 compared to all IR groups (Figure 8-4 C). ANOVA testing revealed a significant main effect of training day ($F(4, 48) = 11.2, P < 0.0001$). Post hoc analysis showed that only the Sham mice were able to significantly increase the amount of direct finding between day 1 and 5 (Figure 8-4 C; Sham: $P_{1/5} = 0.0012$).

The results indicate that 0.25 Gy and 0.5 Gy irradiated mice improved their performance to the end of the reversal learning phase, although their learning process was still delayed between day 1 and day 2 compared to Sham and 0.125 Gy animals. In addition to that, the ability to use spatial strategies and direct finding to escape from the water was still diminished in the IR groups, albeit a significant deviation between the groups was not detectable.

8.1.5 Reversal Probe Testing Confirmed Proper Formation of Reference Memory

A One-way ANOVA analysis of the following probe trial did not show any significant effect of IR dose on the distance covered (Figure 8-5 A; $F(3, 34) = 0.59, P = 0.63$). Thus, similar effort during probe trial searching was assumed for all groups. Overall, there was a main effect of quadrant ($F(3, 102) = 54.0, P < 0.0001$) but not of IR dose ($F(3, 34) = 0.39, P = 0.77$), thus between-group differences could be ruled out and post-hoc testing was performed for the between-quadrant comparisons of the individual groups. Tukey's multiple comparisons test revealed significantly increased preferences of all groups for the target NE, especially compared to the SW sector (Figure 8-5 B;

Sham: $P_{NE/SW} < 0.0001$; 0.125 Gy: $P_{NE/SW} < 0.0001$; 0.25 Gy: $P_{NE/SW} = 0.0006$; 0.5 Gy: $P_{NE/SW} < 0.0001$). Kruskal-Wallis analyses for evaluation of search precision revealed significant effects on frequency in the new vs. the old critical zone ($H = 51.1$, $P < 0.0001$). Dunn's follow-up test showed significantly increased frequencies for all groups in the new critical zone (Figure 8-5 C; Sham: $P = 0.007$; 0.125 Gy: $P < 0.0001$; 0.25 Gy: $P = 0.04$; 0.5 Gy: $P = 0.004$).

These results demonstrate that the mice primarily searched in the target quadrant and there very specifically in the newly learned platform position. Accordingly, the animals could oblivate the old platform position to a great extent in favour of a new position. Furthermore, the probe trial confirmed the improvement of the IR groups during the second half of the reversal training.

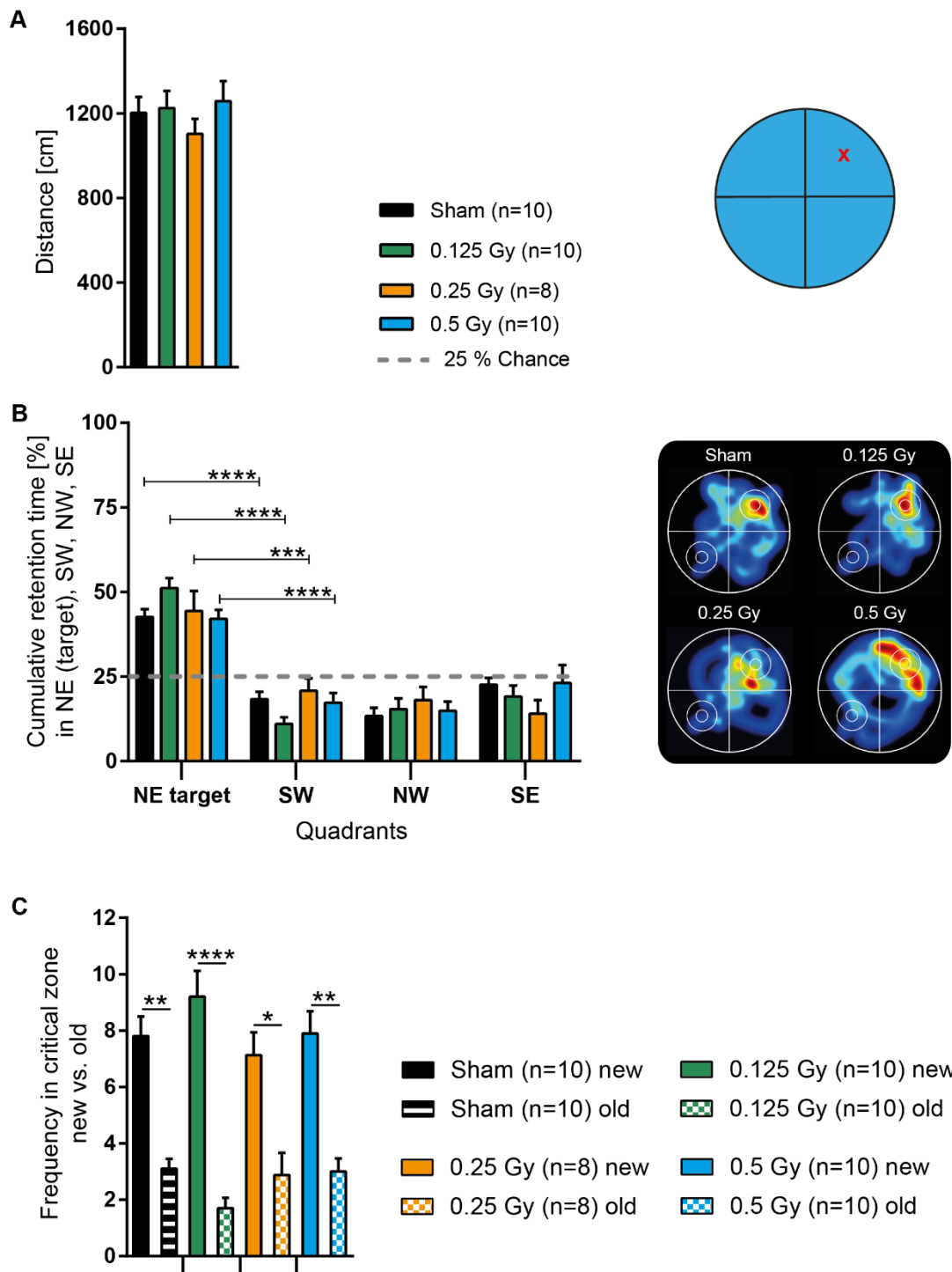


Figure 8-5: E14.5 MWM reversal probe trial showed that the IR groups could develop proper reference memories for a new platform position. (A) Swimming distance [cm] and swimming velocity [cm/s] during the 60-second probe trial. Statistics: One-way ANOVA (B) Cumulative retention time [%] in North-East (NE) target quadrant, South-West (SW), North-West (NW), South-East (SE). The dashed grey line represents 25 % chance. Statistics: Two-way RM ANOVA followed by Tukey's multiple comparisons test. Representative heat maps depicting both former positions of platform/critical zone (new vs. old) and areas of long retention time (red colors) and areas of short retention time (blue colors) within the MWM pool. (C) Frequency in critical zone new vs. old. Statistics: Kruskal-Wallis test followed by Dunn's multiple comparisons test, * = $P < 0.05$, ** = $P < 0.01$, **** = $P < 0.0001$. Plain/striped black bars represent Sham (n = 10), plain/checkered green bars represent 0.125 Gy (n = 10), plain/checkered orange bars represent 0.25 Gy (n = 8), plain/checkered red bars represent 0.5 Gy (n = 10). All values are expressed as mean (SEM).

8.1.6 Conclusion – Chapter I (E14.5)

In summary, it can be stated that the initial learning phase of the MWM unveiled deficiencies regarding the initial learning process in irradiated mice. Interestingly, the observed effects were more pronounced with increasing irradiation dose. Therefore, prenatal irradiation at E14.5 caused dose-dependent effects. The 0.125 Gy animals showed a learning delay compared to Sham animals that could be caught up almost completely during training. In contrast to that, the 0.25 Gy and the 0.5 Gy mice displayed learning deficits even towards the end of the initial learning phase. Search patterns were characterized by decreasing efficiency with increasing dose. Especially, the development of straight swimming paths was affected by irradiation. Direct swim patterns to the hidden platform represent the most efficient spatial escape strategy and are thus the silver bullet to success in the MWM test. Proper spatial platform targeting mirrors the proper functioning of the hippocampus-dependent allocentric place navigation and thus the formation of an adequate spatial map. During the MWM, start positions were semi-randomly chosen for each trial, so that the mice had to navigate allocentrically to the platform by remembering its coordinates relative to distant extramaze visual cues. (Moghaddam & Bures, 1996; Morris et al., 1982, 1986; Vorhees & Williams, 2014). Consequently, the results show that allocentric place navigation was affected after irradiation.

Unexpectedly, the irradiated mice performed better during reversal learning. The amount of spatial searching increased in the irradiated groups, indicating the formation of an allocentric spatial map. However, the precision of allocentric place navigation was still affected, as only the Sham mice significantly increased the percentage of direct platform localization. The irradiated animals were principally able to learn a platform position but especially the initial confrontation with the MWM test was caused them some problems and revealed a delay in spatial map formation.

9 Chapter II – Evaluation of Long-term Radiation Risk and Sensitivity for the Time Point P10

The second chapter of this thesis deals with the long-term effects of postnatal low-dose irradiation in C57BL/6 mice. As for the time point E14.5, the mice were characterized in a series of behavioural tests addressing the motor abilities, activity-/exploration- and anxiety-related properties and the development of spatial reference memory. Single low X-ray doses from 0 Gy (Sham) to 0.5 Gy were whole-body applied at P10. The offspring was analyzed for the different behavioural aspects at the age of two months to evaluate the risk of radiation exposure and the sensitivity of this specific phase of brain maturation.

9.1 Results

9.1.1 Effects on Motor Performance and Activity/Exploration Behaviour (P10)

The analysis of motor function with the accelerating Rotarod did not reveal any difference between Sham and the IR groups regarding the time spent on the rotating bar (Fig. 9-1 A; Kruskal-Wallis test; $H = 2.59$, $P = 0.46$). All mice were able to maintain balance on the Rotarod and reached about 90 % of the maximum time on average. Hence, the motor function was unaffected by postnatal irradiation and a physical handicap during the following tests could be excluded.

Next, the Elevated Zero Maze (EZM) was performed to test the exploration/activity and anxiety of the animals. The mice were allowed to move within the maze for 30 minutes. A Kruskal-Wallis statistic revealed significant differences among the group means of the distance covered and the velocity during exploration (Figure 9-1 B; distance: $H = 8.71$, $P = 0.033$; velocity: $H = 12.42$, $P = 0.0061$).

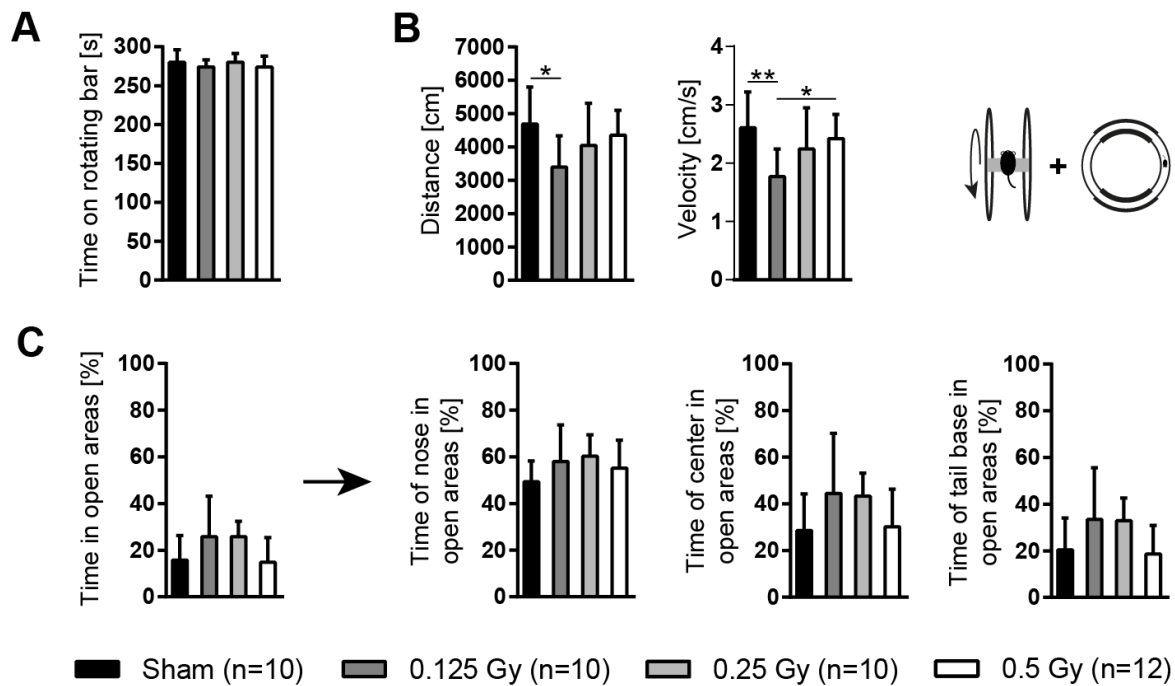


Figure 9-1: LDIR did not affect motor performance (Rotarod) but caused dose-specific effects on activity behaviour (Elevated Zero Maze). 0.125 Gy mice showed a reduced distance covered and a reduced velocity in the EZM. (A) Time spent on the rotating bar [s]. Statistics: Kruskal-Wallis test. (B) Distance [cm] and velocity [cm/s] during the 30-minute EZM testing phase. Statistics: One-way ANOVA followed by Tukey's multiple comparisons test. * = $P < 0.05$, ** = $P < 0.01$ (C) Time [%] spent in open areas of the EZM for the case when animals left the sheltered areas with the entire body contour and for the three individually tracked body points (nose, center, tail base). Statistics: Kruskal-Wallis test. Black bars represent Sham (n = 10), dark grey bars represent 0.125 Gy (n = 10), light grey bars represent 0.25 Gy (n = 10), white bars represent 0.5 Gy (n = 12). All values are expressed as mean (SD).

The follow-up analysis with Tukey's multiple comparisons test showed a significantly reduced mean distance for the 0.125 Gy mice compared to Sham ($P = 0.042$). Moreover, the mean velocity was significantly diminished in the 0.125 Gy group compared to Sham ($P = 0.007$) and 0.5 Gy ($P = 0.028$). The discrepancy between 0.125 Gy and 0.25 Gy was not significant (Figure 9-1 B). Obviously, the activity and exploration behaviour was affected in 0.125 Gy animals, as seven out of ten 0.125 Gy animals were clearly below the average of the Sham control group. Seemingly, irradiation at the postnatal time point influenced another behavioural component of the EZM test than irradiation at the prenatal time point regarding the same dose (for comparison see Figure 8-1). Furthermore, a Kruskal-Wallis analysis, did not show effects among the time spent in open areas that describes the case when all body points are situated in the open areas. It was apparent that all groups preferred the closed over the open areas, as indicated by a minor percentage between 15 % and 25 % (Figure 9-1 C). The more detailed evaluation of the three individual body points suggested

increased retention times outside the sheltered areas for center and tail base in 0.125 Gy and 0.25 Gy animals. However, Kruskal-Wallis testing could not uncover significant effects on nose, center or tail base. Consequently, the results did not indicate an altered anxiety level in 0.125 Gy, 0.25 Gy and 0.5 Gy mice compared to Sham.

9.1.2 Initial Learning Uncovers Dose-dependent Learning Delays

The mice were trained for five days in the initial learning phase of the MWM and analyzed for hippocampus-dependent learning deficits. The platform was constantly located in the center of the SW quadrant, as during analysis of time point E14.5.

On the first day of training, the Kaplan-Meier plots of Sham, 0.25 Gy and 0.5 Gy had similar curve shapes while the 0.125 plot was characterized by a slight right shift. However, a significant deviation in the cumulative incidence of escape from control could not be detected (Figure 9-2 A). Generally, a left shift of the Sham curve was observed over the training course, displaying a clear decrease in escape latencies already on training day 2. In contrast to that, the animals irradiated with the highest dose of 0.5 Gy hardly improved their performance. Both the 0.125 Gy mice and the 0.25 Gy mice ranged between Sham and 0.5 Gy and could catch up to Sham on the last training day, as also indicated by their median overall swimming times (MOST). Significant differences in the Kaplan-Meier curves were detected on day 2 between Sham and 0.25 Gy/0.5 Gy (Figure 9-2 A; $P_{S/0.25} = 0.005$; $P_{S/0.5} = 0.001$) and on day 4 between Sham and 0.5 Gy (Figure 9-2 A; $P_{S/0.5} = 0.008$). Despite the fact that the 0.5 Gy curve still showed animals with increased escape latencies or even animals that could not localized the platform once within 4 trials on day 5, a significant deviation from control could not be shown (Figure 9-2 A). On none of the days, the percentage of 0.5 Gy animals succeeding in platform localization reached 100 %.

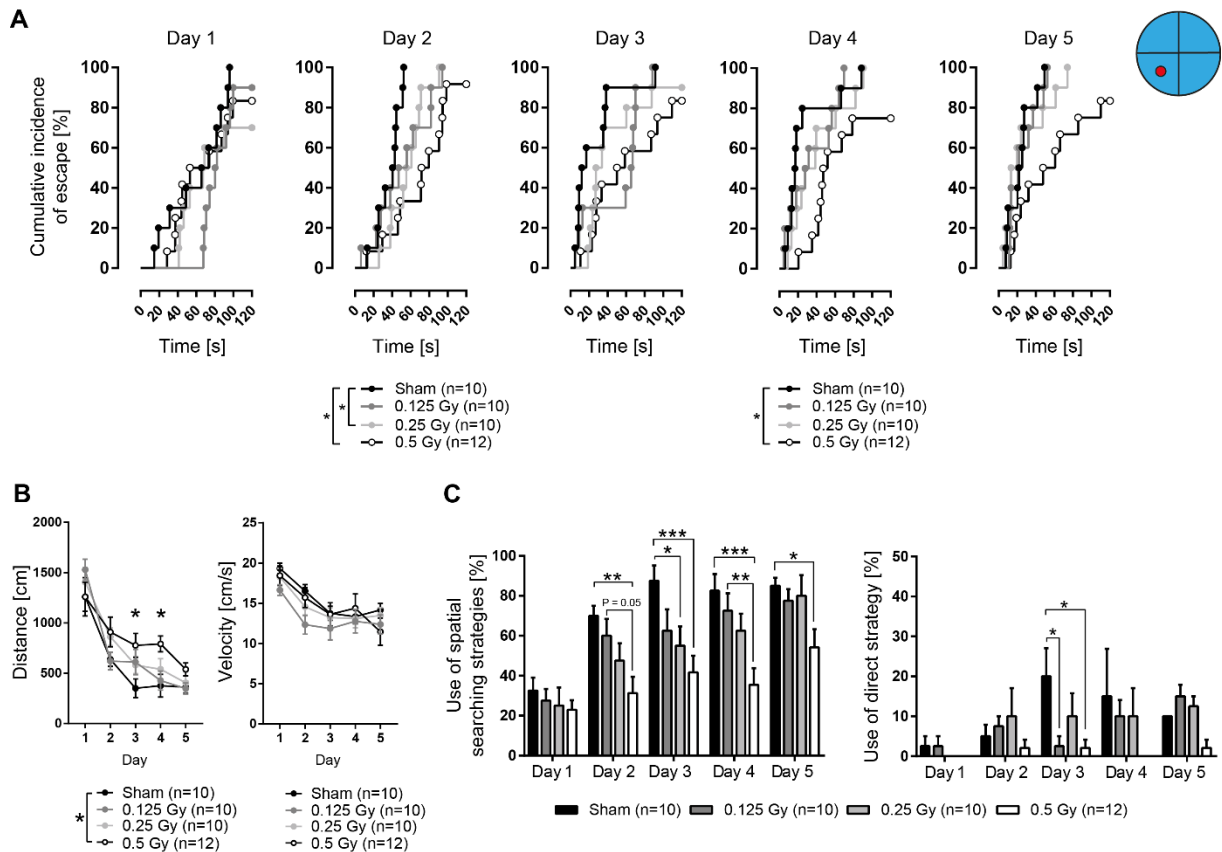


Figure 9-2: P10 MWM initial learning phase revealed dose-dependent impairment after irradiation, expressed by a delayed learning process and a reduced percentage of spatial searching. (A) Cumulative incidence of escape [%] from Day 1 – Day 5. Statistics: Log-rank test followed by Bonferroni correction, * = $P < 0.0083$. Each data point represents the mean of four training trials. **(B)** Swimming distance [cm] and swimming velocity [cm/s] over the course of five training days. Statistics: Two-way RM ANOVA followed by Tukey’s multiple comparisons test, * = $P < 0.05$. Values are expressed as mean (SEM). **(C)** Use of spatial searching strategies [%] and direct finding [%] over the course of five training days. Statistics: Two-way RM ANOVA followed by Tukey’s multiple comparisons test, * = $P < 0.05$, ** = $P < 0.01$, *** = $P < 0.001$. Values are expressed as mean (SEM). Black curves/bars represent Sham ($n = 10$), dark grey curves/bars represent 0.125 Gy ($n = 10$), light grey curves/bars represent 0.25 Gy ($n = 10$), black curves with open circles/bars represent 0.5 Gy ($n = 12$).

The swimming distances, as depicted in Figure 9-2 B, were alike on day 1 and decreased with ongoing training in all groups. The Sham animals showed the strongest decline on day 3 and stayed on this plateau until day 5. By contrast, the 0.5 Gy animals showed a slower decrement in distance and never reached the same level as Sham. Both 0.125 Gy and 0.25 Gy mice showed slightly increased distances compared to Sham on day 3. Two-way RM ANOVA testing revealed a significant effect of training day ($F(4, 152) = 66.2, P < 0.0001$). Tukey’s follow-up test showed significantly increased distances in 0.5 Gy mice compared to Sham on day 3 (Figure 9-2 B; $P = 0.029$) and day 4 (Figure 9-2 B; $P = 0.035$). The swimming velocities decreased slightly in all groups during the training phase. Overall, Two-way RM ANOVA yielded a main effect of training day ($F(4, 152) = 36.13, P < 0.0001$) but not of IR dose ($F(3, 38) = 0.78, P = 0.5$). Post-hoc

testing did not reveal any significant difference between the group means (Figure 9-2 B).

Each MWM trial was further classified into spatial and non-spatial based on the prevailing search pattern. The daily percentage of spatial searching was statistically compared using a Two-way RM ANOVA followed by Tukey's post hoc test. Overall, there was a significant main effect of training day ($F(4, 152) = 26.1, P < 0.0001$) and applied dose ($F(3, 38) = 8.3, P = 0.0002$). Figure 9-2 C shows the corresponding bar graph. On day 1, all groups started with a similar amount of spatial searching (Figure 9-2 C). Despite the similar baseline, follow-up testing revealed a significant difference between Sham and 0.5 Gy and a first trend for less spatial searching in 0.5 Gy compared to 0.125 Gy on day 2 (Figure 9-2 C; $P_{S/0.5} = 0.0036, P_{0.125/0.5} = 0.05$). The 0.25 Gy group did not significantly differ from any of the other groups on this day. Sham and 0.125 Gy animals used similar amounts of spatial strategies from day 1 to day 5, with a greater deviation on day 3 (Figure 9-2 C). The third training day, revealed a significant reduction of spatial searching in 0.25 Gy and 0.5 Gy animals compared to control (Figure 9-2 C; $P_{S/0.25} = 0.03, P_{S/0.5} = 0.0004$). On day 4, both the 0.125 Gy and the 0.25 Gy group could improve, ending up with a significant disparity between 0.125 Gy and 0.5 Gy, while the 0.25 Gy group could not be statistically distinguished anymore from Sham. The Sham mice still showed significantly more spatial searching than 0.5 Gy animals on this day (Figure 9-2 C; $P_{S/0.5} = 0.0002, P_{0.125/0.5} = 0.006$). The last training day revealed that 0.125 Gy and 0.25 Gy animals were able to nearly reach the Sham level while spatial searching in the 0.5 Gy group was still significantly reduced (Figure 9-2 C; $P_{S/0.5} = 0.03$). The results highlight that the development of efficient spatial searching strategies was impaired in a dose-dependent manner, prominent on all training days except day 1. Thus, low-dose irradiation at P10 also impaired the hippocampus-dependent allocentric place navigation and the formation of a spatial map.

Overall, a Two-way RM ANOVA of direct platform localization indicated effects of IR dose ($F(3, 12) = 3.4, P = 0.05$) and training day ($F(4, 48) = 2.5, P = 0.06$). Tukey's test revealed statistically significant deviations from Sham for 0.125 Gy and 0.5 Gy mice on day 3 (Figure 9-2 C; $P_{S/0.125} = 0.038, P_{S/0.5} = 0.032$). Generally, the 0.5 Gy animals were unable to develop considerable direct finding to localize the platform, as indicated

by permanently and substantially low percentage values for this strategy (Figure 9-2 C).

In summary, it can be stated that the results highlight a dose-dependent impairment of spatial learning in an initial MWM phase after low-dose irradiation at P10, reflecting the lack of a proper allocentric spatial map.

9.1.3 Disturbed Reference Memory during Probe Trial

After finishing the training phase, a probe trial without platform should reveal if the mice developed a proper reference memory of the platform position.

First, a One-way ANOVA was conducted to compare the effect of IR dose on the distance covered. The analysis revealed an overall dose effect on the group means of distance (Figure 9-3 A; $F(3, 38) = 3.0, P = 0.04$). The corresponding graph shows a strong trend towards a decline after irradiation with 0.5 Gy compared to Sham and 0.25 Gy, however, post-hoc analysis with Tukey's test was not significant (Figure 9-3 A; $P_{S/0.5} = 0.087, P_{0.25/0.5} = 0.063$). Nevertheless, the effort during the 60 s probe testing was assumed to be reduced in 0.5 Gy mice, when the escape from water by finding the platform was impossible.

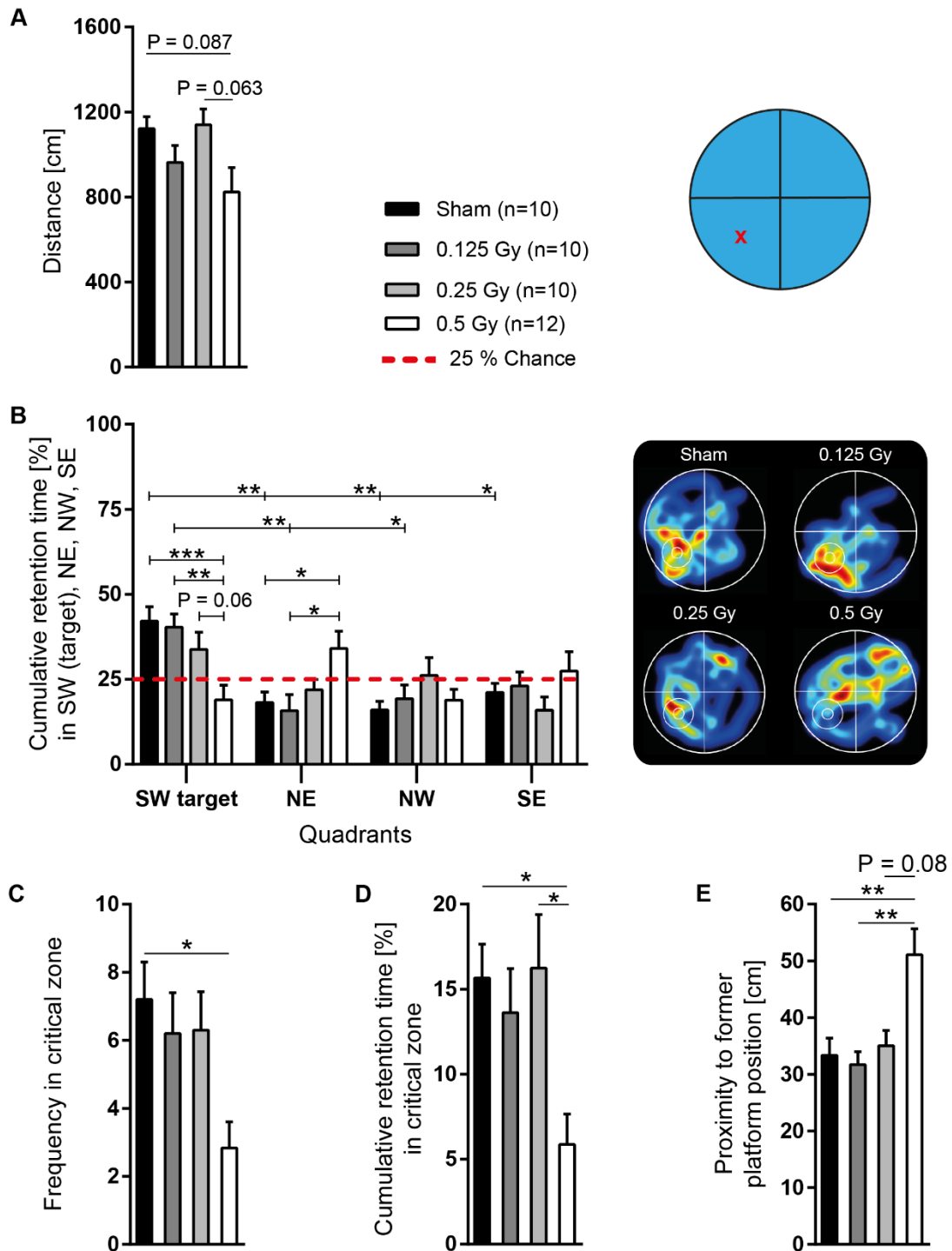


Figure 9-3: P10 MWM initial probe trial without platform revealed a dose-dependent decline in the preference for target zones. (A) Swimming distance [cm] during the 60-second probe trial. Statistics: One-way ANOVA followed by Tukey's multiple comparisons test. (B) Cumulative retention time [%] in South-West (SW) target quadrant, North-East (NE), North-West (NW), South-East (SE). The dashed red line represents 25 % chance. Statistics: Two-way RM ANOVA followed by Tukey's multiple comparisons test, * = $P < 0.05$, ** = $P < 0.01$, *** = $P < 0.001$. Representative heat maps depicting both former position of platform/critical zone and areas of long retention time (red colors) and areas of short retention time (blue colors) within the MWM pool. (C) Frequency in critical zone. Statistics: Kruskal-Wallis test followed by Dunn's multiple comparisons test, * = $P < 0.05$. (D) Cumulative retention time [%] in critical zone. Statistics: Kruskal-Wallis test followed by Dunn's multiple comparisons test, * = $P < 0.05$. (E) Proximity to former platform position [cm]. Statistics: Kruskal-Wallis test followed by Dunn's multiple comparisons test, ** = $P < 0.01$. Black bars represent Sham ($n = 10$), dark grey bars represent

0.125 Gy (n = 10), light grey bars represent 0.25 Gy (n = 10), white bars represent 0.5 Gy (n = 12). All values are expressed as mean (SEM).

The cumulative retention times within each of the four quadrants were compared, using a Two-way RM ANOVA followed by Tukey's multiple comparisons test. Overall, there was a significant main effect of quadrant ($F(3, 114) = 6.47, P = 0.0004$) and applied dose ($F(3, 38) = 4.24, P = 0.011$). Generally, in contrast to the 0.5 Gy group, Sham, 0.125 Gy and 0.25 Gy mice exceeded the statistical 25 % chance level within the SW sector but not in NE, NW and SE, indicating a preference for the target quadrant. Follow-up testing to show between-group differences within the individual quadrants revealed significant differences in the cumulative retention time in the target quadrant between Sham and 0.5 Gy and between 0.125 Gy and 0.5 Gy (Figure 9-3 B; $P_{S/0.5} = 0.0007, P_{0.125/0.5} = 0.0021$). Even though, the 0.25 Gy animals outreached the 25 % chance level for SW, this difference was not significant towards the 0.5 Gy group (Figure 9-3 B; $P_{0.25/0.5} = 0.06$). Significantly increased retention times in the NE quadrant were observed for 0.5 Gy compared Sham and 0.125 Gy (Figure 9-3 B; $P_{S/0.5} = 0.038, P_{0.125/0.5} = 0.012$). Analysis of between-quadrant differences showed that only the Sham group prioritized SW significantly over all remaining three quadrants ($P_{SW/NE} = 0.006, P_{SW/NW} = 0.002, P_{SW/SE} = 0.02$). Significant differences for the 0.125 Gy group were detected between SW and NE ($P_{SW/NE} = 0.004$) and between SW and NW ($P_{SW/NW} = 0.02$). A substantial difference between SW and the other quadrants could not be ascertained for both the 0.25 Gy animals and the 0.5 Gy animals (Figure 9-3 B). Additionally, heat maps also indicated a less focused, but rather a broadly expanded search window in mice irradiated with 0.25 Gy and 0.5 Gy (representative examples in Figure 9-3 B). Effects of IR dose on the precision of search were investigated next. A Kruskal-Wallis statistic was employed to compare the group means of frequency and cumulative retention time in the critical zone as well as the proximity to the former platform position (Figure 9-3 C, D and E). In general, the 0.125 Gy and 0.25 Gy dose had only minor effects on these parameters when compared to Sham. In contrast to that, 0.5 Gy animals showed a substantially reduced frequency and cumulative retention time in the critical zone as well as an increased distance to the former platform position. Overall, there were significant effects of IR dose on the frequency ($H = 10.2, P = 0.017$) and the cumulative retention time ($H = 10.3, P = 0.016$) in the critical zone. Additionally, there was an effect on the proximity to the former platform position ($H = 12.8, P =$

0.005). Dunn's post-hoc test showed significant differences between Sham and 0.5 Gy for each of the three analyzed parameters. In addition to that, the 0.5 Gy group showed significantly increased distances to the former platform position compared to the 0.125 Gy animals. Moreover, the 0.5 Gy group showed a significant deviation from 0.25 Gy for the parameter cumulative retention time in critical zone. The comparison of 0.5 Gy and 0.25 Gy for the proximity to former platform position was not significant, even if a difference was obvious (Figure 9-3 C, D and E; Frequency in critical zone: $P_{S/0.5} = 0.02$; Cumulative retention time in critical zone: $P_{S/0.5} = 0.04$, $P_{0.25/0.5} = 0.04$; Proximity to the former platform position: $P_{S/0.5} = 0.0099$, $P_{0.125/0.5} = 0.0056$, $P_{0.25/0.5} = 0.08$).

9.1.4 Performance of Irradiated Mice was Improved during Reversal Training

In the next step, the platform was centered in the North-East (NE) quadrant and reversal learning was performed to test the memory acquisition for a new platform location.

When analyzing the cumulative incidence of escape on the first reversal training day, the animals needed more time to find the platform compared to day 5 of initial learning, as indicated by prolonged escape latencies and their increased MOST on reversal day 1 (Figure 9-4 A) compared to initial day 5 (Figure 9-2 A).

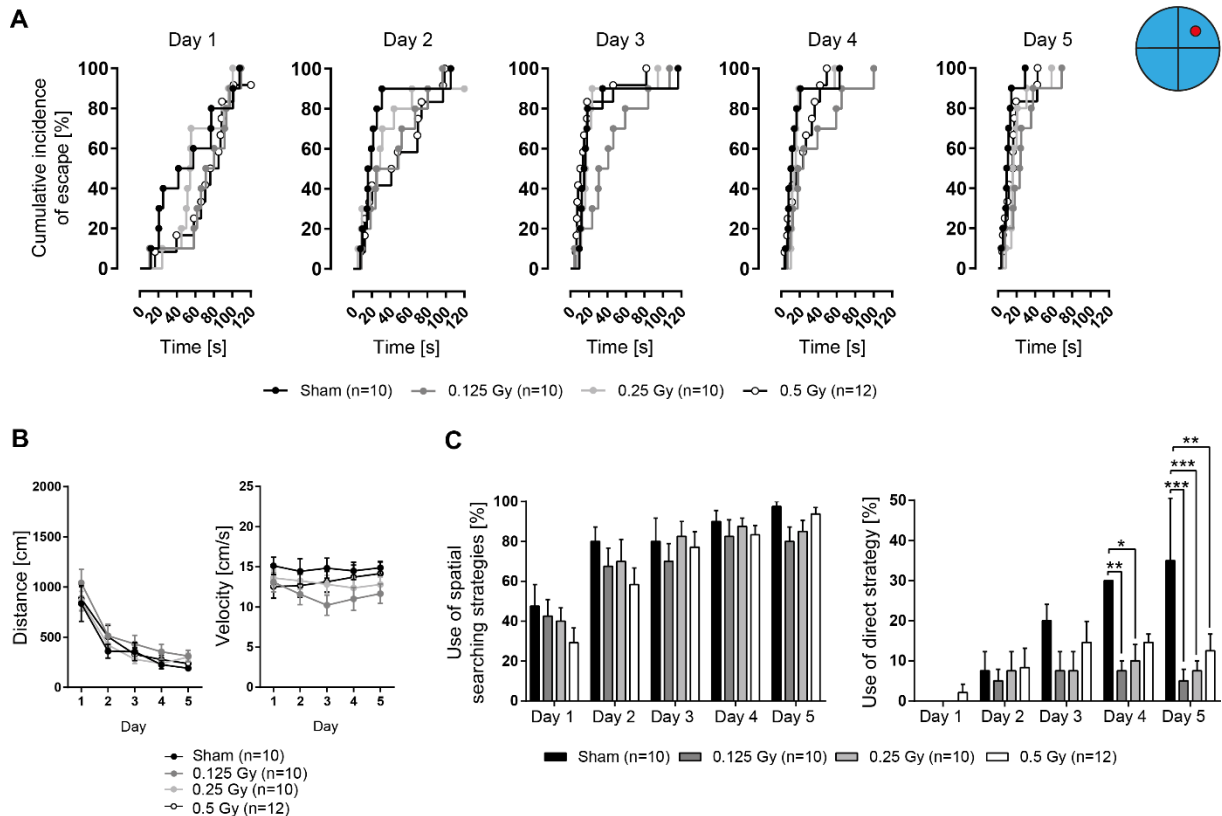


Figure 9-4: P10 IR groups improved their MWM performance in a reversal learning phase. However, differences in direct platform localization were evident. (A) Cumulative incidence of escape [%] from Day 1 to Day 5. Statistics: Log-rank test followed by Bonferroni correction, * = $P < 0.0083$. Each data point represents the mean of four training trials. **(B)** Swimming distance [cm] and swimming velocity [cm/s] over the course of five training days. Statistics: Two-way RM ANOVA followed by Tukey's multiple comparisons test. Values are expressed as mean (SEM). **(C)** Use of spatial searching strategies [%] and direct finding [%] over the course of five training days. Statistics: Two-way RM ANOVA followed by Tukey's multiple comparisons test. * = $P < 0.05$, ** = $P < 0.01$, *** = $P < 0.001$. Values are expressed as mean (SEM). Black curves/bars represent Sham (n = 10), dark grey curves/bars represent 0.125 Gy (n = 10), light grey curves/bars represent 0.25 Gy (n = 10), black curves with open circles/bars represent 0.5 Gy (n = 12).

From day 2 on, all groups strongly improved their performance within the five training days as indicated by the left shift of the Kaplan-Meier plots, similarly reduced MOST on day five (Figure 9-4 A) and by their declining swimming distances (Figure 9-4 B). The mean velocity remained constant in all groups during the training phase with slightly reduced velocities in the 0.125 Gy group on day 3 (Figure 9-4 B). However, Two-way RM ANOVA testing could neither reveal any significant effect of training day ($F(4, 152) = 1.1, P = 0.35$) nor IR dose ($F(3, 38) = 1.3, P = 0.28$). Moreover, each group started with a reduced amount of spatial searching on the first day but strongly improved their search from day 2 onwards, reaching 80 % and more spatial searching on day 5 (Figure 9-4 C). A Two-way RM ANOVA analysis showed a significant effect of training day ($F(4, 152) = 41.6, P < 0.0001$) but not of IR dose ($F(3, 38) = 0.87, P = 0.46$).

Interestingly, all irradiated groups showed deficits in the development of a direct strategy compared to Sham on day 4 and 5 (Figure 9-4 C). Two-way RM ANOVA testing revealed a significant main effect of training day ($F(4, 48) = 6.5, P = 0.0003$) and IR dose ($F(3, 12) = 8.9, P = 0.0022$). Post-hoc analysis showed that the Sham mice localized the platform significantly more often with the direct strategy than the irradiated groups (Figure 9-4 C; day 4: $P_{S/0.125} = 0.0093, P_{S/0.25} = 0.025$; day 5: $P_{S/0.125} = 0.0003, P_{S/0.25} = 0.001, P_{S/0.5} = 0.0093$).

Overall, the results show that the irradiated mice improved their spatial learning performance during a reversal learning phase, although they still had difficulties in developing a direct search pattern as seen in control animals, suggesting the formation of a less precise spatial map.

9.1.5 Reversal Probe Test Confirmed Improved Reference Memory

A One-way ANOVA analysis of the following probe trial showed a significant effect of IR dose on the distance covered (Figure 9-5 A; $F(3, 38) = 4.69, P = 0.007$). Post-hoc analysis with Tukey's test revealed a significantly decreased distance in 0.125 Gy mice compared to Sham (Figure 9-5 A; $P_{S/0.125} = 0.0045$). Overall, Two-way RM ANOVA testing showed a main effect of quadrant ($F(3, 114) = 55.3, P < 0.0001$) on the cumulative retention time. Post-hoc testing was performed for the between-quadrant comparisons of the individual groups. Here, significantly increased preferences of all groups for the target NE were observed compared to the old target sector SW (Figure 9-5 B; Sham: $P_{NE/SW} < 0.0001$; 0.125 Gy: $P_{NE/SW} = 0.013$; 0.25 Gy: $P_{NE/SW} < 0.0001$; 0.5 Gy: $P_{NE/SW} < 0.0001$). Additionally, a Kruskal-Wallis analysis showed a significant effect on frequency ($H = 55.3, P < 0.0001$) in the new vs. the old critical zone. Dunn's follow-up test revealed significantly increased frequencies in Sham, 0.25 Gy and 0.5 Gy mice for the comparisons between new and old critical zone. The 0.125 Gy animals did not differ statistically between new and old critical zone (Figure 9-5 C; Sham: $P = 0.001$; 0.125 Gy: $P = 0.76$; 0.25 Gy: $P = 0.0006$; 0.5 Gy: $P < 0.0001$).

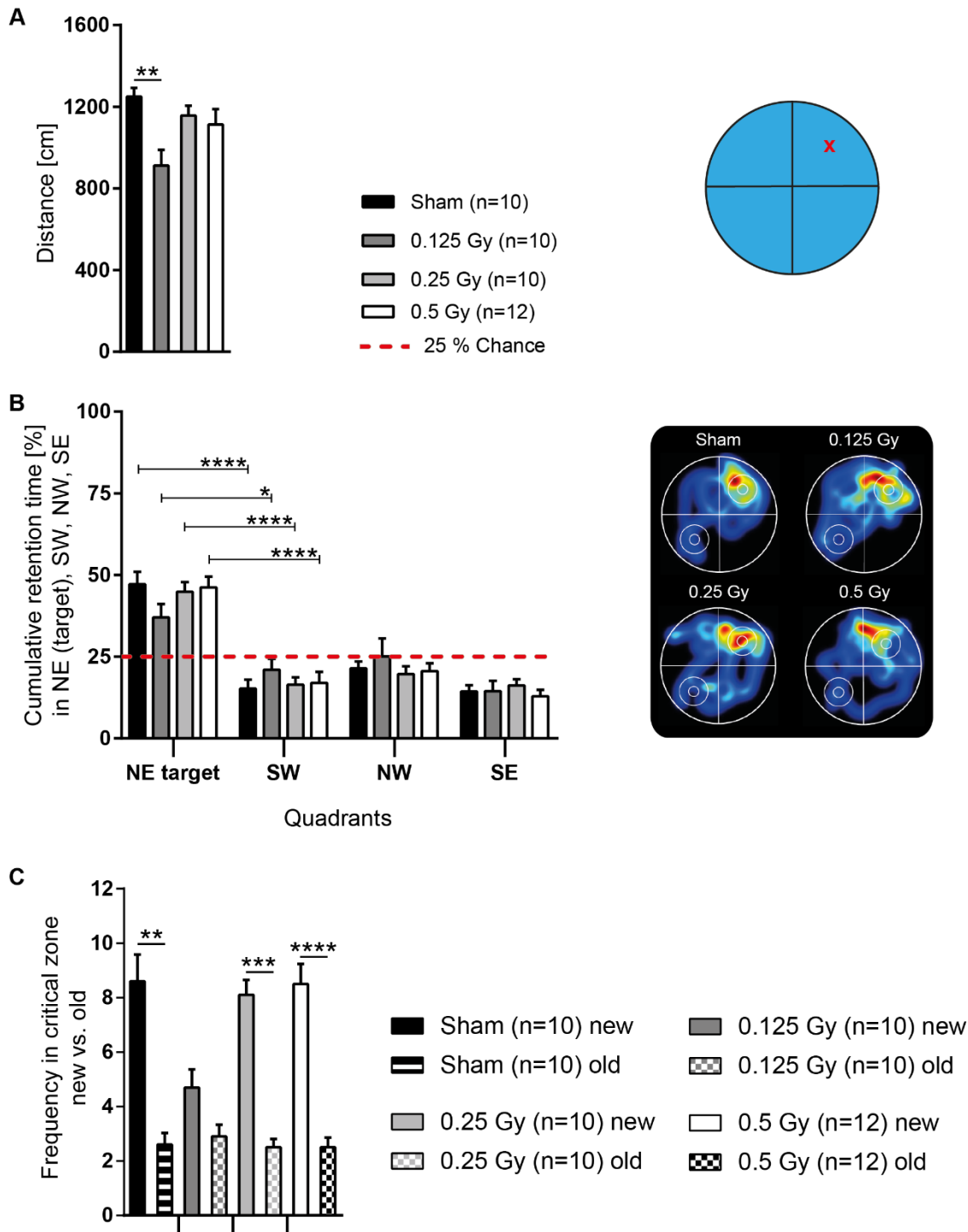


Figure 9-5: MWM reversal probe trial showed that IR groups developed proper reference memory for a new platform position. However, the 0.125 Gy group performed slightly worse than the other groups. (A) Swimming distance [cm] during the 60-second probe trial. Statistics: One-way ANOVA followed by Tukey’s multiple comparisons test. ** = $P < 0.01$. **(B)** Cumulative retention time [%] in North-East (NE) target quadrant, South-West (SW), North-West (NW), South-East (SE). The dashed red line represents 25 % chance. Statistics: Two-way RM ANOVA followed by Tukey’s multiple comparisons test. Representative heat maps depicting both former positions of platform/critical zone (new vs. old) and areas of long retention time (red colors) and areas of short retention time (blue colors) within the MWM pool. **(C)** Frequency in critical zone new vs. old. Statistics: Kruskal-Wallis test followed by Dunn’s multiple comparisons test, ** = $P < 0.01$, *** = $P < 0.001$, **** = $P < 0.0001$. Plain/striped black bars represent Sham control ($n = 10$), plain/checkered dark grey bars represent 0.125 Gy ($n = 10$), plain/checkered light grey bars represent 0.25 Gy ($n = 10$), plain/checkered white bars represent 0.5 Gy ($n = 12$). All values are expressed as mean (SEM).

The results demonstrate that all mice principally searched in the target quadrant. However, a very specific search for the newly learned platform position within a critical zone was only observed for Sham, 0.25 Gy and 0.5 Gy. The 0.125 Gy animals were less precise in searching for the new platform location. Additionally, their search pattern was associated with less effort. Accordingly, animals irradiated with the two higher doses could obliterate the old platform position to a great extent in favour of a new position. Furthermore, mice irradiated with the lowest dose had minor difficulties in learning a new position.

9.2 Conclusion – Chapter II (P10)

In summary, it can be stated that the initial learning phase of the MWM unveiled deficiencies regarding the learning process in postnatally irradiated mice similar to an irradiation at E14.5. The observed impairment was also stronger with increasing irradiation dose. Thus, postnatal irradiation at P10 caused dose-dependent effects. Both the 0.125 Gy and the 0.25 Gy animals showed a learning delay compared to Sham animals that could be caught up almost completely during training. In contrast to that, the 0.5 Gy mice displayed learning deficits even towards the end of the learning phase. The efficiency of spatial searching was diminished with increasing dose. As shown for E14.5, the development of straight swimming paths was likewise affected by irradiation. Consequently, the formation of an allocentric spatial map and place navigation was impaired after irradiation. The probe trial results show that at least the 0.5 Gy irradiation impaired the learning process during the training phase to the extent that the development of proper spatial reference memory was disturbed. The weakened performance during the probe test could partially be due to a reduced searching effort in the 0.5 Gy group. The IR mice improved during reversal learning, however, the development of direct localization was still present, as only the Sham mice significantly increased the percentage of direct platform localization. It seems that the irradiated animals were principally able to learn a platform position but especially the initial phase of the MWM test procedure was characterized by the absence of a proper allocentric spatial map, resulting in worse performance.

10 Chapter III – Effects of LDIR on MWM Learning Phases

After the evaluation of low-dose radiation exposure during critical phases of brain development and maturation, the next step addressed the question if low-dose irradiation (0.5 Gy) influences MWM performance when it is applied during different stages of the spatial learning test in the young adult mouse.

The mice were divided into three distinct cohorts according to the irradiation time point. Each cohort consisted of a IR group (0.5 Gy) and a separate Sham control group. Cohort 1 was irradiated seven days prior to the beginning of the MWM, Cohort 2 was irradiated immediately after training day 1 of the MWM initial learning, and Cohort 3 was irradiated immediately after the probe trial on day 6 of the MWM initial learning. MWM testing followed the same protocol as for the time points E14.5 and P10 with the exception that two reversal probe trials (60 s each) were performed. The first probe trial 24 h after the last reversal training day tested, as always, for the proper development of reference memory in the groups. The second probe trial, performed five days after the last reversal training day should additionally evaluate the persistence of this reference memory.

10.1 Results

10.1.1 Similar Rotarod and EZM Performance in all Cohorts

All cohorts showed similar levels of motor performance, as shown by their retention time on the rotating bar in Figure 10-1. Mann-Whitney tests were conducted to analyze differences in group means. There were no significant differences for any of the cohorts. Apparently, the motor function was not affected by irradiation, thus, any physical handicap during swimming in the Morris Water Maze could be excluded.

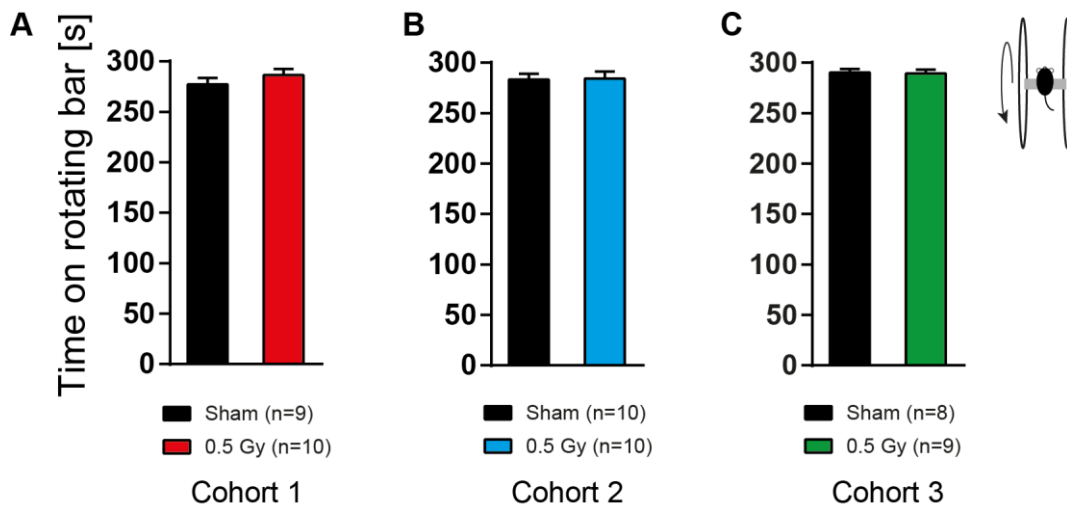


Figure 10-1: The Rotarod test did not reveal any difference in motor coordination or balance. Time spent on the rotating bar [s]. **(A) Cohort 1:** Black bar represents Sham (277.4 (6.2); n = 9), red bar represents 0.5 Gy (286.6 (6.0); n = 10). **(B) Cohort 2:** Black bar represents Sham (283.2 (5.8); n = 10), blue bar represents 0.5 Gy (284.4 (7.0); n = 10). **(C) Cohort 3:** Black bar represents Sham control (290.2 (3.4); n = 8), green bar represents 0.5 Gy (289.5 (3.6); n = 9). Statistics: Mann-Whitney test. All values are expressed as mean (SEM).

Next, the mice were allowed to explore the Elevated Zero Maze (EZM) for 30 minutes to evaluate their activity/exploration and anxiety behaviour. Cohort 1 neither showed a significant difference regarding time in open areas nor regarding frequency in open areas which both describe the case when the mice entered the unsheltered sectors with all body points simultaneously (Figure 10-2 A; Mann-Whitney test). These findings indicate similar basic activity, exploration and anxiety levels in Sham and 0.5 Gy irradiated animals of Cohort 1.

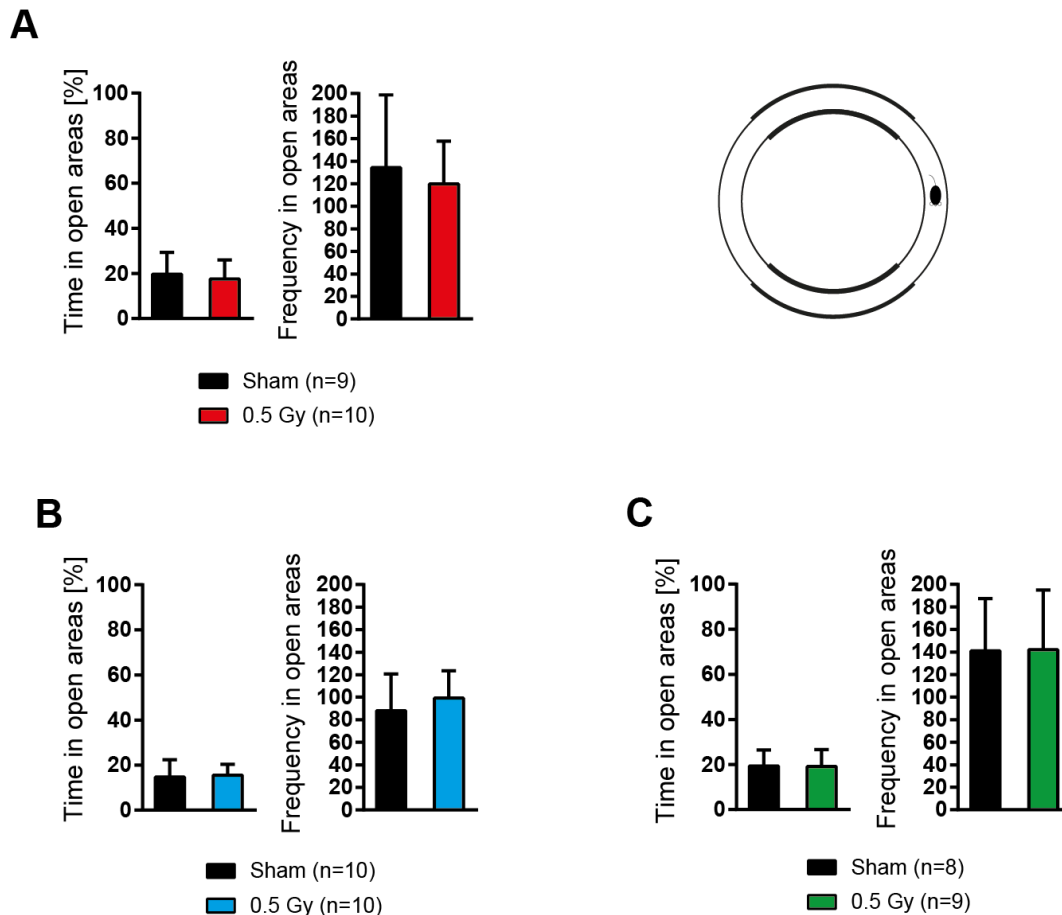


Figure 10-2: Elevated Zero Maze testing could not reveal significant differences in activity/exploration or anxiety behaviour in any of the cohorts. (A) Cohort 1: Time spent in open areas of the EZM [%] and frequency in open areas. Black bars represent Sham (n = 9), red bars represent 0.5 Gy (n = 10). **(B) Cohort 2:** Time spent in open areas of the EZM [%] and frequency in open areas. Black bars represent Sham (n = 10), blue bars represent 0.5 Gy (n = 10). **(C) Cohort 3:** Time spent in open areas of the EZM [%] and frequency in open areas. Black bars represent Sham (n = 8), green bars represent 0.5 Gy (n = 9). Statistics: Mann-Whitney test. All values are expressed as mean (SD).

Furthermore, Cohort 2 did not differ in the parameters time or frequency in open areas (Figure 10-2 B; Mann-Whitney test). Accordingly, normal activity/exploration and anxiety levels were assumed for Cohort 2.

The groups of Cohort 3 neither showed a significant difference regarding time in open areas nor regarding frequency in open areas (Figure 10-2 C; Mann-Whitney test). Overall, the results also indicate similar activity/exploration and anxiety levels in the Sham and 0.5 Gy irradiated animals of Cohort 3.

Next, each cohort was first trained for five days in an initial learning phase of the MWM and analyzed for their hippocampus-dependent spatial learning abilities.

10.1.2 Minimal Difference in the Acquisition of Spatial Memory in Cohort 1

During the initial learning phase, the platform was constantly centered in the SW quadrant. Generally, mice irradiated with 0.5 Gy seven days prior to the MWM performed a little worse in locating the hidden platform (Figure 10-3 A). They showed slightly increased escape latencies on the first training day, as also indicated by their median overall swimming time (MOST) compared to Sham. However, Log-rank testing could not detect any significant difference in the survival distributions of the two samples. On day 2, 100 % of the Sham animals were able to localize the platform within the maximum time of 120 s while only 70 % of the 0.5 Gy animals passed the test within the given time. Nevertheless, the MOST of both groups declined to a similar level. Here, the Log-rank analysis was not significant as well. The third training day revealed increased escape latencies for several of the 0.5 Gy animals, as it was also reflected by the prolonged MOST of the 0.5 Gy group (Figure 10-3 A). However, the log-rank analysis could not ascertain any significant alteration between the groups. Even if two more training days were still not sufficient for a few 0.5 Gy mice to reach Sham levels, the MOST on both days was equal (Figure 10-3 A). Log-rank analyses of day 4 and 5 could not detect significant effects of irradiation on the survival distributions.

The use of spatial searching strategies increased in both groups over the course of the training with apparent differences between the groups on day 3, 4 and 5 (Figure 10-3 B). Overall, a Two-way RM ANOVA revealed a main effect of training day on spatial searching (Figure 10-3 B; $F(4, 68) = 36.4, P < 0.0001$). Tukey's post-hoc test showed a significant increase of spatial searching strategies from day 1 to day 2 in both groups (Figure 10-3 B; Sham: $P_{1/2} = 0.014$; 0.5 Gy: $P_{1/2} = 0.0005$). Moreover, the Sham mice were able to significantly expand their spatial searching further when comparing day 2 with day 3 and to maintain a significantly elevated level of spatial searching until day 5 while the 0.5 Gy mice only significantly differed again between day 2 and day 5 (Figure 10-3 B; Sham: $P_{2/3} = 0.006, P_{2/4} = 0.006, P_{2/5} = 0.003$; 0.5 Gy: $P_{2/3} = 0.13, P_{2/4} = 0.32, P_{2/5} = 0.04$).

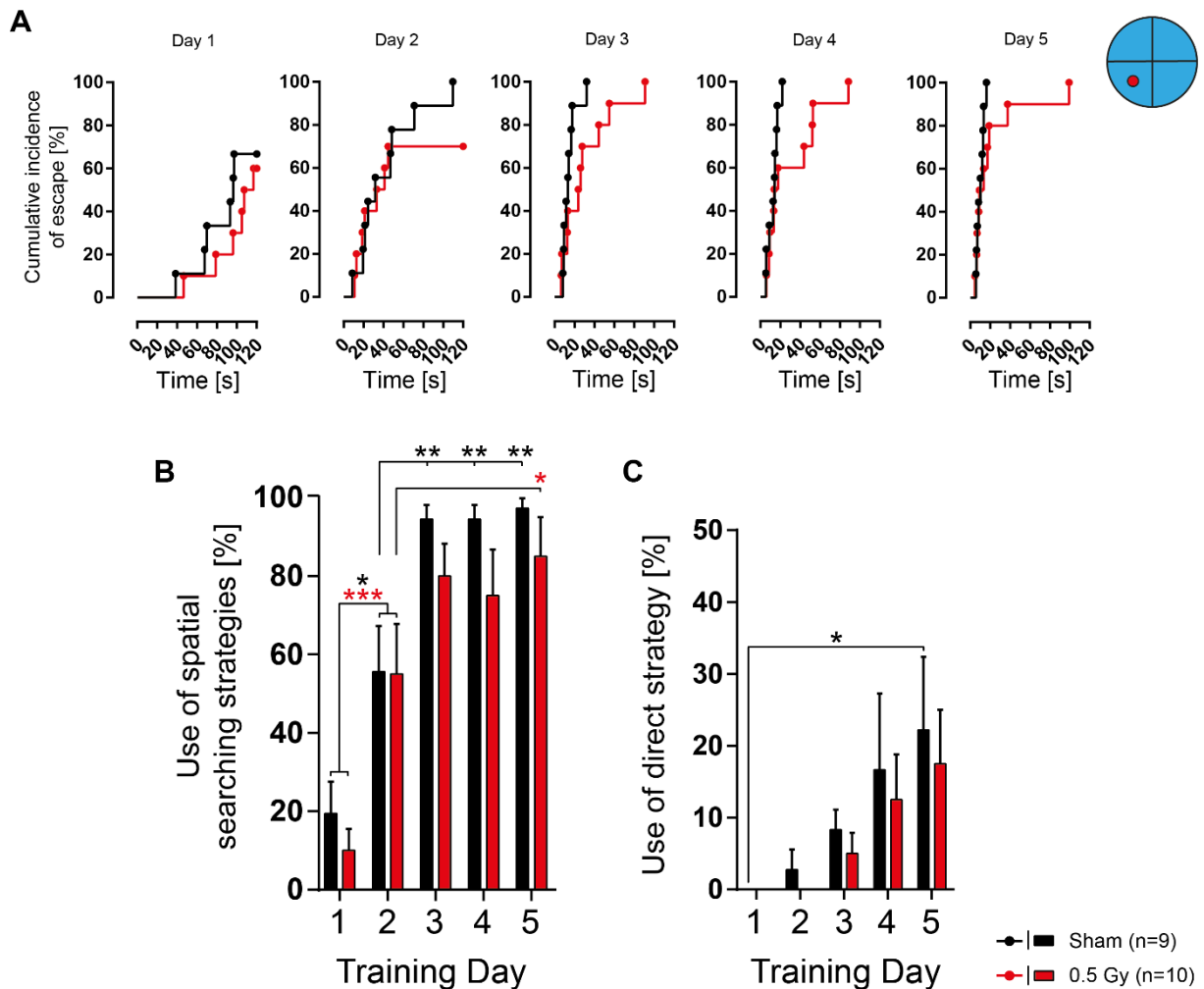


Figure 10-3: Cohort 1 – MWM initial learning revealed minor differences in the acquisition of spatial memory. (A) Cumulative incidence of escape [%] on Day 1 – Day 5. Statistics: Log-rank test followed by Bonferroni correction. Each data point represents the mean of four training trials. (B) Use of spatial searching strategies [%] over the course of five training days. Statistics: Two-way RM ANOVA followed by Tukey’s multiple comparisons test. * = $P < 0.05$, ** = $P < 0.01$, *** = $P < 0.001$. Values are expressed as mean (SEM). (C) Use of direct strategy [%] over the course of five training days. Statistics: Two-way RM ANOVA followed by Tukey’s multiple comparisons test. * = $P < 0.05$. Values are expressed as mean (SEM). Black curves/bars represent Sham ($n = 9$), red curves/bars represent 0.5 Gy ($n = 10$).

The percentage of direct platform localization increased in both groups over the training period (Figure 10-3 C). Two-way RM ANOVA testing revealed a main effect of training day ($F(4, 24) = 5.41, P = 0.0030$). Both Sham and 0.5 Gy animals reached their highest values on day 4 and 5. Tukey’s post-hoc test showed a significant increase in direct localization from day 1 to day 5 in the Sham group (Figure 10-3 C; $P_{1/5} = 0.042$). Probe testing (60 s) without platform 24 h after the last training day could not show any serious difference regarding the reference memory between 0.5 Gy and Sham. Both groups clearly passed the 25 % chance level, thus indicating a preference for the target quadrant in SW (Figure 10-4 A). A Two-way RM ANOVA analysis revealed a main effect

of quadrant ($F(3, 51) = 42.2, P < 0.0001$). Tukey's test could ascertain significantly prolonged retention times in the target sector for both groups compared to the three remaining quadrants (Figure 10-4 A; Sham: $P_{SW/NE}|P_{SW/NW}|P_{SW/SE} < 0.0001$; 0.5 Gy: $P_{SW/NE}|P_{SW/NW}|P_{SW/SE} < 0.0001$). In addition to that, there were no significant differences between the groups in respect of the distance covered (Figure 10-4 B; Mann-Whitney test), frequency in critical zone and cumulative retention time in critical zone (Figure 10-4 C; Mann-Whitney test).

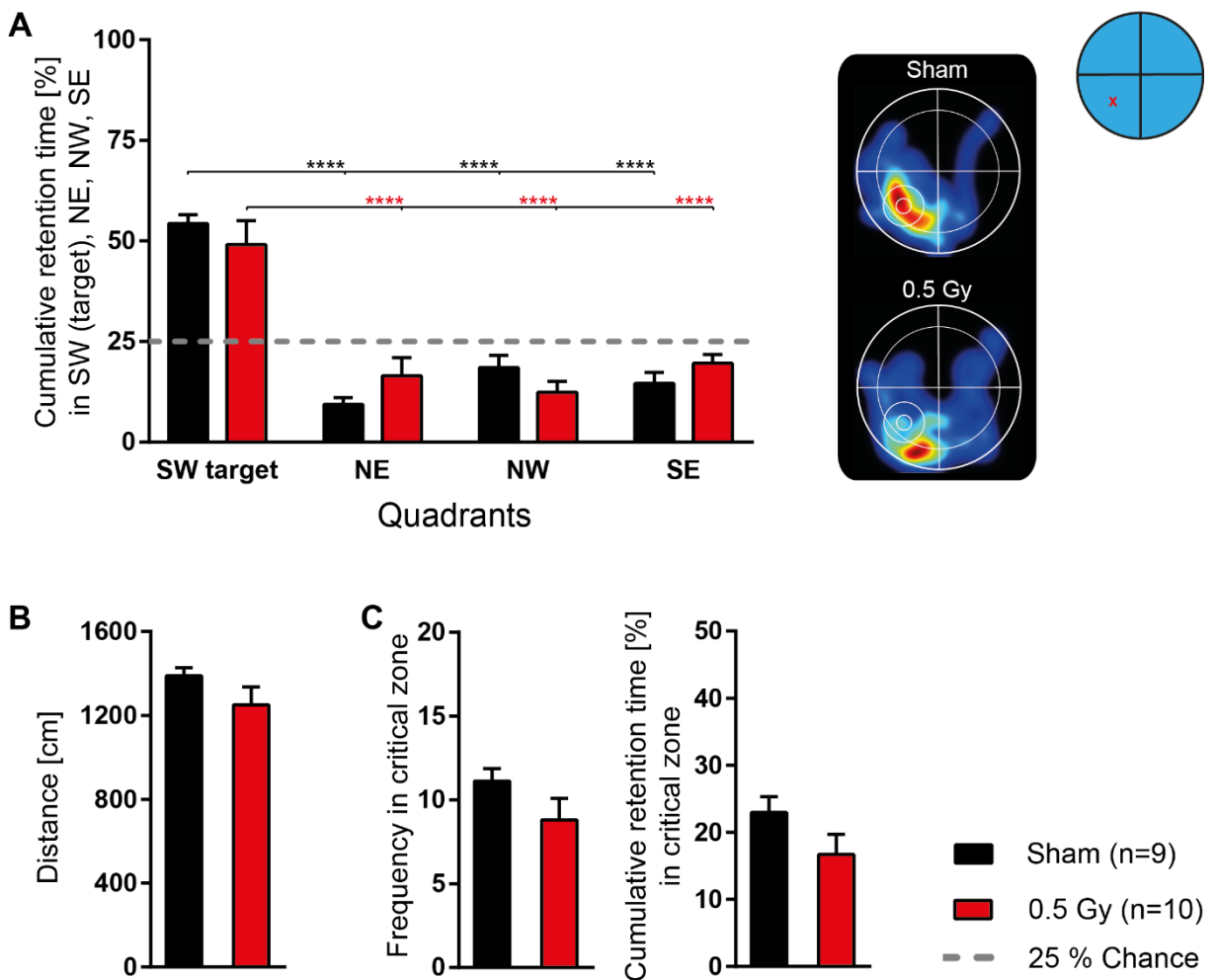


Figure 10-4: Cohort 1 – MWM initial probe trial indicated a preference for the periphery of the pool in the 0.5 Gy group. (A) Cumulative retention time [%] in South-West (SW) target quadrant, North-East (NE), North-West (NW), South-East (SE). The dashed grey line represents 25 % chance. Representative heat maps depicting former position of platform/critical zone/thigmotactic zone and areas of long retention time (red colors) and areas of short retention time (blue colors) within the MWM pool. Statistics: Two-way RM ANOVA followed by Tukey's multiple comparisons test. **** = $P < 0.0001$. (B) Swimming distance [cm] during the 60-second probe trial. Statistics: Mann Whitney test. (C) Frequency and cumulative retention time [%] in critical zone. Statistics: Mann Whitney test. * = $P < 0.05$. Black bars represent Sham ($n = 9$), red bars represent 0.5 Gy ($n = 10$). All values are expressed as mean (SEM).

For reversal learning, the platform was centered in the North-East (NE) quadrant. In general, increased escape latencies were observed for Sham and 0.5 Gy on the reversal training day 1, compared to day 5 of initial learning.

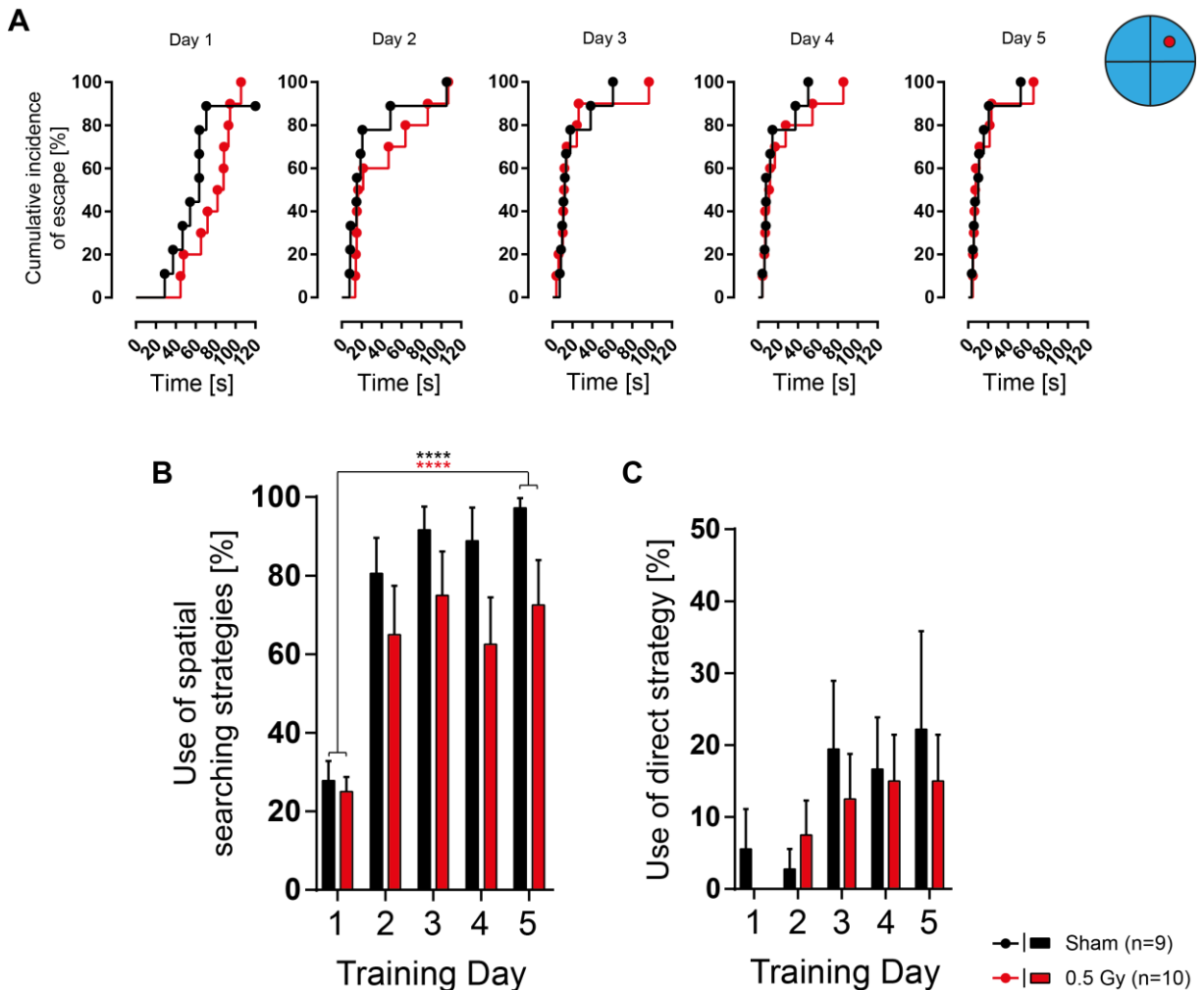


Figure 10-5: Cohort 1 – MWM reversal learning indicated that 0.5 Gy animals had slight problems with the development of spatial searching. (A) Cumulative incidence of escape [%] on Day 1 – Day 5. Statistics: Log-rank test followed by Bonferroni correction. Each data point represents the mean of four training trials. (B) Use of spatial searching strategies [%] over the course of five training days. Statistics: Two-way RM ANOVA followed by Tukey’s multiple comparisons test. **** = $P < 0.0001$. Values are expressed as mean (SEM). (C) Use of direct strategy [%] over the course of five training days. Statistics: Two-way RM ANOVA. Values are expressed as mean (SEM). Black curves/bars represent Sham ($n = 9$), red curves/bars represent 0.5 Gy ($n = 10$).

This was also shown by their increased MOST on day 1 (Figure 10-5 A). Thus, the preference for the former target in SW was obviously still present on day 1. Interestingly, the majority of mice irradiated with 0.5 Gy seven days prior to the MWM showed prolonged escape latencies compared to Sham (Figure 10-5 A). However, the log-rank analysis could not reveal any statistically significant difference between the groups. In the further course of the training between day 2 and day 5, the Sham and

the 0.5 Gy animals could not be distinguished anymore. Both groups showed a distinct left shift of their Kaplan-Meier curves over the course of the training.

Overall, both Sham and 0.5 Gy started with shorter escape latencies on reversal day 1 compared to initial day 1, reflecting their already formed procedural knowledge about the learning test. Furthermore, both groups started with higher levels of spatial searching compared to initial day 1 and were able to increase the percentage of more effective strategies during the reversal training. However, differences between the groups from day 2 to day 5 were obvious (Figure 10-5 B). A Two-way RM ANOVA revealed a main effect of training day on the amount of spatial searching strategies ($F(4, 68) = 30.0, P < 0.0001$). Follow-up testing with Tukey's test showed that Sham and 0.5 Gy mice used significantly more spatial searching on day 5 than on the first reversal training day (Figure 10-5 B; Sham: $P_{1/5} < 0.0001$; 0.5 Gy: $P_{1/5} < 0.0001$).

The percentage of direct platform localization increased in both groups over the training period (Figure 10-5 C). Both Sham and 0.5 Gy animals reached their highest values between day 3 and 5.

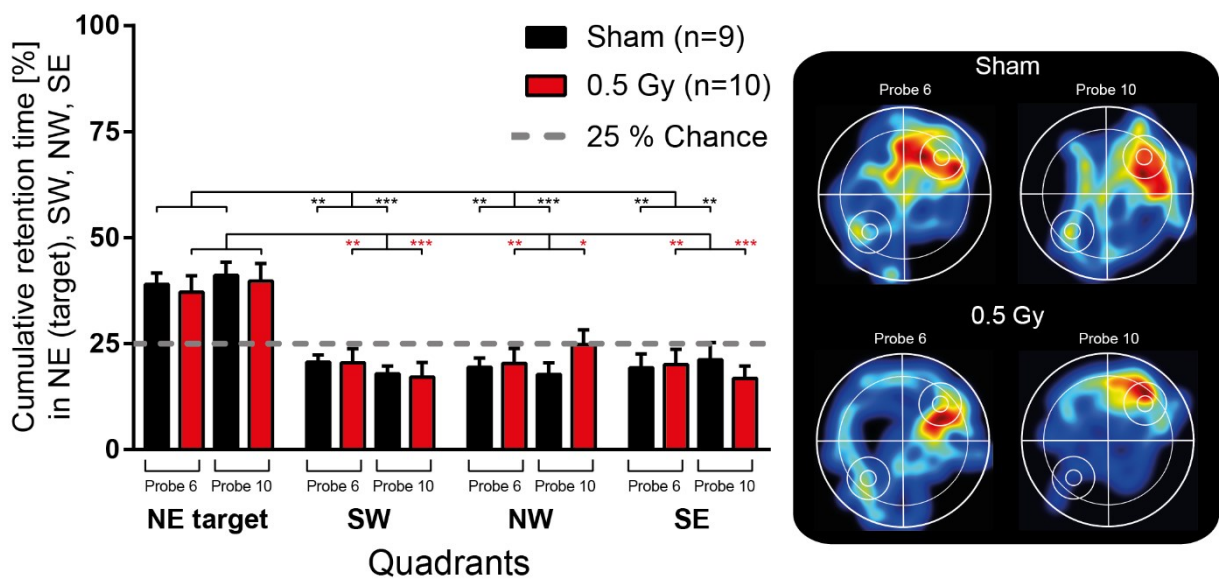


Figure 10-6: Cohort 1 – Both groups showed a similar preference for the target quadrant during the reversal probe trials on day 6 and day 10. Cumulative retention time [%] in North-East (NE) target quadrant, South-West (SW), North-West (NW), South-East (SE). The dashed grey line represents 25 % chance. Representative heat maps depicting former positions of platform/critical zone/thigmotactic zone and areas of long retention time (red colors) and areas of short retention time (blue colors) within the MWM pool. Statistics: Two-way RM ANOVA followed by Tukey's multiple comparisons test. * = $P < 0.05$, ** = $P < 0.01$, *** = $P < 0.001$. Values are expressed as mean (SEM). Black bars represent Sham ($n = 9$), red bars represent 0.5 Gy ($n = 10$).

In the further course of the investigation, the two reversal probe trials were performed.

The cumulative retention time in the target quadrant NE was clearly above the 25 % chance level for both groups and both probe trials (Figure 10-6). Overall, Two-way RM ANOVA revealed a main effect of quadrant ($F(3, 102) = 27.4, P < 0.0001$) on the retention time. The following Tukey's test for the comparison of the individual quadrants demonstrated that the preference for the target sector NE was statistically significant in Sham and 0.5 Gy for each of the probe trials over the remaining sectors SW, NW and SE (Figure 10-6; Sham Probe 6: $P_{NE/SW} = 0.006, P_{NE/NW} | P_{NE/SE} = 0.003$; 0.5 Gy Probe 6: $P_{NE/SW} | P_{NE/NW} = 0.009, P_{NE/SE} = 0.007$; Sham Probe 10: $P_{NE/SW} = 0.0003, P_{NE/NW} = 0.0002, P_{NE/SE} = 0.002$; 0.5 Gy Probe 10: $P_{NE/SW} = 0.0002, P_{NE/NW} = 0.024, P_{NE/SE} = 0.0001$).

10.1.3 Mice in Cohort 2 Displayed Equal Spatial Learning Abilities

During the initial leaning phase of the MWM, the platform was constantly centered in the SW quadrant. Cohort 2 was irradiated immediately after training day 1 of the MWM initial learning phase. Overall, the Kaplan-Meier plots showed a distinct left shift with ongoing training in both groups. The irradiated mice could not be distinguished statistically from Sham on any of the five initial training days, as also shown by their MOST (Figure 10-7 A). The log-rank analyses of the survival distributions on the different training days did not reveal any statistically significant difference.

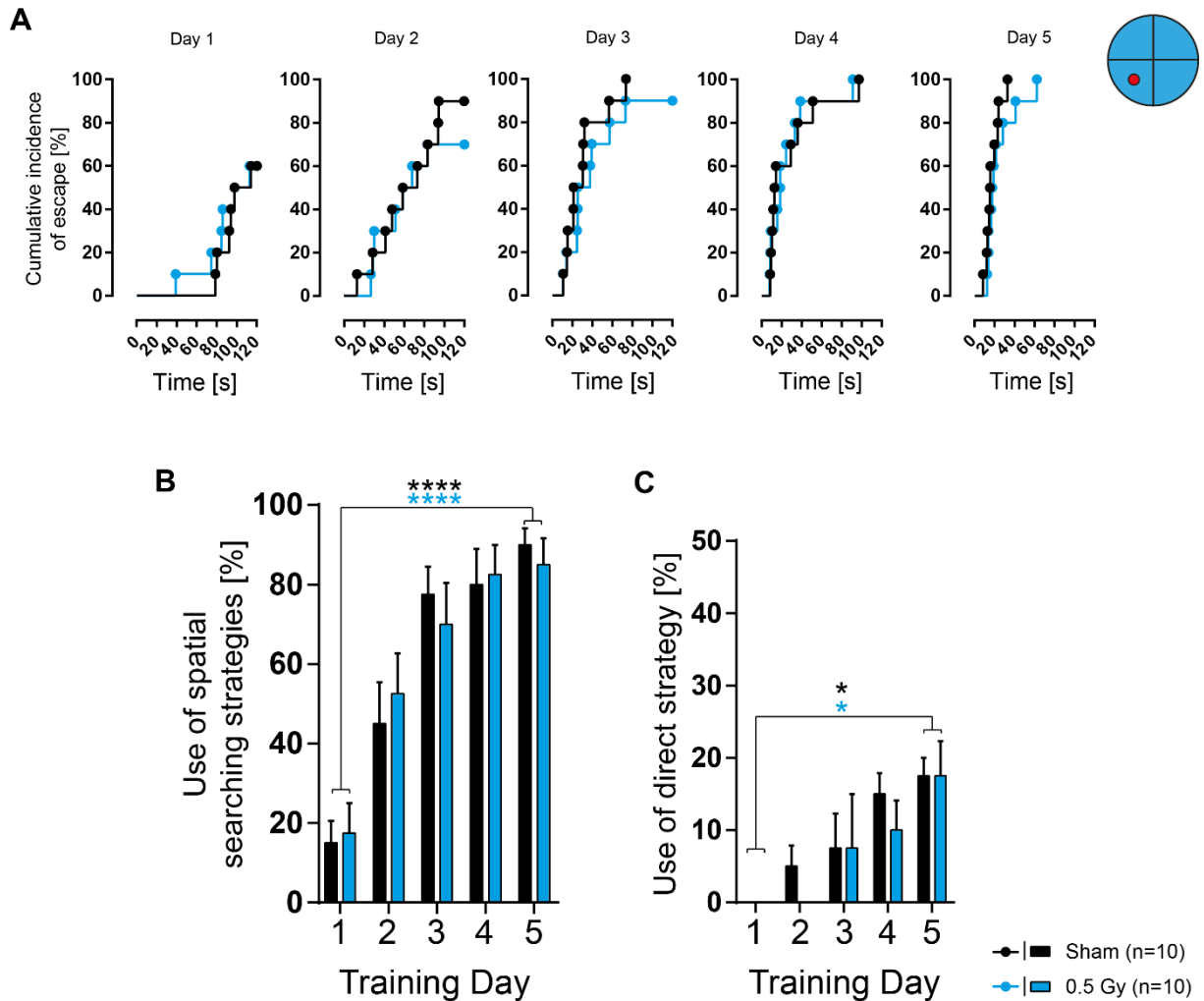


Figure 10-7: Cohort 2 – MWM initial learning could not reveal any serious difference in the acquisition of spatial memory. (A) Cumulative incidence of escape [%] on Day 1 – Day 5. Statistics: Log-rank test followed by Bonferroni correction. Each data point represents the mean of four training trials. (B) Use of spatial searching strategies [%] over the course of five training days. Statistics: Two-way RM ANOVA followed by Tukey’s multiple comparisons test. **** = $P < 0.0001$. Values are expressed as mean (SEM). (C) Use of direct strategy [%] over the course of five training days. Statistics: Two-way RM ANOVA followed by Tukey’s multiple comparisons test. * = $P < 0.05$. Values are expressed as mean (SEM). Black curves/bars represent Sham ($n = 10$), blue curves/bars represent 0.5 Gy ($n = 10$).

The use of spatial searching strategies increased in both groups over the course of the training without serious differences between the groups. Overall, a Two-way RM ANOVA revealed a main effect of training day on spatial searching (Figure 10-7 B; $F(4, 72) = 37.41$, $P < 0.0001$). Tukey’s test confirmed a significant increase from day 1 to day 5 in both groups (Figure 10-7 B; Sham: $P_{1/5} < 0.0001$; 0.5 Gy: $P_{1/5} < 0.0001$).

The percentage of direct platform localization increased in both groups over the training period (Figure 10-7 C). Two-way RM ANOVA testing revealed a main effect of training day ($F(4, 24) = 6.56, P = 0.0010$). Follow-up comparison with Tukey's test showed a significant increase from day 1 to day 5 in both the Sham and 0.5 Gy group (Figure 10-7 C; Sham: $P_{1/5} = 0.033$; 0.5 Gy: $P_{1/5} = 0.033$).

A probe test (60 s) without platform 24 h after the last training day could not show any serious difference regarding the reference memory between 0.5 Gy and Sham. Both groups clearly passed the 25 % chance level, thus indicating a preference for the target quadrant SW (Figure 10-8 A). A Two-way RM ANOVA revealed a main effect of quadrant on the cumulative retention time ($F(3, 54) = 27.1, P < 0.0001$). Tukey's test demonstrated significantly prolonged retention times in the target sector for both groups compared to the three remaining quadrants (Figure 10-8 A; Sham: $P_{SW/NE} | P_{SW/NW} | P_{SW/SE} < 0.0001$; 0.5 Gy: $P_{SW/NE} < 0.0001, P_{SW/NW} = 0.005, P_{SW/SE} = 0.0006$). Additionally, there were no significant differences between the groups in respect of the distance covered, the frequency in critical zone and the cumulative retention time in critical zone (Figure 10-8 B and C; Mann-Whitney test).

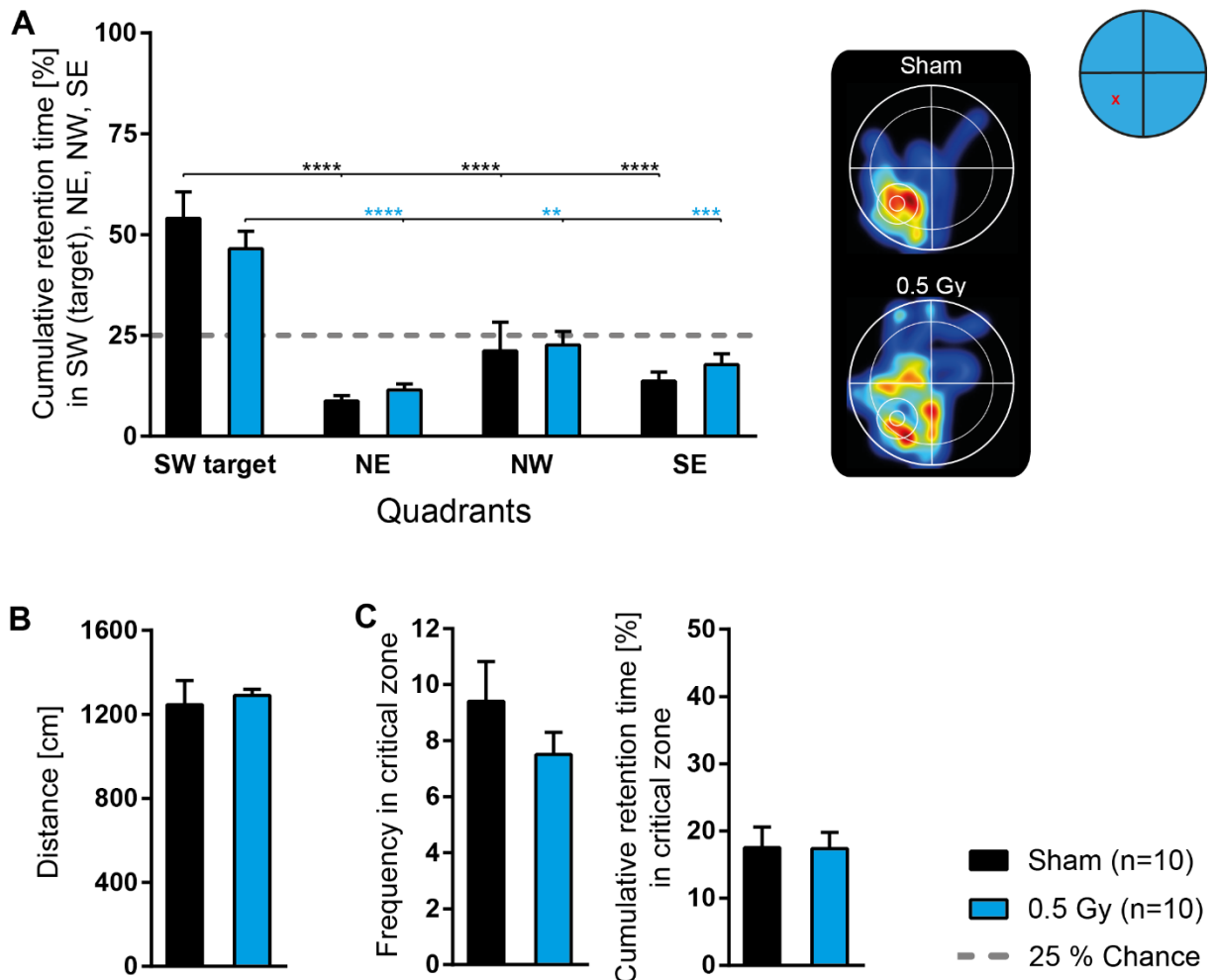


Figure 10-8: Cohort 2 – MWM initial probe trial could not unveil any serious alteration after irradiation. (A) Cumulative retention time [%] in South-West (SW) target quadrant, North-East (NE), North-West (NW), South-East (SE). The dashed grey line represents 25 % chance. Representative heat maps depicting former position of platform/critical zone/thigmotactic zone and areas of long retention time (red colors) and areas of short retention time (blue colors) within the MWM pool. Statistics: Two-way RM ANOVA followed by Tukey’s multiple comparisons test. ** = $P < 0.01$, *** = $P < 0.001$, **** = $P < 0.0001$. (B) Swimming distance [cm] during the 60-second probe trial. Statistics: Mann Whitney test. (C) Frequency and cumulative retention time [%] in critical zone. Statistics: Mann Whitney test. Black bars represent Sham ($n = 10$), blue bars represent 0.5 Gy ($n = 10$). All values are expressed as mean (SEM).

The reversal learning with the platform in the North-East sector (NE) showed increased escape latencies for Sham and 0.5 Gy on the reversal training day 1, compared to day 5 of initial learning. This was also shown by their increased MOST on reversal day 1 (Figure 10-9 A). A log-rank analysis could not reveal any statistically significant difference between the groups. In the further course of the training between day 2 and day 5, Sham and 0.5 Gy performed similar. Both groups showed a clear left shift of their Kaplan-Meier curves with progression of the training phase (Figure 10-9 A).

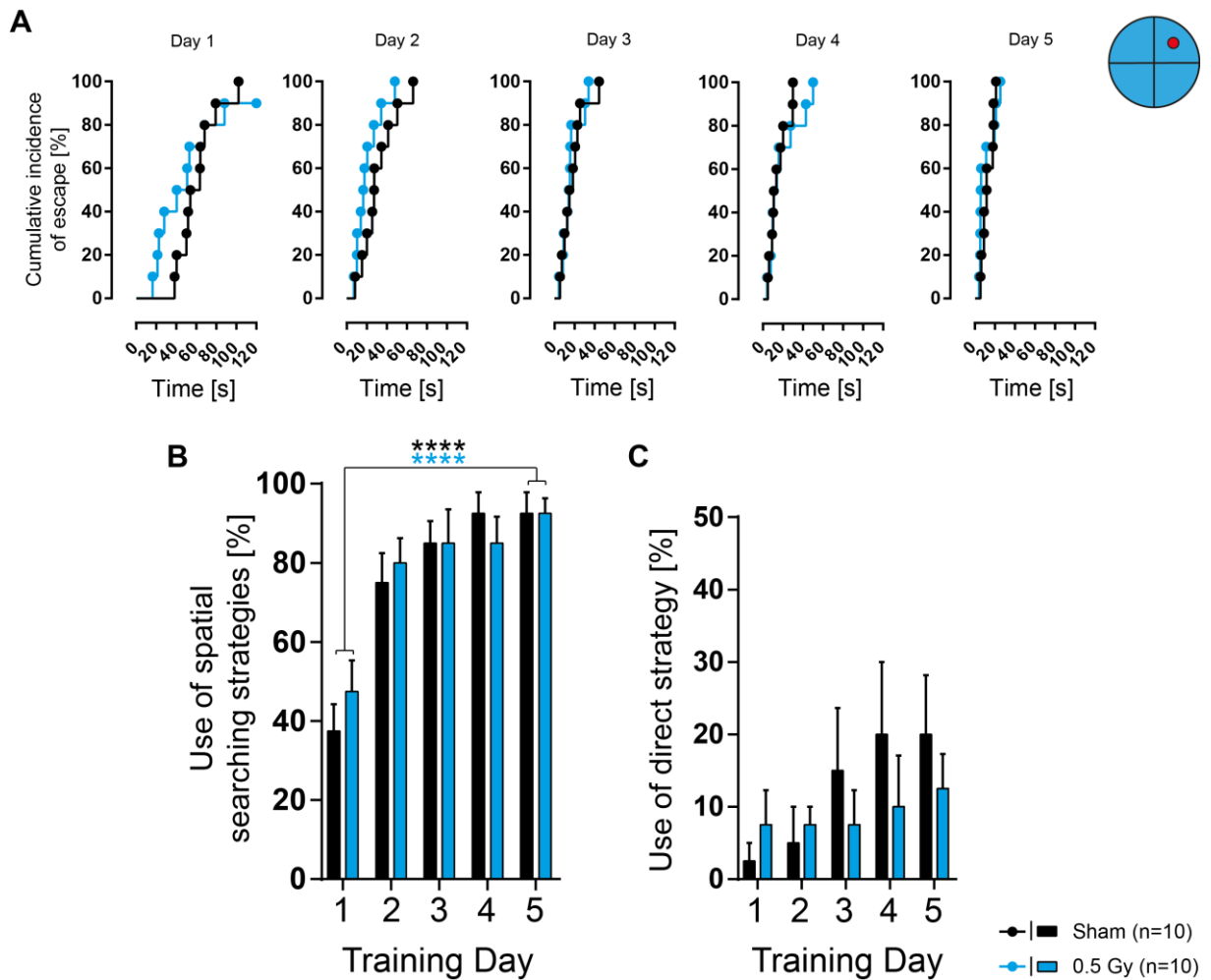


Figure 10-9: Cohort 2 – MWM reversal learning revealed similar performance in Sham and 0.5 Gy animals. (A) Cumulative incidence of escape [%] on Day 1 – Day 5. Statistics: Log-rank test followed by Bonferroni correction. Each data point represents the mean of four training trials. (B) Use of spatial searching strategies [%] over the course of five training days. Statistics: Two-way RM ANOVA followed by Tukey’s multiple comparisons test. **** = $P < 0.0001$. Values are expressed as mean (SEM). (C) Use of direct strategy [%] over the course of five training days. Statistics: Two-way RM ANOVA followed by Tukey’s multiple comparisons test. * = $P < 0.05$. Values are expressed as mean (SEM). Black curves/bars represent Sham ($n = 10$), blue curves/bars represent 0.5 Gy ($n = 10$).

Both groups started with higher levels of spatial searching compared to initial day 1 and were able to significantly increase the percentage of the more effective spatial strategies during the reversal training. Differences between the groups from day 1 to day 5 could not be observed (Figure 10-9 B). A Two-way RM ANOVA revealed a main effect of training day on the amount of spatial searching strategies ($F(4, 72) = 26.4, P < 0.0001$). Follow-up testing identified that Sham and 0.5 Gy mice used significantly more spatial searching on day 5 than on the first reversal training day (Figure 10-9 B; Sham: $P_{1/5} < 0.0001$; 0.5 Gy: $P_{1/5} < 0.0001$). The percentage of direct platform localization increased in both groups over the training period (Figure 10-9 C). However, this increase was more pronounced in Sham mice than in 0.5 Gy mice between day 3

and 5. In the further course of the investigation, the two reversal probe trials (60 s each) were performed.

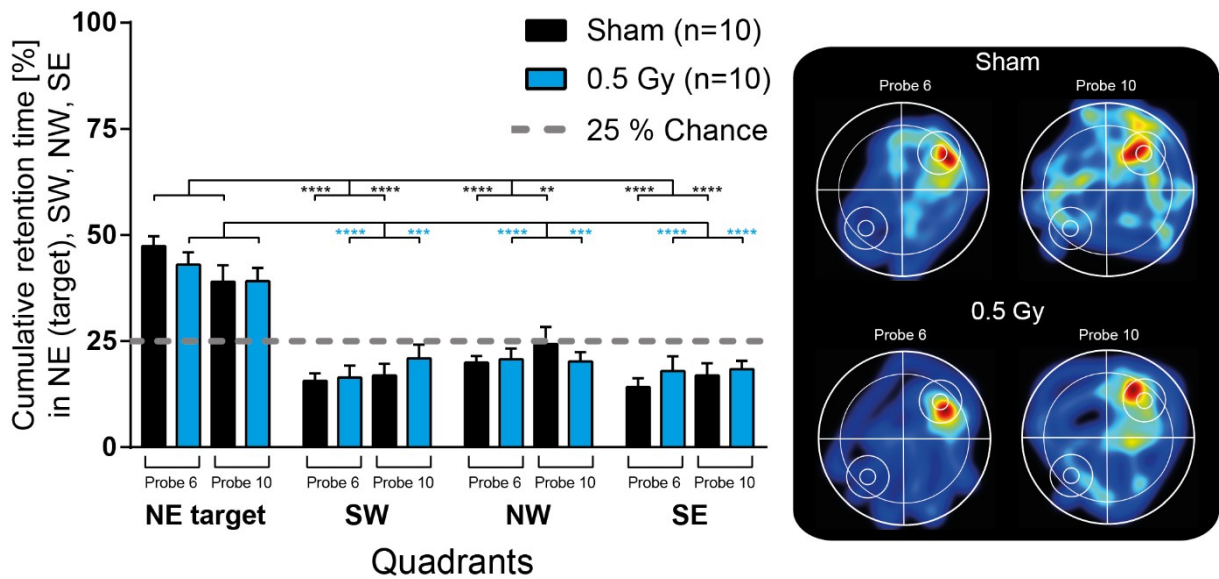


Figure 10-10: Cohort 2 – Both groups showed a similar preference for the target quadrant during the reversal probe trials on day 6 and day 10. Cumulative retention time [%] in North-East (NE) target quadrant, South-West (SW), North-West (NW), South-East (SE). The dashed grey line represents 25 % chance. Representative heat maps depicting former positions of platform/critical zone/thigmotactic zone and areas of long retention time (red colors) and areas of short retention time (blue colors) within the MWM pool. Statistics: Two-way RM ANOVA followed by Tukey’s multiple comparisons test. ** = $P < 0.01$, *** = $P < 0.001$, **** = $P < 0.0001$. Values are expressed as mean (SEM). Black bars represent Sham (n = 10), blue bars represent 0.5 Gy (n = 10).

The cumulative retention time in the target quadrant NE was clearly above the 25 % chance level for both groups and both probe trials (Figure 10-10). Overall, Two-way RM ANOVA revealed a main effect of quadrant ($F(3, 108) = 54.1, P < 0.0001$) on the retention time. Tukey’s test demonstrated that the preference for the target sector NE was statistically significant in Sham and 0.5 Gy for each of the probe trials over the remaining sectors SW, NW and SE (Figure 10-10; Sham Probe 6: $P_{NE/SW} | P_{NE/NW} | P_{NE/SE} < 0.0001$; 0.5 Gy Probe 6: $P_{NE/SW} | P_{NE/NW} | P_{NE/SE} < 0.0001$; Sham Probe 10: $P_{NE/SW} | P_{NE/SE} < 0.0001, P_{NE/NW} = 0.0099$; 0.5 Gy Probe 10: $P_{NE/SW} = 0.0008, P_{NE/NW} = 0.0004, P_{NE/SE} < 0.0001$). The analysis of the two probe trials could not reveal any serious differences between Sham and 0.5 Gy animals.

10.1.4 IR Mice of Cohort 3 Performed Worse at the Start of Reversal Learning

During the initial leaning phase of the MWM, the platform was constantly centered in the SW quadrant. Cohort 3 was irradiated immediately after the probe trial on day 6 of the MWM initial learning phase. Altogether, the Kaplan-Meier plots of the cumulative incidence of escape clearly shifted to the left with ongoing training in both groups, as also shown by their MOST (Figure 10-11 A). Even if the escape latencies of the designated IR group were slightly shorter on day 1 compared to the designated Sham group, the 0.5 Gy animals could not be distinguished statistically from the Sham animals on any of the five initial training days, as also confirmed by the Log-rank analyses of the survival distributions.

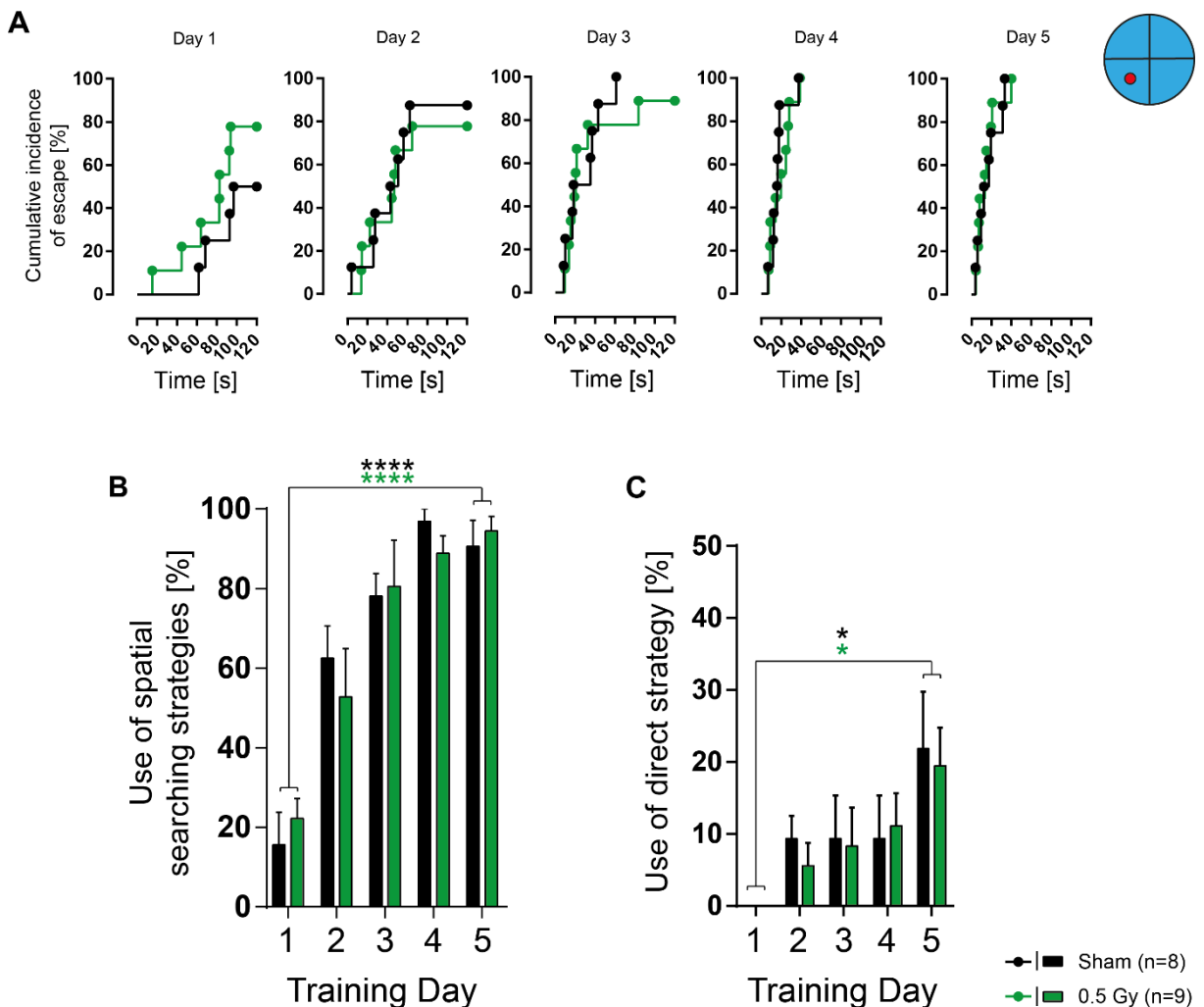


Figure 10-11: Cohort 3 – MWM initial learning could not reveal any serious difference in spatial memory acquisition. (A) Cumulative incidence of escape [%] on Day 1 – Day 5. Statistics: Log-rank test followed by Bonferroni correction. Each data point represents the mean of four training trials. (B) Use of spatial searching strategies [%] over the course of five training days. Statistics: Two-way RM ANOVA followed by Tukey’s multiple comparisons test. **** = $P < 0.0001$. Values are expressed as mean (SEM). (C) Use of direct strategy [%] over the course of five training days. Statistics: Two-way RM ANOVA followed by Tukey’s multiple comparisons test. Values are expressed as mean (SEM). Black curves/bars represent Sham (n = 8), green curves/bars represent 0.5 Gy (n = 9).

The use of spatial searching strategies increased in both groups over the course of the training without serious differences. A Two-way RM ANOVA showed a main effect of training day on spatial searching (Figure 10-11 B; $F(4, 60) = 45.3, P < 0.0001$). The following Tukey's test unveiled a significant increase from day 1 to day 5 in both groups (Figure 10-11 B; Sham: $P_{1/5} < 0.0001$; 0.5 Gy: $P_{1/5} < 0.0001$).

The percentage of direct platform localization increased in both groups over the training period (Figure 10-11 C). Two-way RM ANOVA testing revealed a main effect of training day ($F(4, 24) = 5.45, P = 0.0029$). Follow-up comparison with Tukey's test showed a significant increase from day 1 to day 5 in the Sham and 0.5 Gy group (Figure 10-11 C; Sham: $P_{1/5} = 0.016$; 0.5 Gy: $P_{1/5} = 0.039$).

In a probe test (60 s) without platform 24 h after the last training day, Sham and 0.5 Gy mice behaved equally regarding their reference memory. Both groups clearly passed the 25 % chance level, indicating a preference for the target quadrant SW (Figure 10-12 A). A Two-way RM ANOVA revealed a main effect of quadrant ($F(3, 45) = 26.2, P < 0.0001$). Follow-up testing demonstrated significantly increased retention times in the target sector for both groups compared to the three remaining quadrants (Figure 10-12 A; Sham: $P_{SW/NE} | P_{SW/NW} | P_{SW/SE} < 0.0001$; 0.5 Gy: $P_{SW/NE} = 0.001, P_{SW/NW} | P_{SW/SE} < 0.0001$). Additionally, there were no significant differences between the groups regarding the swimming distance, frequency in critical zone and cumulative retention time in critical zone (Figure 10-12 B and C; Mann-Whitney test).

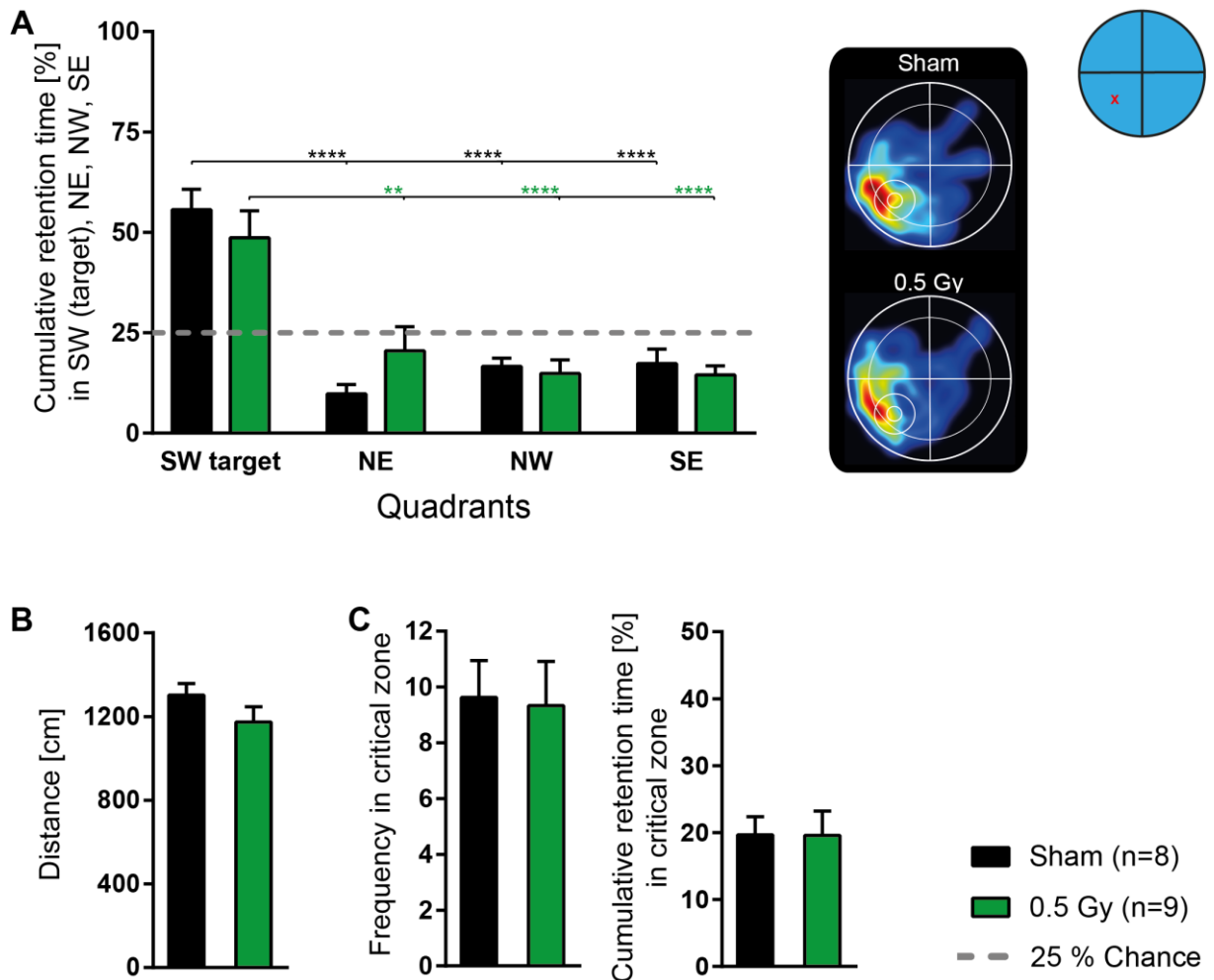


Figure 10-12: Cohort 3 – Both groups showed similar performance in the MWM initial probe trial. (A) Cumulative retention time [%] in South-West (SW) target quadrant, North-East (NE), North-West (NW), South-East (SE). The dashed grey line represents 25 % chance. Representative heat maps depicting former position of platform/critical zone/thigmotactic zone and areas of long retention time (red colors) and areas of short retention time (blue colors) within the MWM pool. Statistics: Two-way RM ANOVA followed by Tukey’s multiple comparisons test. ** = $P < 0.01$, **** = $P < 0.0001$. (B) Swimming distance [cm] during the 60-second probe trial. Statistics: Mann Whitney test. (C) Frequency and cumulative retention time [%] in critical zone. Statistics: Mann Whitney test. Black bars represent Sham ($n = 8$), green bars represent 0.5 Gy ($n = 9$). All values are expressed as mean (SEM).

During reversal learning with the platform centered in NE, increased escape latencies were observed for Sham and 0.5 Gy on day 1, compared to day 5 of initial learning. This was also shown by the increased MOST. The corresponding Log-rank analysis revealed a statistically significant prolongation of the escape latencies after irradiation with 0.5 Gy (Figure 10-13 A; $P = 0.046$). The Log-rank tests of the remaining training days could not reveal any statistically significant difference between the groups. Altogether, both groups showed a clear left shift of their Kaplan-Meier curves during the training period.

Overall, both groups started with shorter escape latencies on reversal day 1 compared to initial day 1, as shown by their reduced MOST, reflecting their functional procedural knowledge about the learning test. However, the 0.5 Gy mice showed significantly increased escape latencies on the first reversal learning day compared to the Sham group. Thus, irradiation after the initial probe trial obviously impaired the MWM performance on the first reversal training day.

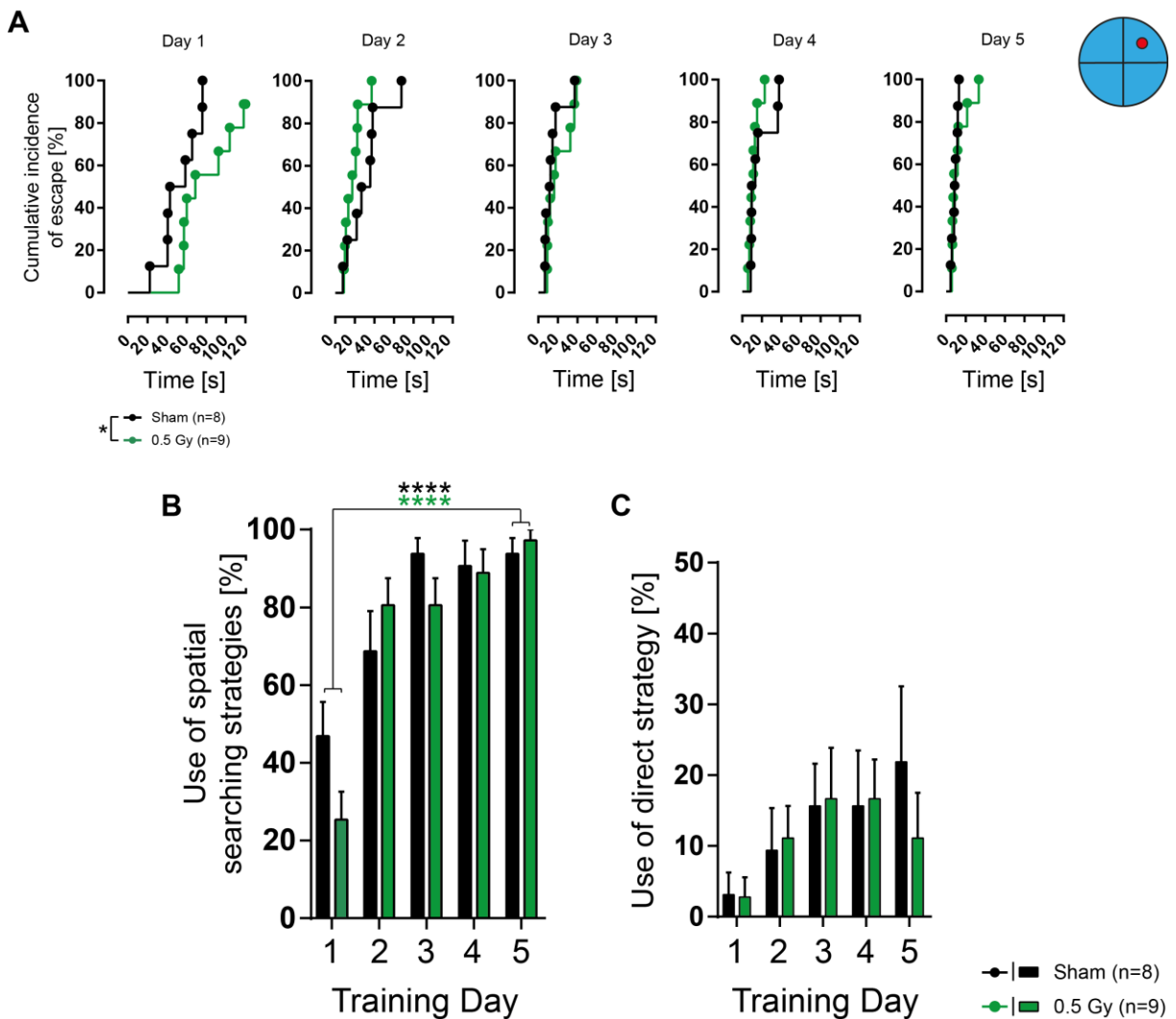


Figure 10-13: Cohort 3 – MWM reversal learning revealed a significantly impaired performance of 0.5 Gy animals on the first training day. (A) Cumulative incidence of escape [%] on Day 1 – Day 5. Statistics: Log-rank test followed by Bonferroni correction. * = $P < 0.0083$. Each data point represents the mean of four training trials. (B) Use of spatial searching strategies [%] over the course of five training days. Statistics: Two-way RM ANOVA followed by Tukey’s or Sidak’s multiple comparisons test. **** = $P < 0.0001$. Values are expressed as mean (SEM). (C) Use of direct strategy [%] over the course of five training days. Statistics: Two-way RM ANOVA. Values are expressed as mean (SEM). Black curves/bars represent Sham ($n = 8$), green curves/bars represent 0.5 Gy ($n = 9$).

The Sham mice started with higher levels of spatial searching compared to initial day 1. In contrast to that, the use of spatial strategies was clearly reduced in the 0.5 Gy

group. Altogether, both groups were able to increase the amount of spatial searching in the course of the five training days (Figure 10-13 B). A Two-way RM ANOVA revealed a main effect of training day on the amount of spatial searching strategies ($F(4, 60) = 32.4, P < 0.0001$). Sidak's post-hoc test for the comparison of group differences on the training days suggested that irradiation directly following the initial probe trial could prevent the usually observed elevated percentage of spatial searching on reversal learning day 1 (Figure 10-13 B; $P = 0.05$). Further differences between the groups from day 2 to day 5 could not be observed. Follow-up testing with Tukey's test illustrated that Sham and 0.5 Gy mice used significantly more spatial searching on day 5 than on the first reversal day (Figure 10-13 B; Sham: $P_{1/5} < 0.0001$; 0.5 Gy: $P_{1/5} < 0.0001$). The percentage of direct platform localization increased in both groups over the training period (Figure 10-13 C). On day 5, 0.5 Gy animals differed from Sham animals by decreased percentage of direct localization, however, ANOVA testing did not reveal any significant effect.

Next, the two reversal probe trials (60 s each) were performed. Both groups clearly exceeded the 25 % chance level regarding the cumulative retention time in the target sector NE in both probe trials (Figure 10-14). Overall, a Two-way RM ANOVA revealed a main effect of quadrant ($F(3, 90) = 61.5, P < 0.0001$) on the retention time. The following Tukey's test for the comparison of the individual quadrants demonstrated that the preference for the target sector NE was statistically significant in Sham and 0.5 Gy for each of the probe trials over the remaining sectors SW, NW and SE (Figure 10-14; Sham Probe 6: $P_{NE/SW} | P_{NE/NW} | P_{NE/SE} < 0.0001$; 0.5 Gy Probe 6: $P_{NE/SW} | P_{NE/NW} | P_{NE/SE} < 0.0001$; Sham Probe 10: $P_{NE/SW} | P_{NE/NW} | P_{NE/SE} < 0.0001$; 0.5 Gy Probe 10: $P_{NE/SW} | P_{NE/NW} | P_{NE/SE} < 0.0001$).

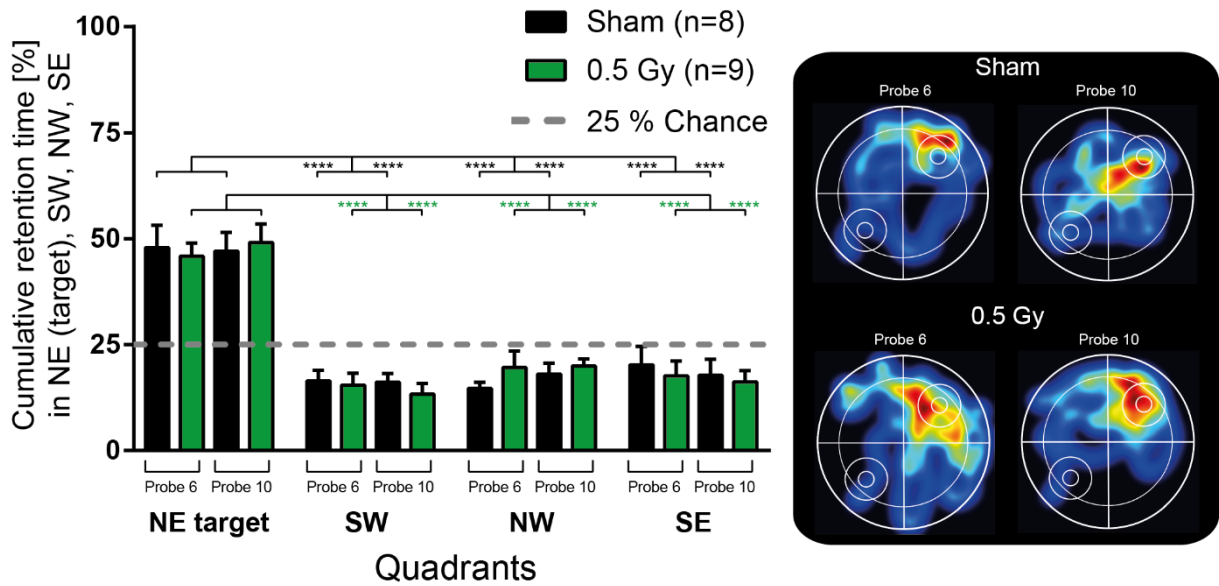


Figure 10-14: Cohort 3 – Both groups equally preferred the target sector over the remaining quadrants during the reversal probe trials on day 6 and day 10. Cumulative retention time [%] in North-East (NE) target quadrant, South-West (SW), North-West (NW), South-East (SE). The dashed grey line represents 25 % chance. Representative heat maps depicting former positions of platform/critical zone/thigmotactic zone and areas of long retention time (red colors) and areas of short retention time (blue colors) within the MWM pool. Statistics: Two-way RM ANOVA followed by Tukey’s multiple comparisons test. **** = $P < 0.0001$. Values are expressed as mean (SEM). Black bars represent Sham ($n = 8$), green bars represent 0.5 Gy ($n = 9$).

On the whole, the results of Cohort III did not reveal serious effects of irradiation after the probe trial and before the start of the reversal learning.

10.2 Conclusion – Chapter III (learning phases)

Taken together, low-dose irradiation (0.5 Gy) applied during different learning phases of the MWM had only minor influence on the spatial learning capacity and the formation of an allocentric spatial map. Each of the investigated groups was able to develop proper reference memory of the two learned platform positions, as shown by their performance during an initial and a reversal probe testing. Firmness and persistence of this reference memory was demonstrated by similar retention times in the target quadrant during a second reversal probe trial compared to Sham animals. Nevertheless, insignificant alterations were observed after irradiation 7 days before the start of the MWM test (Cohort 1) which resulted in slightly decreased spatial searching during initial and reversal learning. Furthermore, irradiation after the initial probe trial (Cohort 3) was associated with significantly decreased escape latencies and reduced

spatial searching on the first reversal training day. However, irradiated mice of Cohort 3 performed equally to control during the remaining days of the MWM reversal phase.

11 Chapter IV – Immunohistological Analysis of Neural Progenitors in the Dentate Gyrus

The hippocampal network plays an essential role for spatial memory formation (Hartley et al., 2014; M. Moser et al., 2015). Especially, the subgranular zone of the dentate gyrus (DG) harbours neural stem cells which provide the basis for the generation of progenitor cells that differentiate into new granule cells. These cells then integrate into the existing hippocampal circuitry and add an additional level of complexity to neural plasticity (Colangelo et al., 2019; Taupin & Gage, 2002; Toni et al., 2008; Urban & Guillemot, 2014). Several studies on adult hippocampal neurogenesis have linked this process to learning and memory (Döbrössy et al., 2003; Drapeau et al., 2003; Kempermann & Gage, 2002; Leuner et al., 2004).

Chapter IV covers the influence of low-dose ionizing radiation on a specific cell type, the DCX⁺ immature progenitor cell type that can be used as a marker of neurogenesis (J. Brown et al., 2003; Couillard-Despres et al., 2005; Rao & Shetty, 2004). Doublecortin (DCX) is microtubule-associated protein which is characterized by a specific temporal expression pattern. It is essential for regular migration of neurons and is a marker of cells committed to a neuronal lineage in both the developing and the adult brain (Hodge & Hevner, 2011; Kempermann et al., 2015).

Therefore, immunohistological analysis and quantification of those immature nerve cells was performed next, to examine if low-dose irradiation at E14.5 or P10 affected neurogenesis and the hippocampal morphology in the two months old mouse.

11.1 Results

11.1.1 Irradiation with 0.5 Gy Reduced DCX⁺ Progenitor Cells and Resulted in Diminished DG Area

The number of DCX⁺ progenitor cells in the dentate gyrus was apparently reduced in both E14.5 and P10 animals exposed to 0.5 Gy compared to Sham control animals (Figure 11-1 C, D, E and F). A statistical analysis showed a significant reduction of DCX⁺ progenitor cells in animals irradiated with 0.5 Gy at E14.5 (Figure 11-1 E; Mann-Whitney test, $P = 0.013$). Additionally, measurements of the dentate gyrus area showed that the significant loss of the DCX⁺ progenitor cells in 0.5 Gy mice of the time point E14.5 was associated with a significantly reduced area (Figure 11-1 E; Mann-Whitney test, $P = 0.029$). The observed loss of DCX⁺ cells in two months old mice after irradiation at P10 was not significant (Figure 11-1 F; Mann-Whitney test, $P = 0.38$). Furthermore, the DG area was unaffected after irradiation at P10 (Figure 11-1 F; Mann-Whitney test, $P = 0.78$).

Consequently, irradiation with 0.5 Gy reduced the number of DCX⁺ progenitor cells in the adult dentate gyrus in both the embryonic and the postnatal time point. However, this cell loss was more pronounced in the embryonic than in the early postnatal time point. IR at E14.5 caused about 35 % less progenitor cells and a DG area reduction of 15 %. In contrast to that, IR at P10 reduced the cell number by 17 % while the DG took up an area of approximately 6 % less compared to Sham (Figure 11-1 E and F).

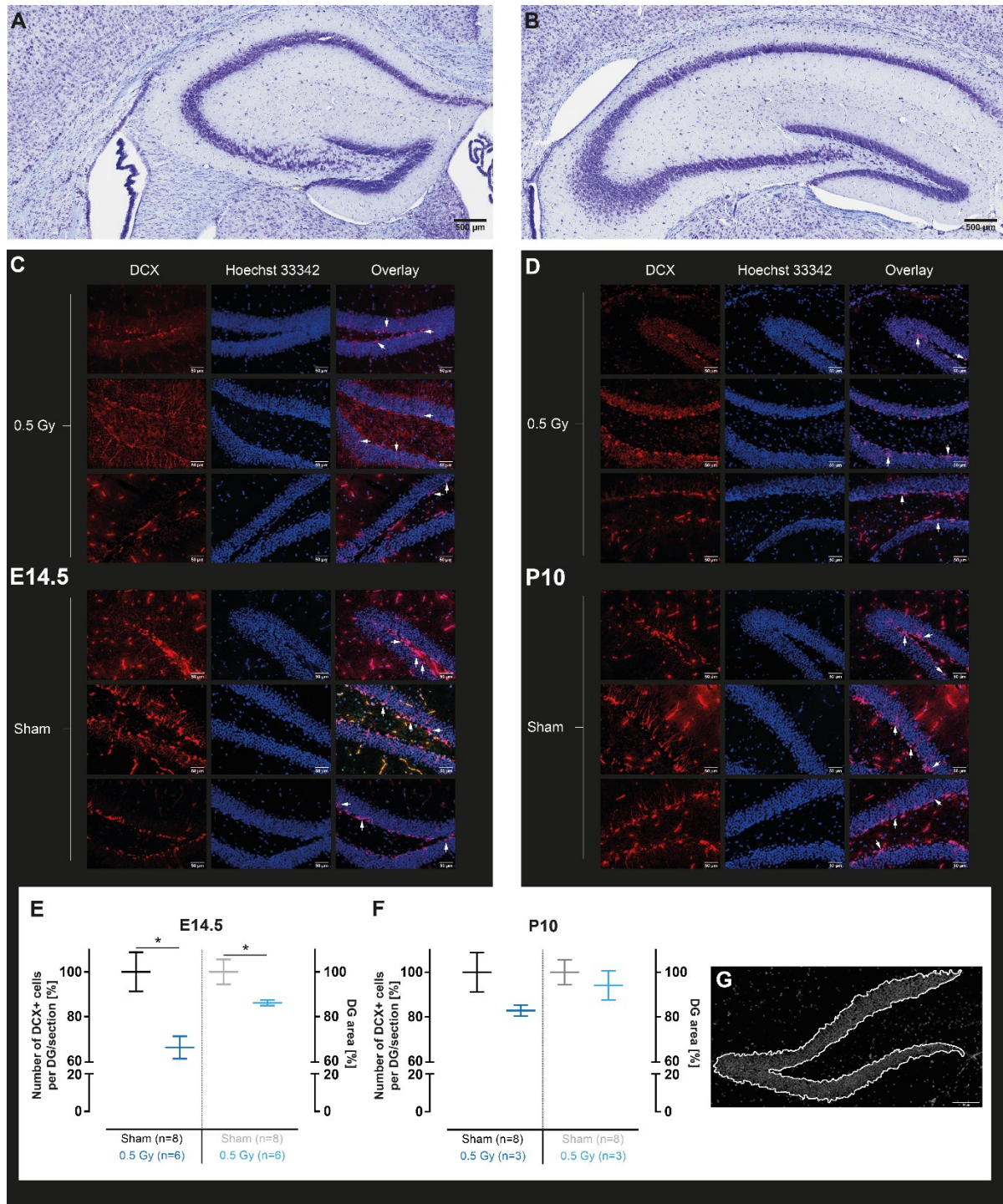


Figure 11-1: IHC analysis of the DG revealed significantly less DCX⁺ progenitor cells and reduced DG area in mice irradiated with 0.5 Gy at E14.5. (A) Nissl staining of hippocampus at Bregma -1.34. Scale bar corresponds to 500 μ m. (B) Nissl staining of hippocampus at Bregma -2.70. Scale bar corresponds to 500 μ m. (C) IHC stainings of DCX⁺ progenitor cells within the DG of two months old mice irradiated with 0.5 Gy or Sham at E14.5. Scale bars correspond to 50 μ m. (D) IHC stainings of DCX⁺ progenitor cells within the DG of two months old mice irradiated with 0.5 Gy or Sham at P10. Scale bars correspond to 50 μ m. (E) Number of DCX⁺ cells within DG per section [%] and DG area [%] for time point E14.5. (F) Number of DCX⁺ cells within DG per section [%] and DG area [%] for time point P10. (G) Representative image of DG showing a measurement of area with ImageJ. Sham (n = 8) is shown in black, E14.5 0.5 Gy (n = 6) is shown in blue. P10 0.5 Gy (n = 3) is shown in grey. DCX⁺ cells are depicted in red and Hoechst33342 staining in blue. White arrows in overlay indicate DCX⁺ cells. All values are expressed as mean (SEM). Statistics: Mann-Whitney test. * = P < 0.05. DG = dentate gyrus. IHC = immunohistology.

11.2 Conclusion – Chapter IV (Immunohistological Analysis)

Low-dose irradiation with 0.5 Gy was sufficient to reduce the number of necessary progenitor cells within the hippocampal dentate gyrus. Those cells normally integrate into the hippocampus and contribute to the proper function of trisynaptic circuitry. In the case of an irradiation at E14.5, this reduction was significant and associated with a reduced area of the dentate gyrus. A decrease of DCX⁺ cell numbers was also noticed at P10, however, a statistically significance could not be shown.

Taken together, these results could explain at least partially the occurrence of aberrant spatial learning and memory abilities in the MWM test, as the hippocampus plays an essential role in the formation of spatial maps (E. Moser et al., 2017).

12 Chapter V – Overarching Comparison of the Distinct Irradiation Time Points

This chapter focuses on the direct comparison of all investigated irradiation time points and thus contributes to the assessment of the radiosensitivity of specific phases of brain development and maturation. The development of proper spatial searching and reference memory during the Morris Water Maze test represent the most important parameters for the evaluation of performance and hippocampal function. Moreover, the generation of allocentric spatial maps within the hippocampus plays an essential role for navigation and is mirrored by the development of spatial strategies. Together, this reflects the proper functioning of hippocampus-dependent allocentric place navigation (Moghaddam & Bures, 1996; Morris, 1984; Morris et al., 1982, 1986; Vorhees & Williams, 2014). For reasons of complexity reduction, this chapter compares these two main parameters with focus on the five different groups irradiated with the highest dose of 0.5 Gy. Moreover, the comparison of all investigated control animals demonstrates equal experimental conditions. A pooled Sham control group is integrated in the graphs just as an orientation guide and without plotting values of significance.

12.1 Results

12.1.1 Different Sham Groups Performed Similar in the MWM Task

First of all, the escape latencies and the amount of spatial searching of the different Sham groups were statistically compared to allow pooling of the control groups. All Sham groups performed similar during the initial and reversal learning phase of the MWM test. Figure 12-1 shows the plots for the cumulative incidence of escape on day 3 and 5 of the initial (Figure 12-1 A) and the reversal learning phase (Figure 12-1 C). The statistical analysis of the survival distributions did not reveal any significant divergence between the different Sham groups. Furthermore, Two-way RM ANOVA testing demonstrated main effects of training day on spatial searching strategies and direct localization for both the initial (Figure 12-1 B; Spatial: $F(4, 168) = 104.1, P < 0.0001$; Direct: $F(4, 60) = 9.3, P < 0.0001$) and the reversal (Figure 12-1 D; Spatial: $F(4, 168) = 72.4, P < 0.0001$; Direct: $F(4, 60) = 9.2, P < 0.0001$) MWM phase. Significant differences between the Sham groups could not be detected.

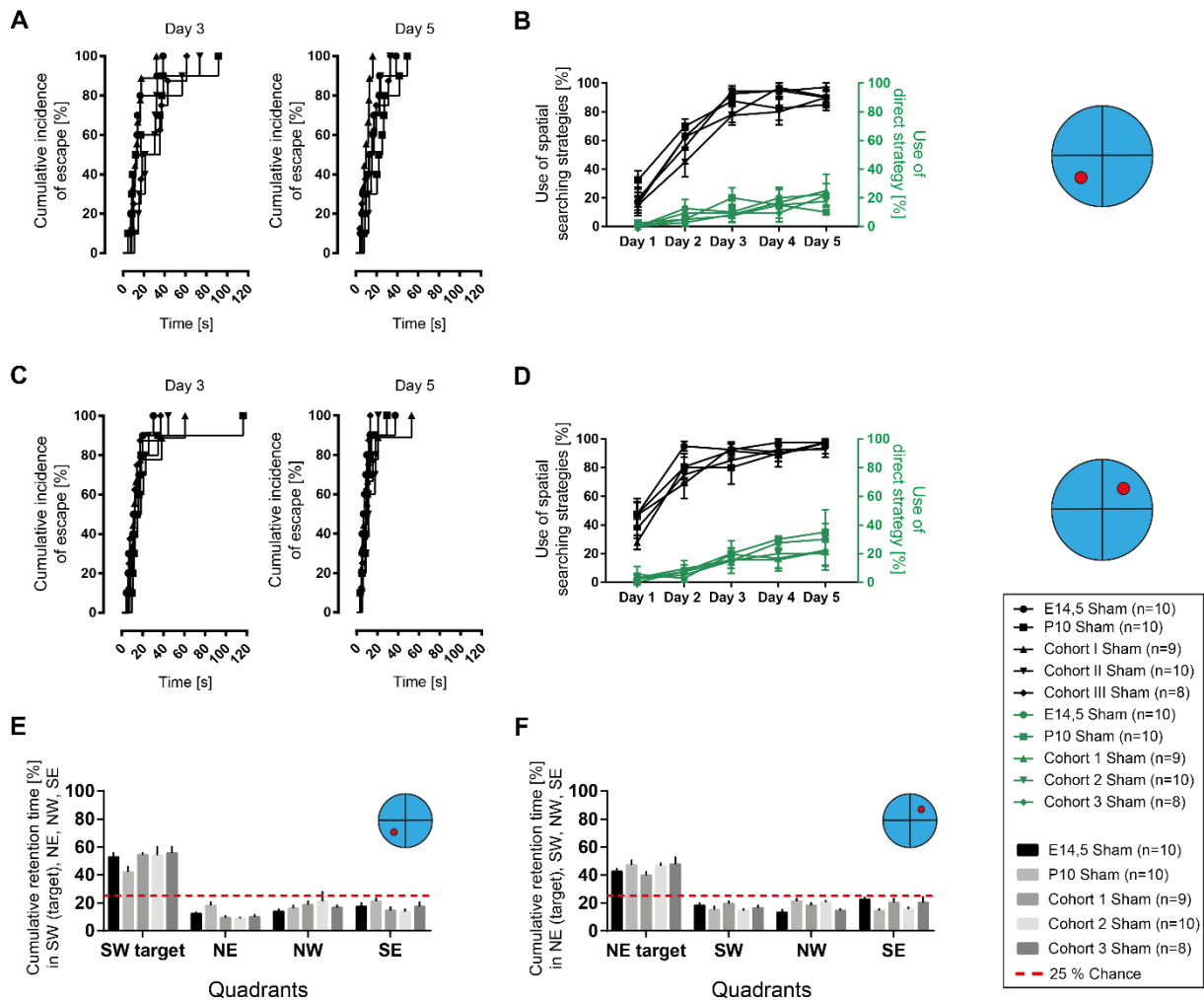


Figure 12-1: All Sham groups performed similar during the initial and reversal phase of the MWM. (A) Cumulative incidence of escape [%] on Day 3 and Day 5 of initial MWM phase. Statistics: Log-rank test followed by Bonferroni correction. Each data point represents the mean of four training trials. (B) Use of spatial and direct (green) strategies for platform localization. Statistics: Two-way RM ANOVA followed by Tukey’s multiple comparisons test. Values are expressed as mean (SEM). (C) Cumulative incidence of escape [%] on Day 3 and Day 5 of reversal MWM phase. Statistics: Log-rank test followed by Bonferroni correction. Each data point represents the mean of four training trials. (D) Use of spatial and direct (green) strategies for platform localization. Statistics: Two-way RM ANOVA followed by Tukey’s multiple comparisons test. Values are expressed as mean (SEM). (E) Cumulative retention time [%] in South-West (SW) target quadrant, North-East (NE), North-West (NW), South-East (SE) during initial MWM phase. Statistics: Two-way RM ANOVA followed by Tukey’s multiple comparisons test. Values are expressed as mean (SEM). (F) Cumulative retention time [%] in North-East (NE) target quadrant, South-West (SW), North-West (NW), South-East (SE) during reversal MWM phase. Statistics: Two-way RM ANOVA followed by Tukey’s multiple comparisons test. Values are expressed as mean (SEM). The dashed red lines represent 25 % chance. E14.5 Sham (n = 10), P10 Sham (n = 10), Cohort 1 Sham (n = 9), Cohort 2 Sham (n = 10), Cohort 3 Sham (n = 8).

The similarity of all control groups independent of the different sample period allowed the proper comparison of the five 0.5 Gy groups.

12.1.2 Differences in Spatial Searching and Reference Memory Depending on Irradiation Time Point

Two-way RM ANOVA testing showed main effects of IR group ($F(4, 46) = 5.1, P = 0.0018$) and training day ($F(4, 184) = 49.1, P < 0.0001$) on the amount of spatial searching in the investigated groups (Figure 12-2). Post-hoc analysis with Tukey's test revealed that irradiation at E14.5 and P10 resulted in significantly less spatial searching on three out of five initial training days compared to irradiation during learning phases in the young adult mice (Figure 12-2 A; Day 3: $P_{E/C1} = 0.011, P_{E/C3} = 0.012, P_{P/C1} = 0.019, P_{P/C3} = 0.022$; Day 4: $P_{P/C1} = 0.014, P_{P/C2} = 0.0018, P_{P/C3} = 0.0004$; Day 5: $P_{E/C1} = 0.034, P_{E/C2} = 0.034, P_{E/C3} = 0.0046, P_{P/C3} = 0.016$).

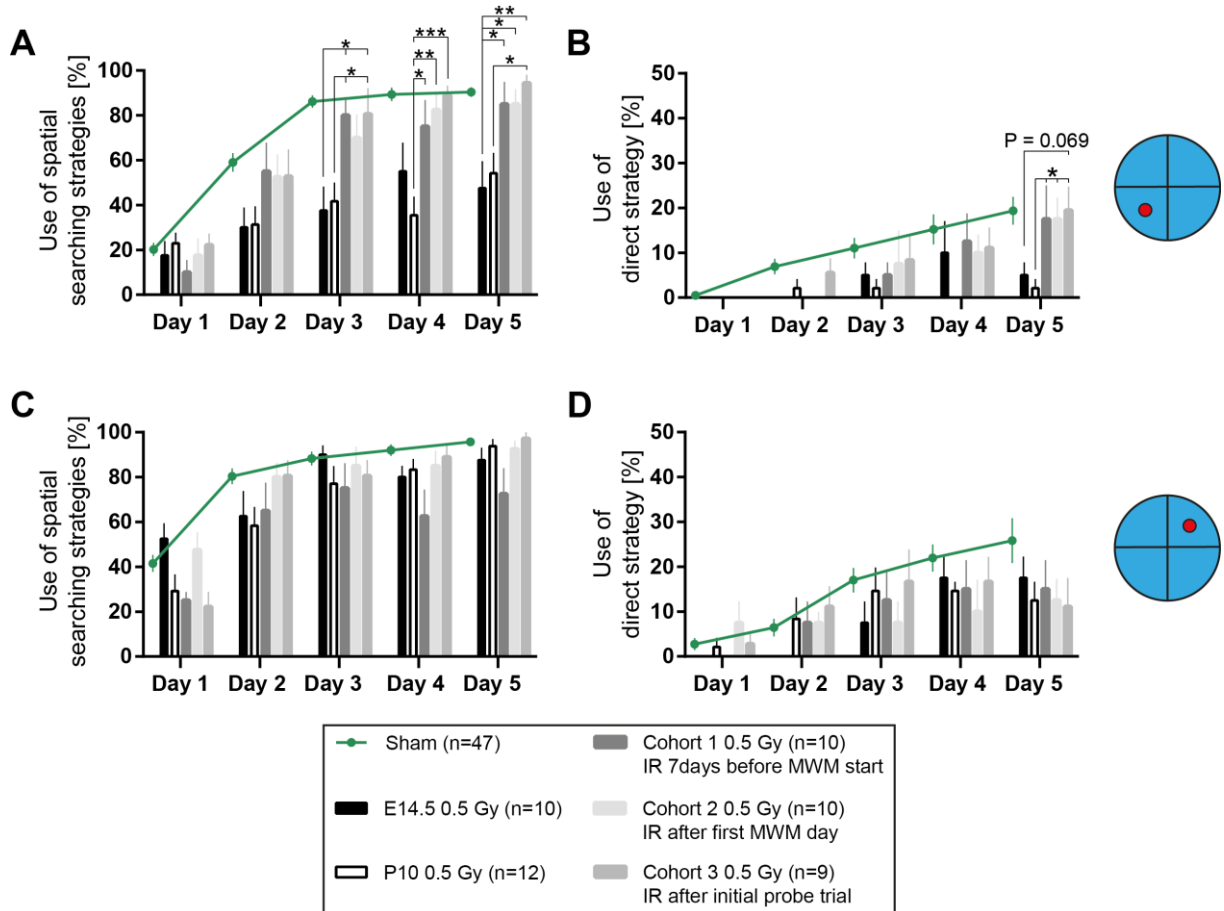


Figure 12-2: Irradiation during learning phases of the MWM did not affect spatial searching compared to irradiation at E14.5 or P10. (A) Use of spatial searching strategies [%] over the course of the initial training. Statistics: Two-way RM ANOVA followed by Tukey's multiple comparisons test, * = $P < 0.05$, ** = $P < 0.01$, *** = $P < 0.001$. (B) Use of direct strategy [%] over the course of the initial training. Statistics: Two-way RM ANOVA followed by Tukey's multiple comparisons test, * = $P < 0.05$. (C) Use of spatial searching strategies [%] over the course of the reversal training. Statistics: Two-way RM ANOVA followed by Tukey's multiple comparisons test. (D) Use of direct strategy [%] over the course of the reversal training. Statistics: Two-way RM ANOVA. Green curves represent Sham ($n = 47$), Black bars represent E14.5 0.5 Gy ($n = 10$), white bars represent P10 0.5 Gy ($n = 12$), dark grey bars represent Cohort 1 0.5 Gy ($n = 10$), light grey bars represent Cohort 2 0.5 Gy ($n = 10$), medium grey bars represent Cohort 3 0.5 Gy ($n = 9$). All values are expressed as mean (SEM).

Moreover, Two-way RM ANOVA analysis revealed a main effect of training day ($F(4, 60) = 9.96, P < 0.0001$). E14.5 and P10 animals showed a reduced amount of direct platform localization on initial day 5 compared to the three learning phase cohorts, as shown by post-hoc testing (Figure 12-2 B; $P_{P/C1} = 0.044, P_{P/C2} = 0.044, P_{P/C3} = 0.017; P_{E/C3} = 0.069$).

The amount of spatial searching strategies on reversal day 1 varied between the groups, suggesting that the early relearning process might be influenced by different irradiation time points. However, the five irradiation groups performed similar during the remaining days (Figure 12-2 C and D). All groups increased their amount of spatial searching until day 5. Even if cohort 1 displayed slightly decreased spatial searching compared to the other groups, they showed similar amounts of direct platform localization.

Two-way RM ANOVA testing of reference memory during the probe trials revealed main effects of quadrant ($F(3, 276) = 31.8, P < 0.0001$) and IR group ($F(5, 92) = 3.3, P = 0.0087$) on the cumulative retention time in the target quadrant SW during the initial probe trial. Follow-up testing showed significantly reduced retention times in SW of E14.5 and P10 animals compared to mice irradiated during one of the three learning phases (Figure 12-3 A; $P_{E/C1} = 0.0005, P_{E/C2} = 0.0027, P_{E/C3} = 0.001, P_{P/C1} < 0.0001, P_{P/C2} < 0.0001, P_{P/C3} < 0.0001$).

The groups did not differ in the cumulative retention time in the new target NE during the reversal probe testing (Figure 12-3 B).

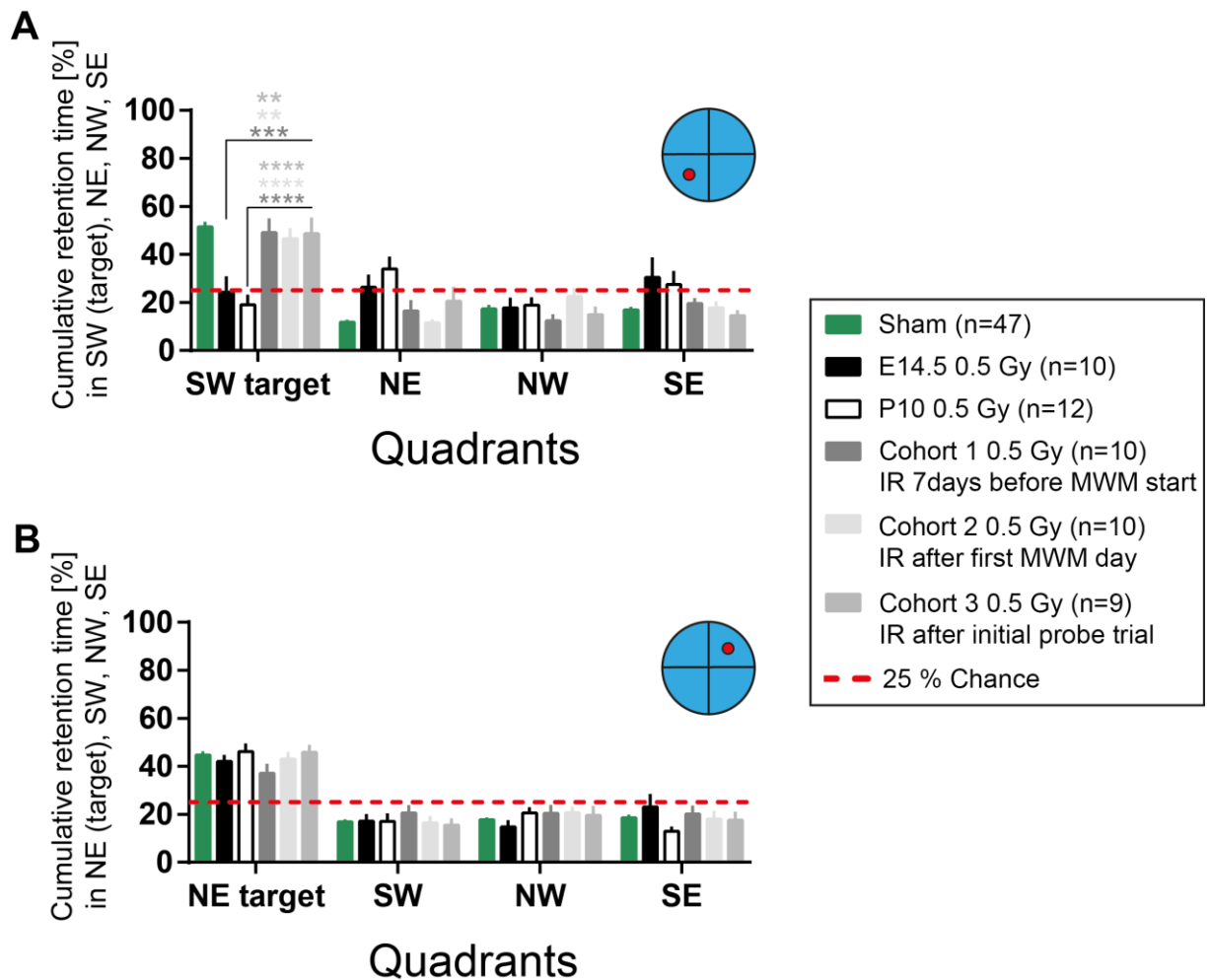


Figure 12-3: Irradiation during learning phases of the MWM did not affect reference memory compared to irradiation at E14.5 or P10. (A) Cumulative retention time [%] during initial probe trial in South-West (SW) target quadrant, North-East (NE), North-West (NW), South-East (SE). Statistics: Two-way RM ANOVA followed by Tukey’s multiple comparisons test, ** = $P < 0.01$, *** = $P < 0.001$, **** = $P < 0.0001$. (B) Cumulative retention time [%] during reversal probe trial in North-East (NE) target quadrant, South-West (SW), North-West (NW), South-East (SE). Statistics: Two-way RM ANOVA. Green bars represent Sham ($n = 47$), Black bars represent E14.5 0.5 Gy ($n = 10$), white bars represent P10 0.5 Gy ($n = 12$), dark grey bars represent Cohort 1 0.5 Gy ($n = 10$), light grey bars represent Cohort 2 0.5 Gy ($n = 10$), medium grey bars represent Cohort 3 0.5 Gy ($n = 9$). The dashed red lines represent 25 % chance. All values are expressed as mean (SEM).

Overall, radiation effects were detectable in E14.5 and P10 animals while irradiation during learning phases in the young adult mouse revealed only marginal influence on the development of spatial searching and the generation of spatial maps in the hippocampus. Therefore, the early irradiation time points were assumed to be more radiosensitive and thus critical for proper hippocampal function.

12.1.3 Evaluation of Searching Strategy Profiles

For further comparisons, it was interesting to evaluate how search patterns in the different groups were distributed. Figure 12-4 provides overviews about the range of searching strategies used by the different groups during day 3, 4 and 5 of initial training in the MWM, as these days were associated with the biggest differences in spatial searching. The strategy profile of the pooled Sham group clearly peaked at the orienting strategy (day 3: 52.6 %, day 4: 54.7 %, day 5: 55.9 %) and nicely showed that training day 3, 4 and 5 were hardly to distinguish (Figure 12-4 A). Thus, the Sham animals reached a proper and constant performance level already after a few training days. In contrast to that, it was conspicuous that the strategy profile of E14.5 mice always peaked at the scanning strategy independent of the training day (Figure 12-4 B; day 3: 42.5 %, day 4: 35.0 %, day 5: 45.0 %). This strategy is characterized by a shift away from the periphery of the pool and searching proceeds more in the pool center. However, mice do not yet show focused search. Overall, scanning indicates a progression away from less efficient strategies, however, it is not a spatial strategy. The strategy profile of the P10 animals was more widespread on the three training days, containing almost the whole range of available strategies. While day 4 was dominated by the scanning strategy (37.5 %), the P10 group shifted to a peak at the orienting strategy (39.6 %) on day 5. Nevertheless, the amount of orienting in the P10 animals was lower than in the Sham animals on that day (Figure 12-4 A and C). Both E14.5 and P10 animals were characterized by a lower amount of direct localization compared to Sham on the three days (Figure 12-4 A, B and C).

Generally, strategy use of cohort 1, 2 and 3 resembled the Sham profile. They also peaked at the orienting strategy on day 3, 4 and 5, leveling off at 42.5 % (C1), 65.0 % (C2) and 50.0 % (C3) orienting on day 5 (Figure 12-4 D, E and F). Additionally, they also showed similar amounts of direct localization on day 5 (Figure 12-4 D, E and F).

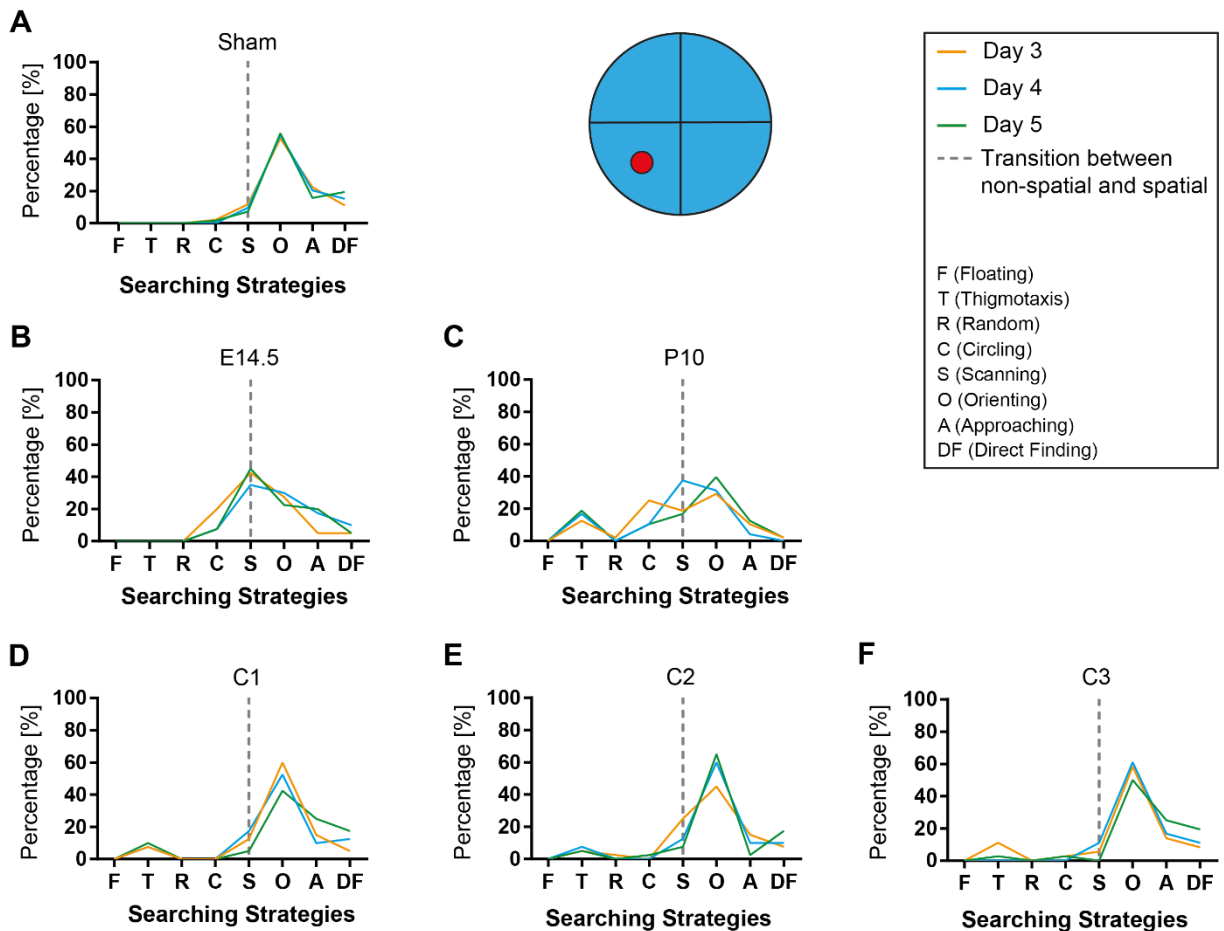


Figure 12-4: Searching profiles showing the distribution of the different searching strategies on day 3, 4 and 5 of initial learning. Percentage [%] of spatial strategies (A) Sham (n = 47). (B) E14.5 (n = 10). (C) P10 (n = 12). (D) Cohort 1 (C1, n = 10), IR 7 days before MWM start. (E) Cohort 2 (C2, n = 10), IR after first MWM day. (F) Cohort 3 (C3, n = 9), IR after initial probe trial. Orange curves represent Day 3, blue curves represent Day 4 and green curves represent Day 5. The dashed grey lines represent the transition between non-spatial and spatial strategies. All values are expressed as mean.

Figure 12-4 provides overviews about the range of searching strategies used by the different groups during day 3, 4 and 5 of reversal training in the MWM. The strategy profile of the Sham group was very similar in shape to the initial profile. Sham mice peaked again at the orienting strategy (Figure 12-5 A; day 3: 54.0 %, day 4: 53.8 %, day 5: 51.0 %) and their curves again overlapped on all three training days.

The strategy profiles of the E14.5 and P10 group observed during reversal learning shifted to a higher amount of spatial strategies. The E14.5 mice showed peaks at the orienting strategy on each of the three training days (Figure 12-5 B; day 3: 62.5 %, day 4: 47.5 %, day 5: 45.0 %) as well as increased amount of direct platform localization. The P10 group displayed similar percentages of orienting and approaching on day 3 (O: 29.2 %, A: 33.3 %), a peak at approaching on day 4 (39.6 %) and a peak at orienting on day 5 (54.2 %). In addition to that, direct localization was also increased in P10 animals compared to the initial learning (Figure 12-5 C). The three learning phase cohorts slightly differed in their strategy profiles, however, higher amounts of orienting were obvious in each of three cohorts on day 3, 4 and 5 (Figure 12-5 D, E and F).

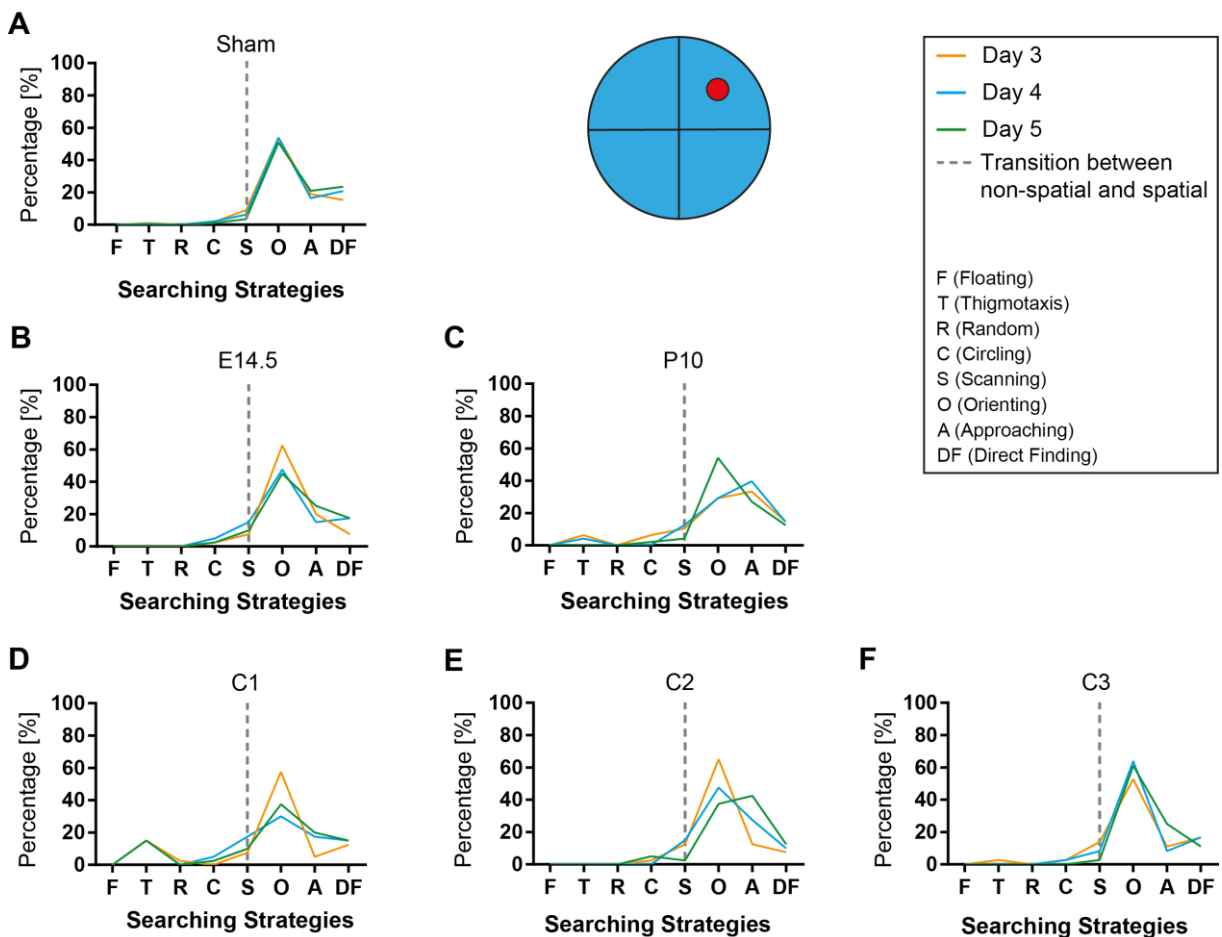


Figure 12-5: Searching profiles showing the distribution of the different searching strategies on day 1, 3 and 5 of reversal learning. Percentage [%] of spatial strategies (A) Sham (n = 47). (B) E14.5 (n = 10). (C) P10 (n = 12). (D) Cohort 1 (C1, n = 10), IR 7 days before MWM start. (E) Cohort 2 (C2, n = 10), IR after first MWM day. (F) Cohort 3 (C3, n = 9), IR after initial probe trial. Orange curves represent Day 3, blue curves represent Day 4 and green curves represent Day 5. The dashed grey lines represent the transition between non-spatial and spatial strategies. All values are expressed as mean.

12.2 Conclusion – Chapter V (Overarching Comparison)

Overall, both E14.5 and P10 mice differed from the learning phase cohorts in the initial phase of the MWM regarding their spatial searching and the formation of reference memory during training. Here, E14.5 and P10 performed quite similar both during initial and reversal learning. The three cohorts among themselves differed only marginally. Even if cohort 1 showed slightly decreased spatial searching during reversal learning, they used similar amounts of direct platform localization.

The analysis of the searching strategy profiles revealed that orienting turned out to be a prevailing strategy with progression of MWM training. Animals irradiated during different learning phases were able to develop Sham-like strategy profiles during the initial and reversal phase of the MWM test. Contrary to that, E14.5 and P10 needed more training to do so and could catch-up with the three cohorts and with Sham not until the reversal phase of the MWM.

Taken together, clear radiation effects were detectable in E14.5 and P10 animals while irradiation during learning phases in the young adult mouse revealed only marginal influence on the development of spatial searching and the generation of spatial maps in the hippocampus. Therefore, the early irradiation time points were assumed to be more sensitive to radiation and thus critical for proper hippocampal function. Furthermore, these results indicate an impairment or rather a delayed generation of allocentric spatial maps of the maze environment within the hippocampus after low-dose irradiation during critical developmental phases.

13 Discussion

Our modern society widely accepts the exposure to or the use of ionizing radiation in different contexts, especially if it is medically necessary and facilitates medical treatment conditions. This central base lead to an increase in the use of medical radiation over the past decades and accounts for the major source of exposure to ionizing radiation in the general population (Bernier et al., 2012; Mettler Jr et al., 2008, 2000). In spite of possible advantages, undesirable side effects for human health are often recognized. Especially, exposure to ionizing radiation may result in serious adverse consequences for normal brain development.

Several epidemiological studies have provided evidence for neurological impairments in children that were exposed prenatally to ionizing radiation. Studies on the terrible bombings of Hiroshima and Nagasaki revealed that *in utero* irradiation resulted in higher risk of developing small head size, mental retardation, lower IQ values and seizures. In particular, irradiation within the gestational weeks 8 to 15 and 16 to 25 turned out to be most harmful (Otake & Schull, 1993; Schull et al., 1990; Verheyde & Benotmane, 2007). This indicates a time-dependent sensitivity towards irradiation.

This study makes a contribution to the current discussion of low-dose ionizing radiation exposure. It focuses on the comparison between pre- and postnatal irradiation and the sensitivity of specific phases of brain development and maturation. Furthermore, my results contribute to the estimation of possible threshold doses and take a closer look at the influence of irradiation during learning and memory phases of the MWM in the young adult mouse. Thus, this study addresses the question if low doses interfere with specific learning processes. Finally, my results emphasize spatial searching strategies based on the formation of hippocampal cognitive maps as important read-out parameters to evaluate radiation effects in the mouse model. Cognitive maps enable animals to solve newly emerged spatial problems by making their spatial behaviour more flexible and efficient. Therefore, my results extend beyond the most widely used parameters for the analysis MWM performance (measuring of escape latencies and path lengths) that do not allow to address specifically the hippocampal contribution to MWM performance (Garthe & Kempermann, 2013). Taken together, this thesis adds

additional information to the understanding of the multifaceted impact of low-dose irradiation on hippocampal cognitive processes.

Generally, the current data situation regarding low-dose irradiation and effects on cognition is very complex, so that the risk possibly arising from exposure to low-dose radiation is still part of intensive and ongoing debates. Current results continue to be a matter of controversy. Oftentimes, available studies differ in many aspects and lack comparable testing procedures. On the one hand, animal studies suggest detrimental effects of treatments with low-dose ionizing radiation, involving genetic and epigenetic aberrations and a variety of physiological impairments (Tang et al., 2017). Various sequelae, like alterations during brain development resulting in impaired cognitive function, changes in the immune system and a shortened life-span can occur (Bellone et al., 2015, 2014; Nelson et al., 2014; Snijders et al., 2012; Takai et al., 2011; Tanaka et al., 2007; Yin et al. 2003). On the other hand, there are some studies describing beneficial long-term effects after low-dose exposure. The decline of tumorigenesis, a prolonged lifespan or the alleviation of diabetic nephropathy are a few examples (Ina & Sakai, 2004; Nomura et al., 2011; Sakai et al., 2006). The diverse outcomes of the reported observations are due to equally diverse experimental conditions. Those studies are based on varying irradiation procedures, different radiation types, several genetic backgrounds of the animals, different animal species, distinct pre- and postnatal irradiation time points and deviating experimental designs. Generally, studies also indicate that for example rats and mice differ in the use of strategies during spatial learning tasks (Frick et al., 2000) and that even distinct strains of the same species demonstrate task-dependent variations in their cognitive abilities (Yoshida et al., 2001). Taken together, the complexity and variability of low-dose ionizing radiation effects hampers their interpretation. It becomes apparent that our knowledge about the consequences of low-dose radiation exposure is still limited regarding the facets of cognitive function that can be affected and the radiation sensitivity of specific irradiation time points towards a specific dose range.

My experiments provide evidence for LDIR-induced aberrations during mouse brain development and maturation, resulting in long-term cognitive dysfunctioning. Changes

of hippocampal neurogenesis and failing of proper integration of new neurons into the hippocampal circuitry might both contribute to the observed aberrant behaviours.

13.1 Impact of LDIR on Motor Function and Anxiety-like Behaviour

Rotarod Results

The accelerating Rotarod performance test (Jones & Roberts, 1968) was used as a pretest to ensure that the investigated animals exhibited similar gross motor abilities. The mice must permanently walk forward to prevent falling off a rotating bar. Mice with motoric impairments or deficits in balance would drop down the rotating bar usually during the first minute of the test, while mice with intact motor coordination have no difficulties in maintaining balance for several minutes.

My results demonstrate that irradiated C57BL/6 mice (E14.5 and P10) performed properly on the accelerating Rotarod. Thus, low-dose irradiation ≤ 0.5 Gy did not result in motor or coordination deficits, proving adequate motor function (Figure 8-1 A; Figure 9-1 A). The mice assigned to the different learning phase cohorts showed likewise proper motor function (Figure 10-1 A, B and C).

Other studies with C57BL/6 mice (Koturbash et al., 2017; Verreet et al., 2015) partially report motoric differences in the Rotarod test after single whole-body irradiation with 1.0 Gy during embryonic development (E11) or after fractionated low-dose radiation (0.1-0.5 Gy) in adult animals and following skilled ladder walking test. This indicates that specific time points of brain development, however, might be susceptible to moderate irradiation doses, leading to motoric deficits. Furthermore, accumulation of fractionated low-dose radiation represents a particular challenge that can impair motor function even in adult animals.

However, this was clearly not the case in my experiments. Thus, adequate motor performance in the following cognitive tests was assumed.

EZM Results

The Elevated Zero Maze (Heisler et al., 1998; Shepherd et al., 1994) is based on a natural conflict in rodents between exploration of novel environments and the aversive properties of brightly lit, exposed areas (Lister, 1987; Montgomery, 1955; Pellow et al., 1985). On the one hand, mice tend to explore novel environments. On the other hand, they avoid to expose themselves and instead seek for shelter by hiding away or

exhibiting thigmotactic behaviour. The EZM provides both sheltered and aversive features that allow the investigation of the anxiety, exploration and activity status of the animals.

My results demonstrate normal activity levels in mice irradiated at E14.5 (Figure 8-1 B). Even if overall anxiety levels were quite similar compared to Sham, irradiation with 0.125 Gy reduced the time of the nose-point in the open areas (Figure 8-1 C). This might indicate that the lowest applied dose could elicit elevated anxiety responses for this body point. Based on the nocturnal activity of some rodents, including mice, behaviours like whisking (Gao et al., 2001; Knutsen et al., 2006) and exploratory sniffing (Kepecs et al., 2007; Wesson et al., 2008) are crucial to actively acquire information from the environment. In this respect, the nose point data appears interesting and is worth mentioning, since this body part provides the mouse with a lot of sensory information. Mice are using nose-contact and olfaction to interact with their environment, thus it constitutes an essential sense that is used among others for exploration and avoidance of potentially dangerous conflicts (Gillis & Datta, 2017). In direct comparison to that, irradiation with 0.125 Gy at P10 might be responsible for the hypoactivity that was indicated by a decreased distance and reduced velocity compared to Sham and 0.5 Gy mice (Figure 9-1 B).

Thus, application of a low dose in the range of medical treatments might generate different read-outs in the Elevated Zero Maze depending on the irradiation time point. Consequently, it might be assumed that the radio sensitivity of different vulnerable stages of brain development manifests in distinct altered behavioural attributes.

Interestingly, Verreet et al. (2015) analyzed the circadian horizontal cage activity in their mice and reported that exposure to 0.5 Gy at E11 caused hyperactivity during the dark cycle. Furthermore, exposure to 0.2 Gy, 0.5 Gy and 1.0 Gy at E12 caused both hyperactivity during the light cycle and hypoactivity during the dark cycle. Their observed alterations of activity status highly depended on the developmental time point and the applied dose (Verreet et al., 2015).

The study by Koturbash et al. (2017) revealed that C57BL/6 mice exposed to fractionated low-dose radiation performed worse in an open field task. At least irradiation with 0.4 Gy and 0.5 Gy reduced the retention times in the center of the open field, suggesting elevated anxiety levels (Koturbash et al., 2017).

Another publication (Baskar & Devi, 2000) analyzed effects of *in utero* exposure (E11.5, E12.5, E14.5 and E17.5) to low-level gamma radiation (0.25 Gy, 0.35 Gy, 0.5 Gy) on postnatal behaviour in a 3 months old Swiss albino mouse model. They observed a dose-dependent reduction of line crossings (E11.5-E14.5) and rearings (E11.5-E17.5) during open-field testing, indicating deficient locomotor and emotional activity. In a light/dark arena test, mice showed a dose-dependent decrease in numbers of line crossings in the dark sector for either of the irradiation time points with significant differences after 0.35 Gy or 0.5 Gy irradiation (E11.5-E14.5). Furthermore, 0.5 Gy mice showed reduced retention times in the dark area of the apparatus. All in all, their data point to disturbances of locomotor activity, anxiety-related and exploratory behaviours, respectively.

A further study compared effects of postnatal low-dose irradiation on spontaneous behaviour in a novel environment in NMRI and C57BL/6 mice (Eriksson et al., 2016). Irradiation at P3 or P10 but not P19 with 0.5 Gy significantly reduced locomotion, rearings and total activity during the first third of the test in two months old NMRI mice while the same parameters were significantly increased in the last third of the test. The assessment of dose-response (0.02 Gy, 0.1 Gy, 0.5 Gy, 1 Gy) showed that P10 was most sensitive to irradiation with 0.5 Gy and 1 Gy. Results were similar in C57BL/6 mice. In essence, this study shows that exposure to low or moderate irradiation doses during critical postnatal stages is involved in the induction of behavioural disorders. A radiation-sensitive period seems to be around P3 to P10 in mice.

Altogether, the data of others point out that whole body irradiation could interfere with various behavioural facets concerning the motoric system, anxiety responses and activity levels during exploration of novel environments. Especially early developmental phases could be particularly sensitive to low radiation doses. In conclusion, my data gives cautious hints that it might be possible to disturb normal behavioural attributes even with a very low dose and that effects could differ depending on irradiation time point. However, keeping in mind that the EZM test procedure depicts a snapshot, the observed preliminary effects in my mice might also be influenced by factors like the form on the day of testing. Therefore, further analyses will be necessary to ascertain if changes in anxiety or activity behaviour are likely to occur with our irradiation protocol. A set of assays to evaluate baseline activity (circadian cage activity), approach and

avoidant behaviours (light/dark box, social interaction, open field test, novelty suppressed feeding test) or defensive behaviours (acoustic startle response, freezing behaviour) could be helpful in further investigations.

13.2 Impact of LDIR on Hippocampus-dependent Spatial Navigation

The reference memory protocol used during my MWM experiments is characterized by distant visual cues, constant hidden platform positions during initial and reversal learning and probe trials without platform. With such a protocol, mice normally acquire memory about the platform position within a few days while escape latencies decrease to constant low levels and probe testing results indicate successful spatial memory by a clear preference for the target quadrant.

However, when comparing similar studies, one has to keep in mind that the read-out is influenced by several factors like the size of the MWM pool, the number and complexity of visual cues as well as the age and the traits of the trained animal models (Garthe & Kempermann, 2013). Taken together, my reference memory protocol used here tests allocentric spatial learning and thus the development and modification of cognitive maps providing information about both the general layout of the maze and concrete locations within the maze as part of a route that can be used in subsequent trials. Start positions were semi-randomly chosen for each trial, so that allocentric navigation to the platform by remembering its coordinates relative to distant extramaze visual cues was reinforced and should dominate over egocentric navigation (Moghaddam & Bures, 1996; Morris et al., 1982, 1986; Vorhees & Williams, 2014).

13.2.1 Initial MWM Phase

My MWM data revealed long-term deficiencies regarding the initial learning process in two month old C57BL/6 mice irradiated at E14.5 or P10. Results of both time points highlight a dose-dependent impairment of MWM performance, characterized by decreasing efficiencies in spatial searching and disturbed reference memory with increasing irradiation dose (Figure 8-2; Figure 9-2). Especially, the development of straight swimming paths, reflecting the precision of search, was affected by irradiation (Figure 8-2 C; Figure 9-2 C). Spatial swim patterns represent the most efficient escape strategies for localization of the hidden platform and are thus the silver bullet to success in the MWM test. Spatial platform targeting mirrors the proper functioning of the

hippocampus-dependent allocentric place navigation and thus the proper formation of a cognitive map (Buzsáki & Moser, 2013; Rogers et al., 2017; Vorhees & Williams, 2014). Additionally, the probe testing without platform of the 0.5 Gy animals (E14.5 and P10) revealed reduced retention times in the target quadrant, indicating a decreased preference for this zone (Figure 8-3; Figure 9-3). Consequently, my results indicate that allocentric place navigation, the formation of a cognitive map and the reference memory for the platform position in the initial MWM phase was disturbed by low-dose irradiation at E14.5 and P10.

In contrast to that, mice of the learning phase cohorts (Figure 7-3) displayed nearly Sham like performance in all parameters of the MWM test independent of the distinct MWM learning phase (Chapter III; Figure 12-2; Figure 12-3; Figure 12-4 D, E and F; Figure 12-5 D, E and F). This suggests that MWM learning is robust and resistant to LDIR when it is applied during a short-term pre-test phase (Cohort 1), during an early phase critical to cognitive map formation and memory consolidation (Cohort 2) and prior to relearning processes (Cohort 3). In the direct comparison, both E14.5 and P10 mice also differed from the learning phase cohorts in the initial phase of the MWM task in regard to their spatial searching and the formation of reference memory during training. The three cohorts among themselves differed only marginally (Figure 12-2; Figure 12-3). In the searching strategy profiles of Sham control and learning phase animals (Figure 12-4 A, D, E and F), beside approaching and direct finding, orienting turned out to be the prevailing strategy with progression of MWM training. In contrast to that, both the E14.5 and the P10 group displayed high amounts of inefficient strategies like scanning, circling or thigmotaxis (Figure 12-4 B and C), indicating malformation or dysfunctioning of the cognitive map.

Normally, mice pass through different stages of MWM learning, characterized by different searching strategies (Dalm et al., 2000; Graziano et al., 2003). First, they typically show thigmotactic or random swimming behaviours which are followed by an increase of distance to the edge of the pool. Circling and Scanning emerge as further strategies which often result in platform discovery. The development of the Scanning strategy indicates a more systematic search, but it is still associated with random searching of other regions of the arena (Gehring et al., 2015). Therefore, it was considered as non-spatial in my results, but was used to demarcate the transition to

spatial searching. Non-spatial patterns have been found to persist in animals with hippocampal impairment (Hodges, 1996). The use of spatial strategies marks the onset of allocentric navigation, when focused searching using the distant visual cues has priority. Spatial searching refines from orienting over approaching until mice show direct finding of platform the position (Rogers et al., 2017; Wolfer & Lipp, 2000).

Interestingly, Gil-Mohapel et al. investigated all phases of the neurogenic process: cell proliferation, neuronal differentiation, cell survival and overall neurogenesis, throughout the lifespan of C57Bl/6 mice and analyzed age effects on learning and memory in a MWM test (Gil-Mohapel et al., 2013). They showed that both neurogenesis and learning and memory performance were highest around the age of 1.5 months. Following this peak, they observed a steady decrease in neurogenesis with age. Interestingly, they could show a correlation between levels of overall neurogenesis and the observed searching strategies. Higher levels of neurogenesis in younger animals coincided with more efficient spatial strategies while older mice with lower levels of neurogenesis showed more inefficient search patterns. This observation indicates that levels of neurogenesis could predict searching strategies used in spatial learning tasks.

Taken together, two specific critical phases of murine brain development and maturation turned out to be particularly sensitive to LDIR. The long-term consequence was the impaired formation of cognitive spatial maps of the maze environment in the hippocampal formation which is crucial for the development of proper spatial searching in the MWM. Therefore, I could demonstrate that low-dose irradiation specifically affected the hippocampal contribution to the MWM performance.

In terms of experimental design, the study by Verreet et al. (2015) allows a suitable comparison to my investigations. They analyzed the impact of low-dose ionizing radiation at the beginning of neurogenesis on three different time points E10, E11 and E12. Therefore, mice were exposed to different X-ray doses, ranging between 0 and 1 Gy. Behavioural analysis took place when the mice were 3 months old. The MWM set-up that was used differed in diameter (150 cm) and the training procedure deviated from the test protocol in this thesis by four additional training days and the absence of

a reversal learning phase. Furthermore, Verreet et al. performed longer probe trials (100 s) four days after the last training day.

The authors reported that irradiation at E10 did not result in aberrations during MWM memory acquisition. However, an impairment of reference memory consolidation during the probe trial after irradiation with 0.2 Gy and 1 Gy at E10 was salient, as those mice did not prefer the predefined target sector. Conspicuous for me were the elevated escape latencies in the 0.2 Gy group during the first half of their training blocks, even if those did not reach a statistical significance. Interestingly, irradiation with 1 Gy at E11 also impaired spatial learning during the acquisition phase of the MWM. Here, significantly increased escape latencies over the whole training period of eight days were observed. Moreover, these animals displayed significantly reduced retention times in the target quadrant compared to their controls. Consequently, mice irradiated with 1 Gy at E11 were characterized by deficits of both spatial learning and memory. Mice irradiated at E12 did not differ in the MWM acquisition phase or in the corresponding probe trials. Taken together, Verreet et al. obtained the strongest effects on spatial learning and long-term memory with a dose of 1 Gy at time point E11, but even lower doses of 0.2 Gy were sufficient to disturb spatial memory at E10. Unfortunately, they did not comment on the use of spatial searching strategies or put their results into relation with the formation of cognitive maps. Generally, the degree of radiation sensitivity seems to differ within very narrow time windows during embryonic development between the onset of neurogenesis around E10 (Hatten, 1999; Rice & Barone Jr., 2000) and the subsequent migration of dentate precursor cells at E14.5 (Urban & Guillemot, 2014), as my results demonstrate.

A study by Baskar & Devi (2000) reports impairment of learning and memory functions after low-dose irradiation at prenatal time points. In a modified hole board test with three consecutive training days, irradiation increased the numbers of hole pokes, indicating disturbed learning. Strongest impairments were observed on day 1 and 2 of testing after irradiation at E11.5 with 0.35 Gy and 0.5 Gy. Exposure at E12.5 also increased the number of hole pokes with significant differences on the first and second training day after irradiation with 0.5 Gy. On training day 3, mice irradiated on both E11.5 and E12.5 performed as good as controls, clearly indicating a learning delay. Irradiation with 0.5 Gy at E14.5 significantly increased hole pokes on the first training

day. Baskar & Devi further used an active avoidance test box equipped with two grid areas connected to separate electric circuits for assessment of learning and memory deficits. During the test, mice learn that a 10 s discriminative stimulus predicts electric foot shocks that can be avoided by crossing the box to the opposing side during the 10 s time interval. Mice exposed to 0.5 Gy at E11.5, E12.5 and E14.5 showed significantly extended retention scores which reflect the impairment of learning and memory function. Irradiation with 0.35 Gy at E11.5 resulted at least in a noticeable negative effects in this test.

Cognitive long-term deficits were also detected after postnatal irradiation of ten days old NMRI mice (Kempf et al., 2014). The authors reported significant reductions in cognitive performance. In detail, they observed alterations in spontaneous behaviour in a novel environment at two and four months of age following a single 0.5 Gy or 1 Gy irradiation. They also concluded that neurocognitive deficits in adult animals could result from exposure to low or moderate radiation doses at this early postnatal stage.

A further study using NMRI mice suggests that 0.35 Gy seems to be a tentative threshold dose for eliciting negative persistent behavioural deficits. The same study revealed that 0.5 Gy at P10 were suitable to significantly increase levels of tau protein in the cerebral cortex in 6 months old mice (Buratovic et al., 2014).

As a member of the microtubule-associated protein family, tau plays a role in the outgrowth of neural processes and in the stabilization and maintenance of normal neuronal morphology (Biswas & Kalil, 2018; Wang & Liu, 2008). Increased levels of phosphorylated tau have been observed to impair memory and learning in humans and are a diagnostic sign of Alzheimer's disease.

Taken together, my data and those of others point to threshold doses below 0.5 Gy that are sufficient to influence behaviour. Interestingly, even doses as low as 0.125 Gy and 0.25 Gy applied at E14.5 and P10, respectively, were sufficient to influence the learning process in my experiments. Therefore, it is conceivable that the tentative threshold dose of 0.35 Gy suggested by Buratovic et al. could even be reduced further.

13.2.2 Initial Deficit in Spatial Navigation Could Result from Impairment of the Neurogenic Niche

The hippocampal circuitry is crucial for spatial memory formation (Hartley et al., 2014; M. Moser et al., 2015). Integration of new granule cells into the existing hippocampal network adds an additional level of complexity to neural plasticity (Colangelo et al., 2019; Taupin & Gage, 2002; Toni et al., 2008; Urban & Guillemot, 2014). Several studies on adult hippocampal neurogenesis have linked this process to learning and memory (Döbrössy et al., 2003; Drapeau et al., 2003; Kempermann & Gage, 2002; Leuner et al., 2004).

My immunohistological results show that irradiation with 0.5 Gy reduced the number of DCX⁺ progenitor cells in the adult dentate gyrus of naïve mice after both the embryonic and the early postnatal irradiation (Figure 11-1). However, this cell loss was stronger in mice irradiated at E14.5 compared to the P10. LDIR at E14.5 resulted in approximately 35 % less progenitor cells and was associated with a reduction of DG area about 15 %. Contrary to that, IR at P10 reduced the cell number by 17 % while the DG took up an area of approximately 6 % less compared to Sham. My mice were further investigated after the MWM task by Prof. Dr. Andreas Hess and his research group. Interestingly, they observed that irradiation with 0.5 Gy at E14.5 caused a decrease in brain size, as shown by voxel-based morphometry (data not shown; MRI experiments were performed in the lab of Prof. Dr. Andreas Hess, University of Erlangen).

Vulnerability of the neurogenic niche in the dentate gyrus

Doublecortin (DCX) is a microtubule-associated protein and can be used as a marker of neurogenesis (J. Brown et al., 2003; Rao & Shetty, 2004). DCX is essential for regular migration of neurons and one of the earliest differentiation markers in neuronal differentiation, thus expressed by cells committed to a neuronal lineage in both the developing and the adult brain (Hodge & Hevner, 2011; Kempermann et al., 2015; von Bohlen und Halbach, 2007, 2011). In particular, expression of DCX in adult dentate progenitor cells starts with the type-2b IPC phenotype, is maintained during the type-3 neuroblast stage and persists up to the first two to three weeks of postmitotic maturation of immature dentate granule cells (for details see section 4.2.4; Figure 4.3).

Based on its presence in neuronal leading processes during migration and in axons of differentiating neurons, DCX is suggested to play a role in the outgrowth of neuronal processes (Francis et al., 1999).

The observed changes in the numbers of DCX⁺ progenitor cells in my naïve mice could explain the worsened performance in the MWM learning task after low-dose irradiation. It would be conceivable that my observed reduction of progenitor cell number after irradiation associated with impairment of efficient spatial searching could to some extent mirror a stage of premature hippocampal aging that would match with the results described in the study of Gil-Mohapel et al. (2013).

In line with my results, the observed deficits in spatial learning and memory after low-dose irradiation described by Verreet et al. (2015), were associated with a significant decrease in proliferating Ki67⁺ progenitor cells and beyond that with substantially reduced numbers of Sox2⁺ progenitor cells in the juvenile hippocampus. In addition to that, they also observed significant reductions of cortical thickness (24 h after irradiation at E11), brain volume and ventricle size (both 1 week after irradiation at E11).

Mizumatsu et al. (2003) could show that irradiation of two months old C57BL/6 mice with 2 Gy reduced the DCX⁺ cell number by approximately 20 % 48 h later. They also reported that the number of Ki67⁺ proliferating cells was exceedingly reduced by 75 % after 1 Gy and by 90 % after 2 Gy (Mizumatsu et al., 2003). Ki67 is commonly used as a marker for actively proliferating progenitor cells which exclusively express the Ki67 protein (Cavegn et al., 2013; Juríková et al., 2016).

A further study conducted by Kim et al. (2008) investigated cell death and neurogenesis in two months old ICR mice after whole-body gamma-irradiation with 0.5 Gy, 2 Gy or 4 Gy. They observed significant dose-dependent reductions in Ki67⁺ and DCX⁺ cells with increasing dose in the dentate gyrus. In addition to that, their mice were impaired in object recognition memory which is also hippocampus-dependent. Thus, the observed memory dysfunction was in accordance with the alterations in neurogenesis following irradiation.

Furthermore, Raber et al. (2004) report that numbers of Ki67⁺ proliferating and DCX⁺ immature neurons were reduced by 90 % in 5 months old C57BL/6 mice that were irradiated with a high dose of 10 Gy three months earlier. These results were related to the impaired performance in another test for the analysis of spatial learning and

memory, the Barnes Maze. Here, irradiated mice used significantly less spatial search patterns, covered longer distances and showed an increased error rate during localization of the escape tunnel (Raber et al., 2004).

A further study by Rola et al. (2004) showed that whole brain irradiation with 2 to 10 Gy in three weeks old C57BL/6 mice dose-dependently reduced proliferating cells in the subgranular zone and immature neurons 48 h later. They could further demonstrate by BrdU stainings that irradiation with 5 Gy resulted in decreased production of new granule cells 1 and 3 months after irradiation. The observed impairment of neurogenesis was associated with spatial memory retention deficits in the Morris water maze task three months after irradiation (Rola et al., 2004).

In comparison to fully developed neurons, neurogenic areas harboring stem and neural precursor cells are considered as radiosensitive (Fike et al., 2009; Mizumatsu et al., 2003; Rola et al., 2004). My data and those of others clearly demonstrate that the neurogenic niche in the dentate gyrus reacts very sensitive to radiation exposure, even if doses are low, and that alterations in neurogenesis are associated with learning and memory deficits. As my observed impact on neurogenesis was differently pronounced in naïve animals irradiated at E14.5 or P10, whereas the observed cognitive effects were quite similar, a reduction of progenitor cell numbers in the adult animals and thus less integration of new cells into the hippocampal network was probably not the only relevant trigger for cognitive impairment. It is conceivable that a combination of underlying processes is responsible for the observed learning deficiencies after irradiation at E14.5 or P10 and that the components of this combination have a different impact depending on the specific irradiation time point. On the one hand, irradiation-induced progenitor cell loss during embryonic development and a disturbed migration of neuroblasts to their target areas could be of more significance for long-term cognitive deficiencies after irradiation at E14.5. On the other hand, it is conceivable that irradiation at P10 has a greater impact on synaptic wiring and slightly less impact on neurogenesis. Subsequently, this would lead to insufficient integration of immature granule cells into the hippocampal network, as the predominant factor. The formation of synapses is important for learning and memory processes.

Effects on Migration

Embryonic development of the dentate gyrus is characterized by migration of proliferative progenitor cells and the formation of the dentate migratory stream (DMS) that starts from the dentate neuroepithelium (primary matrix) and spreads out to the future dentate gyrus in late embryonic development (Altman & Bayer, 1990a, 1990b; Nelson et al., 2020; Urban & Guillemot, 2014). The primary matrix is a part of the ventricular zone and becomes discernible from embryonic day 14.5 on, the time point of initial DMS formation. Embryonic day 14.5 coincides with the start of migration of precursors and immature neurons in direction of the pial surface and hippocampal fissure, a process that is conveyed by Cajal-Retzius cells (Altman & Bayer, 1990a, 1990b; Del Río et al., 1997; Nelson et al., 2020; Rickmann et al., 1987; Urban & Guillemot, 2014). Thus, E14.5 represents a crucial time point during the development of the dentate gyrus in regard to migratory events that could be particularly susceptible to irradiation.

On their further way, the progenitor cells form a new migratory population called the secondary matrix while simultaneously glial scaffolding starts. This, together with Cajal-Retzius cells, has crucial functions in the organization of progenitor and dentate granule cells (Urban & Guillemot, 2014). A proliferative tertiary matrix is formed when the progenitor cells arrive and accumulate in the hippocampal fissure around E17.5. Subsequently, the granule cell layer is built up and adapts its final shape to the surrounding Cajal-Retzius cells that secrete reelin, acting as a positioning signal. In early postnatal life, the tertiary matrix remains the only source of dentate progenitors and granule cells (Frotscher, 1998; Li et al., 2009; Nelson et al., 2020; Urban & Guillemot, 2014). Subsequently, regarding a disturbed migration of neuronal progenitors to their target areas, E14.5 turns out to be a crucial step during dentate gyrus development.

It is conceivable that irradiation during such a sensitive phase influences normal cell adhesion by changing gene expression. Thus, it could be possible that migrating progenitors miss their designated target areas after irradiation, leading to aberrant formation of the tertiary matrix and contributing to the observed significant reduction in DCX positive progenitor cells in my naïve animals after irradiation at E14.5.

In line with this, a recent study reports that gene expression was dose-dependently changed by chronic low-dose irradiation of cultured human neural progenitor cells

(Katsura et al., 2016). Besides a decreased area of neural cells and a reduced length of neurites after irradiation with 0.496 Gy, the authors could show that 0.124 Gy and 0.496 Gy of radiation affected several cell adhesion pathways, including molecules like NCAM (neural cell adhesion molecule) which is important during axon guidance and neuronal migration (Maness & Schachner, 2007). PSA-NCAM (polysialylated NCAM) which is also involved in the regulation of chain migration in the rostral migratory stream (Chazal et al., 2000) is downregulated during adulthood and limited to specific areas that maintain their neurogenic potential and their ability of structural and functional plasticity, like the dentate gyrus (Seki & Arai, 1993).

A further study in rats showed effects of *in utero* exposure to doses as low as 15 cGy which resulted in decelerated neuronal migration and decreased expression of NCAM after irradiation at E16 (Fushiki et al., 1996).

In line with this, Inouye et al. (1993) reported that neuronal migration of cortical cells was impaired by low-dose gamma irradiation with 0.24 Gy at E17 in mice, as shown by comparative BrdU labeling at E16 and E17. The authors demonstrated that two days old irradiated mice exhibited more BrdU labeled cells remaining in the ventricular zone compared to Sham controls. In a long-term analysis, they found less BrdU labeled cells in cortical layers II-III and more BrdU labeled cells in cortical layers IV-VI in six week old mice that were prenatally irradiated and compared to Sham (Inouye et al., 1993).

Effects on Synaptogenesis

Generally, a sensitive period towards neurotoxic treatments causing behavioural alterations in the adult animal seems to exist in the neonatal mouse around postnatal day 10 (Eriksson 1997). This stage also represents a critical period characterized by the peak of brain growth spurt and synaptogenesis. The transmission of chemical signals through synapses represents the main channel of communication in the brain. In species with more complex brains such as primates, synaptogenesis extends over a protracted period starting prenatally and proceeding into postnatal life (Chen et al., 2017). In humans, synaptogenesis is reported to begin around gestational week 8. It continues beyond birth, peaking in the first year of life (Herschkowitz et al., 1997). Synaptogenesis is characterized by rapid and specific changes of synapse numbers, morphologies and protein expression and generally takes place at low rates throughout life (Chen et al., 2017; Meredith, 2015; Rice & Barone Jr., 2000). In rodents, the

majority of synaptogenesis occurs during the first three weeks after birth and is most active in the first two weeks (Crain et al., 1973; O’Kusky et al., 2000; Semple et al., 2013; Steward & Falk, 1986). In particular, the bulk of synaptogenesis in mice is limited to the first two postnatal weeks, with a sudden increase in synaptic density at P10 (Chen et al., 2017; Semple et al., 2013; Waites et al., 2005). Consequently, regarding alterations in synaptogenesis of neuronal progenitors, P10 turns out to be a decisive step during dentate gyrus maturation.

Concerning my P10 results, it is conceivable that irradiation of cells at this time point, disturbed synaptogenesis and underlying molecular mechanisms. In particular, the rapid increase in synapse numbers allows neurons to establish and strengthen synaptic connections to other neurons, thereby adapting, refining and stabilizing their synaptic contacts (Gonzalez-Lozano et al., 2016; Harms & Dunaevsky, 2007). Generally, exposure to ionizing radiation during sensitive developmental periods has been linked to altered synaptogenesis (Rice & Barone Jr., 2000; Sotelo & Beaudet, 1979). As a consequence, it is conceivable that irradiated immature cells are only poorly integrated into the hippocampal network.

In agreement with this, modifications of the Rac1-Cofilin signaling pathway in the cortex and hippocampus of six to seven months old NMRI mice have been described after irradiation with 0.5 Gy or 1.0 Gy at P10 (Kempf et al., 2014). This pathway is related to synaptic actin remodeling, spine and synapse formation as well as maturation (Saneyoshi et al., 2010). Kempf et al. further showed that genes involved in synaptic plasticity like Arc, c-Fos and CREB were downregulated in hippocampus and cortex after 1 Gy irradiation. The authors further observed elevated levels of miR-132, miR-134 and miR-212 microRNA after 0.5 Gy and 1 Gy in both hippocampus and cortex, also linking effects of low-dose irradiation to epigenetic modulation.

Thus, similar effects of low-dose irradiation in ten days old C57BL/6 mice seem likely, even if the question remains of how the different age of investigation (2 vs. 6-7 months) influences the severity of impairment.

A following study (Kempf et al., 2015) reports that prenatal irradiation of C57BL/6 mice at E11 also had long-term effects on hippocampal and cortical signaling pathways related to CREB-dependent synaptic plasticity. In detail, six months old mice showed decreased phosphorylated CREB levels in the cortex after irradiation with 0.5 Gy or 1 Gy at E11. Hippocampal levels of phosphorylated CREB were significantly reduced after

0.1 Gy, 0.5 Gy and 1 Gy. Importantly, reduction of CREB phosphorylation affects synaptic plasticity in the hippocampus (Bourtchuladze et al., 1994; Miyamoto, 2006). Furthermore, Kempf et al. also observed a strengthened expression of PSD95, suggesting effects on synaptic plasticity in neuronal dendrites. In line with this, studies have shown that PSD95 is critically involved in balancing the ratio of excitatory and inhibitory synapses and that alterations in PSD95 levels can lead to learning impairments (Migaud et al., 1998; Prange et al., 2004).

How far irradiation at E14.5 would affect the same signaling pathways has to be analyzed, just like the comparison of time point E14.5 and P10 to elucidate to what extent synaptic actin remodeling, spine and synapse formation as well as maturation are affected.

Taken together, an accumulation of the above effects could contribute to my observed cognitive deficits after *in utero* and early postnatal irradiation. Further experiments addressing the influence of low-dose irradiation at E14.5 and P10 on synapse formation could help to elucidate to what extent aberrant integration of newly generated granule cells into the hippocampus plays a role. Thus, it will be necessary to analyze the different progenitor subpopulations in more detail. Immature granule cells and fully developed granule cells should be characterized according to the development, structure and complexity of their dendritic trees, their synaptic gene expression and corresponding protein profiles after irradiation. Further, it will be interesting to analyze to what extent mice irradiated at E14.5 and P10 show impaired migration.

In my histological experiments, I used naïve mice that did not perform the set of behavioural tasks. Therefore, it would be necessary to analyze the radiation impact on the dentate gyrus in mice that went through the behavioural analysis, including the MWM learning task. By using mice from different learning phases and a combination with BrdU/EdU stainings, it would be possible to elucidate numbers of newly generated cells in the dentate gyrus for the corresponding time points. Thus, the conditions over the course of the whole spatial training could be analyzed in more detail. A combination of BrdU and EdU labeling would also be suitable to elucidate migratory deficits with special regard to the hippocampal formation.

Moreover, the investigation of non-naïve mice would also provide some indication to what extent passing the behavioural tests per se influences the hippocampal

morphology after irradiation. Factors like enriched environment or voluntary running are known to enhance neurogenic processes in the hippocampus (Fordyce & Wehner, 1993; Kempermann et al., 1997; van Praag et al., 1999, 2000; Wainwright et al., 1993). Thus, the confrontation of the animals with challenging and complex hippocampus-dependent tasks probably has similar effects (Gould et al., 1999).

Thinking one step further, it also will be interesting to take epigenetic changes into consideration, as recent studies report on increase or loss in global genomic methylation, dysregulation of DNA methyltransferases and methyl-binding proteins after irradiation (Koturbash et al., 2017, 2008, 2006; Pogribny et al., 2005). Epigenetic regulation of genes involves the coordination of DNA methylation and histone modifications to maintain the transcriptional status. There is evidence that the regulation of the chromatin status provides crucial control mechanisms in memory-associated transcriptional regulation. Thus, aberrant epigenetic reactivation or silencing of numerous genes could also elicit memory impairment and should not be underestimated for this reason in regard to irradiation effects (Chwang et al., 2006; Korzus et al., 2004; C. Miller & Sweatt, 2007; M. Wood et al., 2005).

13.2.3 Reversal MWM Phase

The present study illustrates that acquiring spatial navigation in the MWM test which requires the formation of a cognitive hippocampal map was disturbed in young adult C57BL/6 mice that were irradiated at E14.5 or P10, while irradiation during distinct learning phases in two months old mice did not result in serious deficits, even when relearning was required by choosing a new platform position during reversal learning. Generally, relearning or reversal learning is a very rapid process because the allocentric spatial relationship of the distant visual cues remains the same when the platform position is switched. The animals only have to learn the new platform location and not a completely new set of landmarks which is important for efficient escape (Morris, 1984).

Mice irradiated at E14.5 or P10 improved their performance during the reversal phase, even if a deficit of allocentric place navigation was still obvious, as shown by reduced amounts of direct platform localization in both groups (Figure 8-4 C; Figure 9-4 C) and significantly reduced spatial searching in the beginning of the reversal learning in mice irradiated at E14.5 (Figure 8-4 C).

Thus, irradiated animals were principally able to learn and remember a platform position but especially the initial confrontation with the MWM test procedure caused them some problems.

Consequently, the initial read-out of my data, the long-term cognitive impairment, turned out to be rather a delayed learning improvement. As switching the platform position had no similar negative effect on performance levels in irradiated mice, it seems likely that a delayed formation of allocentric spatial maps was causative. As these cognitive maps are crucial for the correct representation of the maze environment in the hippocampal formation, proper development of spatial searching strategies was also initially impaired.

Cognitive Spatial Maps

When reconsidering the issue of irradiation-induced premature hippocampal aging associated with disturbed spatial map formation, suggested above, it is quite interesting to note that many older people develop strategies of avoiding new routes, reflecting a coping mechanism that helps them during navigation (Burns, 1999). Indeed, it has been shown in a study on age-dependent formation and use of cognitive maps that older subjects were delayed in forming spatial maps of their environment compared to younger individuals. Additionally, they were not able to use these maps as efficiently as the younger participants (Iaria et al., 2009).

In this regard, another interesting study by Barnes et al. investigated the quality and stability of hippocampal cognitive maps in old rats (Barnes et al., 1997). Rats were exposed to two consecutive episodes in a figure-8 maze. Between episodes, the rats were removed from the testing room for one hour. Young rats showed highly correlated reliable place field maps both during the first and the second exposure of the maze. Old animals displayed likewise precise and robust place field maps within the initial exposure, however, those were completely rearranged during re-exposure in one third of the session. The authors concluded that the observed place field stability during the initial exposure in both old and young rats indicates that old animals have difficulties with selecting the correct cognitive map for a given environment, not with maintaining it.

These results fit to the initially observed search strategy profiles of my E14.5 and P10 animals (Figure 12-4 B and C) which demonstrate that irradiation caused a clear

preference for the non-spatial scanning strategy in the case of E14.5 mice and a wider distribution, including inefficient strategies like thigmotaxis, circling and scanning in the case of P10 animals. The fact that both groups were generally able to develop different strategies for platform localization and to improve them to some extent, indicates that cognitive map formation per se was not affected, but rather the use or selection of a correct spatial map.

In a water maze task, Barnes et al. could further demonstrate that both young and old rats showed a bimodal distribution of their swimming paths in the beginning of the training, meaning that both groups covered sometimes longer and sometimes shorter distances. Interestingly, only the young rats were able to reduce their swimming distance until the last training day, now displaying a unimodal distribution. The old rats continued to show strong bimodality.

The bimodal distribution observed in the young rats at the beginning of training could indicate that place fields are initially rearranged at higher rates until the animals have gained more experience with the learning task and the selection of spatial maps begins to stabilize.

As place cells are also found in the dentate gyrus (Hartley et al., 2014) and based on my observation of less DCX⁺ cells, it might be conceivable that this higher incidence of place field rearrangement initially observed, could be prolonged after irradiation-induced reduction of dentate progenitor cell numbers or failed integration. This could lead to difficulties in the selection process of the correct map needed to localize the hidden platform.

Processes Involved in Allocentric Navigation and Spatial Mapping

As described in more detail in section 4.2.5, place cells in the dentate gyrus and the hippocampus proper and grid cells in the entorhinal cortex, interact by the nature of their specific activity profiles to encode spatial coordinates. Additional cell types in the entorhinal cortex involved in the GPS-like neural positioning system are head direction cells and border cells. Firing of head direction cells may play important roles for the spatial tuning of grid cells and place cells and thus provides animals with an internal neural compass. Border cells may have a role in the calculation of allocentric distances by triangulation and in fitting the grid size to the specific environment (Butler et al., 2017; Buzsáki & Moser, 2013; Calton et al., 2003; Fyhn et al., 2008, 2004; Hafting et

al., 2005; O'Keefe & Dostrovsky, 1971; O'Keefe & Nadel, 1978; Solstad et al., 2008; Taube et al., 1990). In contrast to place cells that exhibit varying firing patterns dependent on the specific environment (Muller & Kubie, 1987), grid cells, head direction cells and border cells display interrelated firing activities in any environment (Solstad et al., 2008). This continuous firing indicates that the entorhinal cortex generates an overarching metric system that is universally usable independent of the environment (Hafting et al., 2005; McNaughton et al., 2006; E. Moser et al., 2008).

The combined activity of place cells in a specific environment is thought to serve as a specific cognitive map, providing the spatial framework for navigation (Buzsáki & Moser, 2013; O'Keefe & Nadel, 1978). Their stability and specificity are important to allow proper remapping of a particular environment and avoid disturbance of spatial memory (Kentros et al., 1998; McHugh et al., 2007; Muller & Kubie, 1987). Place fields are established quite fast in novel environments (Frank et al., 2004; Hill, 1978). They remain stable between visits to an environment (Thompson & Best, 1990) and improve further over longer timescales (S. Kim et al., 2020; Lever et al., 2002; Mankin et al., 2012).

Thus, it seems reasonable that irradiation-induced loss of potential place cells or their failed integration into the dentate gyrus impairs location specific firing and the specificity of spatial maps. As different place cells have different firing locations or place fields (O'Keefe, 1976), it might be possible that the generated cognitive map of the environment is less precise. Consequently, the initially observed frequent rearrangement of place fields during water maze learning could be extended towards later training days due to the reduction of map specificity. Thus, the delayed acquisition of spatial search strategies could reflect deficits in the selection process of a correct spatial map due to missing accuracy.

In this case, the question would be how incoming and outgoing dentate gyrus-mediated information flow is changed by the observed cell loss?

The autonomic, modular organization of grid cells along the dorsal-ventral axis of the entorhinal cortex probably enables the system to adapt independently to changes in the environmental geometry, resulting in numerous alternative combinations of hippocampal inputs. Normally, by reducing interference between similar spatial contents in the hippocampus, it is possible to form a vast number of individual cognitive maps, each representing a specific environment characterized by specific place cell

activity and place fields (Buzsáki & Moser, 2013; Fyhn et al., 2007). The underlying hippocampal process responsible for successful retrieval of competing spatial environments, called pattern separation, takes place in the dentate gyrus and its mossy fiber projections to the CA3 subregion (Yassa & Stark, 2011).

The full functional integration of newly generated granule cells into the hippocampal network takes approximately 4-7 weeks (Ehninger & Kempermann, 2008; Gonçalves et al., 2016; Hodge & Hevner, 2011; van Praag et al., 2002). Interestingly, studies report that immature granule cells extend axons into CA3 very rapidly, already within 4 to 11 days after their generation (Hastings & Gould, 1999; Markakis & Gage, 1999; Zhao et al., 2006), leading to the conclusion that these cells could influence normal hippocampal function despite their immature stage. Indeed, newly generated immature granule cells display different features compared to mature granule cells during their integration into the existing circuitry. Thus, newborn granule cells are for example hyperexcitable and show strengthened synaptic plasticity compared to mature cells (Ge et al., 2008; Ming & Song, 2011; Sahay, Wilson, et al., 2011). Such properties of newly generated granule cells could be important for a role in pattern separation and thus for the precision of memory encoding. Subsequently, limitations of pattern separation due to irradiation-induced loss of new granule cells or their failed integration into the dentate gyrus could result in spatial navigation deficits.

In line with this, a study on adult hippocampal neurogenesis and its function during pattern separation (Clelland et al., 2009) showed that irradiation of eight weeks old C57BL/6 mice resulted in impaired spatial discrimination for similar spatial locations in a radial arm maze test and in a mouse touch screen discrimination paradigm two months later.

Furthermore, Sahay et al. could demonstrate that enhanced adult neurogenesis can improve pattern separation (Sahay, Scobie, et al., 2011). The authors used a genetic gain-of-function strategy including a tamoxifen-inducible Cre/Nestin mouse line and a conditional Bax knockout mouse line. Thus, Bax which normally mediates programmed cell death in adult-generated hippocampal cells (Sun et al., 2004), can be eliminated selectively in neural stem cells. Consequently, the survival of adult-generated granule cells is enhanced. In a contextual fear discrimination task, the authors showed that mice in which Bax was eliminated had significantly higher levels of discrimination between

the two contexts than controls. This improvement in contextual fear-discrimination learning is indicative of strengthened pattern separation.

In line with this, increased neurogenesis through voluntary running was shown to improve the discrimination between locations of two neighbouring, identical stimuli in three months old C57BL/6 mice (Creer et al., 2010). In contrast to that, 22 months old mice exhibited worsened spatial discrimination and low generation of new cells that could hardly be modified by running. Consequently, the addition of newly generated granule cells probably reinforces the dentate gyrus in pattern separation, avoiding interfering information to be mingled.

Taken together, these points clarify that the irradiation-induced reduction of cell numbers in the dentate gyrus of my E14.5 and P10 mice could impair the animals' ability to dissolve similar incoming spatial information and that new integrated neurons are required for pattern separation in dentate gyrus dependent behavioural tasks. Subsequently, choosing a correct spatial map for a specific environment which depends on proper pattern separation would pose difficulties.

In line with this, the observation of Gil-Mohapel et al. that older mice (less neurogenesis) developed more inefficient and imprecise search patterns and worse memory performance during probe testing compared to younger animals (more neurogenesis), leads to the conclusion that increased neurogenesis might improve not only the way mice learn the task but also their ability to learn the task faster.

A peak of dentate neurogenesis is classically described within the first two weeks of postnatal development, followed by a slower rate throughout life (Altman & Bayer, 1975, 1990b, 1990a; Altman & Das, 1965). In addition to that, Gil-Mohapel et al. observed that in mice neurogenesis sharply drops around 1.5 months of age (Gil-Mohapel et al., 2013). This implies that a preservation of neurogenesis during the first months of postnatal development may further provide the animals with a reserve pool of potential granule cells, thus compensating for unexpected functional loss.

Based on that, the reduced number of progenitor cells in my adult naïve mice after both irradiations at E14.5 and partially at P10 could mirror a lack of potential granule cells in the reserve pools. This, could explain my observed impairment in MWM performance, as decreased neurogenesis causes learning deficits (Gil-Mohapel et al., 2013; Kempermann et al., 1997; Lemaire et al., 2000; Shors et al., 2001; van Praag et al.,

1999). Further, this would also explain why irradiation at the age of two months, as performed in my 2 months old cohorts, had no effect on spatial learning. In those animals the reserve pool could be established properly and thus compensate for an irradiation-induced cell loss.

Place cell recordings in the dentate gyrus and hippocampus proper of mice irradiated during sensitive phases could provide insights into the dynamics of spatial map arrangement and the effect of decreased progenitor cell numbers on the process of pattern separation and may explain the failures of place recognition in the MWM. This may further reveal a lack of hippocampal place cell recruitment and subsequent sparse coding, as place fields are based on activity in smaller sets of granule cells. Additionally, it would be necessary to elucidate how the observed delay might be compensated for in those animals and which extra-hippocampal mechanisms may contribute. Based on my escape latency results, it will also be necessary to elucidate to what extent the individual radiation sensitivity of specific animals contributes to the overall observed cognitive deficits in the irradiated groups. It appears that not all irradiated mice, even those of the groups exposed to the highest radiation dose, performed equally bad during the water maze task. It is probable that the overall effects arise from different populations of animals within the groups with differing radiation sensitivity.

Further, it will be quite interesting to take a closer look at the link between spatial learning and the timing of neurogenesis at the cellular level and the ratio of addition and removal of new cell, respectively, especially after treatments like irradiation.

In this regard, it has been shown that learning itself can have paradoxical effects on neurogenesis. Generally, hippocampus-mediated learning depends on the rate of neurogenesis (Drapeau et al., 2003). Furthermore, enhanced neurogenesis is related to improved memory performance while reduced neurogenesis causes learning deficits (Gil-Mohapel et al., 2013; Kempermann et al., 1997; Lemaire et al., 2000; Shors et al., 2001; van Praag et al., 1999). In addition to that, spatial learning increases cell proliferation (Döbrössy et al., 2003; Lemaire et al., 2000) and the survival of newly generated granule cells (Gould et al., 1999). However, spatial learning depends not only on the addition of new granule cells but also on their removal. Surprisingly, it was demonstrated that a decline in numbers of newly generated granule cells or neurogenesis is correlated to spatial learning abilities in water maze tasks (Ambrogini

et al., 2004; Döbrössy et al., 2003; Ehninger & Kempermann, 2006). According to Döbrössy et al. (2003), the late learning phase of a water maze task reduced the number of cells generated during the early learning phase. In essence, they show that late phase learning has a multifaceted effect on neurogenesis, depending on the birth date of newly-born cells and that rats with lower numbers of new-born cells showed better memory performance. Indeed, it seems that mechanisms involved in neurogenesis generate paradoxical effects, far from being understood.

Related to this, another study showed that training in a more difficult MWM task with reduced cues decreased cell survival in their animals (Epp et al., 2010). It is conceivable that absent distant visual landmarks caused a strategy switch for platform localization. In turn, this resulted in reduced, instead of enhanced cell survival in the dentate gyrus. Taken together, this indicates that different types of spatial navigation can have variable impact on cell survival.

Additionally, the inhibition of neurogenesis by using the telomerase inhibitor azidothymidine has been shown to improve performance in a water maze task (Kerr et al., 2010).

Overall, these studies show that the relationship between water maze training and the timing of neurogenesis as well as the ratio of addition and removal of new cell is not a simple case of more is better.

Nevertheless, my results strongly suggest that certain aspects of spatial navigation, like the proper development of efficient spatial searching strategies, are dependent on the rate of hippocampal neurogenesis. Furthermore, the reduction of newly generated granule cells turned out to be an important factor that can impair pattern separation in the dentate gyrus and thus the precision of memory encoding and cognitive spatial mapping.

13.3 Relevance of Medical Radiation Treatments for Human Brain Development

The amount of medical radiation is increasing and represents the major source of exposure in the general population (Bernier et al., 2012; Mettler Jr et al., 2008, 2000). According to the Federal Office for Radiation Protection in Germany, the estimated total number of X-ray examinations in 2016 amounted to approximately 135 million. This number does not include the dental sector which additionally comprised approximately 80 million examinations. Between 2007 and 2017, a steady increase by about 45 % in CT examinations was very prominent (<https://www.bfs.de/DE/themen/ion/anwendung-medizin/diagnostik/roentgen/haeufigkeit-exposition.html>; Status: 13 February 2020).

Therefore, it is particularly urgent to acquire knowledge about the risks of the increased use of CTs, especially related to cognitive abilities in children. The risk possibly arising from exposure to low-dose radiation is still part of intensive and ongoing debates, demonstrating that current results are still controversial.

In my PhD project, I characterized specific brain developmental phases according to their sensitivity towards low-dose ionizing radiation. The results from the time points E14.5 and P10 in the mouse model show that those specific stages of brain development and maturation are particularly vulnerable towards low-dose irradiation.

Epidemiological studies indicate that long-term radiation effects on the human nervous system occur after radiation exposure between the gestational weeks 8 and 15 or less severe between weeks 16 and 25 (Dunn et al., 1990; Otake & Schull, 1998). Obviously, specific developmental phases are crucial for the occurrence of long-term radiation-induced deficiencies in humans.

Mouse models are increasingly used to analyze the developmental basis of impairments in humans. The identification and characterization of neurological deficiencies in these models require information about specific developmental stages and their normal organ and cellular composition. The fact that the timing of key developmental events differs between mice and humans must also be taken into consideration.

Generally, comparative analysis of brain developmental stages can only be conducted by approximation, as temporal placement of key processes, such as neurogenesis,

migration and synaptogenesis are protracted in mice and humans (Figure 13-1). Generally, neuronal development in humans is characterized by a substantial amount of prenatal maturation, whereas a large portion of neurogenesis and synaptogenesis in rodents is shifted to early postnatal life (Stagni et al., 2015). Figure 13-1 contains a summary of the key developmental processes in mice that have been discussed in this thesis and provides an overview about corresponding processes in humans. Thus, this figure roughly allows an estimation of radiation sensitive developmental phases in humans.

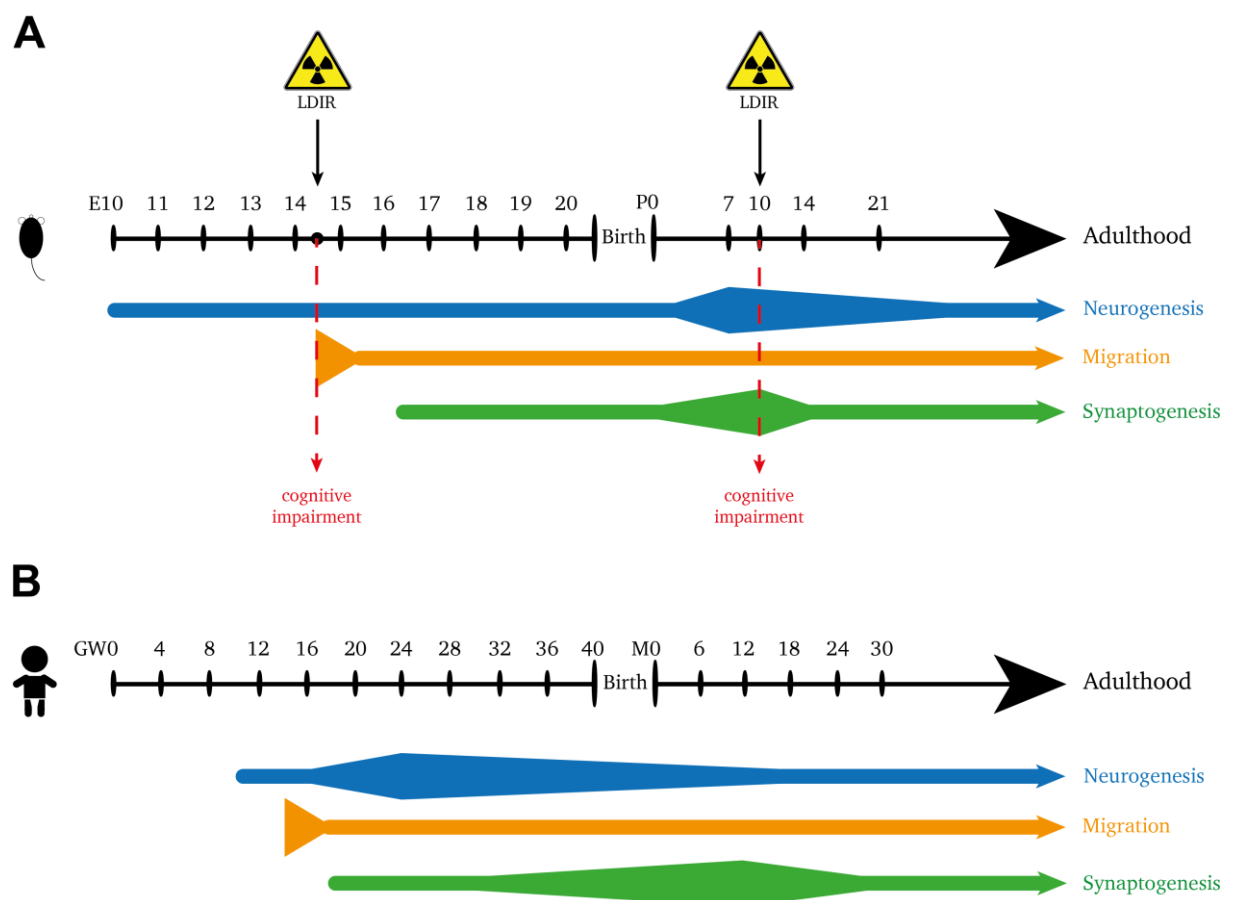


Figure 13-1: Comparison of key developmental steps in the brain of mice and humans. (A) Mouse: The timeline displays key processes of brain development between E10 and early postnatal life. **(B) Humans:** The timeline displays key processes of brain development between GW0 and early postnatal life. The timing of key developmental events differs between mice and humans. Neuronal development in humans is characterized by a substantial amount of prenatal maturation, whereas in rodents it is shifted to early postnatal life. Dentate neurogenesis is depicted in blue, dentate migration is shown in orange and dentate synaptogenesis is depicted in green. LDIR = low-dose ionizing radiation, E = embryonic day, P = postnatal day, GW = gestational week, M = month.

While dentate neurogenesis starts around E10 in mice (Hatten, 1999; Rice & Barone Jr., 2000), it is suggested that its most sensitive phase towards radiation lies between

E12 and E16 (Workman et al., 2013). Indeed, in my experiments, cognitive impairment was observed after irradiation at E14.5. In the mouse, this time point coincides with the onset of dentate migration as shown in Figure 13-1 A (Urban & Guillemot, 2014). The corresponding time point in humans is approximately around gestational week 14 (Figure 13-1 B), matching the suggested radiation sensitive phase between gestational week 8 and 15 (Dunn et al., 1990; Otake & Schull, 1998; Stagni et al., 2015).

Irradiation at P10 coincides in the mouse with peaks in dentate neurogenesis (Altman & Bayer, 1975, 1990b, 1990a; Altman & Das, 1965) and synaptogenesis (Chen et al., 2017; Semple et al., 2013) and also resulted in cognitive impairment as shown in Figure 13-1 A. In humans, dentate neurogenesis starts approximately at gestational week 10-12 and is almost accomplished within the first year after birth as shown in Figure 13-1 B (Howdeshell, 2002; Rice & Barone Jr., 2000; Seress et al., 2001). The corresponding peak in human dentate neurogenesis is approximately between gestational week 18 and 26 as shown in Figure 13-1 B (Stagni et al., 2015), matching the suggested radiation sensitive phase between gestational week 16 and 25 (Dunn et al., 1990; Otake & Schull, 1998). The corresponding peak for synaptogenesis in humans is approximately within the first two years after birth as shown in Figure 13-1 B (Herschkowitz et al., 1997; Howdeshell, 2002).

Subsequently, considering the timeline of human brain development, irradiation between week 14 and 26 of pregnancy may have a large influence on dentate neurogenesis and migration. Irradiation between late gestation and the first two years after birth may principally modulate neuronal maturation and synapse formation.

14 List of figures

Figure 4-1: Stages of hippocampal development in the dorsal telencephalon of the mouse.....	7
Figure 4-2: Schematic overview about the hippocampal network.....	9
Figure 4-3: Adult hippocampal neurogenesis in the subgranular zone of the dentate gyrus.....	15
Figure 4-4: Place cell.....	19
Figure 4-5: Grid cell.....	21
Figure 4-6: Border cells and head direction cells.....	23
Figure 7-1: Experimental timeline for immunohistochemical (IHC) analysis.....	30
Figure 7-2: Experimental timelines for the analysis of sensitive phases of brain development/maturation.....	31
Figure 7-3: Experimental timelines for the analysis of short-term IR effects during learning phases.....	32
Figure 7-4: Schematic figure of the Rotarod.....	34
Figure 7-5: Schematic figure of the Elevated Zero Maze.....	35
Figure 7-6: Schematic figure of the Morris Water Maze (MWM).....	37
Figure 7-7: Starting positions MWM Initial learning phase.....	38
Figure 7-8: Starting positions MWM Reversal learning phase.....	39
Figure 7-9: Zone definitions and dimensions for the Elevated Zero Maze (EZM).....	41
Figure 7-10: Trial control settings for Elevated Zero Maze data acquisition.....	42
Figure 7-11: Zone definitions and dimensions for the Morris Water Maze (MWM) during initial and reversal learning.	44
Figure 7-12: Trial control settings for data acquisition during the MWM training period.....	44
Figure 7-13: Trial control settings for data acquisition during probe trials.....	45
Figure 7-14: Murine coronal sections stained with Nissl.....	47
Figure 7-15: Schematic examples of non-spatial and spatial searching strategies.....	15
Figure 8-1: E14.5 LDIR did not affect motor performance (Rotarod) but caused dose-specific effects on anxiety/exploration behaviour (Elevated Zero Maze).....	54
Figure 8-2: E14.5 MWM initial learning phase revealed dose-dependent deficiencies after irradiation, expressed by a delayed learning process and a reduced amount of spatial searching.....	56
Figure 8-3: E14.5 MWM initial probe trial without platform revealed a dose-dependent decline in the preference for the target zones.....	61
Figure 8-4: E14.5 MWM reversal learning phase revealed deficits after irradiation in the beginning of the training for a new platform location.....	62
Figure 9-1: LDIR did not affect motor performance (Rotarod) but caused dose-specific effects on activity behaviour (Elevated Zero Maze).....	69
Figure 9-2: P10 MWM initial learning phase revealed dose-dependent impairment after irradiation, expressed by a delayed learning process and a reduced percentage of spatial searching.....	71
Figure 9-3: P10 MWM initial probe trial without platform revealed a dose-dependent decline in the preference for target zones.....	74
Figure 9-4: P10 IR groups improved their MWM performance in a reversal learning phase. However, differences in direct platform localization were evident.....	77
Figure 9-5: MWM reversal probe trial showed that IR groups developed proper reference memory for a new platform position.....	79
Figure 10-1: The Rotarod test did not reveal any difference in motor coordination or balance.....	82

Figure 10-2: Elevated Zero Maze testing could not reveal significant differences in activity/exploration or anxiety behaviour in any of the cohorts.....	83
Figure 10-3: Cohort 1 – MWM initial learning revealed minor differences in the acquisition of spatial memory.....	85
Figure 10-4: Cohort 1 – MWM initial probe trial indicated a preference for the periphery of the pool in the 0.5 Gy group.....	86
Figure 10-5: Cohort 1 – MWM reversal learning indicated that 0.5 Gy animals had slight problems with the development of spatial searching.....	87
Figure 10-6: Cohort 1 – Both groups showed a similar preference for the target quadrant during the reversal probe trials on day 6 and day 10.....	88
Figure 10-7: Cohort 2 – MWM initial learning could not reveal any serious difference in the acquisition of spatial memory.....	90
Figure 10-8: Cohort 2 – MWM initial probe trial could not unveil any serious alteration after irradiation.....	92
Figure 10-9: Cohort 2 – MWM reversal learning revealed similar performance in Sham and 0.5 Gy animals.....	93
Figure 10-10: Cohort 2 – Both groups showed a similar preference for the target quadrant during the reversal probe trials on day 6 and day 10.....	94
Figure 10-11: Cohort 3 – MWM initial learning could not reveal any serious difference in spatial memory acquisition.	95
Figure 10-12: Cohort 3 – Both groups showed similar performance in the MWM initial probe trial.....	97
Figure 10-13: Cohort 3 – MWM reversal learning revealed a significantly impaired performance of 0.5 Gy animals on the first training day.....	98
Figure 10-14: Cohort 3 – Both groups equally preferred the target sector over the remaining quadrants during the reversal probe trials on day 6 and day 10.....	100
Figure 11-1: IHC analysis of the DG revealed significantly less DCX ⁺ progenitor cells and reduced DG area in mice irradiated with 0.5 Gy at E14.5.....	104
Figure 12-1: All Sham groups performed similar during the initial and reversal phase of the MWM.....	107
Figure 12-2: Irradiation during learning phases of the MWM did not affect spatial searching compared to irradiation at E14.5 or P10.....	108
Figure 12-3: Irradiation during learning phases of the MWM did not affect reference memory compared to irradiation at E14.5 or P10.....	110
Figure 12-4: Searching profiles showing the distribution of the different searching strategies on day 3, 4 and 5 of initial learning.....	112
Figure 12-5: Searching profiles showing the distribution of the different searching strategies on day 1, 3 and 5 of reversal learning.....	113
Figure 13-1: Comparison of key developmental steps in the brain of mice and humans.....	141

15 List of tables

Table 7-1: Number of animals investigated at E14.5 and P10.....	31
Table 7-2: Number of animals investigated during short-term experiments.....	32
Table 7-3: Protocol of Nissl staining.....	46
Table 7-4: Searching strategies.....	51

16 References

- Akers, K. G., Martinez-Canabal, A., Restivo, L., Yiu, A. P., De Cristofaro, A., Hsiang, H. L., Wheeler, A. L., Guskjolen, A., Niibori, Y., Shoji, H., Ohira, K., Richards, B. A., Miyakawa, T., Josselyn, S. A., & Frankland, P. W. (2014). Hippocampal neurogenesis regulates forgetting during adulthood and infancy. *Science*, *344*(6184), 598–602. <https://doi.org/10.1126/science.1248903>
- Altman, J., & Bayer, S. (1975). Postnatal development of the hippocampal dentate gyrus under normal and experimental conditions. *The Hippocampus Vol. I, eds RL Isa*, 95–122.
- Altman, J., & Bayer, S. (1990a). Migration and distribution of two populations of hippocampal granule cell precursors during the perinatal and postnatal periods. *The Journal of Comparative Neurology*, *301*(3), 365–381. <https://doi.org/10.1002/cne.903010304>
- Altman, J., & Bayer, S. (1990b). Mosaic organization of the hippocampal neuroepithelium and the multiple germinal sources of dentate granule cells. *The Journal of Comparative Neurology*, *301*, 325–342. <https://doi.org/10.1002/cne.903010302>
- Altman, J., & Das, G. (1965). Autoradiographic and histological evidence of postnatal hippocampal neurogenesis in rats. *Journal of Comparative Neurology*, *124*, 319–336.
- Amaral, D., Lavenex, P. (2007). The Hippocampus Book: Hippocampal Neuroanatomy (Chapter 3). *Oxford University Press*, Edited by Andersen, P., Morris, R., Amaral, D., Bliss, T., O’Keefe, J., 37–114.
- Amaral, D., Scharfman, H., & Lavenex, P. (2007). The dentate gyrus: fundamental neuroanatomical organization (dentate gyrus for dummies). *Progress in Brain Research*, *163*, 3–22. [https://doi.org/10.1016/S0079-6123\(07\)63001-5](https://doi.org/10.1016/S0079-6123(07)63001-5)
- Ambrogini, P., Orsini, L., Mancini, C., Ferri, P., Ciaroni, S., & Cuppini, R. (2004). Learning may reduce neurogenesis in adult rat dentate gyrus. *Neuroscience Letters*, *359*, 13–16. <https://doi.org/10.1016/j.neulet.2003.12.123>
- Andersen, J., Urbán, N., Achimastou, A., Ito, A., Simic, M., Ullom, K., Martynoga, B., Lebel, M., Göritz, C., Frisén, J., Nakafuku, M., & Guillemot, F. (2014). A Transcriptional Mechanism Integrating Inputs from Extracellular Signals to Activate Hippocampal Stem Cells. *Neuron*, *83*, 1085–1097. <https://doi.org/10.1016/j.neuron.2014.08.004>
- Anderson, M., & Jeffery, K. (2003). Heterogeneous modulation of place cell firing by changes in context. *The Journal of Neuroscience*, *23*(26), 8827–8835. <https://doi.org/10.1523/jneurosci.23-26-08827.2003>
- Annese, J., Schenker-Ahmed, N. M., Bartsch, H., Maechler, P., Sheh, C., Thomas, N., Kayano, J., Ghatan, A., Bresler, N., Frosch, M. P., Klaming, R., & Corkin, S. (2014). Postmortem examination of patient H.M.’s brain based on histological sectioning and digital 3D reconstruction Jacopo. *Nature Communications*, *5*(3122), 1–9. <https://doi.org/10.1038/ncomms4122>
- Bakker, A., Kirwan, C. B., Miller, M., & Stark, C. E. L. (2008). Pattern Separation in the Human Hippocampal CA3 and Dentate Gyrus. *Science*, *319*(5870), 1640–1642. <https://doi.org/10.1126/science.1152882>.Pattern

-
- Barnes, C., Suster, M., Shen, J., & McNaughton, B. (1997). Multistability of cognitive maps in the hippocampus of old rats. *Nature*, *388*, 272–275. <https://doi.org/10.1038/40859>
- Barry, C., Hayman, R., Burgess, N., & Jeffery, K. (2007). Experience-dependent rescaling of entorhinal grids. *Nature Neuroscience*, *10*(6), 682–684. <https://doi.org/10.1038/nn1905>
- Baskar, R., & Devi, P. (2000). Influence of gestational age to low-level gamma irradiation on postnatal behavior in mice. *Neurotoxicology and Teratology*, *22*(4), 593–602. [https://doi.org/10.1016/S0892-0362\(00\)00076-3](https://doi.org/10.1016/S0892-0362(00)00076-3)
- Basu, J., & Siegelbaum, S. (2015). The Corticohippocampal Circuit, Synaptic Plasticity, and Memory. *Cold Spring Harbor Perspectives in Biology*, 1–26.
- Bayer, S., Yackel, J., & Puri, P. (1982). Neurons in the rat dentate gyrus granular layer substantially increase during juvenile and adult life. *Science*, *216*(4548), 890–892. <https://doi.org/10.1126/science.7079742>
- Bellone, J., Rudbeck, E., Hartman, R., Szücs, A., & Vlkolinský, R. (2015). A Single Low Dose of Proton Radiation Induces Long-Term Behavioral and Electrophysiological Changes in Mice. *Radiation Research*, *184*(2), 193–202. <https://doi.org/10.1667/RR13903.1>
- Bergonié, J., & Tribondeau, L. (1906). Interprétation de quelques résultats de la Radiothérapie et essai de fixation d'une technique rationnelle. *Comptes Rendus Hebdomadaires de l'Académie Des Sciences*, 983–985.
- Bergonié, J., & Tribondeau, L. (1959). Interpretation of some results of radiotherapy and an attempt at determining a logical technique of treatment | De Quelques Resultats de la Radiotherapie et Essai de Fixation d'une Technique Rationnelle. *Radiation Research*, *11*(4), 587–588. <https://doi.org/10.2307/3570812>
- Bernier, M., Rehel, J., Brisse, H., Wu-Zhou, X., Caer-Lorho, S., Jacob, S., Chateil, J., Aubert, B., & Laurier, D. (2012). Radiation exposure from CT in early childhood: A French large-scale multicentre study. *The British Journal of Radiology*, *85*(1009), 53–60. <https://doi.org/10.1259/bjr/90758403>
- Biebl, M., Cooper, C., Winkler, J., & Kuhn, H. (2000). Analysis of neurogenesis and programmed cell death reveals a self-renewing capacity in the adult rat brain. *Neuroscience Letters*, *291*, 17–20. [https://doi.org/10.1016/S0304-3940\(00\)01368-9](https://doi.org/10.1016/S0304-3940(00)01368-9)
- Biswas, S., & Kalil, K. (2018). The microtubule-associated protein tau mediates the organization of microtubules and their dynamic exploration of actin-rich lamellipodia and filopodia of cortical growth cones. *The Journal of Neuroscience*, *38*(2), 291–307. <https://doi.org/10.1523/JNEUROSCI.2281-17.2017>
- Blot, W. (1975). Review of thirty years study of Hiroshima and Nagasaki atomic bomb survivors. II. Biological effect. C. Growth and development following prenatal and children exposure to atomic radiation. *Journal of Radiation Research*, *16*(Supplement), 82–88.
- Boccaro, C., Sargolini, F., Thoresen, V., Solstad, T., Witter, M., Moser, E., & Moser, M. (2010). Grid cells in pre-and parasubiculum. *Nature Neuroscience*, *13*(8), 987–994. <https://doi.org/10.1038/nn.2602>
- Bolus, N. (2017). Basic review of radiation biology and terminology. *Journal of Nuclear Medicine Technology*, *45*(4), 259–264. <https://doi.org/10.2967/jnmt.117.195230>
-

-
- Bostock, E., Muller, R., & Kubie, J. (1991). Experience-dependent modifications of hippocampal place cell firing. *Hippocampus*, *1*(2), 193–206. <https://doi.org/10.1002/hipo.450010207>
- Bourtchuladze, R., Frenguelli, B., Blendy, J., Cioffi, D., Schutz, G., & Silva, A. (1994). Deficient long-term memory in mice with a targeted mutation of the cAMP-responsive element-binding protein. *Cell*, *79*, 59–68. [https://doi.org/10.1016/0092-8674\(94\)90400-6](https://doi.org/10.1016/0092-8674(94)90400-6)
- Brandt, M., Jessberger, S., Steiner, B., Kronenberg, G., Reuter, K., Bick-Sander, A., von der Behrens, W., & Kempermann, G. (2003). Transient calretinin expression defines early postmitotic step of neuronal differentiation in adult hippocampal neurogenesis of mice. *Molecular and Cellular Neuroscience*, *24*, 603–613. [https://doi.org/10.1016/S1044-7431\(03\)00207-0](https://doi.org/10.1016/S1044-7431(03)00207-0)
- Brenner, D., & Hall, E. (2007). Computed tomography--an increasing source of radiation exposure. *The New England Journal of Medicine*, *357*(22), 2277–2284. <https://doi.org/10.1056/NEJMra072149>
- Brill, M., Ninkovic, J., Winpenny, E., Hodge, R., Ozen, I., Yang, R., Lepier, A., Gascón, S., Erdelyi, F., Szabo, G., Parras, C., Guillemot, F., Frotscher, M., Berninger, B., Hevner, R., Raineteau, O., & Götz, M. (2009). Adult generation of glutamatergic olfactory bulb interneurons. *Nature Neuroscience*, *12*(12), 1524–1533. <https://doi.org/10.1038/nn.2416>
- Brill, M., Snappyan, M., Wohlfrom, H., Ninkovic, J., Jawerka, M., Mastick, G., Ashery-Padan, R., Saghatelian, A., Berninger, B., & Götz, M. (2008). A Dlx2- and Pax6-dependent transcriptional code for periglomerular neuron specification in the adult olfactory bulb. *The Journal of Neuroscience*, *28*(25), 6439–6452. <https://doi.org/10.1523/JNEUROSCI.0700-08.2008>
- Brown, J., Couillard-Després, S., Cooper-Kuhn, C., Winkler, J., Aigner, L., & Kuhn, H. (2003). Transient Expression of Doublecortin during Adult Neurogenesis. *Journal of Comparative Neurology*, *467*, 1–10. <https://doi.org/10.1002/cne.10874>
- Brown, T., Ross, R., Ph, D., Tobyne, S., Stern, C., & Phil, D. (2012). Cooperative interactions between hippocampal and striatal systems support flexible navigation. *Neuroimage*, *60*(2), 1316–1330. <https://doi.org/10.1016/j.neuroimage.2012.01.046>. Cooperative
- Brun, V., Solstad, T., Kjelstrup, K., Fyhn, M., Witter, M., Moser, E., & Moser, M. (2008). Progressive increase in grid scale from dorsal to ventral medial entorhinal cortex. *Hippocampus*, *18*, 1200–1212. <https://doi.org/10.1002/hipo.20504>
- Buratovic, S., Stenerlöv, B., Fredriksson, A., Sundell-Bergman, S., Viberg, H., & Eriksson, P. (2014). Neonatal exposure to a moderate dose of ionizing radiation causes behavioural defects and altered levels of tau protein in mice. *NeuroToxicology*, *45*, 48–55. <https://doi.org/10.1016/j.neuro.2014.09.002>
- Burgess, N., & O'Keefe, J. (2011). Models of place and grid cell firing and theta rhythmicity. *Current Opinion in Neurobiology*, *21*, 734–744. <https://doi.org/10.1016/j.conb.2011.07.002>
- Burns, P. (1999). Navigation and the mobility of older drivers. *Journals of Gerontology - Social Sciences*, *54 B*(1), 49–55. <https://doi.org/10.1093/geronb/54B.1.S49>
- Butler, W., Smith, K., van der Meer, M., & Taube, J. (2017). The Head-Direction Signal Plays a Functional Role as a Neural Compass during Navigation. *Current Biology*, *27*(9), 1259–1267. <https://doi.org/10.1016/j.cub.2017.03.033>

-
- Buzsáki, G., Leung, L., & Vanderwolf, C. (1983). Cellular bases of hippocampal EEG in the behaving rat. *Brain Research Reviews*, 6, 139–171. [https://doi.org/10.1016/0165-0173\(83\)90037-1](https://doi.org/10.1016/0165-0173(83)90037-1)
- Buzsáki, G., & Llinas, R. (2017). Space and Time in the brain. *Science*, 358, 482–485.
- Buzsáki, G., & Moser, E. (2013). Memory, navigation and theta rhythm in the hippocampal-entorhinal system. *Nature Neuroscience*, 16(2), 130–138. <https://doi.org/10.1038/nn.3304>
- Calton, J., Stackman, R., Goodridge, J., Archev, W., Dudchenko, P., & Taube, J. (2003). Hippocampal Place Cell Instability after Lesions of the Head Direction Cell Network. *The Journal of Neuroscience*, 23(30), 9719–9731. <https://doi.org/10.1523/jneurosci.23-30-09719.2003>
- Cavegn, N., van Dijk, R., Menges, D., Brettschneider, H., Phalanndwa, M., Chimimba, C., Isler, K., Lipp, H., Slomianka, L., & Amrein, I. (2013). Habitat-specific shaping of proliferation and neuronal differentiation in adult hippocampal neurogenesis of wild rodents. *Frontiers in Neuroscience*, 7(59), 1–11. <https://doi.org/10.3389/fnins.2013.00059>
- Chazal, G., Durbec, P., Jankovski, A., Rougon, G., & Cremer, H. (2000). Consequences of neural cell adhesion molecule deficiency on cell migration in the rostral migratory stream of the mouse. *The Journal of Neuroscience*, 20(4), 1446–1457. <https://doi.org/10.1523/jneurosci.20-04-01446.2000>
- Chen, V., Morrison, J., Southwell, M., Foley, J., Bolon, B., & Elmore, S. (2017). Histology Atlas of the Developing Prenatal and Postnatal Mouse Central Nervous System, with Emphasis on Prenatal Days E7.5 to E18.5. *Toxicologic Pathology*, 45(6), 705–744. <https://doi.org/10.1177/0192623317728134.Histology>
- Chevalyere, V., & Siegelbaum, S. (2010). Strong CA2 pyramidal neuron synapses define a powerful disinhibitory cortico-hippocampal loop. *Neuron*, 66, 560–572. <https://doi.org/10.1016/j.neuron.2010.04.013>
- Chwang, W., O’Riordan, K., Levenson, J., & Sweatt, J. (2006). ERK/MAPK regulates hippocampal histone phosphorylation following contextual fear conditioning. *Learning and Memory*, 13(3), 322–328. <https://doi.org/10.1101/lm.152906>
- Clelland, C., Choi, M., Romberg, C., Clemenson, G., Fragniere, A., Tyers, P., Jessberger, S., Saksida, L., Barker, R., Gage, F., & Bussey, T. (2009). A Functional Role for Adult Hippocampal Neurogenesis in Spatial Pattern Separation. *Science*, 325(5937), 210–213. <https://doi.org/10.1126/science.1173215>
- Colangelo, A., Cirillo, G., Alberghina, L., Papa, M., & Westerhoff, H. (2019). Neural plasticity and adult neurogenesis: the deep biology perspective. *Neural Regeneration Research*, 14(2), 201–205. <https://doi.org/10.4103/1673-5374.244775>
- Couillard-Despres, S., Winner, B., Schaubeck, S., Aigner, R., Vroemen, M., Weidner, N., Bogdahn, U., Winkler, J., Kuhn, H., & Aigner, L. (2005). Doublecortin expression levels in adult brain reflect neurogenesis. *European Journal of Neuroscience*, 21, 1–14. <https://doi.org/10.1111/j.1460-9568.2004.03813.x>
- Crain, B., Cotman, C., Taylor, D., & Lynch, G. (1973). A quantitative electron microscopic study of synaptogenesis in the dentate gyrus of the rat. *Brain Research*, 63, 195–204. [https://doi.org/10.1016/0006-8993\(73\)90088-7](https://doi.org/10.1016/0006-8993(73)90088-7)

-
- Creer, D., Romberg, C., Saksida, L., van Praag, H., & Bussey, T. (2010). Running enhances spatial pattern separation in mice. *PNAS*, *107*(5), 2367–2372. <https://doi.org/10.1073/pnas.0911725107>
- Crespo, D., Stanfield, B., & Cowan, W. (1986). Evidence that late-generated granule cells do not simply replace earlier formed neurons in the rat dentate gyrus. *Experimental Brain Research*, *62*(3), 541–548. <https://doi.org/10.1007/BF00236032>
- Cui, Z., Gerfen, C., & Young, W. (2013). Hypothalamic and other connections with dorsal CA2 area of the mouse hippocampus. *Journal of Comparative Neurology*, *521*(8), 1844–1866. <https://doi.org/10.1002/cne.23263>
- Dalm, S., Grootendorst, J., de Kloet, E., & Oitzl, M. (2000). Quantification of swim patterns in the Morris water maze. *Behavior Research Methods, Instruments, and Computers*, *32*(1), 134–139. <https://doi.org/10.3758/BF03200795>
- Del Río, J., Heimrich, B., Borrell, V., Förster, E., Drakew, A., Alcántara, S., Nakajima, K., Miyata, T., Ogawa, M., Mikoshiba, K., Derer, P., Frotscher, M., & Soriano, E. (1997). A role for Cajal-Retzius cells and reelin in the development of hippocampal connections. *Nature*, *385*, 70–74.
- Deng, W., Aimone, J., & Gage, F. (2010). New neurons and new memories: how does adult hippocampal neurogenesis affect learning and memory? *Nature Reviews Neuroscience*, *11*(5), 339–350. <https://doi.org/10.1038/nrn2822>
- Deng, W., Saxe, M., Gallina, I., & Gage, F. (2009). Adult-born hippocampal dentate granule cells undergoing maturation modulate learning and memory in the brain. *The Journal of Neuroscience*, *29*(43), 13532–13542. <https://doi.org/10.1523/jneurosci.3362-09.2009>
- Döbrössy, M., Drapeau, E., Aourousseau, C., Le Moal, M., Piazza, P., & Abrous, D. (2003). Differential effects of learning on neurogenesis: Learning increases or decreases the number of newly born cells depending on their birth date. *Molecular Psychiatry*, *8*, 974–982. <https://doi.org/10.1038/sj.mp.4001419>
- Douchamps, V., Jeewajee, A., Blundell, P., Burgess, N., & Lever, C. (2013). Evidence for encoding versus retrieval scheduling in the hippocampus by theta phase and acetylcholine. *The Journal of Neuroscience*, *33*(20), 8689–8704. <https://doi.org/10.1523/JNEUROSCI.4483-12.2013>
- Dragoi, G., & Buzsáki, G. (2006). Temporal Encoding of Place Sequences by Hippocampal Cell Assemblies. *Neuron*, *50*, 145–157. <https://doi.org/10.1016/j.neuron.2006.02.023>
- Drapeau, E., Mayo, W., Aourousseau, C., Le Moal, M., Piazza, P., & Abrous, D. (2003). Spatial memory performances of aged rats in the water maze predict levels of hippocampal neurogenesis. *PNAS*, *100*(24), 14385–14390. <https://doi.org/10.1073/pnas.2334169100>
- Dunn, K., Yoshimaru, H., Otake, M., Annegers, J., & Schull, W. (1990). Prenatal exposure to ionizing radiation and subsequent development of seizures. *American Journal of Epidemiology*, *131*(1), 114–123. <https://doi.org/10.1093/oxfordjournals.aje.a115464>
- Ehninger, D., & Kempermann, G. (2006). Paradoxical effects of learning the Morris water maze on adult hippocampal neurogenesis in mice may be explained by a combination of stress and physical activity. *Genes, Brain and Behavior*, *5*(1), 29–39. <https://doi.org/10.1111/j.1601-183X.2005.00129.x>

-
- Ehninger, D., & Kempermann, G. (2008). Neurogenesis in the adult hippocampus. *Cell and Tissue Research*, 331, 243–250. <https://doi.org/10.1007/s00441-007-0478-3>
- Encinas, J., Vaahtokari, A., & Enikolopov, G. (2006). Fluoxetine targets early progenitor cells in the adult brain. *PNAS*, 103(21), 8233–8238. <https://doi.org/10.1073/pnas.0601992103>
- Epp, J., Haack, A., & Galea, L. (2010). Task difficulty in the Morris water task influences the survival of new neurons in the dentate gyrus. *Hippocampus*, 20(7), 866–876. <https://doi.org/10.1002/hipo.20692>
- Eriksson, P. (1997). Developmental neurotoxicity of environmental agents in the neonate. *NeuroToxicology*, 18, 719–726.
- Eriksson, P., Buratovic, S., Fredriksson, A., Stenerlöv, B., & Sundell-Bergman, S. (2016). Neonatal exposure to whole body ionizing radiation induces adult neurobehavioural defects: Critical period, dose-response effects and strain and sex comparison. *Behavioural Brain Research*, 304, 11–19. <https://doi.org/10.1016/j.bbr.2016.02.008>
- Esposito, M. S. (2005). Neuronal Differentiation in the Adult Hippocampus Recapitulates Embryonic Development. *Journal of Neuroscience*, 25(44), 10074–10086. <https://doi.org/10.1523/JNEUROSCI.3114-05.2005>
- Ferbinteanu, J., & McDonald, R. J. (2000). Dorsal and ventral hippocampus: Same or different? *Psychobiology*, 28(3), 314–324.
- Fiete, I., Burak, Y., & Brookings, T. (2008). What grid cells convey about rat location. *The Journal of Neuroscience*, 28(27), 6858–6871. <https://doi.org/10.1523/JNEUROSCI.5684-07.2008>
- Fike, J., Rosi, S., & Limoli, C. (2009). Neural Precursor Cells and CNS Radiation Sensitivity. *Seminars in Radiation Oncology*, 19(2), 122–132. <https://doi.org/10.1016/j.semradonc.2008.12.003>
- Fordyce, D., & Wehner, J. (1993). Physical activity enhances spatial learning performance with an associated alteration in hippocampal protein kinase C activity in C57BL/6 and DBA/2 mice. *Brain Research*, 619, 111–119. [https://doi.org/10.1016/0006-8993\(93\)91602-O](https://doi.org/10.1016/0006-8993(93)91602-O)
- Foster, D., & Wilson, M. (2007). Hippocampal Theta Sequences. *Hippocampus*, 17, 1093–1099. <https://doi.org/10.1002/hipo>
- Francis, F., Koulakoff, A., Boucher, D., Chafey, P., Schaar, B., Vinet, M., Friocourt, G., McDonnell, N., Reiner, O., Kahn, A., McConnell, S., Berwald-Netter, Y., Denoulet, P., & Chelly, J. (1999). Doublecortin is a developmentally regulated, microtubule-associated protein expressed in migrating and differentiating neurons. *Neuron*, 23(2), 247–256. [https://doi.org/10.1016/S0896-6273\(00\)80777-1](https://doi.org/10.1016/S0896-6273(00)80777-1)
- Frank, L., Stanley, G., & Brown, E. (2004). Hippocampal plasticity across multiple days of exposure to novel environments. *The Journal of Neuroscience*, 24(35), 7681–7689. <https://doi.org/10.1523/JNEUROSCI.1958-04.2004>
- Frick, K., Stillner, E., & Berger-Sweeney, J. (2000). Mice are not little rats: Species differences in a one-day water maze task. *NeuroReport: Learning and Memory*, 11(16), 3461–3465. <https://doi.org/10.1097/00001756-200011090-00013>
- Frotscher, M. (1998). Cajal-Retzius cells, Reelin, and the formation of layers. *Current Opinion in*

-
- Neurobiology*, 8, 570–575. [https://doi.org/10.1016/S0959-4388\(98\)80082-2](https://doi.org/10.1016/S0959-4388(98)80082-2)
- Fuhrmann, F., Justus, D., Sosulina, L., Kaneko, H., Beutel, T., Friedrichs, D., Schoch, S., Schwarz, M., Fuhrmann, M., & Remy, S. (2015). Locomotion, Theta Oscillations, and the Speed-Related Firing of Hippocampal Neurons Are Controlled by a Medial Septal Glutamatergic Circuit. *Neuron*, 86, 1253–1264. <https://doi.org/10.1016/j.neuron.2015.05.001>
- Fukuda, A., Fukuda, H., Swanpalmer, J., Hertzman, S., Lannering, B., Marky, I., Björk-Eriksson, T., & Blomgren, K. (2005). Age-dependent sensitivity of the developing brain to irradiation is correlated with the number and vulnerability of progenitor cells. *Journal of Neurochemistry*, 92(3), 569–584. <https://doi.org/10.1111/j.1471-4159.2004.02894.x>
- Fushiki, S., Matsushita, K., Yoshioka, H., & Schull, W. (1996). In utero exposure to low-doses of ionizing radiation decelerates neuronal migration in the developing rat brain. *International Journal of Radiation Biology*, 70(1), 53–60. <https://doi.org/10.1080/095530096145328>
- Fyhn, M., Hafting, T., Treves, A., Moser, M., & Moser, E. (2007). Hippocampal remapping and grid realignment in entorhinal cortex. *Nature*, 446(7132), 190–194. <https://doi.org/10.1038/nature05601>
- Fyhn, M., Hafting, T., Witter, M., Moser, E., & Moser, M. (2008). Grid cells in mice. *Hippocampus*, 18, 1230–1238. <https://doi.org/10.1002/hipo.20472>
- Fyhn, M., Molden, S., Witter, M., Moser, E., & Moser, M. (2004). Spatial representation in the entorhinal cortex. *Science*, 305, 1258–1264. <https://doi.org/10.1126/science.1099901>
- Gage, F. (2000). Mammalian Neural Stem Cells. *Science*, 287(5457), 1433–1438. <https://doi.org/10.1126/science.287.5457.1433>
- Galanski, M., Nagel, H., & Stamm, G. (2007). *Paediatric CT Exposure Practice in the Federal Republic of Germany: Results of a Nation-wide Survey in 2005 / 06*. 56.
- Gao, P., Bermejo, R., & Zeigler, H. (2001). Whisker deafferentation and rodent whisking patterns: Behavioral evidence for a central pattern generator. *The Journal of Neuroscience*, 21(14), 5374–5380. <https://doi.org/10.1523/jneurosci.21-14-05374.2001>
- Garthe, A., & Kempermann, G. (2013). An old test for new neurons: refining the Morris water maze to study the functional relevance of adult hippocampal neurogenesis. *Frontiers in Neuroscience*, 7(63), 1–11. <https://doi.org/10.3389/fnins.2013.00063>
- Gatz S., Ju L., Gruber R., Hoffmann E., Carr A., Wang Z., Liu C., Jeggo P. (2011). Development/Plasticity/Repair Requirement for DNA Ligase IV during Embryonic Neuronal Development: Damage Response in the Embryonic Brain. *The Journal of Neuroscience*, 32(27), 10088–10100. doi:10.1523/JNEUROSCI.1324-11.2011
- Ge, S., Sailor, K., Ming, G., & Song, H. (2008). Synaptic integration and plasticity of new neurons in the adult hippocampus. *Journal of Physiology*, 586(16), 3759–3765. <https://doi.org/10.1113/jphysiol.2008.155655>
- Gehring, T., Luksys, G., Sandi, C., & Vasilaki, E. (2015). Detailed classification of swimming paths in the Morris Water Maze: Multiple strategies within one trial. *Scientific Reports*, 5, 1–15. <https://doi.org/10.1038/srep14562>
-

-
- Gil-Mohapel, J., Brocardo, P., Choquette, W., Gothard, R., Simpson, J., & Christie, B. (2013). Hippocampal neurogenesis levels predict WATERMAZE search strategies in the aging brain. *PLoS One*, 8(9), e75125. <https://doi.org/10.1371/journal.pone.0075125>
- Gillis, W., & Datta, S. (2017). Knowing where the nose is. *BMC Biology*, 15(42), 1–3. <https://doi.org/10.1186/s12915-017-0382-6>
- Gonçalves, J., Schafer, S., & Gage, F. (2016). Adult Neurogenesis in the Hippocampus: From Stem Cells to Behavior. *Cell*, 167(4), 897–914. <https://doi.org/10.1016/j.cell.2016.10.021>
- Gonzalez-Lozano, M., Klemmer, P., Gebuis, T., Hassan, C., van Nierop, P., van Kesteren, R., Smit, A., & Li, K. (2016). Dynamics of the mouse brain cortical synaptic proteome during postnatal brain development. *Scientific Reports*, 6(35456), 1–15. <https://doi.org/10.1038/srep35456>
- Goodroe, S., Starnes, J., & Brown, T. (2018). The Complex Nature of Hippocampal-Striatal Interactions in Spatial Navigation. *Frontiers in Human Neuroscience*, 12(250), 1–9. <https://doi.org/10.3389/fnhum.2018.00250>
- Götz, M., & Huttner, W. (2005). The cell biology of neurogenesis. *Nature Reviews Molecular Cell Biology*, 6(10), 777–788. <https://doi.org/10.1038/nrm1739>
- Götz, M., Nakafuku, M., & Petrik, D. (2016). Neurogenesis in the Developing and Adult Brain - Similarities and Key Differences. *Cold Spring Harbor Perspectives in Biology*, 1–23. <https://doi.org/10.1101/cshperspect.a018853>
- Gould, E., Beylin, A., Tanapat, P., Reeves, A., & Shors, T. J. (1999). Learning enhances adult neurogenesis in the hippocampal formation. *Nat Neurosci*, 2(3), 260–265. <https://doi.org/10.1038/6365>
- Graziano, A., Petrosini, L., & Bartoletti, A. (2003). Automatic recognition of explorative strategies in the Morris water maze. *Journal of Neuroscience Methods*, 130(1), 33–44. [https://doi.org/10.1016/S0165-0270\(03\)00187-0](https://doi.org/10.1016/S0165-0270(03)00187-0)
- Gupta, A., van der Meer, M., Touretzky, D., & Redish, A. (2012). Segmentation of spatial experience by hippocampal theta sequences. *Nature Neuroscience*, 15(7), 1032–1039. <https://doi.org/10.1038/nn.3138>
- Haber, S., & Knutson, B. (2010). The reward circuit: Linking primate anatomy and human imaging. *Neuropsychopharmacology*, 35, 4–26. <https://doi.org/10.1038/npp.2009.129>
- Hack, M., Saghatelian, A., de Chevigny, A., Pfeifer, A., Ashery-Padan, R., Lledo, P., & Götz, M. (2005). Neuronal fate determinants of adult olfactory bulb neurogenesis. *Nature Neuroscience*, 8(7), 865–872. <https://doi.org/10.1038/nn1479>
- Hafting, T., Fyhn, M., Molden, S., Moser, M., & Moser, E. (2005). Microstructure of a spatial map in the entorhinal cortex. *Nature*, 436, 801–806. <https://doi.org/10.1038/nature03721>
- Hall, P., Adami, H., Trichopoulos, D., Pedersen, N., Lagiou, P., Ekblom, A., Ingvar, M., Lundell, M., & Granath, F. (2004). Effect of low doses of ionising radiation in infancy on cognitive function in adulthood : Swedish population based cohort study. *British Medical Journal*, 328, 1–5.
- Harms, K., & Dunaevsky, A. (2007). Dendritic spine plasticity: Looking beyond development. *Brain Research*, 1184, 65–71. <https://doi.org/10.1016/j.brainres.2006.02.094>
- Hartley, T., Lever, C., Burgess, N., & O'Keefe, J. (2014). Space in the brain: How the hippocampal

- formation supports spatial cognition. *Philosophical Transactions of the Royal Society B: Biological Sciences*, 369, 1–18. <https://doi.org/10.1098/rstb.2012.0510>
- Hartley, T., Maguire, E., Spiers, H., & Burgess, N. (2003). The well-worn route and the path less traveled: Distinct neural bases of route following and wayfinding in humans. *Neuron*, 37(5), 877–888. [https://doi.org/10.1016/S0896-6273\(03\)00095-3](https://doi.org/10.1016/S0896-6273(03)00095-3)
- Hasselmo, M., Bodelón, C., & Wyble, B. (2002). A proposed function for hippocampal theta rhythm: Separate phases of encoding and retrieval enhance reversal of prior learning. *Neural Computation*, 14, 793–817. <https://doi.org/10.1162/089976602317318965>
- Hastings, N., & Gould, E. (1999). Rapid extension of axons into the CA3 region by adult-generated granule cells. *The Journal of Comparative Neurology*, 413, 146–154. [https://doi.org/10.1002/\(SICI\)1096-9861\(19991011\)413:1<146::AID-CNE10>3.0.CO;2-B](https://doi.org/10.1002/(SICI)1096-9861(19991011)413:1<146::AID-CNE10>3.0.CO;2-B)
- Hatten, M. (1999). Central nervous system neuronal migration. *Annual Review of Neuroscience*, 22, 511–539. <https://doi.org/10.1146/annurev.neuro.22.1.511>
- Hebb, D. (1949). *The Organization of Behavior; A Neuropsychological Theory*. <https://doi.org/10.2307/1418888>
- Heisler, L., Chu, H.-M., Brennan, T., Danao, J., Bajwa, P., Parsons, L., & Tecott, L. (1998). Elevated anxiety and antidepressant-like responses in serotonin 5-HT1A receptor mutant mice. *PNAS*, 95, 15049–15054. <https://doi.org/10.1109/icsmc.2002.1176091>
- Herschkowitz, N., Kagan, J., & Zilles, K. (1997). Neurobiological bases of behavioral development in the first year. *Neuropediatrics*, 28, 296–306. <https://doi.org/10.1055/s-2007-973495>
- Hill, A. (1978). First occurrence of hippocampal spatial firing in a new environment. *Experimental Neurology*, 62(2), 282–297. [https://doi.org/10.1016/0014-4886\(78\)90058-4](https://doi.org/10.1016/0014-4886(78)90058-4)
- Hitti, F., & Siegelbaum, S. (2014). The hippocampal CA2 region is essential for social memory. *Nature*, 508, 88–92. <https://doi.org/10.1038/nature13028>
- Hodge, R., & Hevner, R. (2011). Expression and Actions of Transcription Factors in Adult Hippocampal Neurogenesis. *Developmental Neurobiology*, 71, 680–689. <https://doi.org/10.1002/dneu.20882>
- Hodges, H. (1996). Maze procedures: The radial-arm and water maze compared. *Cognitive Brain Research*, 3, 167–181. [https://doi.org/10.1016/0926-6410\(96\)00004-3](https://doi.org/10.1016/0926-6410(96)00004-3)
- Howdeshell, K. (2002). A model of the development of the brain as a construct of the thyroid system. *Environmental Health Perspectives*, 110(Suppl 3), 337–348. <https://doi.org/10.1289/ehp.02110s3337>
- Iaria, G., Palermo, L., Committeri, G., & Barton, J. (2009). Age differences in the formation and use of cognitive maps. *Behavioural Brain Research*, 196, 187–191. <https://doi.org/10.1016/j.bbr.2008.08.040>
- Iaria, G., Petrides, M., Dagher, A., Pike, B., & Bohbot, V. (2003). Cognitive strategies dependent on the hippocampus and caudate nucleus in human navigation: Variability and change with practice. *The Journal of Neuroscience*, 23(13), 5945–5952. <https://doi.org/10.1523/jneurosci.23-13-05945.2003>
- Ina, Y., & Sakai, K. (2004). Prolongation of Life Span Associated with Immunological Modification by Chronic Low-Dose-Rate Irradiation in MRL-Ipr / Ipr Mice. *Radiation Research*, 161, 168–173.

-
- Inouye, M., Hayasaka, S., Sun, X., & Yamamura, H. (1993). Disturbance of Neuronal Migration in Mouse Cerebral Cortex by Low-Dose Gamma-Radiation. *Journal of Radiation Research*, *34*, 204–213.
- Jacquet, P. (2004). Sensitivity of germ cells and embryos to ionizing radiation. *Journal of Biological Regulators and Homeostatic Agents*, *18*(2), 106–114.
- Jahn-Eimermacher, A., Lasarzik, I., & Raber, J. (2011). Statistical analysis of latency outcomes in behavioral experiments. *Behavioural Brain Research*, *221*(1), 271–275. <https://doi.org/10.1016/j.bbr.2011.03.007>.Statistical
- Jeewajee, A., Lever, C., Burton, S., O'Keefe, J., & Burgess, N. (2008). Environmental novelty is signaled by reduction of the hippocampal theta frequency. *Hippocampus*, *18*, 340–348. <https://doi.org/10.1002/hipo.20394>
- Jones, B., & Roberts, D. (1968). The quantitative measurement of motor inco-ordination in naive mice using an accelerating rotarod. *Journal of Pharmacy and Pharmacology*, *20*(4), 302–304. <https://doi.org/10.1111/j.2042-7158.1968.tb09743.x>
- Jung, M., Wiener, S., & McNaughton, B. (1994). Comparison of spatial firing characteristics of units in dorsal and ventral hippocampus of the rat. *The Journal of Neuroscience*, *14*(12), 7347–7356. <https://doi.org/10.1523/jneurosci.14-12-07347.1994>
- Juríková, M., Danihel, L., Polák, Š., & Varga, I. (2016). Ki67, PCNA, and MCM proteins: Markers of proliferation in the diagnosis of breast cancer. *Acta Histochemica*, *118*, 544–552. <https://doi.org/10.1016/j.acthis.2016.05.002>
- Kajiwara, R., Wouterlood, F., Sah, A., Boekel, A., Baks-te Bulte, L., & Witter, M. (2008). Convergence of entorhinal and CA3 inputs onto pyramidal neurons and interneurons in hippocampal area CA1 - An anatomical study in the rat. *Hippocampus*, *18*, 266–280. <https://doi.org/10.1002/hipo.20385>
- Katsura, M., Cyon-Nakamine, H., Zen, Q., Zen, Y., Nansai, H., Amagasa, S., Kanki, Y., Inoue, T., Kaneki, K., Taguchi, A., Kobayashi, M., Kaji, T., Kodama, T., Miyagawa, K., Wada, Y., Akimitsu, N., & Sone, H. (2016). Effects of Chronic Low-Dose Radiation on Human Neural Progenitor Cells. *Scientific Reports*, *6*(20027), 1–12. <https://doi.org/10.1038/srep20027>
- Kelsey, C., Heintz, P., Sandoval, D., Chambers, G., Adolphi, N., & Paffett, K. (2014). Radiation Biology of Medical Imaging. *Wiley Blackwell*, Chapter 4, 61–79. <https://doi.org/10.1002/9781118517154.ch4>
- Kempermann, G., & Gage, F. (2002). Genetic determinants of adult hippocampal neurogenesis correlate with acquisition, but not probe trial performance, in the water maze task. *European Journal of Neuroscience*, *16*(1), 129–136. <https://doi.org/10.1046/j.1460-9568.2002.02042.x>
- Kempermann, G., Jessberger, S., Steiner, B., & Kronenberg, G. (2004). Milestones of neuronal development in the adult hippocampus. *Trends in Neurosciences*, *27*(8), 447–452. <https://doi.org/10.1016/j.tins.2004.05.013> \nS0166223604001675 [pii]
- Kempermann, G., Kuhn, H., & Gage, F. (1997). More hippocampal neurons in adult mice living in an enriched environment. In *Nature* (Vol. 386, pp. 493–495). <https://doi.org/10.1038/386493a0>
- Kempermann, G., Song, H., & Gage, F. (2015). Neurogenesis in the adult hippocampus. *Cold Spring Harbor Perspectives in Biology*, *7*, 1–14. <https://doi.org/10.1101/cshperspect.a018812>
-

-
- Kempf, S., Casciati, A., Buratovic, S., Janik, D., von Toerne, C., Ueffing, M., Neff, F., Moertl, S., Stenerl w, B., Saran, A., Atkinson, M., Eriksson, P., Pazzaglia, S., & Tapio, S. (2014). The cognitive defects of neonatally irradiated mice are accompanied by changed synaptic plasticity, adult neurogenesis and neuroinflammation. *Molecular Neurodegeneration*, *9*(57), 1–17. <https://doi.org/10.1186/1750-1326-9-57>
- Kempf, S., von Toerne, C., Hauck, S., Atkinson, M., Benotmane, M., & Tapio, S. (2015). Long-term consequences of in utero irradiated mice indicate proteomic changes in synaptic plasticity related signalling. *Proteome Science*, *13*(26), 1–7. <https://doi.org/10.1186/s12953-015-0083-4>
- Kentros, C., Hargreaves, E., Hawkins, R., Kandel, E., Shapiro, M., & Muller, R. (1998). Ablation of Long Term Stability of New Hippocampal Place Cell Maps by NMDA Receptor Blockade. *Science*, *280*, 2121–2126.
- Kepecs, A., Uchida, N., & Mainen, Z. (2007). Rapid and precise control of sniffing during olfactory discrimination in rats. *Journal of Neurophysiology*, *98*, 205–213. <https://doi.org/10.1152/jn.00071.2007>
- Kerr, A., Steuer, E., Pochtarev, V., & Swain, R. (2010). Angiogenesis but not neurogenesis is critical for normal learning and memory acquisition. *Neuroscience*, *171*(1), 214–226. <https://doi.org/10.1016/j.neuroscience.2010.08.008>
- Kim, E., Leung, C., Reed, R., & Johnson, J. (2007). In vivo analysis of Ascl1 defined progenitors reveals distinct developmental dynamics during adult neurogenesis and gliogenesis. *The Journal of Neuroscience*, *27*(47), 12764–12774. <https://doi.org/10.1523/JNEUROSCI.3178-07.2007>
- Kim, S., Jung, D., & Royer, S. (2020). Place cell maps slowly develop via competitive learning and conjunctive coding in the dentate gyrus. *Nature Communications*, *11*(4550), 1–15. <https://doi.org/10.1038/s41467-020-18351-6>
- Kjelstrup, K., Solstad, T., Brun, V., Hafting, T., Leutgeb, S., Witter, M., Moser, E., & Moser, M. (2008). Finite scale of spatial representation in the hippocampus. *Science*, *321*, 140–143. <https://doi.org/10.1126/science.1157086>
- Knierim, J. (2002). Dynamic interactions between local surface cues, distal landmarks, and intrinsic circuitry in hippocampal place cells. *The Journal of Neuroscience*, *22*(14), 6254–6264. <https://doi.org/10.1523/jneurosci.22-14-06254.2002>
- Knierim, J., Kudrimoti, H., & McNaughton, B. (1995). Place cells, head direction cells, and the learning of landmark stability. *The Journal of Neuroscience*, *15*(3), 1648–1659. <https://doi.org/10.1523/jneurosci.15-03-01648.1995>
- Knierim, J., & Neunuebel, J. (2016). Tracking the flow of hippocampal computation: Pattern separation, pattern completion, and attractor dynamics. *Neurobiology of Learning and Memory*, *129*, 38–49. <https://doi.org/10.1016/j.nlm.2015.10.008>
- Knutsen, P., Pietr, M., & Ahissar, E. (2006). Haptic object localization in the vibrissal system: Behavior and performance. *The Journal of Neuroscience*, *26*(33), 8451–8454. <https://doi.org/10.1523/JNEUROSCI.1516-06.2006>
- Kohara, K., Pignatelli, M., Rivest, A., Jung, H., Kitamura, T., Suh, J., Frank, D., Kajikawa, K., Mise, N.,

-
- Obata, Y., Wickersham, I., & Tonegawa, S. (2014). Cell type-specific genetic and optogenetic tools reveal hippocampal CA2 circuits. *Nature Neuroscience*, 17(2), 269–279. <https://doi.org/10.1038/nn.3614>
- Kohwi, M., Osumi, N., Rubenstein, J., & Alvarez-Buylla, A. (2005). Pax6 is required for making specific subpopulations of granule and periglomerular neurons in the olfactory bulb. *The Journal of Neuroscience*, 25(30), 6997–7003. <https://doi.org/10.1523/JNEUROSCI.1435-05.2005>
- Korzus, E., Rosenfeld, M., & Mayford, M. (2004). CBP histone acetyltransferase activity is a critical component of memory consolidation. *Neuron*, 42(6), 961–972. <https://doi.org/10.1016/j.neuron.2004.06.002>
- Koturbash, I., Jadavji, N., Kutanzi, K., Rodriguez-Juarez, R., Kogosov, D., Metz, G., & Kovalchuk, O. (2017). Fractionated low-dose exposure to ionizing radiation leads to DNA damage, epigenetic dysregulation, and behavioral impairment. *Environmental Epigenetics*, 2(4), 1–13. <https://doi.org/10.1093/eep/dvw025>
- Koturbash, I., Kutanzi, K., Hendrickson, K., Rodriguez-Juarez, R., Kogosov, D., & Kovalchuk, O. (2008). Radiation-induced bystander effects in vivo are sex specific. *Mutation Research*, 642, 28–36. <https://doi.org/10.1016/j.mrfmmm.2008.04.002>
- Koturbash, I., Rugo, R., Hendricks, C., Loree, J., Thibault, B., Kutanzi, K., Pogribny, I., Yanch, J., Engelward, B., & Kovalchuk, O. (2006). Irradiation induces DNA damage and modulates epigenetic effectors in distant bystander tissue in vivo. *Oncogene*, 25(31), 4267–4275. <https://doi.org/10.1038/sj.onc.1209467>
- Kraus, B., Robinson II, R., White, J., Eichenbaum, H., & Hasselmo, M. (2013). Hippocampal “Time Cells”: Time versus Path Integration. *Neuron*, 78(6), 1090–1101. <https://doi.org/10.1161/CIRCULATIONAHA.110.956839>
- Kreuzer M., Auvinen A., Bouffler S., Cardis E., Durante M., Jourdain J., Harms-Ringdahl M., Madas B., Quintens R., Prise K., Pazzaglia S., Ottolenghi A., Sabatier L., (2017). Strategic Research Agenda of the Multidisciplinary European Low Dose Initiative (MELODI)-2017. *MELODI*, 1-22.
- Kreuzer M., Auvinen A., Cardis E., Durante M., Harms-Ringdahl M., Jourdain J., Madas B., Ottolenghi A., Pazzaglia S., Prise K., Quintens R., Sabatier L., Bouffler S. (2018). Multidisciplinary European Low Dose Initiative (MELODI): strategic research agenda for low dose radiation risk research. *Radiation and Environmental Biophysics*, 57(1), 5-15.
- Krieger, H. (2011). Grundlagen der Strahlungsphysik und des Strahlenschutzes. *Springer Spektrum*, 4.
- Kuhn, H., Biebl, M., Wilhelm, D., Li, M., Friedlander, R., & Winkler, J. (2005). Increased generation of granule cells in adult Bcl-2-overexpressing mice: A role for cell death during continued hippocampal neurogenesis. *European Journal of Neuroscience*, 22, 1907–1915. <https://doi.org/10.1111/j.1460-9568.2005.04377.x>
- Lemaire, V., Koehl, M., Le Moal, M., & Abrous, D. (2000). Prenatal stress produces learning deficits associated with an inhibition of neurogenesis in the hippocampus. *PNAS*, 97(20), 11032–11037.
- Leuner, B., Mendolia-Loffredo, S., Kozorovitskiy, Y., Samburg, D., Gould, E., & Shors, T. (2004). Learning enhances the survival of new neurons beyond the time when the hippocampus is required for

- memory. *The Journal of Neuroscience*, 24(34), 7477–7481.
<https://doi.org/10.1523/JNEUROSCI.0204-04.2004>
- Leutgeb, S., Leutgeb, J., Treves, A., Moser, M., & Moser, E. (2004). Distinct ensemble codes in hippocampal areas CA3 and CA1. *Science*, 305, 1295–1298.
<https://doi.org/10.1126/science.1100265>
- Leutgeb, S., Ragozzino, K., & Mizumori, S. (2000). Convergence of head direction and place information in the CA1 region of hippocampus. *Neuroscience*, 100(1), 11–19. [https://doi.org/10.1016/S0306-4522\(00\)00258-X](https://doi.org/10.1016/S0306-4522(00)00258-X)
- Lever, C., Wills, T., Cacucci, F., Burgess, N., & Keefe, J. (2002). Long-term plasticity in hippocampal place-cell representation of environmental geometry. *Nature*, 416, 90–94.
- Li, G., Kataoka, H., Coughlin, S., & Pleasure, S. (2009). Identification of a transient subpial neurogenic zone in the developing dentate gyrus and its regulation by Cxcl12 and reelin signaling. *Development*, 136, 327–335. <https://doi.org/10.1242/dev.025742>
- Lister, R. (1987). The use of a plus-maze to measure anxiety in the mouse. *Psychopharmacology*, 92, 180–185.
- López-Juárez, A., Howard, J., Ullom, K., Howard, L., Grande, A., Pardo, A., Waclaw, R., Sun, Y., Yang, D., Kuan, C., Campbell, K., & Nakafuku, M. (2013). Gsx2 controls region-specific activation of neural stem cells and injury-induced neurogenesis in the adult subventricular zone. *Genes and Development*, 27, 1272–1287. <https://doi.org/10.1101/gad.217539.113>
- Lugert, S., Basak, O., Knuckles, P., Haussler, U., Fabel, K., Götz, M., Haas, C., Kempermann, G., Taylor, V., & Giachino, C. (2010). Quiescent and Active Hippocampal Neural Stem Cells with Distinct Morphologies Respond Selectively to Physiological and Pathological Stimuli and Aging. *Cell Stem Cell*, 6, 445–456. <https://doi.org/10.1016/j.stem.2010.03.017>
- Luo, A., Tahsili-Fahadan, P., Wise, R., Lupica, C., & Aston-Jones, G. (2011). Linking context with reward: A functional circuit from hippocampal CA3 to ventral tegmental area. *Science*, 333, 353–357. <https://doi.org/10.1126/science.1204622>
- MacDonald, C., Carrow, S., Place, R., & Eichenbaum, H. (2013). Distinct hippocampal time cell sequences represent odor memories in immobilized rats. *The Journal of Neuroscience*, 33(36), 14607–14616. <https://doi.org/10.1523/JNEUROSCI.1537-13.2013>
- Maness, P., & Schachner, M. (2007). Neural recognition molecules of the immunoglobulin superfamily: Signaling transducers of axon guidance and neuronal migration. *Nature Neuroscience*, 10(1), 19–26. <https://doi.org/10.1038/nn1827>
- Mankin, E., Sparks, F., Slayyeh, B., Sutherland, R., Leutgeb, S., & Leutgeb, J. (2012). Neuronal code for extended time in the hippocampus. *PNAS*, 109(47), 19462–19467. <https://doi.org/10.1073/pnas.1214107109>
- Markakis, E., & Gage, F. (1999). Adult-generated neurons in the dentate gyrus send axonal projections to field CA3 and are surrounded by synaptic vesicles. *Journal of Comparative Neurology*, 406(4), 449–460. [https://doi.org/10.1002/\(SICI\)1096-9861\(19990419\)406:4<449::AID-](https://doi.org/10.1002/(SICI)1096-9861(19990419)406:4<449::AID-)

- Marr, D. (1971). Simple memory: a theory for archicortex. *Philosophical Transactions of the Royal Society of London: Biological Sciences*, 262(841), 23–81. <https://doi.org/10.1098/rstb.1998.0279>
- Matthews, E. (2019). Radiation Physics, Biology, and Protection. *Radiologic Technology*, 90(5), 471–485.
- McHugh, T., Jones, M., Quinn, J., Balthasar, N., Coppari, R., Elmquist, J., Lowell, B., Fanselow, M., Wilson, M., & Tonegawa, S. (2007). Dentate gyrus NMDA receptors mediate rapid pattern separation in the hippocampal network. *Science*, 317, 94–99. <https://doi.org/10.1126/science.1140263>
- McNaughton, B., Barnes, C., Gerrard, J., Gothard, K., Jung, M., Knierim, J., Kudrimoti, H., Qin, Y., Skaggs, W., Suster, M., & Weaver, K. (1996). Deciphering the hippocampal polyglot: The hippocampus as a path integration system. *The Journal of Experimental Biology*, 199(1), 173–185.
- McNaughton, B., Battaglia, F., Jensen, O., Moser, E., & Moser, M. (2006). Path integration and the neural basis of the “cognitive map.” *Nature Reviews Neuroscience*, 7(8), 663–678. <https://doi.org/10.1038/nrn1932>
- Meredith, R. (2015). Sensitive and critical periods during neurotypical and aberrant neurodevelopment: A framework for neurodevelopmental disorders. *Neuroscience and Biobehavioral Reviews*, 50, 180–188. <https://doi.org/10.1016/j.neubiorev.2014.12.001>
- Mettler Jr, F., Huda, W., Yoshizumi, T., & Mahesh, M. (2008). Effective Doses in Radiology and Diagnostic Nuclear Medicine: A Catalog. *Radiology*, 248(1), 254–263. <https://doi.org/10.1148/radiol.2481071451>
- Mettler Jr, F., Wiest, P., Locken, J., & Kelsey, C. (2000). CT scanning: patterns of use and dose. *Journal of Radiological Protection*, 20, 353–359.
- Michelin S., del Rosario Perez M., Dubner D., Gisone P. (2004). Increased Activity and Involvement of Caspase-3 in Radiation-Induced Apoptosis in Neural Cells Precursors from Developing Rat Brain. *NeuroToxicology*, 25(3), 387-398.
- Migaud, M., Charlesworth, P., Dempster, M., Webster, L., Watabe, A., Makhinson, M., He, Y., Ramsay, M., Morris, R., Morrison, J., O'Dell, T., & Grant, S. (1998). Enhanced long-term potentiation and impaired learning in mice with mutant postsynaptic density-95 protein. *Nature*, 396, 433–439. <https://doi.org/10.1038/24790>
- Miller, C., & Sweatt, J. (2007). Covalent Modification of DNA Regulates Memory Formation. *Neuron*, 53(6), 857–869. <https://doi.org/10.1016/j.neuron.2007.02.022>
- Miller, R. (1969). Delayed Radiation Effects in Atomic-Bomb Survivors Major observations by the Atomic Bomb Casualty Commission are evaluated. *Science*, 166, 569–574.
- Miller, R., & Blot, W. (1972). Small Head Size after in-utero Exposure to Atomic Radiation. *The Lancet*, 300(7781), 784–787.
- Milner, B., Squire, L., & Kandel, E. (1998). Cognitive Neuroscience and the Study of Memory. *Neuron*, 20, 445–468.
- Ming, G., & Song, H. (2011). Adult Neurogenesis in the Mammalian Brain: Significant Answers and Significant Questions. *Neuron*, 70(4), 687–702. <https://doi.org/10.1016/j.neuron.2011.05.001>

-
- Miyamoto, E. (2006). Molecular mechanism of neuronal plasticity: Induction and maintenance of long-term potentiation in the hippocampus. *Journal of Pharmacological Sciences*, *100*, 433–442. <https://doi.org/10.1254/jphs.CPJ06007X>
- Mizumatsu, S., Monje, M., Morhardt, D., Rola, R., Palmer, T., & Fike, J. (2003). Extreme sensitivity of adult neurogenesis to low doses of X-irradiation. *Cancer Research*, *63*(14), 4021–4027. <http://www.ncbi.nlm.nih.gov/pubmed/12874001>
- Mizumori, S., Ragozzino, K., & Cooper, B. (2000). Location and head direction representation in the dorsal striatum of rats. *Psychobiology*, *28*(4), 441–462. <https://doi.org/10.3758/BF03332003>
- Moghaddam, M., & Bures, J. (1996). Contribution of egocentric spatial memory to place navigation of rats in the Morris water maze. *Behavioural Brain Research*, *78*(2), 121–129. [https://doi.org/10.1016/0166-4328\(95\)00240-5](https://doi.org/10.1016/0166-4328(95)00240-5)
- Montgomery, K. (1955). The relation between fear induced by novel stimulation and exploratory behavior. *Journal of Comparative and Physiological Psychology*, *48*(4), 254–260. <https://doi.org/10.1037/h0043788>
- Morris, R. (1984). Developments of a water-maze procedure for studying spatial learning in the rat. *Journal of Neuroscience Methods*, *11*(1), 47–60. [https://doi.org/10.1016/0165-0270\(84\)90007-4](https://doi.org/10.1016/0165-0270(84)90007-4)
- Morris, R., Garrud, P., Rawlins, J., & O'Keefe, J. (1982). Place navigation impaired in rats with hippocampal lesions. In *Nature* (Vol. 297, pp. 681–683). <https://doi.org/10.1038/297681a0>
- Morris, R., Hagan, J., & Rawlins, J. (1986). Allocentric Spatial-Learning by Hippocampotomized Rats - a Further Test of the Spatial-Mapping and Working Memory Theories of Hippocampal Function. In *Quarterly Journal of Experimental Psychology Section B-Comparative and Physiological Psychology* (Vol. 38, Issue 4).
- Moser, E., Kropff, E., & Moser, M. (2008). Place cells, grid cells, and the brain's spatial representation system. *Annual Review of Neuroscience*, *31*, 69–89. <https://doi.org/10.1146/annurev.neuro.31.061307.090723>
- Moser, E., Moser, M., & McNaughton, B. (2017). Spatial representation in the hippocampal formation: A history. *Nature Neuroscience*, *20*(11), 1448–1464. <https://doi.org/10.1038/nn.4653>
- Moser, E., & Paulsen, O. (2001). New excitement in cognitive space: Between place cells and spatial memory. *Current Opinion in Neurobiology*, *11*, 745–751. [https://doi.org/10.1016/S0959-4388\(01\)00279-3](https://doi.org/10.1016/S0959-4388(01)00279-3)
- Moser, M., Rowland, D., & Moser, E. (2015). Place Cells, Grid Cells, and Memory. *Cold Spring Harbor Perspectives in Biology*, *7*(a021808), 1–16.
- Mulisch, M., & Welsch, U. (2010). Romeis - Mikroskopische Technik, Kapitel 3 Färbungen. *Springer Spektrum*, 18th Editi.
- Muller, R., & Kubie, J. (1987). The effects of changes in the environment on the spatial firing of hippocampal complex-spike cells. *The Journal of Neuroscience*, *7*(7), 1951–1968. <https://doi.org/10.1523/jneurosci.07-07-01951.1987>
- Nacher, J., Varea, E., Blasco-Ibañez, J., Castillo-Gomez, E., Crespo, C., Martinez-Guijarro, F., & McEwen, B. (2005). Expression of the transcription factor Pax6 in the adult rat dentate gyrus. *Journal of*

Neuroscience Research, 81, 753–761. <https://doi.org/10.1002/jnr.20596>

- Nakazawa, K., Quirk, M., Chitwood, R., Watanabe, M., Yeckel, M., Sun, L., Kato, A., Carr, C., Johnston, D., Wilson, M., & Tonegawa, S. (2002). Requirement for hippocampal CA3 NMDA receptors in associative memory recall. *Science*, 297, 211–218.
- Nakazawa, K., Sun, L., Quirk, M., Rondi-Reig, L., Wilson, M., & Tonegawa, S. (2003). Hippocampal CA3 NMDA receptors are crucial for memory acquisition of one-time experience. *Neuron*, 38, 305–315. [https://doi.org/10.1016/S0896-6273\(03\)00165-X](https://doi.org/10.1016/S0896-6273(03)00165-X)
- Nelson, B., Hodge, R., Daza, R., Tripathi, P., Arnold, S., Millen, K., & Hevner, R. (2020). Intermediate progenitors support migration of neural stem cells into dentate gyrus outer neurogenic niches. *ELife*, 9(e53777), 1–30. <https://doi.org/10.7554/eLife.53777>
- Neves, G., Cooke, S., & Bliss, T. (2008). Synaptic plasticity, memory and the hippocampus: a neural network approach to causality. *Nature Reviews Neuroscience*, 9, 65–75. <https://doi.org/10.1038/nrn2303> [pii] 10.1038/nrn2303
- Ninkovic, J., Steiner-Mezzadri, A., Jawerka, M., Akinci, U., Masserdotti, G., Petricca, S., Fischer, J., von Holst, A., Beckers, J., Lie, C., Petrik, D., Miller, E., Tang, J., Wu, J., Lefebvre, V., Demmers, J., Eisch, A., Metzger, D., Crabtree, G., ... Götz, M. (2013). The BAF complex interacts with Pax6 in adult neural progenitors to establish a neurogenic cross-regulatory transcriptional network. *Cell Stem Cell*, 13, 1–16. <https://doi.org/10.1016/j.stem.2013.07.002>
- Nomura, T., Li, X., Ogata, H., Sakai, K., Kondo, T., Takano, Y., & Magae, J. (2011). Suppressive effects of continuous low-dose-rate γ irradiation on diabetic nephropathy in type II diabetes mellitus model mice. *Radiation Research*, 176(3), 356–365. <https://doi.org/10.1667/RR2559.1>
- O'Keefe, J. (1976). Place units in the hippocampus of the freely moving rat. *Experimental Neurology*, 51, 78–109. [https://doi.org/10.1016/0014-4886\(76\)90055-8](https://doi.org/10.1016/0014-4886(76)90055-8)
- O'Keefe, J., & Conway, D. (1978). Hippocampal place units in the freely moving rat: Why they fire where they fire. *Experimental Brain Research*, 31, 573–590. <https://doi.org/10.1007/BF00239813>
- O'Keefe, J., & Dostrovsky, J. (1971). The hippocampus as a spatial map. Preliminary evidence from unit activity in the freely-moving rat. *Brain Research*, 34, 171–175. <http://www.ncbi.nlm.nih.gov/pubmed/5124915>
- O'Keefe, J., & Nadel, L. (1978). The Hippocampus as a Cognitive Map. In *Oxford: Clarendon Press*. <https://doi.org/10.5840/philstudies19802725>
- O'Keefe, J., & Recce, M. (1993). Phase Relationship Between Hippocampal Place Units and the EEG Theta Rhythm. *Hippocampus*, 3(3), 317–330.
- O'Kusky, J., Ye, P., & D'Ercole, A. (2000). Insulin-like growth factor-I promotes neurogenesis and synaptogenesis in the hippocampal dentate gyrus during postnatal development. *The Journal of Neuroscience*, 20(22), 8435–8442. <https://doi.org/10.1523/jneurosci.20-22-08435.2000>
- Otake, M., & Schull, W. (1993). Radiation-related small head sizes among prenatally exposed A-bomb survivors. *International Journal of Radiation Biology*, 63(2), 255–270. <https://doi.org/10.1080/09553009314550341>
- Otake, M., & Schull, W. (1998). Review: Radiation-related brain damage and growth retardation among

-
- the prenatally exposed atomic bomb survivors. *International Journal of Radiation Biology*, 74(2), 159–171. <https://doi.org/10.1080/095530098141555>
- Otake, M., Schull, W., Fujikoshi, Y., & Yoshimaru, H. (1988). Effect on school performance of prenatal exposure to ionizing radiation in Hiroshima: a comparison of the T65DR and DS86 dosimetry systems. *RERF Technical Report Series, 2–88*, 1–36.
- Otake, M., Schull, W., & Lee, S. (1996). Threshold for radiation-related severe mental retardation in prenatally exposed A-bomb survivors: A re-analysis. *International Journal of Radiation Biology*, 70(6), 755–763. <https://doi.org/10.1080/095530096144644>
- Otake, M., Yoshimaru, H., & Schull, W. (1987). Severe mental retardation among the prenatally exposed survivors of atomic bombing of Hiroshima and Nagasaki: a comparison of the T65DR and DS86 dosimetry systems. *RERF Technical Report Series, 16–87*, 1–40.
- Packard, M., & McGaugh, J. (1996). Inactivation of hippocampus or caudate nucleus with lidocaine differentially affects expression of place and response learning. *Neurobiology of Learning and Memory*, 65, 65–72. <https://doi.org/10.1006/nlme.1996.0007>
- Paridaen, Jt., & Huttner, W. (2014). Neurogenesis during development of the vertebrate central nervous system. *EMBO Reports*, 15(4), 351–364. <https://doi.org/10.1002/embr.201438447>
- Parras, C., Galli, R., Britz, O., Soares, S., Galichet, C., Battiste, J., Johnson, J., Nakafaku, M., Vescovi, A., & Guillemot, F. (2004). Mash1 specifies neurons and oligodendrocytes in the postnatal brain. *EMBO Journal*, 23, 4495–4505. <https://doi.org/10.1038/sj.emboj.7600447>
- Pastalkova, E., Itskov, V., Amarasingham, A., & Buzsáki, G. (2008a). Internally Internally generated cell assembly sequences in the rat hippocampus. *Science*, 321, 1322–1327. <https://doi.org/10.1126/science.1159775>.Internally
- Pastalkova, E., Itskov, V., Amarasingham, A., & Buzsáki, G. (2008b). Supporting Online Material for Internally Internally generated cell assembly sequences in the rat hippocampus. *Science*, 321, 1322–1327. <https://doi.org/10.1126/science.1159775>
- Paxinos, G., & Franklin, K. (2004). The Mouse Brain in Stereotaxic Coordinates, 2nd edition. In *Elsevier Academic Press*.
- Pellow, S., Chopin, P., File, S., & Briley, M. (1985). Validation of open : closed arm entries in an elevated plus-maze as a measure of anxiety in the rat. *Journal of Neuroscience Methods*, 14(3), 149–167. [https://doi.org/10.1016/0165-0270\(85\)90031-7](https://doi.org/10.1016/0165-0270(85)90031-7)
- Plümpe, T., Ehninger, D., Steiner, B., Klempin, F., Jessberger, S., Brandt, M., Römer, B., Rodriguez, G., Kronenberg, G., & Kempermann, G. (2006). Variability of doublecortin-associated dendrite maturation in adult hippocampal neurogenesis is independent of the regulation of precursor cell proliferation. *BMC Neuroscience*, 7(77), 1–14. <https://doi.org/10.1186/1471-2202-7-77>
- Pogribny, I., Koturbash, I., Tryndyak, V., Hudson, D., Stevenson, S., Sedelnikova, O., Bonner, W., & Kovalchuk, O. (2005). Fractionated low-dose radiation exposure leads to accumulation of DNA damage and profound alterations in DNA and histone methylation in the murine thymus. *Molecular Cancer Research*, 3(10), 553–561. <https://doi.org/10.1158/1541-7786.MCR-05-0074>
- Prange, O., Wong, T., Gerrow, K., Wang, Y., & El-Husseini, A. (2004). A balance between excitatory and
-

-
- inhibitory synapses is controlled by PSD-95 and neuroligin. *PNAS*, *101*(38), 13915–13920.
- Raber, J., Rola, R., LeFevour, A., Morhardt, D., Curley, J., Mizumatsu, S., & Fike, J. (2004). Radiation-induced cognitive impairments are associated with changes in indicators of hippocampal neurogenesis. *Radiation Research*, *162*(1), 39–47.
- Ranck, J. B. Jr. (1984). Head direction cells in the deep layer of dorsal presubiculum in freely moving rats. *Society for Neuroscience Abstracts*, *10*, 599.
- Rao, M., & Shetty, A. (2004). Efficacy of doublecortin as a marker to analyse the absolute number and dendritic growth of newly generated neurons in the adult dentate gyrus. *European Journal of Neuroscience*, *19*, 234–246. <https://doi.org/10.1111/j.1460-9568.2003.03123.x>
- Rice, D., & Barone Jr., S. (2000). Critical periods of vulnerability for the developing nervous system: Evidence from humans and animal models. *Environmental Health Perspectives*, *108*, 511–533. <https://doi.org/10.1289/ehp.00108s3511>
- Rickmann, M., Amaral, D., & Cowan, W. (1987). Organization of radial glial cells during the development of the rat dentate gyrus. *The Journal of Comparative Neurology*, *264*(4), 449–479. <https://doi.org/10.1002/cne.902640403>
- Rogers, J., Churilov, L., Hannan, A., & Renoir, T. (2017). Search strategy selection in the Morris water maze indicates allocentric map formation during learning that underpins spatial memory formation. *Neurobiology of Learning and Memory*, *139*, 37–49. <https://doi.org/10.1016/j.nlm.2016.12.007>
- Rola, R., Raber, J., Rizk, A., Otsuka, S., Vandenberg, S., Morhardt, D., & Fike, J. (2004). Radiation-induced impairment of hippocampal neurogenesis is associated with cognitive deficits in young mice. *Experimental Neurology*, *188*(2), 316–330. <https://doi.org/10.1016/j.expneurol.2004.05.005>
- Rolls, E. (2013). The mechanisms for pattern completion and pattern separation in the hippocampus. *Frontiers in Systems Neuroscience*, *7*(74), 1–21. <https://doi.org/10.3389/fnsys.2013.00074>
- Rolls, E., Stringer, S., & Elliot, T. (2006). Entorhinal cortex grid cells can map to hippocampal place cells by competitive learning. *Network: Computation in Neural Systems*, 447–465. <https://doi.org/10.1080/09548980601064846>
- Rowland, D., Roudi, Y., Moser, M., & Moser, E. (2016). Ten Years of Grid Cells. *Annual Review of Neuroscience*, *39*(1), 19–40. <https://doi.org/10.1146/annurev-neuro-070815-013824>
- Roybon, L., Deierborg, T., Brundin, P., & Li, J. (2009). Involvement of Ngn2, Tbr and NeuroD proteins during postnatal olfactory bulb neurogenesis. *European Journal of Neuroscience*, *29*, 232–243. <https://doi.org/10.1111/j.1460-9568.2008.06595.x>
- Rubin, P., & Casarett, G. (1968). Clinical radiation pathology as applied to curative radiotherapy. *Cancer*, *22*(4), 767–778. [https://doi.org/10.1002/1097-0142\(196810\)22:4<767::AID-CNCR2820220412>3.0.CO;2-7](https://doi.org/10.1002/1097-0142(196810)22:4<767::AID-CNCR2820220412>3.0.CO;2-7)
- Sahay, A., Scobie, K., Hill, A., O'Carroll, C., Kheirbek, M., Burghardt, N., Fenton, A., Dranovsky, A., & Hen, R. (2011). Increasing adult hippocampal neurogenesis is sufficient to improve pattern separation. *Nature*, *472*, 466–470. <https://doi.org/10.1038/nature09817>
- Sahay, A., Wilson, D., & Hen, R. (2011). Pattern Separation: A Common Function for New Neurons in Hippocampus and Olfactory Bulb. *Neuron*, *70*(4), 582–588.
-

<https://doi.org/10.1016/j.neuron.2011.05.012>

- Sakai, K., Nomura, T., & Ina, Y. (2006). Enhancement of bio-protective functions by low dose/dose-rate radiation. *Dose-Response*, 4(4), 327–332. <https://doi.org/10.2203/dose-response.06-115.Sakai>
- Saneyoshi, T., Fortin, D., & Soderling, T. (2010). Regulation of spine and synapse formation by activity-dependent intracellular signaling pathways. *Current Opinion in Neurobiology*, 20, 108–115. <https://doi.org/10.1016/j.conb.2009.09.013>
- Sargolini, F., Fyhn, M., Hafting, T., McNaughton, B., Witter, M., Moser, M., & Moser, E. (2006). Conjunctive representation of position, direction, and velocity in entorhinal cortex. *Science*, 312(5774), 758–762. <https://doi.org/10.1126/science.1125572>
- Schull, W., Norton, S., & Jensch, R. (1990). Ionizing radiation and the developing brain. *Neurotoxicology and Teratology*, 12, 249–260. [https://doi.org/10.1016/0892-0362\(90\)90096-U](https://doi.org/10.1016/0892-0362(90)90096-U)
- Schull, W., & Otake, M. (1986). Effect on intelligence of prenatal exposure to ionizing radiation. *RERF Technical Report Series*, 7–86, 1–26. https://www.rerf.or.jp/library/scidata/tr_all/TR1986-07.pdf
- Scimeca, J., & Badre, D. (2012). Striatal Contributions to Declarative Memory Retrieval. *Neuron*, 75(3), 380–392. <https://doi.org/10.1016/j.neuron.2012.07.014>
- Scoville, W. (1954). The limbic lobe in man. *Journal of Neurosurgery*, 11(1), 64–66. <https://doi.org/10.3171/jns.1954.11.1.0064>
- Scoville, W., & Milner, B. (1957). Loss of recent memory after bilateral hippocampal lesions. *Journal of Neurology, Neurosurgery and Psychiatry*, 20(11), 11–21. <https://doi.org/10.1136/jnnp.20.1.11>
- Seki, T., & Arai, Y. (1993). Highly polysialylated neural cell adhesion molecule (NCAM-H) is expressed by newly generated granule cells in the dentate gyrus of the adult rat. *The Journal of Neuroscience: The Official Journal of the Society for Neuroscience*, 13(June), 2351–2358. <https://doi.org/10.1523/jneurosci.3447-10.2011>
- Semple, B., Blomgren, K., Gimlin, K., Ferriero, D., & Noble-Haeusslein, L. (2013). Brain development in rodents and humans: Identifying benchmarks of maturation and vulnerability to injury across species. *Progress in Neurobiology*, 106–107, 1–16. <https://doi.org/10.1016/j.pneurobio.2013.04.001>
- Seress, L., Ábrahám, H., Tornóczky, T., & Kosztolányi, G. (2001). Cell formation in the human hippocampal formation from mid-gestation to the late postnatal period. *Neuroscience*, 105(4), 831–843. [https://doi.org/10.1016/S0306-4522\(01\)00156-7](https://doi.org/10.1016/S0306-4522(01)00156-7)
- Seri, B., García-Verdugo, J., Collado-Morente, L., McEwen, B., & Alvarez-Buylla, A. (2004). Cell types, lineage, and architecture of the germinal zone in the adult dentate gyrus. *The Journal of Comparative Neurology*, 478, 359–378. <https://doi.org/10.1002/cne.20288>
- Sharp, P. (1997). Subicular cells generate similar spatial firing patterns in two geometrically and visually distinctive environments: Comparison with hippocampal place cells. *Behavioural Brain Research*, 85, 71–92. [https://doi.org/10.1016/S0166-4328\(96\)00165-9](https://doi.org/10.1016/S0166-4328(96)00165-9)
- Shepherd, J., Grewal, S., Fletcher, A., Bill, D., & Dourish, C. (1994). Behavioural and pharmacological characterisation of the elevated “zero-maze” as an animal model of anxiety. *Psychopharmacology*, 116(1), 56–64. <https://doi.org/10.1007/BF02244871>

-
- Shors, T., Miesegaes, G., Beylin, A., Zhao, M., Rydel, T., & Gould, E. (2001). Neurogenesis in the adult is involved in the formation of trace memories. *Nature*, *410*, 372–376. <https://doi.org/10.1038/414938a>
- Si, B., & Treves, A. (2009). The role of competitive learning in the generation of DG fields from EC inputs. *Cognitive Neurodynamics*, *3*, 177–187. <https://doi.org/10.1007/s11571-009-9079-z>
- Snijders, A., Marchetti, F., Bhatnagar, S., Duru, N., Han, J., Hu, Z., Mao, J., Gray, J., & Wyrobek, A. (2012). Genetic Differences in Transcript Responses to Low-Dose Ionizing Radiation Identify Tissue Functions Associated with Breast Cancer Susceptibility. *PLoS ONE*, *7*(10). <https://doi.org/10.1371/journal.pone.0045394>
- Solstad, T., Boccara, C., Kropff, E., Moser, M., & Moser, E. (2008). Representation of geometric borders in the entorhinal cortex. *Science*, *322*(5909), 1865–1868. <https://doi.org/10.1016/j.neuron.2014.02.014>
- Song, H., Kempermann, G., Wadiche, L., Zhao, C., Schinder, A., & Bischofberger, J. (2005). New neurons in the adult mammalian brain: Synaptogenesis and functional integration. *The Journal of Neuroscience*, *25*(45), 10366–10368. <https://doi.org/10.1523/JNEUROSCI.3452-05.2005>
- Sotelo, C., & Beaudet, A. (1979). Influence of experimentally induced agranularity on the synaptogenesis of serotonin nerve terminals in rat cerebellar cortex. *Proceedings of the Royal Society of London - Biological Sciences*, *206*, 133–138. <https://doi.org/10.1098/rspb.1979.0096>
- Spalding, K., Bergmann, O., Alkass, K., Bernard, S., Salehpour, M., Huttner, H., Boström, E., Westerlund, I., Vial, C., Buchholz, B., Possnert, G., Mash, D., Druid, H., & Frisén, J. (2013). Dynamics of hippocampal neurogenesis in adult humans. *Cell*, *153*, 1219–1227, S1–S11. <https://doi.org/10.1016/j.cell.2013.05.002>
- Squire, L. (2009). The Legacy of Patient H.M. for Neuroscience. *Neuron*, *61*(1), 6–9. <https://doi.org/10.1016/j.neuron.2008.12.023>
- Squire, L., Stark, C., & Clark, R. (2004). The Medial Temporal Lobe. *Annual Review of Neuroscience*, *27*, 279–306. <https://doi.org/doi:10.1146/annurev.neuro.27.070203.144130>
- Stagni, F., Giacomini, A., Guidi, S., Ciani, E., & Bartesaghi, R. (2015). Timing of therapies for Down syndrome: the sooner, the better. *Frontiers in Behavioral Neuroscience*, *9*(265), 1–18. <https://doi.org/10.3389/fnbeh.2015.00265>
- Stanfield, B., & Trice, J. (1988). Evidence that granule cells generated in the dentate gyrus of adult rats extend axonal projections. *Experimental Brain Research*, *72*, 399–406. <https://doi.org/10.1007/BF00250261>
- Steiner, B., Klempin, F., Wang, L., Kott, M., Kettenmann, H., & Kempermann, G. (2006). Type-2 Cells as Link Between Glial and Neuronal Lineage in Adult Hippocampal Neurogenesis. *Glia*, *54*, 805–814. <https://doi.org/10.1002/glia>
- Stensola, H., Stensola, T., Solstad, T., Frøland, K., Moser, M., & Moser, E. (2012). The entorhinal grid map is discretized. *Nature*, *492*, 72–78. <https://doi.org/10.1038/nature11649>
- Steward, O., & Falk, P. (1986). Protein-synthetic machinery at postsynaptic sites during synaptogenesis: A quantitative study of the association between polyribosomes and developing synapses. *The*

-
- Journal of Neuroscience*, 6(2), 412–423. <https://doi.org/10.1523/jneurosci.06-02-00412.1986>
- Suh, H., Consiglio, A., Ray, J., Sawai, T., D'Amour, K., & Gage, F. (2007). In Vivo Fate Analysis Reveals the Multipotent and Self-Renewal Capacities of Sox2+ Neural Stem Cells in the Adult Hippocampus. *Cell Stem Cell*, 1, 515–528. <https://doi.org/10.1016/j.stem.2007.09.002>
- Sun, W., Winseck, A., Vinsant, S., Park, O., Kim, H., & Oppenheim, R. (2004). Programmed cell death of adult-generated hippocampal neurons is mediated by the proapoptotic gene bax. *The Journal of Neuroscience*, 24(49), 11205–11213. <https://doi.org/10.1523/JNEUROSCI.1436-04.2004>
- Swanson, L., & Cowan, W. (1979). The connections of the septal region in the rat. *Journal of Comparative Neurology*, 186, 621–656. <https://doi.org/10.1002/cne.901860408>
- Takai, D., Todate, A., Yanai, T., Ichinohe, K., & Oghiso, Y. (2011). Enhanced transplantability of a cell line from a murine ovary granulosa cell tumour in syngeneic B6C3F1 mice continuously irradiated with low dose-rate gamma-rays. *International Journal of Radiation Biology*, 87(7), 729–735. <https://doi.org/10.3109/09553002.2010.545861>
- Tanaka I., Tanaka S. Ichinohe K., Matsushita S., Matsumoto T., Otsu H., Oghiso Y., Sato F. (2007). Cause of Death and Neoplasia in Mice Continuously Exposed to Very Low Dose Rates of Gamma Rays. *Radiation Research*, 167(4), 417–437. <http://dx.doi.org/10.1667/RR0728.1>
- Tang, F., Loke, W., & Khoo, B. (2017). Low-dose or low-dose-rate ionizing radiation-induced bioeffects in animal models. *Journal of Radiation Research*, 58(2), 165–182. <https://doi.org/10.1093/jrr/rrw120>
- Tashiro, A., Sandler, V., Toni, N., Zhao, C., & Gage, F. (2006). NMDA-receptor-mediated, cell-specific integration of new neurons in adult dentate gyrus. *Nature*, 442, 929–933. <https://doi.org/10.1038/nature05028>
- Taube, J. (1995). Head direction cells recorded in the anterior thalamic nuclei of freely moving rats. *The Journal of Neuroscience*, 15(1), 70–86. <https://doi.org/10.1523/jneurosci.15-01-00070.1995>
- Taube, J. (1998). Head direction cells and the neurophysiological basis for a sense of direction. *Progress in Neurobiology*, 55, 225–256. [https://doi.org/10.1016/S0301-0082\(98\)00004-5](https://doi.org/10.1016/S0301-0082(98)00004-5)
- Taube, J. (2007). The head direction signal: Origins and sensory-motor integration. *Annual Review of Neuroscience*, 30, 181–207. <https://doi.org/10.1146/annurev.neuro.29.051605.112854>
- Taube, J., Muller, R., & Ranck, J. (1990). Head-direction cells recorded from the postsubiculum in freely moving rats. I. Description and quantitative analysis. *The Journal of Neuroscience*, 10(2), 420–435. <https://doi.org/10.1523/jneurosci.10-02-00420.1990>
- Taupin, P., & Gage, F. (2002). Adult neurogenesis and neural stem cells of the central nervous system in mammals. *Journal of Neuroscience Research*, 69, 745–749. <https://doi.org/10.1002/jnr.10378>
- Thompson, L., & Best, P. (1990). Long-term stability of the place-field activity of single units recorded from the dorsal hippocampus of freely behaving rats. *Brain Research*, 509(2), 299–308. [https://doi.org/10.1016/0006-8993\(90\)90555-P](https://doi.org/10.1016/0006-8993(90)90555-P)
- Tolman, E. (1948). Cognitive maps in rats and men. *The Psychological Review*, 55(4), 189–208. <https://doi.org/10.1037/h0061626>
- Toni, N., Laplagne, D., Zhao, C., Lombardi, G., Ribak, C., Gage, F., & Schinder, A. (2008). Neurons born
-

-
- in the adult dentate gyrus form functional synapses with target cells. *Nature Neuroscience*, 11(8), 901–907. <https://doi.org/10.1038/nn.2156>
- Toni, N., Teng, E., Bushong, E., Aimone, J., Zhao, C., Consiglio, A., Van Praag, H., Martone, M., Ellisman, M., & Gage, F. (2007). Synapse formation on neurons born in the adult hippocampus. *Nature Neuroscience*, 10(6), 727–734. <https://doi.org/10.1038/nn1908>
- Urban, N., & Guillemot, F. (2014). Neurogenesis in the embryonic and adult brain: same regulators, different roles. *Frontiers in Cellular Neuroscience*, 8(396), 1–19. <https://doi.org/10.3389/fncel.2014.00396>
- van Calsteren, K., & Amant, F. (2014). Cancer during pregnancy. *Acta Obstetrica et Gynecologica Scandinavica*, 93(5), 443–446. <https://doi.org/10.1111/aogs.12380>
- van Praag, H., Christie, B., Sejnowski, T., & Gage, F. (1999). Running enhances neurogenesis, learning, and long-term potentiation in mice. *PNAS*, 96(23), 13427–13431. <https://doi.org/10.1073/pnas.96.23.13427>
- van Praag, H., Kempermann, G., & Gage, F. (2000). Neural consequences of environmental enrichment. *Nature Reviews Neuroscience*, 1, 191–198. <https://doi.org/10.1038/35044558>
- van Praag, H., Schinder, A., Christie, B., Toni, N., Palmer, T., & Gage, F. (2002). Functional neurogenesis in the adult hippocampus. *Nature*, 415, 1030–1034. <https://doi.org/10.1101/cshperspect.a018812>
- van Strien, N., Cappaert, N., & Witter, M. (2009). The anatomy of memory: An interactive overview of the parahippocampal- hippocampal network. *Nature Reviews Neuroscience*, 10, 272–282. <https://doi.org/10.1038/nrn2614>
- Vanderwolf, C. (1969). Hippocampal electrical activity and voluntary movement in the rat. *Electroencephalography and Clinical Neurophysiology*, 26, 407–418. <https://doi.org/10.1053/j.semss.2007.06.005>
- Verheyde, J., & Benotmane, M. (2007). Unraveling the fundamental molecular mechanisms of morphological and cognitive defects in the irradiated brain. *Brain Research Reviews*, 53, 312–320. <https://doi.org/10.1016/j.brainresrev.2006.09.004>
- Verreet, T., Quintens, R., Van Dam, D., Verslegers, M., Tanori, M., Casciati, A., Neefs, M., Leysen, L., Michaux, A., Janssen, A., D'Agostino, E., Vande Velde, G., Baatout, S., Moons, L., Pazzaglia, S., Saran, A., Himmelreich, U., De Deyn, P., & Benotmane, M. (2015). A multidisciplinary approach unravels early and persistent effects of X-ray exposure at the onset of prenatal neurogenesis. *Journal of Neurodevelopmental Disorders*, 7(3), 1–21. <https://doi.org/10.1186/1866-1955-7-3>
- von Bechterew W. (1900). Demonstration eines Gehirns mit Zerstörung der vorderen und inneren Theile der Hirnrinde beider Schläfenlappen. *Neurologisches Zentralblatt*, 19, 990-991.
- von Bohlen und Halbach, O. (2007). Immunohistological markers for staging neurogenesis in adult hippocampus. *Cell and Tissue Research*, 329, 409–420. <https://doi.org/10.1007/s00441-007-0432-4>
- von Bohlen und Halbach, O. (2011). Immunohistological markers for proliferative events, gliogenesis, and neurogenesis within the adult hippocampus. *Cell and Tissue Research*, 345, 1–19. <https://doi.org/10.1007/s00441-011-1196-4>
-

-
- Vorhees, C., & Williams, M. (2006). Morris water maze: procedures for assessing spatial and related forms of learning and memory. *Nature Protocols*, 1(2), 848–858. <https://doi.org/10.1038/nprot.2006.116>
- Vorhees, C., & Williams, M. (2014). Assessing spatial learning and memory in rodents. *ILAR Journal*, 55(2), 310–332. <https://doi.org/10.1093/ilar/ilu013>
- Wainwright, P., Lévesque, S., Krempulec, L., Bulman-Fleming, B., & McCutcheon, D. (1993). Effects of environmental enrichment on cortical depth and morris-maze performance in B6D2F2 mice exposed prenatally to ethanol. *Neurotoxicology and Teratology*, 15, 11–20. [https://doi.org/10.1016/0892-0362\(93\)90040-U](https://doi.org/10.1016/0892-0362(93)90040-U)
- Waites, C., Craig, A., & Garner, C. (2005). Mechanisms of vertebrate synaptogenesis. *Annual Review of Neuroscience*, 28, 251–274. <https://doi.org/10.1146/annurev.neuro.27.070203.144336>
- Walcher, T., Xie, Q., Sun, J., Irmeler, M., Beckers, J., Öztürk, T., Niessing, D., Stoykova, A., Cvekl, A., Ninkovic, J., & Götz, M. (2013). Functional dissection of the paired domain of Pax6 reveals molecular mechanisms of coordinating neurogenesis and proliferation. *Development*, 140(5), 1123–1136. <https://doi.org/10.1242/dev.082875>
- Wang, J., & Liu, F. (2008). Microtubule-associated protein tau in development, degeneration and protection of neurons. *Progress in Neurobiology*, 85(2), 148–175. <https://doi.org/10.1016/j.pneurobio.2008.03.002>
- Wesson, D., Donahou, T., Johnson, M., & Wachowiak, M. (2008). Sniffing behavior of mice during performance in odor-guided tasks. *Chemical Senses*, 33, 581–596. <https://doi.org/10.1093/chemse/bjn029>
- West, M. (1990). Stereological studies of the hippocampus: a comparison of the hippocampal subdivisions of diverse species including hedgehogs, laboratory rodents, wild mice and men. *Progress in Brain Research*, 83, 13–36. <http://www.sciencedirect.com/science/article/pii/S0079612308612388>
- Wiener, S. (1993). Spatial and behavioral correlates of striatal neurons in rats performing a self-initiated navigation task. *The Journal of Neuroscience*, 13(9), 3802–3817. <https://doi.org/10.1523/jneurosci.13-09-03802.1993>
- Wilson, M., & McNaughton, B. (1993). Dynamics of the hippocampal ensemble code for space. *Science*, 261(5124), 1055–1058. <https://doi.org/10.1126/science.8351520>
- Winter, S., Clark, B., & Taube, J. (2015). Disruption of the head direction cell network impairs the parahippocampal grid cell signal. *Science*, 347(6224), 870–874.
- Witter, M., Van Hoesen, G., & Amaral, D. (1989). Topographical organization of the entorhinal projection to the dentate gyrus of the monkey. *The Journal of Neuroscience*, 9(1), 216–228. <https://doi.org/10.1523/jneurosci.09-01-00216.1989>
- Wolfer, D., & Lipp, H. (2000). Dissecting the behaviour of transgenic mice: is it the mutation, the genetic background, or the environment? *Experimental Physiology*, 85(6), 627–634. <https://doi.org/10.1017/s0958067000020959>
- Wood, J., Johnson, K., Omori, Y., Kawamoto, S., & Keehn, R. (1967). Mental retardation in children

-
- exposed in utero to the atomic bombs in Hiroshima and Nagasaki. *American Journal of Public Health*, 57(8), 1381–1389. <https://doi.org/10.2105/AJPH.57.8.1381>
- Wood, M., Kaplan, M., Park, A., Blanchard, E., Oliveira, A., Lombardi, T., & Abel, T. (2005). Transgenic mice expressing a truncated form of CREB-binding protein (CBP) exhibit deficits in hippocampal synaptic plasticity and memory storage. *Learning and Memory*, 12(2), 111–119. <https://doi.org/10.1101/lm.86605>
- Workman, A., Charvet, C., Clancy, B., Darlington, R., & Finlay, B. (2013). Modeling Transformations of Neurodevelopmental Sequences across Mammalian Species. *The Journal of Neuroscience*, 33(17), 7368–7383. <https://doi.org/10.1523/JNEUROSCI.5746-12.2013>
- Yager, L., Garcia, A., Wunsch, A., & Ferguson, S. (2015). The ins and outs of the striatum: Role in drug addiction. *Neuroscience*, 301, 529–541. <https://doi.org/10.1016/j.neuroscience.2015.06.033>
- Yassa, M., & Stark, C. (2011). Pattern separation in the hippocampus. *Trends in Neurosciences*, 34(10), 515–525. <https://doi.org/10.1016/j.tins.2011.06.006>.Pattern
- Yin E., Nelson D., Coleman M., Peterson L., Wyrobek A. (2003). Gene expression changes in mouse brain after exposure to low-dose ionizing radiation. *International Journal of Radiation Biology*, 79(10), 759-775.
- Yoshida, M., Goto, K., & Watanabe, S. (2001). Task-dependent strain difference of spatial learning in C57BL/6N and BALB/c mice. *Physiology & Behavior*, 73, 37–42. [https://doi.org/10.1016/S0031-9384\(01\)00419-X](https://doi.org/10.1016/S0031-9384(01)00419-X)
- Zhang, K., Ginzburg, I., McNaughton, B., & Sejnowski, T. (1998). Interpreting neuronal population activity by reconstruction: Unified framework with application to hippocampal place cells. *Journal of Neurophysiology*, 79(2), 1017–1044. <https://doi.org/10.1152/jn.1998.79.2.1017>
- Zhao, C., Deng, W., & Gage, F. (2008). Mechanisms and functional implications of adult neurogenesis. *Cell*, 132, 645–660. <https://doi.org/10.1016/j.cell.2008.01.033>
- Zhao, C., Teng, E., Jr, R., Ming, G., & Gage, F. (2006). Distinct Morphological Stages of Dentate Granule Neuron Maturation in the Adult Mouse Hippocampus. *The Journal of Neuroscience*, 26(1), 3–11. <https://doi.org/10.1523/JNEUROSCI.3648-05.2006>

17 Acknowledgments

My sincere thanks go to my doctoral adviser Professor Dr. Bodo Laube, thank you for the great opportunity to investigate such an interesting and exciting PhD project in your research group! Thank you very much for the fruitful discussions and your guidance!

Many thanks to Professor Dr. Ralf Galuske for being the co-referee of my thesis and for the straightforward processing of questions regarding the work in the animal facility.

Furthermore, I want to give many thanks to all my colleagues, Henrik, Kiki, Selina, Juliane, Max and Raj. In particular, I want to thank...

...Kirsten, for your support regarding administrative affairs...

...Katja and Basti, for our great conference visits all over the world...

...Katja, for our cooperation during the work in the mouse facility...

...Michi, Kai, Gabi and Vito, for being my office partners in the last years and for discussions about data, statistics and football...

...and thanks to everyone, for the very pleasant working atmosphere!

Thanks to Dr. Florian Frohns (research group of Prof. Dr. Markus Löbrich) and Prof. Dr. Andreas Hess (FAU Erlangen) for our cooperation regarding the planning and processing of animal test proposals.

Jasmin and Carmen, thank you very much, for your help in the mouse facility regarding mouse lines and breedings.

Kirsten (research group of Prof. Galuske), thank you for your help in the histology lab. A very special thanks is due to Maren Breitung who is a very important and valuable person in my life.

I would like to express my sincere appreciation and thanks to my family which always supported me.

18 Curriculum Vitae

Axel Klink



Date of birth	14 April 1985
Place of birth	Neunkirchen Saar
Nationality	German

Academic Profile

2014-2020

PhD candidate in the research group of Prof. Dr. Bodo Laube, Department of Neurophysiology and Neurosensory Systems | Technische Universität Darmstadt

2011-2014

Master of Science in “Developmental, Neural, and Behavioral Biology” | Georg-August Universität Göttingen

Master thesis: “The role of Neuregulin-1 (NRG1) during peripheral nerve development and in acute and chronic diseases of the peripheral nervous system” | Max Planck Institute of Experimental Medicine Göttingen, Department of Neurogenetics, Research group: Molecular and Translational Neurology (Prof. Dr. Michael Sereda)

2007-2011

Bachelor of Science in “Biology” | Georg-August Universität Göttingen

Bachelor thesis: “Morphologische Charakterisierung der CMT-Ratte in Bezug auf die Hypermyelinisierung kleinkalibriger Axone” | Max Planck Institute of Experimental Medicine Göttingen, Department of Neurogenetics, Research group: Molecular and Translational Neurology (Prof. Dr. Michael Sereda)

2004

Abitur | Saar-Pfalz-Gymnasium, Homburg

Poster & Talks

2019

Short talk and poster presentation at Fusion Conference Neurogenesis | Nassau, Bahamas

2018

Poster presentation at Annual Meeting of the Society for Biological Radiation Research | Frankfurt am Main

2017

Poster presentation at British Neuroscience Association Conference | Birmingham, UK

Publications

2019

NRG1 type I dependent autocrine stimulation of Schwann cells in onion bulbs of peripheral neuropathies | Nature Communications, 10(1467)

2014

Soluble neuregulin-1 modulates disease pathogenesis in rodent models of Charcot-Marie-Tooth disease 1A | Nature Medicine, 20(9)

2012

A rat model of Charcot-Marie-Tooth disease 1A recapitulates disease variability and supplies biomarkers of axonal loss in patients | Brain, 135(1)